Dual Role of Sulfite Oxidase in Mitochondrial Bioenergetics and Nitrite-Dependent Nitric Oxide Synthesis

Dissertation

zur

Erlangung des Doktorgrades

der Mathematisch-Naturwissenschaftlichen Fakultät

der Universität zu Köln

vorgelegt von

Titus Gehling

angenommen im Jahr 2025

Abstract

Sulfite oxidase (SOX) is a vital mitochondrial enzyme requiring the molybdenum cofactor (Moco) to oxidize toxic sulfite to sulfate, a key step in sulfur metabolism. SOX deficiency (SOXD) causes neurodegeneration and has recently been linked to mitochondrial dysfunction. Thus, understanding the role of SOX for mitochondrial physiology and its regulation is crucial.

While SOX loss of SOX is known to impact mitochondrial bioenergetics and morphology, the underlying mechanisms remain poorly understood. Additionally, SOX has been implicated in a distinct, non-canonical function: facilitating nitrite-dependent nitric oxide (NO) synthesis, the physiological significance of which has yet to be elucidated. This thesis explores both functional dimensions of SOX and investigates their broader physiological relevance.

By using a combination of respiratory experiments and proteomic approaches this work revealed disruption of mitochondrial bioenergetics upon loss of SOX, specifically, a marked reduction in mitochondrial oxygen consumption and impairment of oxidative phosphorylation expanding from different *In vivo* to *ex vivo* model systems. Proteomics revealed that these impairments correlate with widespread downregulation of proteins involved in the tricarboxylic acid cycle and respiratory complexes and upregulation of glycolytic proteins, indicating metabolic rewiring. Whole-cell proteomic analysis uncovered extensive alterations in extracellular matrix proteins, linking SOX deficiency to impaired mitochondrial function and extracellular matrix remodeling. Additionally, nitrite exposure caused a slight, non-significant decrease in respiration, suggesting a potential role for SOX-dependent nitrite reduction in OXPHOS regulation.

Furthermore, this work uncovered a protective role of SOX in hypoxic vasodilation. In the context of heart failure with preserved ejection fraction (HFpEF), loss of SOX resulted in increased right ventricular hypertrophy and cardiac remodeling. Spectroscopic experiments revealed that cytochrome *c* can serve as an electron donor for SOX in the absence of oxygen, suggesting an adaptive mechanism for NO generation under hypoxic conditions.

Furthermore, characterization of SOX-deficient neuronal cultures revealed a novel mechanism underlying the characteristic neurodegeneration of SOXD. While the typical SSC-mediated neurodegeneration was absent, neuronal cultures exhibited a marked reduction in mitochondrial respiration. In combination with a neurodevelopment deficit in these cultures this highlights the contribution of mitochondrial dysfunction towards the pathomechanism of SOXD.

Finally, regulatory studies identified molybdate supplementation, MOCS1AB overexpression, and the RNA-binding protein CLUH as modulators of SOX activity and expression. These findings offer potential therapeutic avenues for molybdenum cofactor deficiency and related metabolic disorders e.g. by dietary or pharmacological molybdate administration, gene therapy approaches aimed at boosting MOCS1AB expression or modulation of CLUH-mediated RNA regulation.

Collectively, this work elucidates a dualistic role of SOX in sustaining mitochondrial bioenergetics and nitric oxide homeostasis, extending the understanding of sulfur metabolism in health and disease. These insights pave the way for mechanism-based therapeutic strategies aimed at mitigating bioenergetic deficits in SOX-related pathologies, while also identifying possible targets for these strategies.

Zusammenfassung

Sulfite-Oxidase (SOX) ist ein lebenswichtiges mitochondriales Enzym, das den Molybdän-Cofaktor (Moco) benötigt, um toxisches Sulfit zu Sulfat zu oxidieren – ein entscheidender Schritt im Schwefelstoffwechsel. SOX-Defizienz (SOXD) führt zu Neurodegeneration und wurde kürzlich mit mitochondrialer Dysfunktion in Verbindung gebracht. Daher ist das Verständnis der Rolle von SOX für die mitochondriale Physiologie und deren Regulation von großer Bedeutung.
Obwohl bekannt ist, dass der Verlust von SOX die mitochondriale Bioenergetik und Morphologie beeinträchtigt, sind die zugrunde liegenden Mechanismen bislang wenig verstanden. Zudem wird SOX eine nicht-kanonische Funktion zugeschrieben: die Förderung der nitritabhängigen Stickstoffmonoxid-(NO)-Synthese, deren physiologische Bedeutung jedoch noch unklar ist. Diese Arbeit untersucht beide funktionellen Aspekte von SOX und deren übergeordnete physiologische Relevanz.

Durch eine Kombination aus respiratorischen Experimenten und proteomischen Ansätzen wurde gezeigt, dass der Verlust von SOX zu einer Störung der mitochondrialen Bioenergetik führt, insbesondere zu einer deutlichen Reduktion des mitochondrialen Sauerstoffverbrauchs und einer Beeinträchtigung der oxidativen Phosphorylierung – dies wurde von verschiedenen *in vivo*- bis hin zu *ex vivo*-Modellsystemen bestätigt. Die Proteomik zeigte, dass diese Beeinträchtigungen mit einer weitreichenden Herunterregulierung von Proteinen des Tricarbonsäurezyklus und der Atmungskomplexe sowie einer Hochregulierung von glykolytischen Proteinen einhergehen, was auf eine metabolische Umstrukturierung hinweist. Die Proteomanalyse ganzer Zellen offenbarte umfangreiche Veränderungen von extrazellulären Matrixproteinen und verbindet SOX-Mangel somit mit mitochondrialer Dysfunktion und Umgestaltung der extrazellulären Matrix. Darüber hinaus führte Nitrit-Exposition zu einer leicht, jedoch nicht signifikant verminderten Atmung, was auf eine mögliche Rolle der SOX-abhängigen Nitritreduktion bei der Regulation der OXPHOS hindeutet.

Des Weiteren konnte ein schützender Effekt von SOX bei der hypoxischen Vasodilatation nachgewiesen werden. Im Kontext der Herzinsuffizienz mit erhaltener Ejektionsfraktion (HFpEF) führte der Verlust von SOX zu verstärkter Rechtsherzhypertrophie und kardialer Remodellierung. Spektroskopische Untersuchungen zeigten, dass Cytochrom *c* unter Sauerstoffmangel als Elektronendonator für SOX dienen kann, was einen adaptiven Mechanismus zur NO-Generation unter hypoxischen Bedingungen nahelegt.

Die Charakterisierung von SOX-defizienten neuronalen Kulturen deckte zudem einen neuartigen Mechanismus auf, der der charakteristischen Neurodegeneration bei SOXD zugrunde liegt. Während die typische SSC-vermittelte Neurodegeneration fehlte, wiesen die neuronalen Kulturen eine deutliche Abnahme der mitochondrialen Atmung auf. In Kombination mit einer Beeinträchtigung der neuronalen Entwicklung unterstreicht dies die Bedeutung mitochondrialer Dysfunktion für den Pathomechanismus von SOXD.

Abschließend identifizierten regulatorische Studien die Molybdat-Supplementierung, die Überexpression von MOCS1AB sowie das RNA-bindende Protein CLUH als Modulatoren der SOX-Aktivität und -Expression. Die Ergebnisse eröffnen potenzielle therapeutische Ansätze für Molybdän-Cofaktor-Defizienz und verwandte Stoffwechselstörungen, z. B. durch diätetische oder pharmakologische Molybdat-Gabe, gentherapeutische Ansätze zur Steigerung der MOCS1AB-Expression oder Modulation der CLUH-vermittelten RNA-Regulation.

Zusammenfassend zeigt diese Arbeit die duale Rolle von SOX bei der Aufrechterhaltung der mitochondrialen Bioenergetik und des Stickstoffmonoxid-Haushalts auf und erweitert somit das Verständnis des Schwefelstoffwechsels in Gesundheit und Krankheit. Diese Erkenntnisse ebnen den Weg für mechanistisch basierte therapeutische Strategien zur Minderung bioenergetischer Defizite bei SOX-assoziierten Pathologien und identifizieren gleichzeitig mögliche Angriffspunkte für diese Ansätze.

.

Table of Contents

List of Figures and Tables

Abbreviations

AAV	Adeno-Associated Virus
ABA3	Moco sulfurase in plants
ABC transporter	ATP-Binding Cassette transporter
ACSF	Artificial cerebrospinal fluid
AD	Alzeheimer's disease
ADP	Adenosine diphosphate
Agrn	Agrin
AMP	Adenosine monophosphate
AMPK	5' adenosine monophosphate-activated protein kinase
AOX	Aldehyde oxidase
Asc	Ascorbate
ATP	Adenosine triphosphate
BFP	Blue fluorescent protein
Bgn	Biglycan
BN	Blue native
BSA	Bovine serum albumin
CAA	Chloroacetic acid
Cd151	Cluster of differentiation 151
CECAD	Cluster of Excellence for Aging Research
CHAPS	3-[(3-Cholamidopropyl)dimethylammonio]-1-propanesulfonate
CLUH	Clustered mitochondria homolog
CMV	Cytomegalovirus
CoQ	Coenzyme Q
cPMP	Cyclic pyranopterin monophosphate
CV	Column volume
Cyt *c*	Cytochrome *c*
DIV	Days in vitro
DMEM	Dulbecco's modified eagle medium
DPP	Decaprenyl pyrophosphate
DTT	Dithiothreitol
ECM	Extracellular matrix
Ecm1	Extracellular matrix protein 1
EDRF	Endothelium-derived relaxing factor
EDTA	Ethylenediaminetetraacetic acid
EE	Ethylmalonic encephalopathy
eNOS	Endothelial nitric oxide synthase
ETC	Electron transport chain
FAD	Flavin adenine dinucleotide
FADH	Reduced flavin adenine dinucleotide
Fbn1	Fibrillin 1
Fbn2	Fibrillin 2
FBS	Fetal bovine serum
FCCP	Carbonylcyanide-p-trifluoromethoxyphenylhydrazone
FMN	Flavin mononucleotide
FMOC-CL	Fluorenylmethyloxycarbonyl chloride
Fn1	Fibronectin 1

GAPDH	Glyceraldehyde-3-phosphate dehydrogenase
GBSS	Gey’s balanced salt solution
GDP	Guanosine diphosphate
GFAP	Glial fibrillary acidic protein
GFP	Green fluorescent protein
Glut	Glutamate
GPHN	Gephyrin
GSEA	Gene set enrichment analysis
GST	Glutathione S-transferase
GTP	Guanosine triphosphate
4-HB	4-Hydroxybenzoate
HEK	Human embryonic kidney
HFpEF	Heart failure with preserved ejection fraction
HMCS	Human moco sulfurase
HPLC	High-performance liquid chromatography
HRP	Horseradish peroxidase
hSOX	Human sulfite oxidase
hSYN	Human synapsin
IGG	Immunoglobulin G
IMS	Intermembrane space
iNOS	Inducible nitric oxide synthase
LB	Luria-bertani
L-NAME	Nω-Nitro-L-arginine methyl ester
Lox	Lysyl oxidase
LV	Left ventricle
mARC	Mitochondrial amidoxime reducing component
mBBR	Monobromobimane
Mcam	Melanoma cell adhesion molecule
MEFs	Mouse embryonic fibroblasts
mito	Mitochondria
MoCD	Molybdenum cofactor deficiency
Moco	Molybdenum cofactor
MPT	Molybdopterin
mPTP	Mitochondrial permeability transition pore
MTS	Mitochondrial targeting sequence
NAD	Nicotinamide adenine dinucleotide
NADH	Reduced NAD
NADPH	Nicotinamide adenine dinucleotide phosphate (reduced)
NB	Neurobasal
NEB	New England Biolabs
Ni-NTA	Nickel-nitrilotriacetic acid
nNOS	Neuronal nitric oxide synthase
NO	Nitric oxide
NOS	Nitric oxide synthase
NR	Nitrate reductase
O/N	Overnight
OCR	Oxygen consumption rate
OXPHOS	Oxidative phosphorylation
PAGE	Polyacrylamide gel electrophoresis

PAPS	3'-phosphoadenosine-5'-phosphosulfate
PAPSS2	PAPS synthase 2
PC	Pyruvate carboxylase
PCA	Principal component analysis
PDH	Pyruvate dehydrogenase
PEG	Polyethylene glycol
PEI	Polyethylenimine
Pfkfb2	Phosphofructokinase-2
PKA	Protein kinase A
PM	Pyruvate/Malate
PPA2	Pyrophosphatase (Inorganic) 2
PVDF	Polyvinylidene fluoride
ROS	Reactive oxygen species
ROT/AA	Rotenone/Antimycin A
RT	Room temperature
RV	Right ventricle
RVSP	Right Ventricular Systolic Pressure
S	Septum
SAP	Systolic arterial pressure
SDC2	Syndecan-2
SDS	Sodium dodecyl sulfate
sGC	Soluble guanylate cyclase
SOX	Sulfite oxidase
SOXD	Isolated sulfite oxidase d#eficiency
SSC	S-sulfocysteine
STS	Stop-transfer signal
Succ	Succinate
TBS	Tris-buffered saline
TBS-T	TBS with tween-20
TCA	Tricarboxylic acid
TEAB	Triethylammonium Bicarbonate
TIM	Translocase of inner mitochondrial membrane
TMPD	N,N,N',N'-tetramethyl-p-phenylenediamine
Tnc	Tenascin C
TOM	Translocase of outer mitochondrial membrane
UTR	Untranslated region
Vcan	Versican
VDAC	Voltage-dependent anion channel
WB	Western blot
WT	Wild type
XDH	Xanthine dehydrogenase
XOR	Xanthine oxidoreductase

1 Introduction

1.1 The Molybdenum cofactor

The molybdenum cofactor (Moco) is an essential, evolutionarily conserved prosthetic group found in nearly all forms of life, where it enables the catalytic activity of a diverse family of enzymes known as molybdoenzymes. The function depends on the transition metal molybdenum (Mo). The ability of molybdenum to adapt to oxidation states ranging from +IV to +VI in enzymes makes it capable of catalyzing the reaction for various redox reactions, found within metabolism of carbon, nitrogen, and sulfur compounds (Adamus et al., 2024; Magalon and Mendel, 2015). Mammalian Moco is composed of a metal-binding pterin (MPT) scaffold, which features a tricyclic structure with a pyran ring fused to the pterin backbone and substituted at the C6 position (Mendel, 2013). A distinctive feature of this cofactor is the dithiolene group attached at the C1' and C2' positions of the pyran ring. These two sulfur atoms chelate the molybdenum ion and are critical for redox activity (Kramer et al., 1987). While most molybdenum-dependent enzymes utilize this tetrahydropyranopterin-based backbone, prokaryotic nitrogenase is a notable exception, employing a unique iron-sulfur (Fe-S) cluster derived molybdenum containing cofactor (FeMoco) instead (Spatzal et al., 2011). Eukaryotic Moco-dependent enzymes are classified into two groups: the sulfite oxidase (SOX) family and the xanthine oxidase (XO) family. Both share the MPT backbone, the dithiolene moieties, and two oxo ligands (in equatorial and axial positions) coordinating the molybdenum, but differ in the identity of the fifth ligand in the equatorial position. In the SOX family this position is occupied by a sulfur atom originating from a highly conserved cysteine residue, whereas in the XO family it is coordinated by a terminal sulfido ligand (Mendel and Schwarz, 2011).

1.2 Moco biosynthesis

Moco is crucial for numerous enzymatic reactions and its instability makes a continuous supply indispensable. Since free Moco is highly sensitive to oxygen, organisms depend on the *de novo* synthesis (Johnson et al., 1984). Recently, however, studies on Moco-deficient *Caenorhabditis elegans* revealed, once bound to protein, Moco can also be taken up from the diet as another bioavailable source (Warnhoff et al., 2021).

Nonetheless, Moco biosynthesis is a highly orchestrated and evolutionarily conserved multistep process involving six different proteins. The pathway begins in the mitochondrial matrix, where guanosine triphosphate (GTP) is converted to cyclic pyranopterin monophosphate (cPMP) by the enzymes MOCS1A and MOCS1B (Mayr et al., 2020; Santamaria-Araujo et al., 2004). Next, cPMP has been proposed to be transported into the cytosol by the mitochondrial adenosine triphosphate (ATP)-binding cassette (ABC)

transporter 3 (ATM3), a transporter which was initially discovered to play a crucial role in the assembly of cytosolic Fe-S clusters (Teschner et al., 2010). In the cytosol, cPMP is converted to molybdopterin (MPT) through the action of MPT synthase, a complex composed of two large MOCS2A and two small MOCS2B subunits. This step introduces the dithiolene moieties at C1' and C2' positions of the pyran ring. The final step of Moco biosynthesis is catalyzed by gephyrin. While the G-domain of the protein is responsible for the activation of MPT to MPT-AMP, consuming ATP, the E-domain catalyzes the final insertion of the molybdate into the MPT backbone by hydrolyzing the AMP (Kaufholdt et al., 2017).

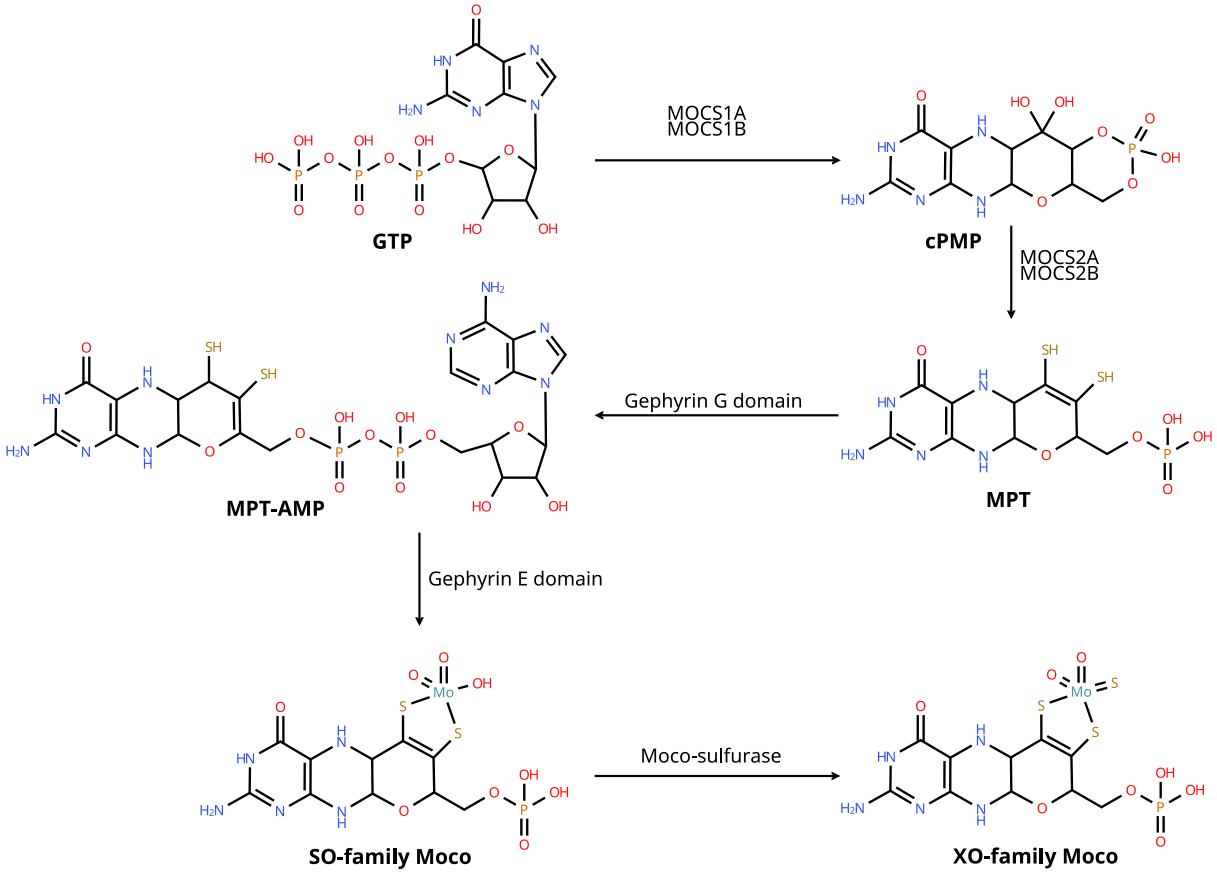

Figure 1: Moco biosynthesis in humans
Biosynthesis begins in the mitochondrial matrix, where MOCS1A/B convert GTP to cPMP. cPMP is then transported to the cytosol and converted to MPT by MOCS2A/B. Gephyrin catalyzes Moco formation in two steps: MPT is adenylated (G domain), then molybdenum is inserted (E domain). For XO-family enzymes, HMCS adds a terminal sulfido ligand in a final maturation step.

Despite its biological importance, the abundance of Mo is rather low, requiring active transport into the cells in form of the oxyanion molybdate (Weber et al., 2023). For enzymes of the SOX family, the biosynthetic pathway concludes with the insertion of Moco. However, in the XO family, Moco undergoes further maturation: the insertion of a terminal sulfido ligand, catalyzed by specific Moco sulfurases abscisic acid-deficient 3 sulfurase (ABA3) in plants and human molybdenum cofactor sulfurase (HMCS) in humans (Bittner et al., 2001; Ichida et al., 2001). A detailed scheme of the biosynthetic pathway is depicted in Figure 1. Dysfunction of Moco

biosynthesis results in molybdenum cofactor deficiency (MoCD), a disease with limited treatment options, which will be discussed elsewhere (1.3.4). Thus, targeting the Moco biosynthetic pathway to restore the activity of the Moco-dependent enzymes holds the potential for therapeutical interventions, however, up to date no studies have focused on that aspect.

1.3 Eukaryotic Moco-dependent enzymes

Eukaryotes possess five Moco-dependent enzymes: aldehyde oxidase (AOX), nitrate reductase (NR), mitochondrial amidoxime reducing component (mARC1/2), sulfite oxidase (SOX), and xanthine oxidase reductase (XOR), whereas bacteria have a much broader diversity of these enzymes (Schwarz et al., 2009). Amongst these, NR is unique to autotrophs and fungi, where it catalyzes the conversion of nitrate to nitrite, an essential step for incorporating inorganic nitrogen into organic molecules (Fischer et al., 2005). The remaining four Moco-dependent enzymes are also present in mammals and their canonical functions will be discussed in the following chapters. While their canonical functions differ, all Moco-dependent enzymes share a common nitrite reducing activity, which will be discussed later (1.6.4, 1.6.5)

1.3.1 Mammalian xanthine oxidase family of Moco enzymes

Two of the four Moco enzymes are members of the XO family: XOR and AOX. XOR is a key enzyme involved in the breakdown of purine nucleotides, catalyzing the sequential oxidation of hypoxanthine to xanthine and then xanthine to uric acid (Aziz and Jamil, 2025). This process is essential for purine catabolism in many organisms, including humans, and is the final step in the production of uric acid from purines. Structurally, XOR is a homodimer with a molecular mass of approximately 300 kDa (Enroth et al., 2000). Each subunit contains one Moco, two 2Fe-2S clusters and one flavin adenine dinucleotide (FAD) cofactor and can act independently during catalysis. The oxidative hydroxylation of hypoxanthine to xanthine and xanthine to uric acid takes place at the molybdenum center reducing Mo^{VI} to Mo^{IV} (Okamoto et al., 2004). Subsequently, the electrons from the Mo are transferred to the FAD via the two Fe-S clusters, and the enzyme is reoxidized (Hille and Nishino, 1995). XOR is initially synthesized as a dehydrogenase (XDH) and is readily converted to its oxidase form in response to inflammation or oxidative stress either reversibly by cysteine modification or irreversibly by proteolysis of lysine residues (Bindoli et al., 1988; Nishino and Nishino, 1997). While both enzymes catalyze the same reaction, XOR is highly susceptible to molecular oxygen and uses dioxygen as the final electron acceptor producing reactive oxygen species (ROS). In contrast, re-oxidation in XDH takes place via reduction of nicotinamide adenine dinucleotide (NAD^+) to NADH (Stein and Kirk, 2015).

The second mammalian member of the XO family is AOX, which shares significant structural and catalytic similarities with XOR. AOX is also a homodimer of about 300 kDa with each monomer consisting of a C-terminal Moco-harboring domain, a central FAD domain and two N-terminal 2Fe-2S clusters (Coelho et al., 2012). Substrate oxidation also takes place at the molybdenum center and the electrons from this reaction are transferred to the FAD via the two Fe-S clusters. Reoxidation of the enzyme takes place at the FAD domain and molecular oxygen serves as the final electron acceptor, resulting in the generating of ROS (Coelho et al., 2012). AOX is known for its substrate specificity and catalyzes the hydroxylation of heterocycles and the oxidation of aldehydes to carboxylic acids (Terao et al., 2020). Additionally, it can reduce N- and S-oxides and hydrolyze amides (Sodhi et al., 2015). Due to its broad substrate range and predominant hepatic localization, AOX is increasingly recognized as a significant factor in drug metabolism and therapeutic development (Gajula et al., 2022; Strelevitz et al., 2012). However, the physiological substrates of AOXs remain a subject of debate (Paragas et al., 2021).

1.3.2 Mitochondrial amidoxime reducing component

The mitochondrial amidoxime reducing component (mARC) is the most recently identified member of the mammalian Moco-dependent enzyme family. Mammalian genomes encode two isoforms, mARC1 and mARC2 (Wahl et al., 2010). Both are monomeric enzymes, unlike all other mammalian Moco-dependent enzymes, which typically function as dimers. Notably, mARC enzymes are the smallest in the family and uniquely bind only Moco, without requiring any additional prosthetic groups (Kubitza et al., 2018). Structural studies have revealed that the molybdenum of the Moco is coordinated by a conserved protein-derived cysteine residue. However, the classification of mARC to the SOX or XO family of Moco enzymes is still under debate (Kubitza et al., 2018; Rajapakshe et al., 2011).

In terms of subcellular localization, mammalian mARC proteins are integrated into the outer mitochondrial membrane, with the N-terminal region acting as a membrane anchor and the C-terminal catalytic domain exposed to the cytosol (Klein et al., 2012). While this mitochondrial localization of mammalian mARC is well established, some studies have also reported possible peroxisomal or cytosolic localization (Islinger et al., 2007; Wiese et al., 2007).

To date, no specific physiological substrate for mARC has been identified. However, *in vitro* studies have shown that mARC forms a functional three-component system with cytochrome *b5* and NADH-dependent cytochrome *b5* reductase, catalyzing the reduction of a broad range of *N*-hydroxylated compounds (Havemeyer et al., 2006; Struwe et al., 2023). This activity links mARC to the metabolism of *N*-hydroxylated prodrugs and detoxification of mutagenic *N*-oxygenated nucleobase analogs. Additionally, human mARC enzymes have been shown to

reduce hydrogen peroxide (H_2O_2), suggesting a potential role in cellular antioxidant defense (Janik et al., 2021; Rixen et al., 2023). In recent years, mARC has also been implicated in lipid metabolism. For example, mARC2 knockout mice are resistant to high-fat diet-induced weight gain, and a common polymorphism in mARC1 (p.A165T) is associated with reduced risk of non-alcoholic fatty liver disease and liver cirrhosis (Emdin et al., 2021, 2020; Rixen et al., 2019). Multiple studies have confirmed that this variant decreases liver fat and lowers the risk of liver disease (Struwe et al., 2023). Although the precise biochemical or cellular pathways by which mARC1 and mARC2 influence lipid metabolism remain to be elucidated, recent evidence suggests a possible role in β-oxidation of fatty acids for mARC1 (Ciociola et al., 2025).

1.3.3 Sulfite oxidase

The only mammalian representative of the SOX family of Moco enzymes is the eponymous SOX. It catalyzes the last step of the cysteine catabolism, the oxidation of toxic sulfite (SO_3^{2-}) to sulfate (SO_4^{2-}). Due to the lethal phenotype caused by loss of function, SOX is considered the most important Moco enzyme. It is important not only for regulating sulfur metabolism, but also for enabling a wide array of downstream physiological functions. The following chapters will summarize the current state of mammalian SOX research.

1.3.3.1 Domain and crystal structure of SOX

The crystal structure of chicken SOX solved in 1997 still serves as the blueprint for structural insights into SOX up to date (Kisker et al., 1997). Mature SOX is a homodimeric enzyme composed of two antiparallel subunits with a molecular weight of approximately 52 kDA each (Figure 2). Each subunit is organized into distinct structural domains: an N-terminal heme domain, a flexible tether of 11 amino acid residues followed by a Moco domain and a C-terminal dimerization domain (Kisker et al., 1997). The flexible tether was shown to be crucial for SOX activity since it enables domain movement of the heme domain (Bender et al., 2019b; Feng et al., 2002, 1.3.3.3). The Moco is deeply buried inside the Moco domain, with only the molybdenum being solvent exposed (Kisker et al., 1997). A highly conserved cysteine residue (C264) and a triade of H361, R366 and K379 coordinate the Moco. The binding pocket of SOX is dominated by positively charged residues (R138, R190, R450, W204 and Y322) enabling a beneficial environment for the negatively charged substrate sulfite and its product sulfate. Besides Moco, SOX also harbors a cytochrome b_5-type heme cofactor within the heme domain. The crystal structure revealed a distance of 32 Å between the two redox centers. Productive electron transfer reactions usually require a distance of 14 Å, indicating the requirement of domain movement for proper SOX activity (Kisker et al., 1997; Page et al., 1999).

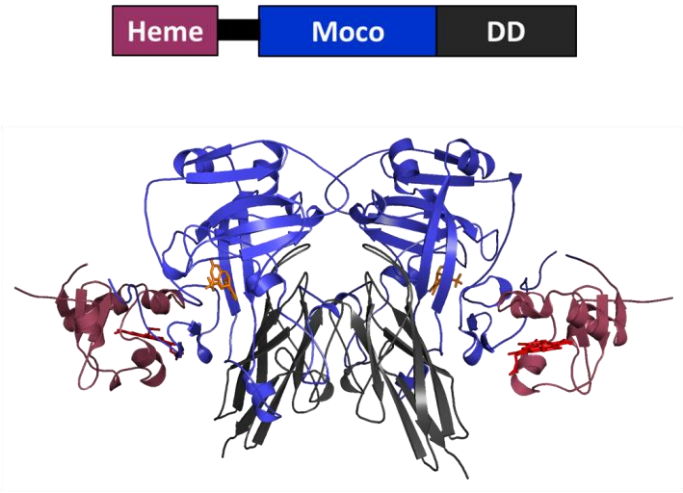

Figure 2: Depiction of the domain structure of chicken sulfite oxidase homodimer
(PDB: 1SOX) SOX is composed of the heme domain (purple) the Moco domain (blue) and the dimerization domain (black). The heme and the Moco domain are linked via a flexible tether domain. The Moco is represented in orange and the heme-cofactor is displayed in red.

1.3.3.2 Maturation of mammalian SOX

Since SOX catalyzes the oxidation of sulfite, which accumulates in mitochondria, and uses cytochrome *c* as a final electron acceptor, SOX localizes to the intermembrane space (IMS). It is encoded by the nuclear *SUOX* gene and synthesized in the cytosol. Since mislocalization of SOX was shown to result in its degradation, a distinct maturation process is crucial (Klein and Schwarz, 2012). Pre-SOX is synthesized with an N-terminal mitochondrial targeting signal (MTS), followed by a hydrophobic stop-transfer signal (STS). Translocation of SOX into the IMS of mitochondria is carried out in an ATP-dependent manner by the translocase of the outer membrane (TOM) (Klein and Schwarz, 2012; Ono and Ito, 1984). Next, the STS is integrated into the inner membrane, presumably by the translocase of the inner membrane (TIM) and a mitochondrial processing peptidase cleaves off the MTS. SOX is released into the IMS by cleavage of the STS carried out by the inner membrane peptidase. Following, folding is initiated by the incorporation of Moco, a step which was shown to be crucial to trap SOX in the IMS. Subsequent to Moco binding, the heme insertion and dimerization can take place independently with no hierarchical order (Klein and Schwarz, 2012). Impairment of Moco binding leads to re-localization to the cytosol and degradation of SOX, a maturation defect which is known to result in SOXD (Bender et al., 2019a; Kaczmarek et al., 2022; Klein and Schwarz, 2012). Once Moco is incorporated, SOX is further processed by binding of the heme cofactor and final folding is achieved by dimerization of the protein.

1.3.3.3 Catalytic cycle of SOX

SOX catalyzes the oxidation of sulfite to sulfate, an oxygen transfer reaction using water as a oxygen donor. The catalytic cycle of SOX can be divided into a reductive and an oxidative half-

reaction, which together facilitate electron transfer from sulfite to cytochrome *c* (Cyt *c*) *(*Figure 3).

In the resting state of the enzyme (Mo^{VI}/ Fe^{III}) the molybdenum active site is surface exposed, allowing nucleophilic sulfite to attack the equatorial oxo-ligand of the molybdenum center (Kisker et al., 1997). This initiates a conformational change mediated by R450, which leads to closure of the active site (Emesh et al., 2009; Kisker et al., 1997). During this process, sulfite displaces the oxo ligand and is oxidized to sulfate, while a water molecule is inserted into the coordination sphere of molybdenum. In turn, two electrons are taken up by the molybdenum in the active center, reducing Mo^{VI} to Mo^{IV} completing the reductive half-reaction. This initial reduction was shown to be fast with a velocity of 541 s^{-1} (Kaczmarek et al., 2019).

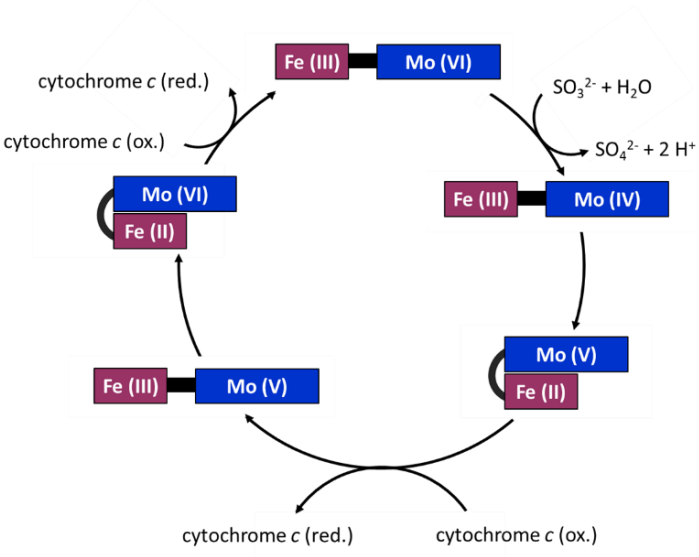

Figure 3: Depiction of the redox changes of the prosthetic groups Mo and Fe during catalytic cycle by SOX
First, sulfite is oxidized to sulfate at the Mo(VI) center, reducing it to Mo(IV). Subsequent IET, requiring domain movement, yields an Mo(V)/Fe(II) state. The heme gets reoxidized by the final electron acceptor cytochrome c. After another IET followed by cytochrome c reduction, the resting state is restored.

The oxidative half-reaction involves two sequential single intramolecular electron transfers (IETs) from the reduced Mo center to the heme iron ($Fe^{III/II}$) and from the heme to cytochrome *c* regenerating the oxidized Mo^{VI}/Fe^{III} resting state of the enzyme. However, the molybdenum and heme centers are spatially separated by ~32 Å, making domain movement essential for electron transfer (Feng et al., 2002; Johnson-Winters et al., 2010). This conformational rearrangement, which brings the heme domain into proximity with the molybdenum center, is influenced by solute viscosity, tether length, and electrostatic interactions between the negatively charged cytochrome b_5-type heme domain and the positively charged Moco domain, including the key residue R160 that stabilizes heme orientation (Emesh et al., 2009; Feng et al., 2003; Kisker et al., 1997; Schrader et al., 2003). The involvement of domain movement significantly slows down the electron transfer rate to 28 s^{-1} or 20 s^{-1} at pH 8.0 or

6.5, respectively, marking the first IET as the rate limiting step in SOX catalysis.(Kaczmarek et al., 2019).

Once Fe^{II} is generated, it donates electrons to cytochrome *c*, the final physiological electron acceptor. This reaction has been studied extensively using laser flash photolysis, revealing rapid rates of up to 700 s^{-1} (Pacheco et al., 1999). Recent studies have demonstrated that IET occurs predominantly within a single subunit of the SOX homodimer. Inter-subunit electron transfer is significantly less efficient, with rates of only 0.02-0.07 s^{-1} for the first electron transfer (from Mo^{IV}) and 0.003-0.02 s^{-1} for the second (from Mo^{V}) (Eh et al., 2022). Following the second IET and the associated cytochrome *c* reduction, the enzyme returns to its Mo^{VI}/Fe^{III} resting state, ready to begin another catalytic cycle.

1.3.4 Sulfite oxidase deficiency

SOXD is caused by complete loss or severe impairments of SOX function, is an ultra-rare autosomal recessive metabolic disorder with a predicted incidence rate of 1 in 1,377,341 births (Kaczmarek et al., 2021). Loss or dysfunction of SOX can be caused either by mutations in the *SUOX* gene, leading to SOXD, or by dysfunctional Moco biosynthesis. Notably, dysfunctions of Moco biosynthesis also affect other Moco-dependent enzymes beyond SOX, resulting in MoCD. MoCD is also an ultra-rare disease and is further classified into three subtypes based on the disturbed proteins involved in Moco biosynthesis: Type A (MOCS1A/B), Type B (MOCS2A/B), and Type C (gephyrin). Although MoCD impairs the function of all Moco-dependent enzymes, the clinical phenotype of MoCD and SOXD is largely indistinguishable, highlighting the unique and essential role of SOX among this enzyme family (Claerhout et al., 2018; Johannes et al., 2022). Both conditions present with early-onset, pharmaco-resistant seizures, severe neurodevelopmental delay, loss of grey matter, and often death in infancy.

The hallmark of SOXD and MoCD is the accumulation of sulfite, a toxic intermediate of cysteine catabolism. On the one hand, sulfite exerts direct toxicity through multiple mechanisms including: disruption of disulfide bonds, ROS generation and inhibition of key metabolic enzymes including glutamate and malate dehydrogenase, which interferes with amino acid metabolism (Vincent et al., 2004; Zhang et al., 2004). On the other hand, sulfite accumulation causes an elevation of sulfur related metabolites such as taurine, thiosulfate and S-sulfocysteine (SSC) (Belaidi and Schwarz, 2013). SSC is generated extracellularly by the reaction of sulfite with the oxidized form of cysteine, cystine. It is a structural homologue of glutamate and thus able to overstimulate N-methyl-D-aspartate (NMDA) receptors leading to excitotoxic calcium influx, calpain-dependent cleavage of synaptic proteins, and loss of inhibitory synapses, causing the observed neurological impairments in SOXD and MoCD (Kumar et al., 2019).

Furthermore, the oxidation product of sulfite, sulfate, serves as a vital substrate for sulfation reactions, mediated by the universal sulfate donor 3'-phosphoadenosine-5'-phosphosulfate (PAPS). Sulfation is an important post-translational modification for several biological processes (Chapman et al., 2004). One of them is the maintenance of proper extracellular matrix (ECM) structure by mediating the interacting of glycosaminoglycans with other ECM components (Ravikumar et al., 2020; Soares Da Costa et al., 2017). The possible contribution of low sulfate levels due to missing sulfite oxidation by SOX, however, is yet unknown.

A recently characterized mouse model of SOXD, generated by a CRISPR/Cas9 mediated 7 bp deletion, has provided new insights into the disease mechanisms (Kohl, 2019). Interestingly, these mice have an average lifespan of 9.6 days but showed no signs of brain damage. In line with these findings, urinary SSC levels were much lower than in human patients. Instead, sulfur is predominantly excreted as thiosulfate, the catabolic oxidation product of hydrogen sulfide (H_2S) and sulfite, indicating elevated H_2S levels in SOXD mice. Strikingly, H_2S is known to impair mitochondrial function by inhibiting cytochrome *c* oxidase (complex IV), thereby reversing the tricarboxylic acid (TCA) cycle and shutting down oxidative phosphorylation (OXPHOS), raising the question of a possible contribution of H2S toxicity towards the pathomechanism of SOXD (Carballal et al., 2021; Grings et al., 2019)

Up to date, the only treatment option for MoCD is a supplementation with cPMP, which can restore Moco biosynthesis and prevent neurodegeneration upon early intervention (Schwahn et al., 2015; Schwarz et al., 2025). However, only MoCD type A can be treated with cPMP. In contrast, no specific treatments exist for MoCD types B and C as well as for SOXD. The only option so far is to reduce the symptoms by dietary restriction of sulfur-containing amino acids to reduce the metabolic flux in the cysteine catabolism and decrease sulfite accumulation (Abe et al., 2021; Boles et al., 1993; Touati et al., 2000).

1.4 The Cysteine Metabolism

Cysteine is a sulfur-containing amino acid that plays a central role in cellular metabolism, not only as a structural component of proteins but also as a precursor for numerous bioactive molecules. One of these is glutathione (GSH) which is synthesized from cysteine, glutamate and glycine in a two step process involving glutamyl-cysteine synthetase (GCL) and GSH synthetase (GSS) (Figure 4). Due to its reactive thiol group, cysteine concentrations must be tightly regulated: insufficient levels impair protein synthesis and antioxidant defense, whereas excess cysteine can promote oxidative stress and cytotoxicity (Paul and Snyder, 2012; Stipanuk, 2004). Cysteine catabolism therefore represents a crucial metabolic hub, linking amino acid turnover, sulfur homeostasis, and energy metabolism (Figure 4).

Cysteine can be taken up by the diet or is generated via a two step transsulfuration pathway. The first step, the condensation of homocysteine and serine, is catalyzed by the enzyme cystathionine β-synthase (CBS) yielding cystathionine (Ctt). The second step is catalyzed by the enzyme cystathionine γ-lyase (CSE), cleaving Ctt into cysteine, α-ketobutyrate and NH_3^+.

The predominant route of cysteine degradation in mammalian tissues is the oxidative pathway, catalyzed by cysteine dioxygenase (CDO) (Figure 4). CDO converts cysteine into cysteine sulfinic acid (CSA), which has two principal fates. First, CSA can undergo oxidative decarboxylation to hypotaurine, which is subsequently oxidized to taurine. Taurine is abundant in mammalian tissues and exerts diverse physiological functions, including bile acid conjugation, osmoregulation, neuromodulation, and antioxidant defense (Huxtable, 1992; Ripps and Shen, 2012). Second, CSA can be transaminated to β-sulfinylpyruvate by glutamate oxaloacetate transaminases (GOT1 (cytosolic) or GOT2 (mitochondrial)), which spontaneously decomposes to pyruvate and sulfite. GOT1 was shown to be the major contributor to sulfite generation in the cysteine catabolism (Mellis et al., 2020). Sulfite is further oxidized to sulfate by SOX, generating a major end-product of sulfur metabolism that is essential for sulfation reactions and detoxification (Dejima et al., 2006). Through this branch, cysteine catabolism contributes both to energy production via pyruvate and to the generation of taurine and sulfate.

The other pathway in cysteine catabolism involves the synthesis and oxidation of H_2S (Figure 4). The synthesis is carried out by three enzymes: CBS, CSE and mercaptopyruvate sulfurtransferase (MPST). On the one hand, CBS and CSE generate H_2S, ammonia, and pyruvate (Kabil and Banerjee, 2014; Kimura, 2014). On the other hand, cysteine can be converted to 3-mercaptopyruvate (3-MP) by a transaminase reaction catalyzed GOT1/2 and further degraded by MPST, producing H_2S and pyruvate (Shibuya et al., 2009).

H_2S oxidation is mediated by three mitochondrial enzymes: sulfide:quinone oxidoreductase (SQOR), persulfide dioxygenase (PDO) and thiosulfate sulfurtransferase (TST) (Figure 4) (Hildebrandt and Grieshaber, 2008). The process begins with SQOR, which oxidizes H_2S and transfers the resulting sulfur atom preferentially to glutathione (GSH). Producing glutathione persulfide (GSSH) (Libiad et al., 2014). The electrons released during H_2S oxidation are transferred to the CoQ, thereby coupling H_2S oxidation to mitochondrial respiration (Marcia et al., 2010). GSSH can subsequently undergo two distinct fates: either it is oxidized by PDO generating sulfite, which is subsequently oxidized by SOX to form sulfate, or it is converted by TST, which catalyzes a trans-sulfuration reaction where sulfite and GSSH are used to form GSH and thiosulfate. Therefore, suggesting thiosulfate can act as a biomarker for intracellular H_2S levels.

H_2S, once regarded as a purely toxic gas, is now recognized as a gasotransmitter. It regulates vascular tone, neurotransmission, and cytoprotection through mechanisms including protein persulfidation and modulation of mitochondrial bioenergetics (Paul and Snyder, 2018; Wang, 2012). However, excessive H_2S can inhibit cytochrome *c* oxidase (complex IV) of the mitochondrial respiratory chain, resulting in impaired oxidative phosphorylation and ATP synthesis (Cooper and Brown, 2008; Tiranti et al., 2009). This dual role highlights the fine balance between beneficial signaling and toxicity. Furthermore, it links H_2S homeostasis to mitochondrial physiology. Specifically, since H_2S oxidation takes place in mitochondria.

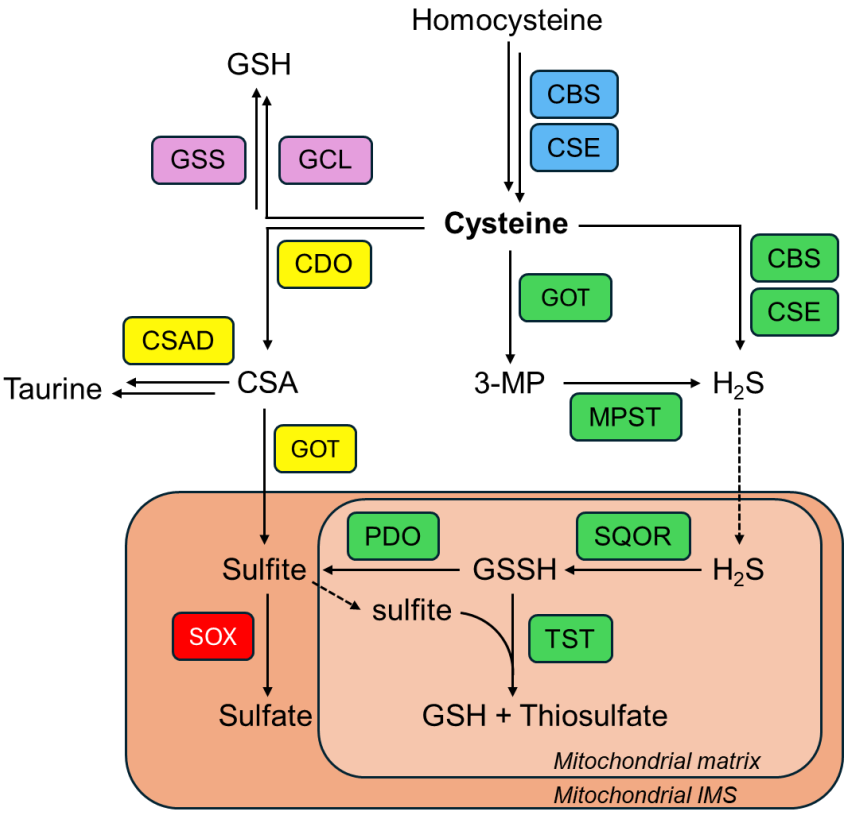

Figure 4:Simplified overview of the cysteine metabolism
The cysteine metabolism starts with the uptake of cysteine from the diet or via its synthesis from homocysteine. Cysteine catabolism can be divided into an oxidative pathway (yellow enzymes), an H_2S related pathway (green enzymes) and the synthesis of glutathione (light purple enzymes). Depending on whether GOT1 (cytosolic) or GOT2 (mitochondrial) catalyze the reaction of cysteine to 3-mercaptopyruvate (3-MP), the reaction takes place in the mitochondrial matrix or the cytosol. Localization of subsequent degradation by MPST to H_2S also depends on the previous step. While the end product of the oxidative pathway are taurine and sulfate, end products of the H_2S related pathway are thiosulfate and sulfate.

1.5 Mitochondrial dynamics and bioenergetics

Mitochondria are essential organelles which fulfill various important cellular functions e.g. production of adenosine triphosphate (ATP) through OXPHOS, regulation of cellular metabolism, and the orchestration of cell death pathways (Friedman and Nunnari, 2014; Nunnari and Suomalainen, 2012; Wallace, 2005). Their proper function is critical for the

survival and health of eukaryotic cells, particularly in tissues with high energy demands such as the brain, heart, and muscles (Herculano-Houzel, 2011; Johannsen and Ravussin, 2009; Murphy et al., 2016). Disruption of mitochondrial integrity and function has been implicated in a wide array of human diseases, including neurodegenerative disorders, metabolic syndromes, and inherited mitochondrial diseases (Schon et al., 2012; Youle and van der Bliek, 2012). To maintain proper function, mitochondria need to adapt to cellular and tissue demands e.g. different cellular nutrient states or the high-energy demand in the heart compared to the high metabolic rate in the liver (Forner et al., 2006; Song et al., 2021). This is achieved by dynamically changing their number by fission and fusion events and/or expression of their proteome e.g. by transcriptional networks regulating the expression of nuclear-encoded proteins (Hock and Kralli, 2009; Scarpulla, 2002; Schatton et al., 2017).

1.5.1 Mitochondrial Morphology

In response to the cellular needs, mitochondria can change their shape, size, number and position by mitochondrial fusion, fission and motility (Tilokani et al., 2018). They are bounded by two distinct membranes: the outer mitochondrial membrane (OMM) and the inner mitochondrial membrane (IMM), which encloses the matrix and forms cristae, olds that increase surface area for oxidative phosphorylation (Vogel et al., 2006).

Mitochondrial dynamics and morphology are mainly regulated by four large GTPases: dynamin-related protein 1 (DRP1), controlling mitochondrial fission, and mitofusin 1 and 2 (MFN1 and MFN2) as well as optic atrophy 1 (OPA1), regulating mitochondrial fusion of the OMM and the IMM, respectively (Tábara et al., 2025). While elongated mitochondrial networks are associated with increased OXPHOS capacity, fragmented mitochondria are commonly observed during apoptosis or cellular stress responses (Glancy et al., 2020; Quintana-Cabrera and Scorrano, 2023). Interestingly, lack of SOX was shown to disturb mitochondrial homeostasis in primary *SUOX*$^{-/-}$ fibroblasts due to reduced mitochondrial motility and elongated mitochondria (Mellis et al., 2021). The latter could be specifically attributed to increased sulfite levels. Furthermore, recent studies on *SUOX*$^{-/-}$ mice revealed smaller lung mitochondria upon loss of SOX (Fu, 2023).

Recent research has highlighted that mitochondrial morphology is not only optimized for ATP production but also provides a mechanism for buffering cellular energy demands and regulating processes such as calcium homeostasis and apoptosis (Faitg et al., 2025; Garcia et al., 2019). Disruptions in the machinery governing mitochondrial dynamics can lead to altered energy metabolism, increased oxidative stress, and are implicated in a range of diseases, including neurodegenerative disorders and mitochondrial myopathies (Quintana-Cabrera and Scorrano, 2023; Rastogi et al., 2019).

In sum, mitochondrial morphology is always changed upon cellular needs, with the aim to maintain the broad physiological functions carried out by mitochondria e.g. ATP generation via the TCA cycle and OXPHOS.

1.5.2 The TCA cycle

Mitochondria are essential for producing cellular energy as ATP via aerobic respiration. The initial stage, glycolysis, occurs in the cytosol, generating two ATP, two NADH, and two pyruvate per glucose, while the TCA cycle and oxidative phosphorylation (OXPHOS) take place in the mitochondrial matrix and inner membrane, respectively.

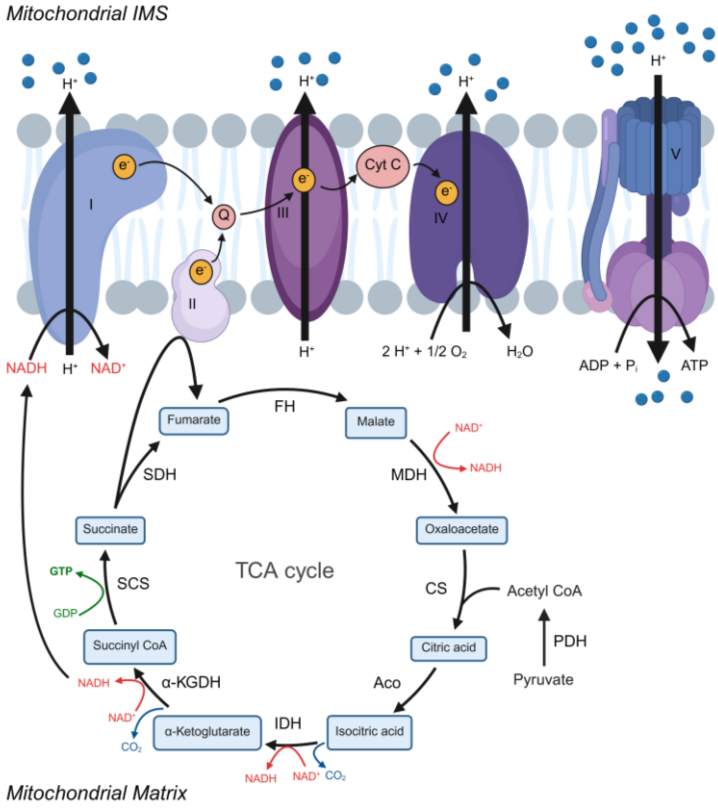

Figure 5: Schematic overview of the TCA cycle and its connection to oxidative phosphorylation
PDH = pyruvate dehydrogenase, CS = citrate synthase, Aco = aconitase, IDH = isocitrate dehydrogenase, α-KGDH = alpha ketoglutarate dehydrogenase, SCS = succinyl-CoA-synthetase, SDH = succinate dehydrogenase, FH = fumarate hydratase, MDH = malate dehydrogenase. Created with BioRender.com.

Pyruvate enters mitochondria and is converted to acetyl-CoA by pyruvate dehydrogenase (PDH), marking the entry point into the TCA cycle (Figure 5). Acetyl-CoA condenses with oxaloacetate (OAA) to form citrate, which is converted to isocitrate and then oxidatively decarboxylated to α-ketoglutarate, producing NADH and CO_2. Next, α-ketoglutarate is further converted to succinyl-CoA (producing NADH and CO_2), then to succinate with GTP formation, which can be readily converted to ATP. Succinate is oxidized to fumarate (reducing FAD to $FADH_2$), then to malate, and finally back to OAA (producing NADH), completing the

cycle. Per pyruvate, the TCA cycle yields three NADH, one $FADH_2$, one GTP, and two CO_2, generating ten reducing equivalents that feed electrons into OXPHOS for ATP production.

1.5.3 Oxidative phosphorylation

The reducing equivalents generated in the TCA cycle drive ATP production via oxidative OXPHOS, the most ATP-productive stage of cellular respiration, occurring in the inner mitochondrial membrane. OXPHOS couples the electron transport chain (ETC) to ATP synthesis: NADH and $FADH_2$ donate electrons to the ETC, which ultimately reduces oxygen to water. Electron flow through complexes I–IV pumps protons into the intermembrane space, generating a proton motive force that drives ATP synthesis via ATP synthase (complex V)

Electrons enter the ETC via two pathways: the NADH-linked N-pathway (complex I) and the $FADH_2$-linked S-pathway (complex II), converging at ubiquinone (CoQ) before passing through complexes III and IV. Complex III transfers electrons to cytochrome *c* while contributing to the proton gradient, and complex IV reduces oxygen to water, further strengthening the proton motive force. At this step, SOX-dependent cytochrome *c* reduction was shown to also contributes to the overall electron flow with about 10% *in vitro*, however, the physiological relevance *in vivo* is yet unknown (Kaczmarek, 2019). ATP synthase (complex V) uses this gradient to convert ADP and phosphate into ATP, producing roughly 26–28 ATP per glucose, depending on tissue type and shuttle efficiency. Several studies have shown that the assembly of ETC complexes into supercomplexes (SCs) or respirasomes increases both the stability and efficiency of electron transfer, while minimizing ROS production (Cogliati et al., 2021).

Maintaining proper TCA cycle and OXPHOS function is crucial for mitochondrial physiology and adaptation to cellular energy needs. One regulator for mitochondrial biogenesis and metabolism is the regulation of translation by mRNA binding protein clustered mitochondria homolog (CLUH). While a common binding motif is yet unknown, CLUH was shown to regulate the translation and stability of a specific subset of mRNA encoding mitochondrial proteins (Gao et al., 2014; Schatton et al., 2017). Interestingly, one of these proteins is SOX, highlighting its importance for mitochondrial homeostasis. Loss of SOX was shown to impair mitochondrial bioenergetics in primary *SUOX*$^{-/-}$ fibroblasts due to decreased ATP levels and decreased membrane potential (Mellis et al., 2021). The underlying mechanism, however, remains elusive. Other studies showed that elevated sulfite can reduce ATP levels via the inhibition of glutamate and malate dehydrogenase (Grings et al., 2014; Vincent et al., 2004; Zhang et al., 2004).

While so far only the canonical function of SOX was considered to impact mitochondrial physiology, the physiological relevance of the non-canonical NO producing function is yet unknown and will be discussed elsewhere (1.6.5).

1.6 Nitric Oxide: Sources, Signaling, and Roles in Health and Disease

1.6.1 Nitric oxide as a signaling molecule

Nitric oxide (NO) has emerged as a versatile and significant signaling molecules in mammalian physiology. Since its identification as the elusive endothelium-derived relaxing factor (EDRF) in 1987, (NO) has transformed our understanding of cellular communication and regulation across multiple biological systems (Furchgott and Zawadzki, 1980; Ignarro et al., 1987). Unlike traditional signaling molecules, NO is lipophilic and diffuses freely across cell membranes. This facilitates its role as a paracrine and autocrine signaling agent, particularly in the cardiovascular, nervous, and immune systems.

In vascular biology, NO induces smooth muscle relaxation through activation of soluble guanylate cyclase (sGC) and the elevation of cyclic guanosine monophosphate (cGMP) levels, leading to vasodilation and blood pressure regulation (Arnold et al., 1977; Palmer et al., 1987). In the central nervous system, NO acts as a non-conventional neurotransmitter, contributing to synaptic plasticity and long-term potentiation (Garthwaite et al., 1988). In the immune system, NO plays a cytotoxic role in host defense, particularly against intracellular pathogens (Wink et al., 2011).

Beyond canonical pathways, NO also exerts its influence through post-translational modifications, most notably S-nitrosylation. This covalent attachment of an NO group to the thiol side chain of cysteine residues in target proteins represents a reversible and highly regulated mechanism of redox-based signal transduction (Stamler, 1994). S-nitrosylation affects protein function, localization, and interactions, and is increasingly recognized as a critical modulator of signaling networks in both physiological and pathological contexts (Stomberski et al., 2019). Unlike cGMP-mediated pathways, S-nitrosylation provides a direct route through which NO can regulate a diverse array of proteins, including enzymes, ion channels, and transcription factors (Hess et al., 2005).

Importantly, aberrant S-nitrosylation has been implicated in various disease states, including neurodegeneration, cancer, and cardiovascular disorders (Oh et al., 2024). For instance, excessive S-nitrosylation of mitochondrial proteins has been linked to neuronal injury in Parkinson’s disease models (Nakamura and Lipton, 2010; Oh et al., 2017). Conversely, controlled S-nitrosylation is essential for vascular homeostasis and immune modulation, highlighting the dualistic nature of NO signaling, beneficial under normal conditions, yet potentially harmful when dysregulated. Thus, it is crucial to understand underlying NO sources and sinks. Extending research on NO-producing proteins including newly identified proteins

such as SOX offer potential to further understand key aspects in NO-dependent health and disease.

1.6.2 Oxygen-dependent NO production

The primary source of NO in mammals is a family of oxygen-dependent enzymes known as nitric oxide synthases (NOS), which catalyze the conversion of the amino acid *L*-arginine into *L*-citrulline and NO. All NOS isoforms share a conserved catalytic mechanism and operate as homodimers, transferring electrons from NADPH through FAD and FMN in the C-terminal reductase domain to the heme group in the N-terminal oxygenase domain (Andrew and Mayer, 1999; Förstermann and Sessa, 2012). This electron flow is essential for oxygen activation at the heme and requires the cofactor tetrahydrobiopterin (BH_4) to enable efficient NO production (Förstermann and Sessa, 2012; Stuehr et al., 2005). Furthermore, all NOS enzymes possess a central calmodulin (CaM) binding domain connecting the C-terminal reductase and the N-terminal oxygenase domain (Crane et al., 1997). In response to an increase in intracellular Ca^{2+} concentrations, calmodulin becomes active and binds to the CaM binding domain of NOS enzymes. This binding event induces conformational changes and activates NOS enzymes enabling NO production (He et al., 2015).

Three major NOS isoforms have been identified in mammals: neuronal NOS (nNOS), endothelial NOS (eNOS) and inducible NOS (iNOS). While nNOS and eNOS are constitutively expressed and regulated in a calcium-dependent manner via calmodulin binding, iNOS is typically inducible, with calmodulin irreversibly bound, rendering its activity calcium-independent (Andrew and Mayer, 1999; Venema et al., 1996). Despite similarities in catalytic mechanisms, the NOS isoforms differ in tissue distribution and physiological roles.

Neuronal NOS is predominantly expressed in neuronal tissues, where it plays key roles in neurogenesis, synaptic plasticity, and learning and memory (Zhou and Zhu, 2009). Its effects are often mediated via transient S-nitrosylation of synaptic proteins, modulating their activity and contributing to signal transduction (Dejanovic and Schwarz, 2014; Ho et al., 2011). In contrast, iNOS is typically absent in resting cells but can be robustly induced in response to inflammatory stimuli such as cytokines and bacterial lipopolysaccharides, particularly in immune cells like macrophages (Förstermann and Kleinert, 1995). However, recent studies have expanded the understanding of iNOS by identifying a constitutively expressed form (ciNOS), which is active under normal physiological conditions in various tissues. CiNOS contributes to essential functions such as heart rate regulation, respiratory gas exchange, and gut microbiome homeostasis (Farahani et al., 2025). Lastly, eNOS is predominantly found in vascular endothelial cells, where it governs vascular tone and blood flow. Current studies revealed eNOS activity in red blood cells, also contributing to vasodilation (Leo et al., 2021).

Beyond vasodilation, eNOS activity contributes to the inhibition of leukocyte adhesion, suppression of vascular inflammation, and the maintenance of endothelial homeostasis (Förstermann and Sessa, 2012; Rafea et al., 2025).

1.6.3 Oxygen-independent NO production

Since hypoxic conditions, e.g. present due to ischemia, abolish NOS-dependent NO production, oxygen-independent generation of NO is vital to sustain NO homeostasis. One such alternative is the nitrate–nitrite–NO pathway, an oxygen-independent route that complements the classical NOS pathway (Carlström et al., 2015; Lundberg et al., 2008). This pathway enables the reduction of circulating nitrate (NO_3^-) and nitrite (NO_2^-) to bioactive NO through non-enzymatic and enzymatic mechanisms, particularly under hypoxic and acidic conditions. At first, nitrate (especially from green leafy or root vegetables) or nitrite (found in vegetables, fruits and cured meat) are taken up by the diet (Hord et al., 2009). Nitrate is absorbed by the salivary glands and enriched in the saliva where it gets reduced to nitrite by NR activity from oral bacteria (Lundberg, 2012). The nitrite-rich saliva is then swallowed and, under the acidic conditions of the stomach, nitrite gets protonated to form nitrous acid (HNO_2), an unstable molecule, which decomposes to generate NO (Lundberg et al., 1994). Residual nitrite is subsequently absorbed via the gut and distributed via systemic circulation (Kleinbongard et al., 2006). During hypoxia, when both pH and oxygen tension are low, nitrite becomes an important substrate for NO generation, supporting vascular and metabolic adaptations. Dietary uptake of nitrite and nitrate was shown to reduce blood pressure and augment the tolerance to ischemia/reperfusion (I/R) injury, a process called pre-conditioning (Bryan, 2022; Shiva et al., 2007). The lowering of blood pressure occurs via the well described activation of soluble guanylate cyclase by NO and subsequent vasodilation. In contrast, the protective effects during I/R injury are attributed to NO's regulatory influence on mitochondrial function (Perrelli et al., 2011). Specifically, S-nitrosylation of mitochondrial complex I during early reperfusion inhibits its activity, thereby reducing ROS generation and mitigating oxidative damage (Shiva et al., 2007).

Another oxygen-independent source of NO is the nitrite reduction by proteins of the globin superfamily (Gladwin and Kim-Shapiro, 2008). These heme-containing proteins – including hemoglobin, myoglobin, neuroglobin, cytoglobin, and most recently androglobin - are capable of reducing nitrite to NO when in their deoxygenated ferrous (Fe^{II}) state (Reeder et al., 2024; Tejero and Gladwin, 2014). The reaction proceeds via formation of a ferric-nitrosyl (Fe^{3+}–NO) intermediate and is favored under acidic and hypoxic conditions (Huang et al., 2005). Notably, these proteins were also reported to act as NO sinks due to the oxygenated hemoglobins reacting with NO to generate nitrate and methemoglobin. This dynamic shift from NO sink to NO source highlights the context-dependent role of globins in NO homeostasis.

Beyond the globin family, nitrite reducing activity (NiR) has also been described in other mammalian heme proteins such as cytochrome *c* (Basu et al., 2008) and indoleamine 2,3-dioxygenase (IDO) (Lim et al., 2019). Both have been shown to catalyze the reduction of nitrite to NO under specific biochemical conditions, further expanding the landscape of enzymatic nitrite reduction.

1.6.4 Nitrite reduction by Moco-dependent enzymes

In addition to heme-dependent nitrite reductions, several studies have expanded the repertoire of oxygen-independent enzymatic nitrite reduction to Moco-dependent enzymes. The diverse nature of Moco with the Mo being able to adapt oxidation states from +IV to +VI, with an stable +V intermediate, allows to also catalyze a one electron transfer reaction such as nitrite reduction. Among these, all four mammalian molybdoenzymes were shown to be capable of reducing nitrite to NO. XOR was the first Moco-dependent enzyme to catalyze this reaction (Zhang et al., 1998).

XOR reduces nitrite to NO, using NADH or xanthine as electron donors. Each oxidized substrate yields two NO molecules. This reaction occurs at the Moco active site, and is significantly enhanced in the oxidase form of the enzyme (XOR), in which oxygen is no longer the preferred electron acceptor (Millar et al., 1998; Zhang et al., 1998). Intriguingly, xanthine-driven NO production leads to inhibition of XOR itself, via a mechanism involving replacement of the essential molybdenum-sulfido ligand with a third terminal oxo group (Enroth et al., 2000). Furthermore, competition studies have shown that xanthine and nitrite both act at the Moco active site, with xanthine acting as a competitive inhibitor of nitrite reduction. This enzymatic activity peaks under hypoxic and acidic conditions, which mimic ischemic tissue microenvironments (Baliga et al., 2012). Under these circumstances, XOR-derived NO has been shown to mediate vasodilation, inhibit platelet aggregation, and protect against ischemia–reperfusion injury. These protective effects are attenuated in the presence of XOR inhibitors such as allopurinol and oxypurinol, or in *XDH*$^{-/-}$ mice (Abe et al., 2009; Dyson et al., 2024; Tripatara et al., 2007; Webb et al., 2004). A recent study by Dyson et al. (2024) demonstrated that hepatocyte-specific and heterozygous *XDH*$^{-/-}$ mice exhibit significantly reduced hepatic and plasma NiR activity, alongside increased systolic blood pressure, cardiac remodeling, leukocyte activation, and endothelial dysfunction - emphasizing the physiological importance of XOR in vascular NO homeostasis.

The AOX, which is structurally and catalytically similar to XOR, was also reported to act as a NiR (Li et al., 2003). AOX can reduce nitrite at the Moco-active site, with electrons donated either directly from aldehyde substrates oxidized at the Moco site or indirectly from NADH via FAD and the iron–sulfur clusters. The reaction is favored under low oxygen tension and mildly

acidic conditions, again resembling ischemic settings (Maia et al., 2015). However, studies assessing the vasodilatory impact of AOX-derived NO, for instance, in rat mesenteric arteries. have yielded inconsistent results (Buerk et al., 2017), leaving its physiological relevance a matter of debate. Nevertheless, given its cytosolic localization and pH sensitivity, AOX likely contributes to NO production in hypoxic or ischemic microenvironments, particularly in the liver, lung, kidney, and heart, which show highest AOX expression.

The mitochondrial Moco enzymes mARC1 and mARC2 were also identified as nitrite reductases. Since their physiological electron donor remains unknown, studies employed a reconstituted artificial electron transfer chain consisting of NADH, cytochrome b_5 reductase, and cytochrome b_5 to support nitrite reduction (Sparacino-Watkins et al., 2014). The reaction was shown to occur at the Moco site and displayed a k_{cat} (~0.1 s^{-1}) comparable to that of AOX (~0.15 s^{-1}) and XOR (~0.3 s^{-1}). Like AOX and XOR, nitrite reduction by mARC is enhanced under acidic conditions and inhibited by oxygen, indicating a shared catalytic mechanism (Cecco et al., 2017; Sparacino-Watkins et al., 2014). Although experiments using HEK cell lysates confirmed that mARC can produce NO under physiological conditions, the biological relevance of this reaction remains unclear. Recent investigations on mARC have focused primarily on its roles in lipid metabolism, redox signaling, and mitochondrial function, rather than its NO-producing capacity (Coyne et al., 2025; Guo et al., 2024; Unrug-Bielawska et al., 2025).

1.6.5 Nitrite reduction by sulfite oxidase

Most recently, SOX has been identified as a novel Moco-dependent NiR. In this dual-function enzyme, nitrite reduction is mechanistically coupled to sulfite oxidation, which serves as the initial electron source (Figure 6). Specifically, sulfite oxidation at the molybdenum center reduces Mo^{VI} to Mo^{IV}, enabling the subsequent inner-sphere electron transfer from Mo^{IV} to nitrite, producing NO (Wang et al., 2015). This step yields an inert Mo^{V} species, which requires an IET to regenerate the catalytically active state. The necessary electron is transferred from Mo^{V} to the heme domain (Fe^{III}), forming Fe^{II}, completing molybdenum reoxidation. Upon a second cycle of sulfite oxidation and nitrite reduction, the enzyme becomes trapped in a Mo^{V}/Fe^{II} state, resulting in a 1:2 stoichiometry of sulfite to nitrite reduction (Bender et al., 2019b). Steady-state NO production is established once a final electron acceptor such as the physiologically relevant cytochrome *c*, accepts the heme-trapped electron.

Importantly, because both sulfite oxidation and nitrite reduction occur at the Moco center, the two reactions are reciprocally regulated, competitively inhibiting each other (Kaczmarek et al., 2019). This competition is also pH-dependent, with nitrite reduction being favored at lower pH values (6.5) due to the requirement for protonation of a Mo-coordinated nitrite intermediate

(Bender et al., 2019b). This pH preference aligns with the environment of the mitochondrial IMS, where SOX resides and where the pH is ~6.8 enhancing SOX activity during oxygen limitation (Kaczmarek et al., 2019; Porcelli et al., 2005).

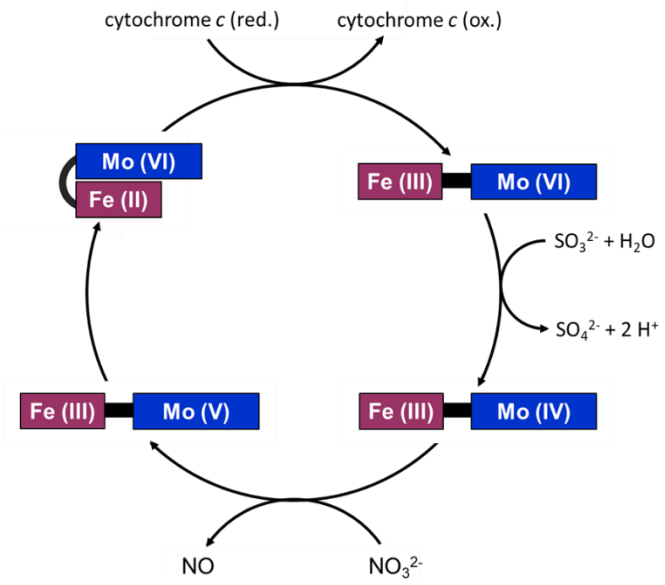

Figure 6: Depiction of the redox changes of the prosthetic groups during steady-state NO production by SOX
First, sulfite is oxidized to sulfate at the Mo(VI) center, reducing it to Mo(IV). Subsequently, Mo(IV) reacts with nitrite to yield NO resulting in a Mo(V) species which is inert for further reaction. An IET from Mo(V) to Fe(III) restore the molybdenum center and subsequent re-oxidation of Fe (II) by cytochrome c restores the resting state (Mo(VI)/Fe(III)) enabling steady-state NO production.

Mechanistic studies showed that nitrite competes with the Fe^{III} heme for the electrons from sulfite oxidation. SOX-dependent nitrite reduction is highly increased upon shortening of the flexible tether, preventing the domain movement required for efficient IET from Mo to heme, or in heme-depleted SOX (Bender et al., 2020, 2019b). The physiological relevance of SOX-dependent nitrite reduction has been demonstrated in human fibroblasts and HEK cells, where SOX-mediated NO production increases under hypoxic conditions (Kaczmarek, 2019; Wang et al., 2015). Recently, the physiological relevance of SOX-dependent nitrite reduction was underlined by a study identifying SOX as the main mediator regulating cerebral blood flow during brain hypoxia (Christie et al., 2023).The authors showed that nitrite is enriched in astrocyte mitochondria and reduced by SOX under hypoxic conditions or during chemical ETC inhibition, suggesting a potential reverse electron flow from the ETC to SOX. While the standard flow of electrons from SOX to complex IV via cytochrome *c* is well-established, the existence of a backward electron transfer mechanism from the ETC to SOX remains to be elucidated. Interestingly, a well-known function of NO is the inhibition of TCA cycle enzymes and the ETC, raising the question whether local NO production by SOX itself could inhibit the ETC and alter mitochondrial bioenergetics.

1.6.6 The role of NO in mitochondrial physiology

In line with previous reports, NO has a moonlighting function in mitochondrial physiology, functioning both as a regulator and a mediator of toxicity (Stomberski et al., 2019). Within mitochondria, NO acts primarily through its interaction with components of the ETC, most notably cytochrome *c* oxidase (complex IV), where it competes with oxygen for binding (Cleeter et al., 1994; Wainio, 1955). This reversible inhibition of cytochrome *c* oxidase by NO modulates mitochondrial respiration, enabling cells to adapt to fluctuating oxygen levels, thereby influencing cellular energy production and metabolic flexibility (Brown, 2007; Erusalimsky and Moncada, 2007).

Beyond this acute and reversible effect, NO and its derivatives, such as reactive nitrogen species (RNS), can induce irreversible modifications at multiple sites within the mitochondrial respiratory chain, leading to altered electron flow and, under certain conditions, mitochondrial dysfunction (Brown, 1999). For instance, complex I can be irreversibly inhibited by NO through S-nitrosylation of critical thiol residues (Clementi et al., 1998; Galkin and Moncada, 2007), tyrosine nitration or removal of iron from its Fe-S-cluster (Brown and Borutaite, 2004; RIOBÓ et al., 2001). Similar mechanisms have been proposed for complexes II and III, with NO targeting their Fe-S clusters (Welter et al., 1996; Wu et al., 2020). Additionally, NO can interfere with electron transfer at the Qo site of complex III by directly reacting with CoQ, resulting in the formation of ubisemiquinone and nitroxyl anion (NO^-), which disrupts the redox state and impairs electron flow (Iglesias et al., 2015; Poderoso et al., 1999, 1996). Although less well characterized, complex V has also been reported to be inhibited by NO, likely through modification of cysteine residues (Brown, 1999; Venkatesh et al., 2009).

The impact of these modifications is highly dependent on NO concentration and exposure duration. At low, physiological levels, NO-mediated S-nitrosylation can be protective, reducing ROS production and mediating tolerance to ischemia/reperfusion injury (Dikalov et al., 2017; Shiva et al., 2007). In contrast, high or prolonged NO exposure leads to increased ROS generation, mitochondrial membrane depolarization, opening of the mitochondrial permeability transition pore (mPTP), and ultimately, induction of apoptosis or necrosis (Brown, 2007; Pappas et al., 2023).

In addition to its effects on OXPHOS, NO disrupts TCA cycle flux by inhibiting key enzymes of the cycle. NO directly inhibits mitochondrial aconitase (Aco2) via interaction with its Fe-S cluster and pyruvate dehydrogenase (PDH) through S-nitrosylation (Castro et al., 1998; Palmieri et al., 2020; Stadler et al., 1991; Yan et al., 2012). In combination with its action on the ETC this leads to metabolic rewiring that shifts cellular energy metabolism towards

glycolysis, a process which is crucial for macrophage activation and inflammatory responses (Palmieri et al., 2020; Pappas et al., 2023).

1.7 Aims of this thesis

In summary, SOX is a mitochondrial enzyme that plays a central role in sulfur metabolism by catalyzing the oxidation of sulfite to sulfate. Beyond this canonical function, recent studies have expanded the physiological significance of SOX, revealing its involvement in mitochondrial respiration and its capacity to reduce nitrite to NO. While SOX is functionally linked to OXPHOS via cytochrome *c*, the precise mechanisms by which it contributes to mitochondrial bioenergetics remain largely unresolved. In particular, the interplay between SOX-dependent NO production and mitochondrial respiration is poorly understood. Furthermore, the physiological relevance of SOX-dependent NO production is yet to be elucidated.

While the pathogenesis of SOXD has been primarily attributed to sulfite accumulation and the neurotoxic effects of SSC, the potential role of SOX-related mitochondrial dysfunction in disease progression remains unexplored.

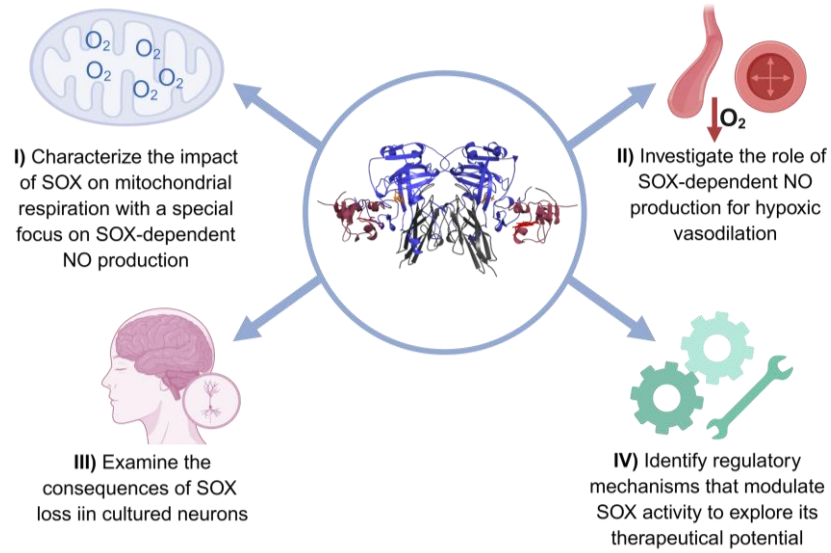

Figure 7: Schematic illustration of the aims of this thesis
This thesis aims to unravel the role of SOX in several cellular and physiological processes as well as to identify routes to regulate SOX activity for therapeutic approaches. First, the impact of SOX on mitochondrial respiration with a special focus on its non-canonical nitrite reducing function will be explored. Second, the implication of SOX-dependent nitrite reduction for vasodilation under hypoxic conditions will be investigated. Third, the role of SOX for the neuronal system will be examined. Lastly, this thesis will explore possible regulatory mechanisms to tune SOX activity, aiming to provide new targets for therapeutical approaches.
Created with BioRender.com.

Taken together, although SOX appears to play a broader role in mitochondrial function and pathology, our understanding of its bioenergetic impact and therapeutic potential remains incomplete. Given the clinical severity of SOXD and the current lack of targeted therapies,

there is a clear need to further investigate the regulation of SOX activity and its implications in mitochondrial health and disease. Thus, this thesis aims to:

I. Characterize the impact of SOX on mitochondrial respiration with a special focus on SOX-dependent NO production
II. Investigate the role of SOX-dependent NO production for hypoxic vasodilation
III. Examine the consequences of SOX loss in cultured neurons
IV. Identify regulatory mechanisms that modulate SOX activity to explore its therapeutical potential

2 Results

2.1 Mitochondrial dysfunction in SOX deficiency

Previously it was reported that SOX-deficiency in MEFs leads to alterations in mitochondrial homeostasis (Mellis et al., 2021). SOX-deficient MEFs displayed elongated mitochondria, a phenotype likely induced by elevated sulfite concentrations and potentially driven by reduced mitochondrial motility. Additionally, these cells demonstrated decreased viability and ATP production under galactose treatment, indicating impaired mitochondrial respiration. This observation is in line with previous studies identifying sulfite as a mediator to decrease ATP-levels (Vincent et al., 2004; Zhang et al., 2004). Recently, sulfite was also shown to disrupt bioenergetics in rat brains and MOCS1 deficient fibroblasts with decreasing activities of TCA cycle enzymes and respiratory chain complexes (Brondani et al., 2025). Here the mitochondrial dysfunction associated with SOX loss was further investigated including the determination of mitochondrial respiration and exploration of proteomic changes using cell culture systems of SOXD.

2.1.1 Impact of SOX-deficiency on mitochondrial respiration

To further investigate the mitochondrial dysfunction associated with SOX loss, we measured the oxygen consumption rate (OCR) of SOX-deficient cells as an indicator of mitochondrial OXPHOS activity. Using a Seahorse XFe96 analyzer mitochondrial function was assessed in both SOX-deficient and wild-type (WT) MEFs (Figure 8).

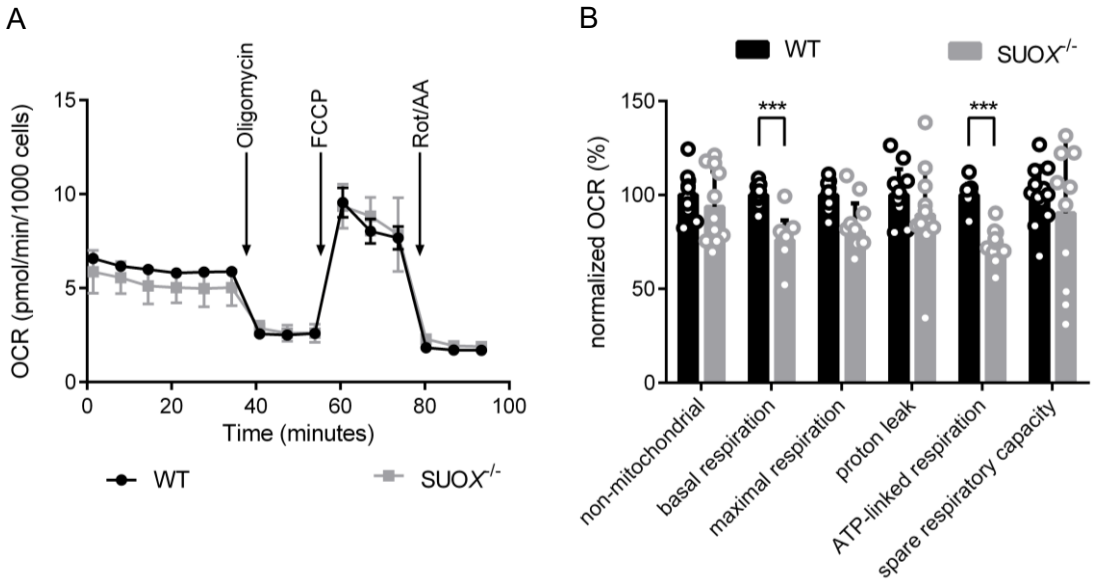

Figure 8: Mitochondrial respiration of MEFs
Oxygen consumption and analysis of mitochondrial respiratory parameters in WT and SUOX-/- MEFs. (A) Representative oxygen consumption traces normalized to cell number from SUOX$^{-/-}$ cells compared to WT cells. The sequential injection of 2 µM oligomycin, 1 µM FCCP and 0.5 µM rotenone/antimycin A was performed (indicated by the arrows). Each dot represents an n=4 technical replicates (B) Evaluation of the OCR normalized to WT. Two-way ANOVA with Sidak's post-hoc test was performed as indicated. p-value **< 0.01

OCR decreased upon addition of the ATP synthase inhibitor oligomycin, increased to maximal respiration after addition of uncoupling agent carbonyl cyanide-p-trifluoromethoxyphenylhydrazone (FCCP), and finally dropped to non-mitochondrial oxygen consumption levels after inhibition of complexes I and III with rotenone and antimycin A (Rot/AA), respectively (Figure 8 A). Further analysis revealed a significant reduction of 25% in basal respiration in SOX-deficient cells. Since the non-mitochondrial oxygen consumption was unchanged, this reduction suggesting an impairment in ETC and provides a potential explanation for the previously reported decrease in ATP-levels associated with sulfite accumulation (Figure 8 B) (Mellis et al., 2021; Vincent et al., 2004; Zhang et al., 2004). The observed decrease in ATP-linked respiration of ~25% aligns with the reduction in basal respiration, as these parameters are directly related. Apart from these changes, no additional alterations in mitochondrial respiration were detected upon SOX loss.

To further investigate the previously observed decrease in basal respiration in SOX-deficient MEFs, the oxygen consumption of isolated mitochondria from these cells was measured using an Oxygraph 2K (Oroboros) and compared to WT controls (Figure 9). First, the success of mitochondrial fractionation was confirmed by immunoblotting for voltage-dependent anion channel (VDAC) and gephyrin as markers for the mitochondrial and cytosolic fractions, respectively, demonstrating efficient enrichment of pure mitochondria (Figure 9 A). Since cytosolic impurities result in high background oxygen consumption, purity of mitochondria is crucial for further analyses.

To assess mitochondrial respiration, oxygen consumption was initially measured in the absence of TCA cycle substrates and no differences between the two cell types were observed (Figure 9 B, C). The subsequent addition of pyruvate and malate, providing substrates for NADH production and electron transfer through complex I, did not reveal any differences in respiration between SOX-deficient and WT mitochondria. Supplementation with ADP to stimulate complex V activity led to a significant increase in respiration, with SOX-deficient mitochondria exhibiting a two-fold lower O_2 flux of 39.4 ± 14.1 pmol*s^{-1}*ml^{-1} compared to 72.3 ± 22.0 pmol*s^{-1}*ml^{-1} in WT cells. Next, the mitochondrial membrane integrity was assessed by addition of cytochrome *c*. Both cell lines showed no response demonstrating intact outer mitochondrial membranes. Supplementation with glutamate, slightly increased mitochondrial respiration, with no significant differences between both cell lines. Introduction of succinate as a complex II substrate disclosed a significantly reduced respiration in SOX-deficient mitochondria compared to WT ones. Maximal respiratory capacity, induced by the uncoupler FCCP, was also significantly reduced by approx. two-fold in SOX-deficient mitochondria (86.3 ± 28.7 pmol*s^{-1}*ml^{-1}) as compared to WT (153.4 ± 33.4 pmol*s^{-1}*ml^{-1}). To ascertain the contribution of complex I and II towards total respiration, both complexes were

sequentially inhibited by using rotenone and antimycin A, respectively. Addition of rotenone resulted in minor changes in oxygen consumption rate, indicating that complex II was the predominant electron source, with WT mitochondria displaying a higher O_2 flux rate compared to those deficient in SOX. Upon addition of antimycin A, no respiration was detected in either SOX-deficient or WT mitochondria. Complex IV activity was assessed by addition of a mixture of the artificial substrate N,N,N',N'-Tetramethyl-p-phenylenediamine dihydrochloride (TMPD) and ascorbate, which serves to maintain TMPD in a reduced state. MEF mitochondria lacking SOX displayed slightly decreased complex IV activity. Finally, the complex IV inhibitor azide was added to abolish mitochondrial oxygen consumption and determine background signal from TMPD autooxidation, revealing no differences between both mitochondria.

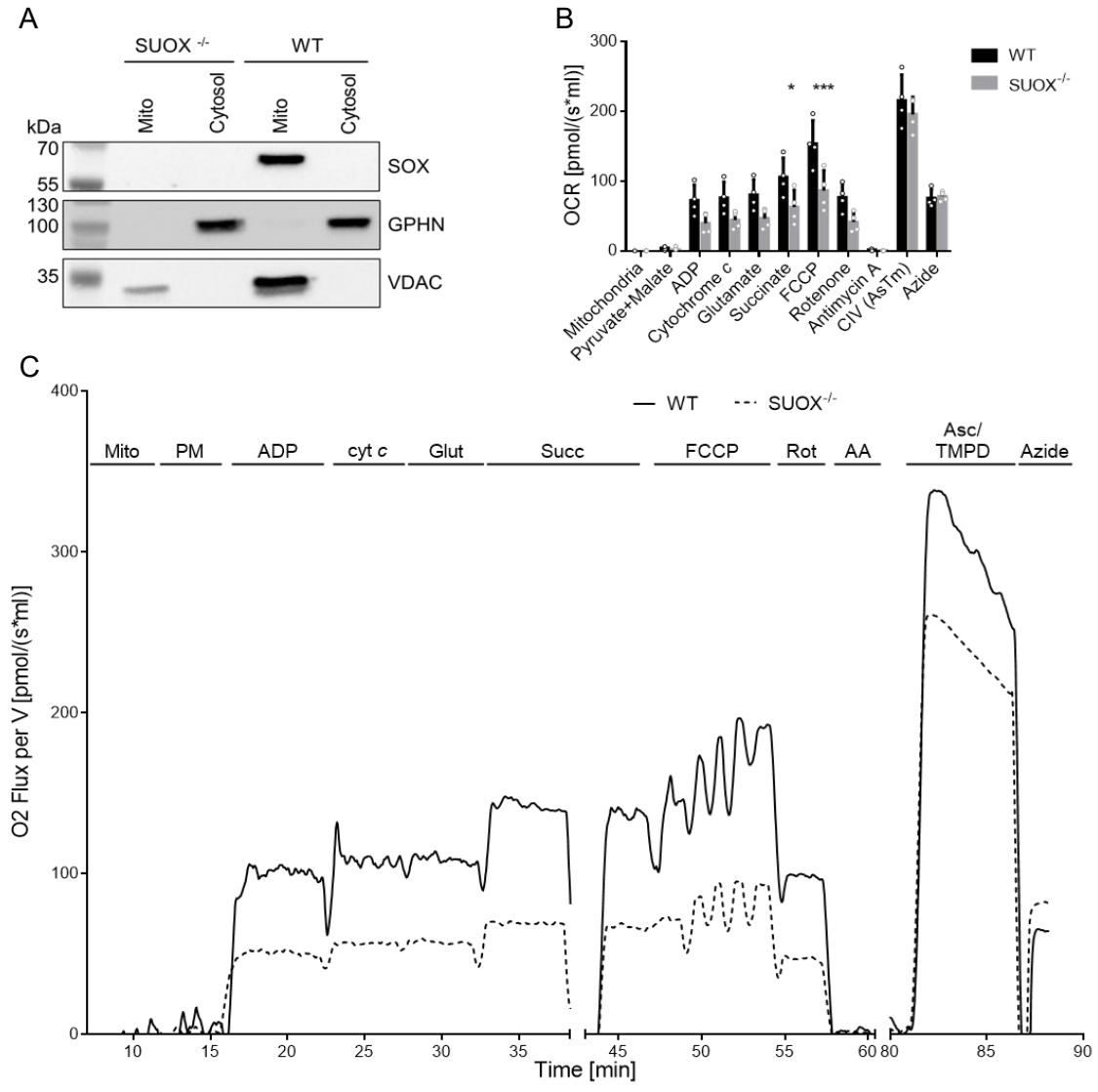

Figure 9: Respiration of enriched mitochondria from SUOX$^{-/-}$ and WT MEFs
(A) Representative WB-based analysis of mitochondrial enrichment from MEFs. 30 µg protein were used, gephyrin (GPHN) and VDAC served as cytosolic and mitochondrial markers, respectively. (B) Analysis of oxygen consumption traces after addition of various substrates (depicted) of enriched mitochondria from SUOX$^{-/-}$ (n=3) and WT MEFs. (n=4). 100 µg pure mitochondria were used. (C) Representative Oxygraph measurements of intact enriched mitochondria of SUOX$^{-/-}$ and WT MEFs. Two-way ANOVA with Sidak's post-hoc test was performed as indicated. p-value**< 0.01, * < 0.05. Mito = Mitochondria, PM = Pyruvate + Malate, cyt *c* = cytochrome *c*, Glut = glutamate, Succ = succinate, Rot = rotenone, AA = antimycine A, Asc = ascorbate

Taken together, the observed decreases in respiration of SOX-deficient mitochondria support previous findings of reduced mitochondrial respiration in MEFs. The reduction was particularly evident for complex II-driven respiration, with only minor changes in complex I activity and unchanged complex IV-dependent oxygen consumption. Unlike the previous study, however, SOX-deficient mitochondria displayed reduced maximal respiration under FCCP, which may reflect substrate limitations in the entire cell-based assay. Such limitations are circumvented in experiments with isolated mitochondria, with excess substrate supply. Nevertheless, both studies rely on in vitro systems, highlighting the need for more physiologically relevant models.

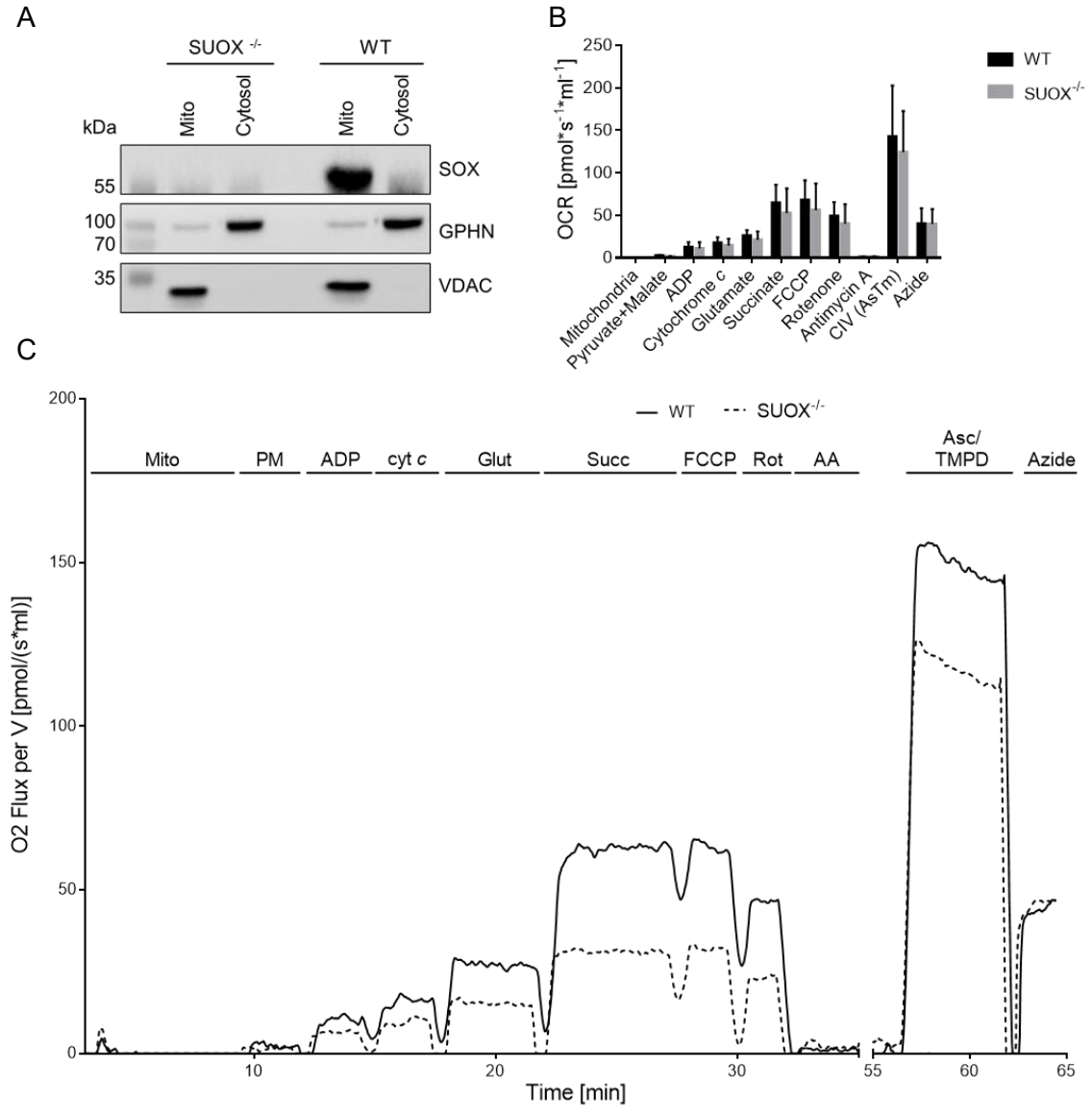

Figure 10: Respiration of enriched hepatocyte mitochondria from SUOX$^{-/-}$ and WT mice
(A) Representative WB-based analysis of mitochondrial enrichment. 30 µg protein were used, gephyrin (GPHN) and VDAC served as cytosolic and mitochondrial markers, respectively. (B) Analysis of oxygen consumption traces after addition of various substrates (depicted) of enriched hepatocyte mitochondria from SUOX$^{-/-}$ (n=4) and WT mice. (n=4). 100 µg pure mitochondria were used. OCR was normalized to WT, Negative values are not shown (n.d.) (C) Representative Oxygraph measurements of enriched hepatocyte mitochondria of SUOX$^{-/-}$ and WT mice. Two-way ANOVA with Sidak's post-hoc test was performed as indicated. p-value **< 0.01, * < 0.05. Mito = mitochondria, PM = pyruvate + malate, cyt *c* = cytochrome *c*, Glut = glutamate, Succ = succinate, Rot = rotenone, AA = antimycine A, Asc = ascorbate

To validate the observed reduction in mitochondrial respiration in SOX-deficient MEFs using a more physiologically relevant system, oxygen consumption in isolated liver mitochondria from mice was assessed using the Oroboros Oxygraph 2k system (Figure 10). Successful mitochondrial isolation was again confirmed by Western blot analysis, demonstrating the enrichment of mitochondrial markers and minimal contamination (Figure 10 A).

Again, the addition of isolated mitochondria alone did not result in measurable oxygen consumption in the absence of substrates (Figure 10 B, C). Overall, both WT and SOX-deficient mitochondria responded appropriately to substrate and inhibitor additions as described previously. However, SOX-deficient mitochondria consistently exhibited a non-significant 20% reduction in oxygen consumption under all tested conditions (Figure 10 B). One contradictory experiment showed a modest increase in respiration in SOX-deficient samples compared to WT (Figure S1), but this result was not representative of the overall trend. In conclusion, these results from liver mitochondria reproduced the reduced mitochondrial respiration phenotype observed in SOX-deficient MEFs. Here complex I, II and IV-driven respiration is slightly reduced. This suggests that the respiration defect was no cell culture artefact but reflected a broader physiological impairment.

2.1.2 Proteomic alterations in SOX-deficient fibroblast mitochondria

To identify the drivers of reduced mitochondrial respiration, OXPHOS protein levels and super complex assembly were assessed using blue native polyacrylamide gel electrophoreses (BN-PAGE) (Figure S2). The BN-PAGE showed no differences between *SUOX*$^{-/-}$ and WT samples, with one WT sample exhibiting reduced overall staining, suggesting technical variability during sample preparation. Thus, analysis of the mitochondrial proteome of immortalized MEFs by mass spectrometry (CECAD proteomics facility) was performed.

Principal component analysis (PCA) demonstrated strong intra-group homogeneity, ensuring reliable comparison (Figure S3 A). In total 3,804 proteins were detected, with 2,760 proteins having a *q*-value < 0.05. Out of these, 1,729 proteins showed at least a 1.5-fold change compared to WT samples (Figure 11 A, Table S4). Amongst those, 689 proteins were down- and 1,040 were upregulated. Given that mitochondria were enriched by sequential centrifugation, which can lead to impurities by co-sedimentations, various proteins associated with other membranes e.g. the cell membrane (Gjb2, Lin7c, Gpc6) were found. Among the proteins with highest fold change, mitochondrial proteins like mitochondrial import receptor subunit TOM5 homolog (Tomm5), Thioredoxin (Tnx2) or presenilin-associated rhomboid-like protein (Parl) were identified (Table S4). Subsequent Gene Set Enrichment Analysis (GSEA) of the 2,759 significantly altered proteins revealed a reduction of 90 proteins linked to OXPHOS

(Figure 11 B, Table S1) including: complex I (29 proteins), complex II (3), complex III (8), complex IV (9) and complex V (14). Additionally, 17 proteins were found to be assembly factors for respiratory chain complexes and ten were found to be associated with OXPHOS including Inorganic pyrophosphatase 2 (Ppa2), which was shown to be essential for maintaining the mitochondrial membrane potential (Guimier et al., 2016, 2016). Furthermore, several proteins involved in the TCA cycle were found to be downregulated in SOX-deficient mitochondria (Figure 11 C, Table S2), namely PDH, MDH, CS, Aco, IDH, αKDH, SDH and FH. Additionally, proteins associated with the TCA cycle such as glutamate dehydrogenase or proteins regulating the function of TCA cycle enzymes e.g. pyruvate dehydrogenase kinase 1 (Pdk1), which regulates PDH activity by phosphorylation, were found to be downregulated (Hitosugi et al., 2011; Li et al., 2016; McFate et al., 2008).

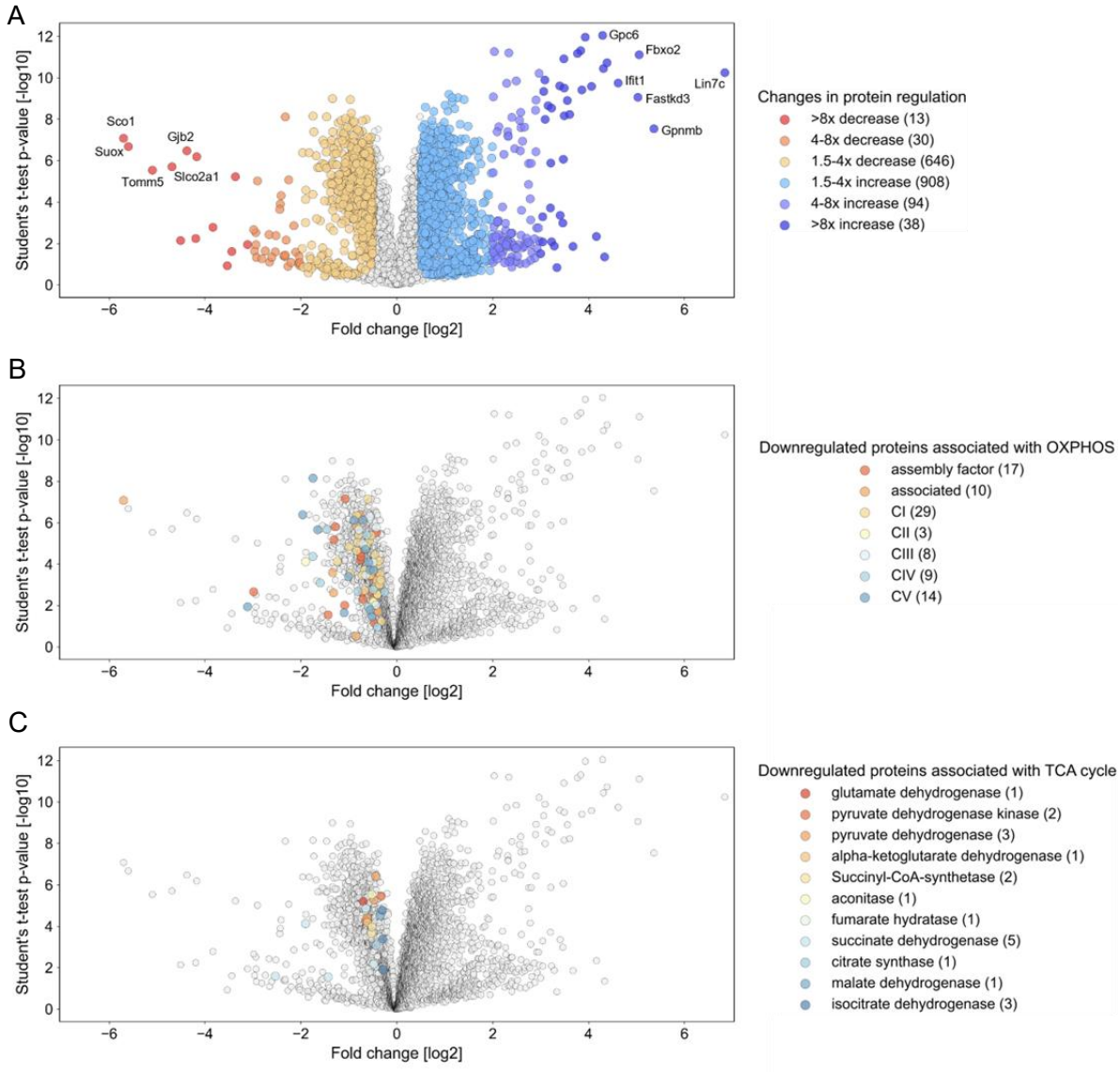

Figure 11: Proteomic profiling of mitochondria from MEFs
(A) Volcano plot depicting significantly up- or downregulated regulated proteins of SUOX$^{-/-}$ mitochondria compared to WT samples (n = 4). Significantly upregulated proteins are displayed in blue, significantly downregulated proteins are displayed in red (q-value < 0.05, absolute log2 fold change ≥0.5). (B) Volcano plot depicting significantly downregulated proteins linked to OXPHOS in SUOX$^{-/-}$ mitochondria compared to WT samples (q-value < 0.05). (C) Volcano plot depicting significantly downregulated proteins linked to the TCA cycle in SUOX$^{-/-}$ mitochondria compared to WT samples (q-value < 0.05).

Taken together, these findings suggest a dysfunction in mitochondrial metabolism underlying the observed reduction of mitochondrial respiration in earlier experiments (2.1.1).

Interestingly, among the upregulated proteins members of the FAS-activated serine/threonine kinase family (Fastkd3-5) were identified, which are important for the regulation of mitochondrial translation and assembly of respiratory chain complexes, thus fine-tuning the balance of mitochondrial energy production, especially under stress conditions (Jourdain et al., 2017; Ohkubo et al., 2021; Simarro et al., 2010). The upregulation of these proteins suggests a possible rescue mechanism to restore the observed reduction in mitochondrial respiration.

2.1.3 Proteomic alterations in SOX-deficient MEFs

Given the extensive alterations observed in mitochondrial metabolism and respiratory chain protein expression in SOX-deficient cells, it was next addressed whether these metabolic disturbances extend to other critical cellular functions. To comprehensively analyze the whole-cell proteome, whole cell lysates, were prepared for mass spectrometry. Principal component analysis (PCA) demonstrated strong intra-group homogeneity, ensuring reliable comparison for subsequent analysis (Figure S3 B). In total 4,649 proteins were detected, of which 282 exhibited statistically significant differences (q-value < 0.05) and an absolute fold change of ≥ 1.5 (Figure 12 A, Table S5). Amongst those, 147 proteins were downregulated and 136 were upregulated. Given that fibroblasts are major producers of extracellular matrix components, numerous ECM proteins were identified (e.g. syndecan-2 (Sdc2), extracellular matrix protein 1 (Ecm1)) as well as proteins involved in ECM regulation (e.g. lysyl oxidase (Lox)) (Frantz et al., 2010). Further analysis revealed a total of 36 ECM-associated proteins, with only four glycoproteins being upregulated (Ecm1, agrin (Agrn), melanoma cell adhesion molecule (Mcam), Cd151) while the majority were downregulated (32 proteins) (Figure 12 A). Of these, 13 were regulators of ECM proteins (e.g. Lox), 17 were proteoglycans and glycoproteins (e.g. fibrillin-2 (Fbn2)) and six were collagens (e.g. collagen type I alpha 2 chain (Col1a2)) (Figure 12 B, Table S3).

Notably, bifunctional 3'-phosphoadenosine 5'-phosphosulfate synthase 2 (Papss2) was also shown to be downregulated, a protein which is responsible for the synthesis of 3'-phosphoadenosine 5'-phosphosulfate (PAPS) from inorganic sulfate, the sulfate donor for sulfation reactions (Dejima et al., 2006). This reduction likely resulted from decreased sulfate availability due to impaired sulfite oxidation in SOX-deficient cells. Importantly, as mentioned earlier (1.3.3), sulfation is a critical post-translational modification required for various biological processes including heparansulfate biosynthesis, and is essential for maintaining proper ECM structure (Chapman et al., 2004; Ravikumar et al., 2020; Soares Da Costa et al., 2017). Consistent with this, Syndecan-2 (Sdc2), Versican (Vcan) and Biglycan (Bgn), sulfate

proteoglycans, as well as Fibronectin (Fn1), Fibrillin-1 and -2 (Fbn1, Fbn2) and Tenascin-C (Tnc), ECM proteins indirectly dependent on sulfated proteins, were also downregulated (Dauth et al., 2016; Galante and Schwarzbauer, 2007; Li et al., 2024).

Collectively, these findings indicate that SOX-deficient cells exhibit a broad reduction in core ECM proteins and key ECM regulators. Importantly, the accumulation of sulfite in SOX-deficient cells has been shown to disrupt disulfide bonds - structural elements that are crucial for ECM stability and integrity (Bächinger et al., 1980; Ilani et al., 2013).

The observed changes in the mitochondrial proteome, particularly in OXPHOS and TCA cycle enzymes, did not emerge in whole-cell proteome profiling (Figure 11, Figure 12). In total, we detected 522 mitochondrial proteins, with only 25 being significantly changed (e.g. acyl-CoA thioesterase 2 (Acot2), lactate dehydrogenase B (Ldhb)) (Table S6). This discrepancy likely attributes to immortalized fibroblasts being inherently glycolytic, displaying limited reliance on mitochondrial respiration and thus less metabolic rewiring in response to decreased mitochondrial respiration (Kondoh et al., 2005; Prieto et al., 2019).

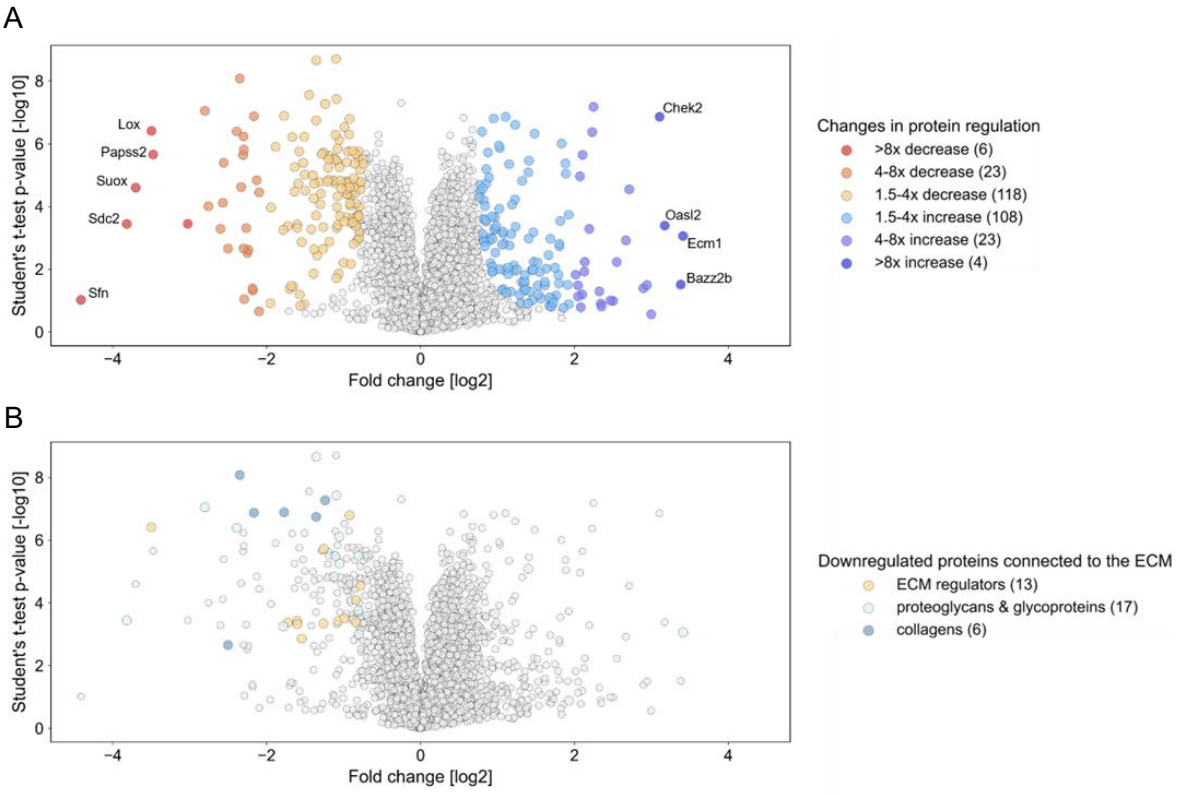

Figure 12: Proteomic profiling of whole cell lysates from MEFs
(A) Volcano plot depicting significantly up-or downregulated regulated proteins of SUOX$^{-/-}$ cells compared to WT samples (n = 4). Significantly up-regulated proteins are displayed in blue, significantly down-regulated proteins are displayed in red (q-value < 0.05, absolute log2 fold change ≥ 0.5). (B) Volcano plot depicting downregulated proteins in SUOX$^{-/-}$ cells compared to WT cells associated with the extracellular matrix (q-value < 0.05).

While the previous studies focused on the complete loss of SOX for mitochondrial bioenergetics, the influence of the non-canonical function of NO production remained elusive.

Thus, the next set of experiments focuses on the impact of SOX-dependent NO production on mitochondrial respiration.

2.2 Impact of SOX-dependent nitrite reduction on mitochondrial respiration

Initial studies on SOX-dependent nitrite reduction focused on unravelling the underlying molecular mechanisms. Although, they revealed first hints about its physiological relevance due to steady-state NO production in the presence of cytochrome *c*, the broad physiological relevance of SOX-mediated NO production was unclear (Bender et al., 2019b; Bender and Schwarz, 2018). Thus, subsequent studies highlighted the physiological relevance of SOX-dependent nitrite reduction by deciphering SOX-dependent NO production in mammalian cells (Kaczmarek, 2019). Importantly, NO was shown to inhibit respiratory chain complexes I-IV (Brown and Borutaite, 2004; Iglesias et al., 2015; Shiva et al., 2001; Valdez* et al., 2012). Since SOX is localized in the IMS of mitochondria and its activity is linked to cytochrome *c* presence, an impact of SOX-dependent nitrite reduction on mitochondrial respiration was suggested. Based on these findings, this work addressed the impact of SOX-derived NO on mitochondrial respiratory dynamics, aiming to improve the understanding of the role of SOX for mitochondrial physiology.

To elucidate the SOX-dependent short-term impact of nitrite exposure on mitochondrial respiration an XFe96 Analyzer was used to monitor the oxygen consumption of MEFs directly after the addition of either cell culture medium or sulfite and/or nitrite. All experimental conditions exhibited the characteristic response profile to the sequential injection of oligomycin, FCCP and Rot/AA (2.1.1) (Divakaruni et al., 2014). Evaluation of the OCR revealed a significant increase in spare respiratory capacity in WT cells upon the addition of sulfite of 40%, an effect that was absent upon loss of SOX activity (Figure 13 C, D). Interestingly, co-administration of nitrite with sulfite attenuated this increase by restoring spare respiratory capacity back to baseline levels. In contrast, nitrite supplementation alone resulted in a slight reduction of spare respiratory capacity.

Taken together, this indicates that SOX-dependent NO production upon short-term nitrite exposure impacts mitochondrial bioenergetics in terms of the spare respiratory capacity. This suggests that, short-term NO production by SOX decreases the cells ability to ramp up ATP production, however, the exact mechanism remains unclear.

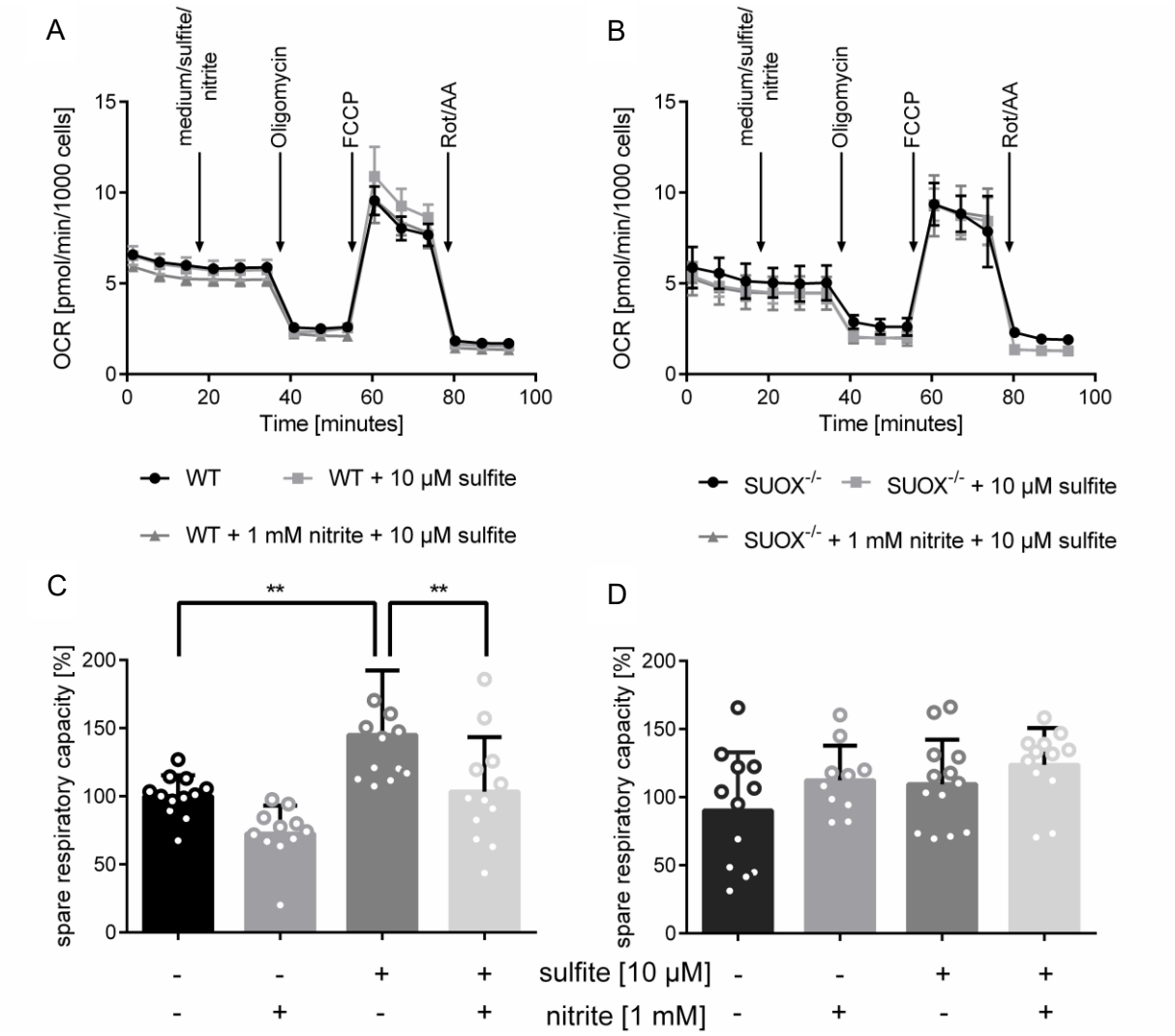

Figure 13: Impact of acute nitrite injection on mitochondrial respiration
Oxygen consumption of SUOX$^{-/-}$ and WT MEFs measured by Seahorse experiments. After the addition of 1 mM nitrite, 10 µM sulfite and a combination of both a sequential injection of 2 µM oligomycin, 1 µM FCCP and 0.5 µM rotenone/antimycin A was performed. (A)-(B) Traces of oxygen consumption of (A) WT and (B) SUOX$^{-/-}$ MEFs normalized to the cell number. Each dot represents n=4. (C)-(D) Analysis of the spare respiratory capacity of SUOX$^{-/-}$ and WT MEFs after the addition of 1 mM nitrite, 10 µM sulfite and a combination of both. Data was normalized to untreated control. One-way ANOVA with Tukey post-hoc test was performed as indicated. p-value **< 0.01.

After identifying SOX-dependent effects in response to short-term nitrite exposure, the question arose whether long-term nitrite exposure similarly impacts mitochondrial bioenergetics. In line with previous experiments, *SUOX*$^{-/-}$ FlpIn^{TM} cells and cells overexpressing human SOX (hSOX) WT were exposed for 72 h with nitrite (Kaczmarek, 2019). Afterwards mitochondria from these cells were enriched and successful mitochondrial fractionation was confirmed by immunoblotting for VDAC and gephyrin as markers for the mitochondrial and cytosolic fraction, respectively (Figure S4). Subsequently, mitochondrial respiration was assessed using an Oxygraph 2K (Oroboros) (Figure 14).

Initial measurements in the absence of substrates revealed no difference in basal oxygen consumption for SOX-expressing mitochondria.

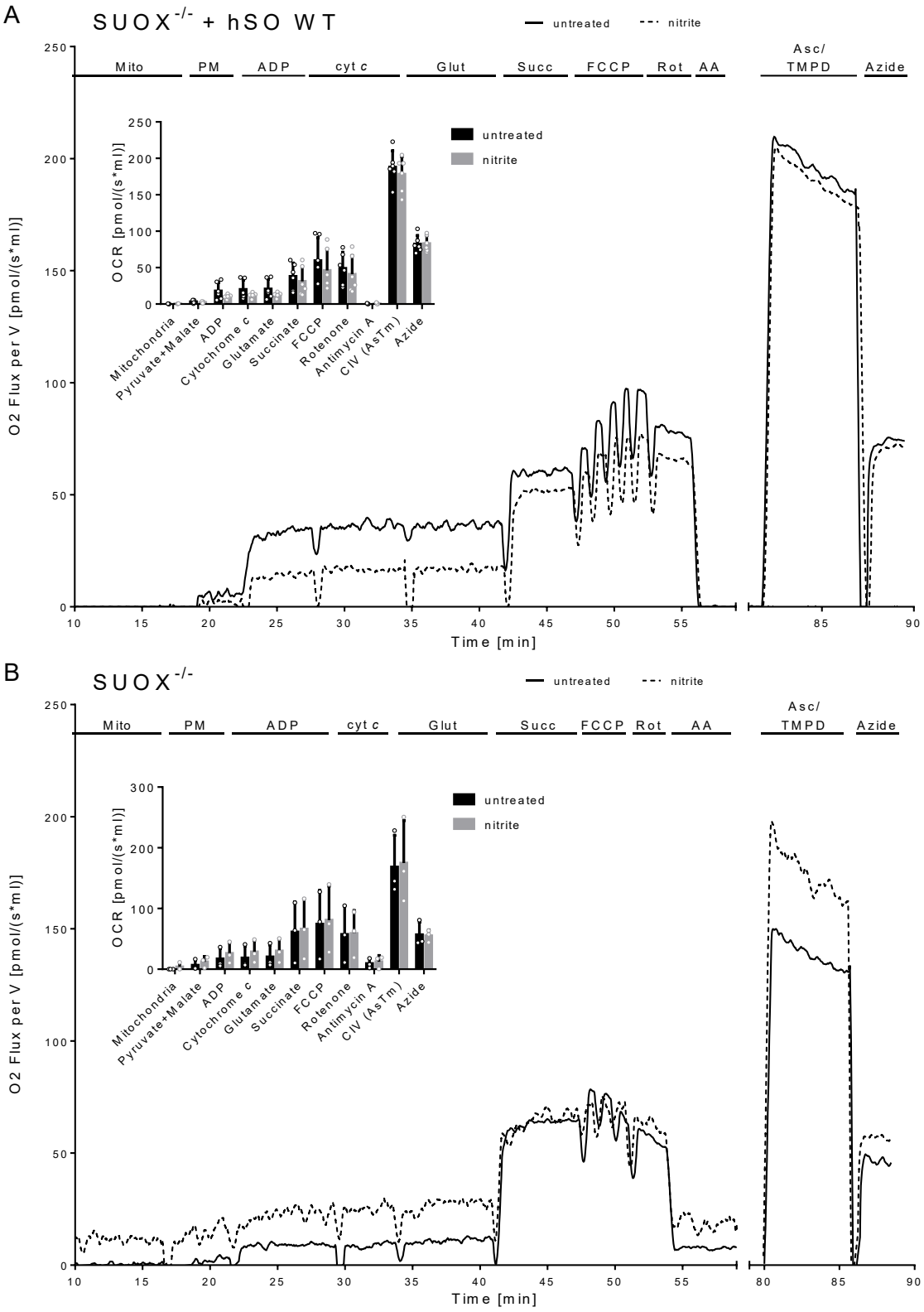

Figure 14: Impact of long-term nitrite treatment on mitochondrial respiration
SUOX$^{-/-}$ and SUOX$^{-/-}$ FlpInTM cells stably expressing hSOX WT (SUOX$^{-/-}$ + hSO WT) were treated with 50 µM nitrite for 72 h before monitoring the mitochondrial respiration. (A)-(B) Representative Oxygraph measurements of pure mitochondria from with the analysis of the oxygraph traces as inlets (A) SUOX$^{-/-}$ cells + hSOX WT (100 µg, n=7) and (B) SUOX$^{-/-}$ cells (25 µg, n=3) after the addition of various substrates (depicted). Two-way ANOVA with Sidak's post-hoc test was performed. p-value: ns > 0.05. Mito = mitochondria, PM = pyruvate + malate, cyt *c* = cytochrome *c*, Glut = glutamate, Succ = succinate, Rot = rotenone, AA = antimycine A, Asc = ascorbate

The addition of pyruvate and malate, substrates fueling NADH production via the TCA cycle, similarly increased oxygen consumption in untreated and nitrite treated SOX-expressing mitochondria. Subsequent supplementation with ADP stimulated OXPHOS, increased oxygen consumption, revealing a non-significant SOX-dependent 1.5-fold decrease in mitochondrial respiration upon nitrite exposure (Figure 14 A). Next, cytochrome *c* addition served as a control for mitochondrial membrane integrity, with only little response, indicating mostly intact outer mitochondrial membranes. Addition of glutamate modestly increased mitochondrial respiration without significant differences. Supplementation of succinate, a complex II substrate, further elevated mitochondrial respiration. At this stage, SOX-expressing mitochondria continued to exhibit a minor non-significant decrease in O_2 flux in response to nitrite exposure. These differences persisted during maximal respiratory stimulation with FCCP. Interestingly, inhibiting complex I with rotenone attenuated the SOX-dependent effect of long-term nitrite treatment on mitochondrial respiration, attributing the observed changes to complex I and the TCA cycle. Subsequent addition of antimycin A resulted in no residual oxygen consumption by SOX-expressing mitochondria. Next, supplementation of complex IV with the artificial electron donor TMPD and its co-substrate ascorbate did not reveal any nitrite-dependent changes. Finally, the background oxygen consumption by autooxidation of TMPD was assessed by blocking complex IV with azide with no differences observed between nitrite treated and control mitochondria.

In *SUOX*$^{-/-}$ mitochondria, nitrite exposure produced an effect opposite to that observed in SOX-expressing mitochondria, causing a slight increase in oxygen consumption. This increase was abolished by succinate addition but was restored upon inhibition of mitochondrial respiration with antimycin A.

In sum, long-term nitrite treatment resulted in a slight, but not significant reduction of mitochondrial respiration in SOX-expressing mitochondria. Strikingly, in SOX-deficient mitochondria this treatment resulted in a contrary effect by slightly, but not significantly, increasing the oxygen consumption (Figure S5).

2.3 Physiological implication of SOX-dependent nitrite reduction

The previous data suggested that the SOX-mediated NO production influences mitochondrial respiration. However, the question of whether this function impacts other physiological roles remains unclear, since NO plays a crucial role for various biological processes (1.6). NO is well known for its role during vasodilation, acting via the main NO receptor sGC (Ignarro et al., 1987). Especially during hypoxia, NO-mediated vasodilation is crucial for improving oxygen delivery to tissues (Umbrello et al., 2013). During hypoxic conditions NO homeostasis is highly dependent on metal-dependent enzymes with nitrite reducing function such as SOX.

SOX-dependent NO production was shown to be favored during hypoxic conditions (Kaczmarek, 2019). To investigate the influence of SOX-dependent nitrite reduction on vasodilation, mice were challenged by inducing heart failure with preserved ejection fraction (HFpEF) and pulmonary hypertension (PH) in cooperation with the AG Rosenkranz (CMMC, Cologne). Based on Schiattarella et al., 2019 mice were either fed a standard ("chow") or a high-fat diet for 18 weeks. Since homozygous SOX-deficient mice (*SUOX*$^{-/-}$) die at 9.5 days of life on average, they were unsuitable and therefore heterozygous SOX-deficient mice (*SUOX*$^{+/-}$) were taken instead (Fu et al., 2024a). On top of the high-fat diet mice were treated with Nω-Nitro-L-arginine methyl ester (L-NAME) to abolish NOS function and induce HFpEF, establishing a state of NO homeostasis relying on metal-dependent enzymes as SOX, and resembling HFpEF in humans. This model for HFpEF was further refined to also induce pulmonary hypertension by exposing mice to hypoxia (10% O_2) for the last 6 weeks of the experiment, establishing favorable conditions for NO production by SOX.

Our collaborators determined systolic arterial pressure (SAP), right ventricular systolic pressure (RVSP) and the fulton index (RV/(LV+S)), representing the ratio between the weight of the right ventricle (RV) to the weight of the left ventricle (LV) and septum (S) (Figure 15). Systolic arterial pressure serves as a general indicator of elevated blood pressure (Gomez-Arroyo et al., 2012; Schiattarella et al., 2019; Zhang et al., 2022).. In mouse models, SAP typically remains unchanged upon the induction of pulmonary hypertension, but is increased in models of heart failure with preserved ejection fraction (HFpEF) (Schiattarella et al., 2019; Thibault et al., 2010). In contrast, RVSP is a specific marker for pulmonary hypertension, while the fulton index provides an objective measure of right ventricular hypertrophy - both are established hallmarks of pulmonary hypertension and right heart overload (Gomez-Arroyo et al., 2012; Zhang et al., 2022).

Notably, in the experiments conducted by our collaborators, hypoxic challenge in chow-fed wild-type (WT) mice significantly increased SAP from 83.7 ± 11.3 mmHg to 115.7 ± 26.7 mmHg (Figure 15 A), contrasting previous reports (Thibault et al., 2010). In *SUOX*$^{+/-}$ mice, however, SAP increased only slightly from 92.9 ± 13.5 mmHg to 99.0 ± 20.2 mmHg. In HFpEF mice, SAP did not change significantly upon induction of pulmonary hypertension, but, consistent with earlier studies, these mice exhibited higher SAP overall compared to chow-fed controls, with averages of ~120 mmHg compared to 100 mmHg, respectively (Figure 15 D) (Schiattarella et al., 2019). Both, RVSP and the fulton index showed a marked hypoxia-dependent increase in both genotypes fed with chow diet (Figure 15 B, C). Interestingly, under HFpEF conditions, the increase in RVSP was maintained in both genotypes, but only SUOX$^{+/-}$ mice exhibited a significant increase in the fulton index, indicating a potential exacerbation of right ventricular hypertrophy with reduced SOX activity (Figure

15 E, F). Notably, *SUOX*$^{+/-}$ mice are phenotypically indistinguishable from their WT litter mates under baseline conditions, as 50% SOX activity is sufficient for survival and normal physiological function, thus complete loss of function in endothelial cells is expected to result in more severe outcomes (Fu et al., 2024a; Shih et al., 1977).

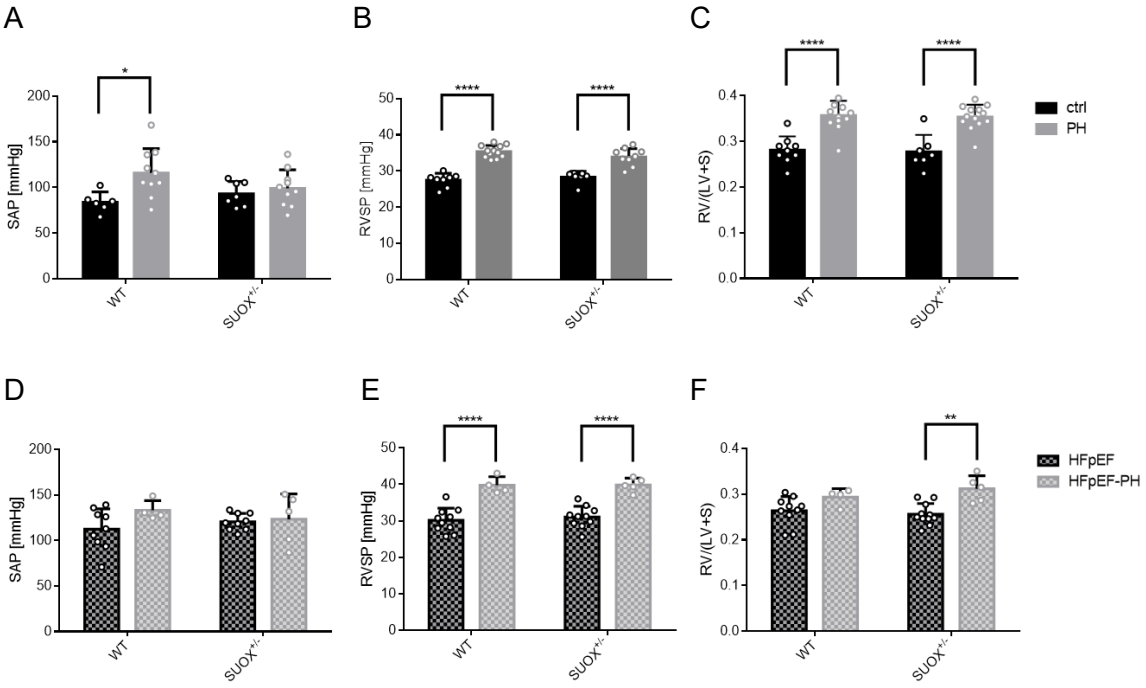

Figure 15:Implication of SOX in HFpEF and pulmonary hypertension
Contribution of SOX towards the regulation of vasodilation, Male C57BL6/N WT and SUOX-/+ mice were implemented in a mouse model for Heart Failure with Preserved Ejection Fraction (HFpEF) and pulmonary hypertension (PH). Mice were fed with either chow diet (ctrl, PH, A-C) or high-fat diet combined with L-NAME treatment (HFpEF, HFpEF-PH, D-F) for 18 weeks to induce HFpEF. Additionally, mice were either kept in normoxic conditions all time (ctrl, HFpEF) or exposed to hypoxia for the last 6 weeks of the experiment (PH, HFpEF-PH), to induce PH. Subsequently, (A, D) systolic arterial pressure (SAP) and (B, E) right-ventricular systolic pressure (RVSP) were determined and mice were sacrificed and the weight of the right-ventricle, the left ventricle and the septum were taken to calculate the (C, F) fulton index (RV/(LV+S). Two-way ANOVA with Sidak's post-hoc test was performed as indicated. p-value ****< 0.0001, *** < 0.001, ** < 0.01, * < 0.05

May cytochrome c provide reverse electron flow into SOX

Despite its limitations, the HFpEF study within this work indicated a role of SOX in the regulation of vasodilation during hypoxia and aligns with a recent report demonstrating a crucial role for SOX in regulating the cerebral blood flow during brain hypoxia (Christie et al., 2023). Specifically, under hypoxic conditions, mitochondrial SOX in astrocytes reduces nitrite to NO, leading to dilation of cortical arterioles and improved brain tissue perfusion. Remarkably, chemically induced hypoxia via ETC inhibition produced similar vasodilatory effects, suggesting that ETC-derived electrons are the source for SOX-dependent nitrite reduction. Given that cytochrome *c* is both a key electron carrier within the ETC and the final electron acceptor of SOX, it was hypothesized that reduced cytochrome *c* could shuttle electrons to SOX during ETC inhibition, providing electrons for subsequent nitrite reduction.

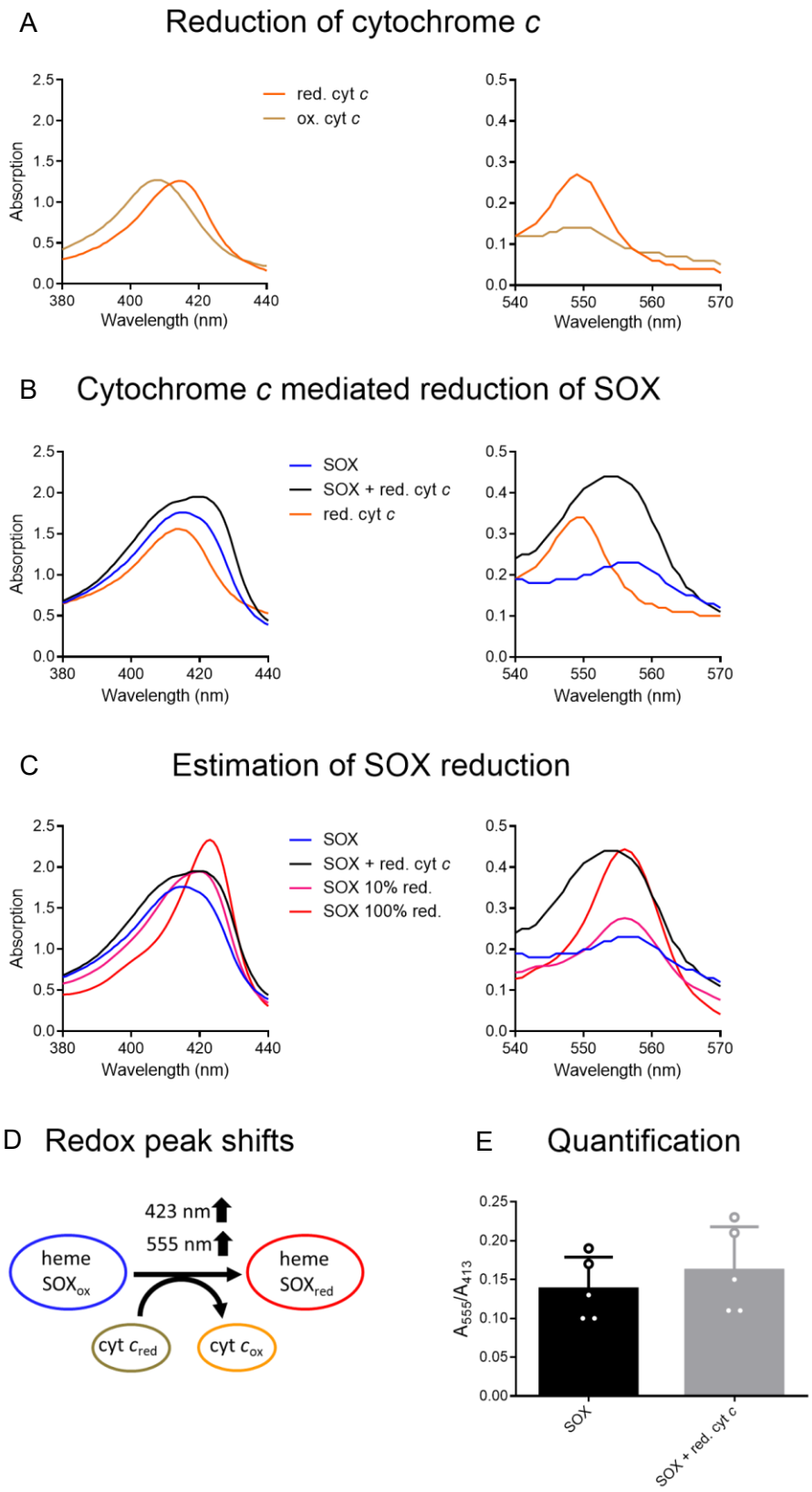

Figure 16: Investigation of the electron transfer from cytochrome c to SOX
Pre-reduced cytochrome *c* was incubated with SOX and afterwards removed by Ni-NTA purification of His-tagged SOX. Substochiometric and full reduction of SOX with sulfite served as an estimated quantification of cytochrome *c* mediated SOX reduction. For better comparison, UV-vis spectra were normalized to the SOX protein at A_{280} if needed.(A) Reduction of cytochrome *c* with ascorbate. (B) SOX reduction by pre-reduced cytochrome *c*. (C) SOX reduction by substochiometric and excess sulfite. (D)Schematic depiction of the redox peak shifts in the heme domain of SOX. (E) Quantification of peak heights at 555 nm. SOX compared to SOX exposed to pre-reduced cytochrome c (n=5).

To test this hypothesis, first cytochrome *c* was pre-reduced with ascorbate (Figure 16 A), then residual ascorbate was removed using a desalting column and afterwards reduced cytochrome *c* was exposed to SOX. After incubation, His-tagged SOX was isolated by Ni-NTA pull-down to remove free cytochrome *c*, and the oxidation state was analyzed by UV–Vis spectroscopy (Figure 16 B, C). For better visualization the baselines of the spectra were normalized to the 280 nm protein peak of SOX, to account for variations in protein yield during pull-down if needed. Full spectra can be found in the supplementary data (Figure S7).

Upon complete reduction, cytochrome *c* displays a peak shift of its heme Soret band from 408 to 415 nm, accompanied by an increased intensity and an increase in α-band peak at 550 nm. Here only partial reduction of cytochrome *c* was achieved with ascorbate as indicated by a Soret peak shift from 408 to 414 nm and an increase in the α-band at 550 nm (Figure 16 A). Neither prolonged exposure time nor increased ascorbate concentrations resulted in complete cytochrome *c* reduction, suggesting that the reduction potential of ascorbate is not sufficient to fully reduce cytochrome *c* (data not shown) (Warren and Mayer, 2010).

Oxidized SOX typically displays a Soret band at 413 nm and no visible peak at 555 nm, characteristic of the oxidized b_5-type cytochrome domain, while reduction of SOX shifts the Soret band to 423 nm and increases peak size at 555 nm. In this preparation, SOX showed a slight Soret shift to 415 nm and a minor 555 nm peak, indicating partial pre-reduction (Figure 16 B). Upon incubation with reduced cytochrome *c*, the Soret band shifted further to 420 nm, and the 555 nm peak increased, consistent with heme reduction, strikingly showing a minor shift to 554 nm (Figure 16 B, C). This minor shift might indicate remaining cytochrome *c* impurities, although no unspecific binding of cytochrome *c* to the beads was observed (Figure S6).To estimate the extent of SOX reduction, these spectra were compared to those obtained from SOX that was partially and fully reduced by sulfite (Figure 16 C). Substoichiometric sulfite reduction (~10%) caused a shift to 420 nm and a slight increase at 555 nm, while full reduction resulted in a Soret shift to 423 nm and a pronounced 555 nm peak. To estimate the reduction achieved by cytochrome *c*, the ratio between peak heights at 413 and 555 nm were compared, enabling a protein concentration independent readout. This comparison indicated a reduction of about 20% (Figure 16 E). These findings support a model in which cytochrome *c* transfers electrons from the ETC to SOX, thereby facilitating NO production under hypoxic conditions in the brain (Christie et al., 2023).

2.4 Characterization of SOX-deficient hippocampal neuronal cultures

MOCD and SOXD are linked to severe neurodegeneration, caused by SSC-mediated toxicity (Kumar et al., 2019). To better understand the mechanisms underlying SOXD, the working

group of Prof. Schwarz developed a SOX-deficient mouse model. These mice die at 9.5 days of age and exhibit normal brain development lacking signs of neurodegeneration, instead showing a general metabolic collapse with reversal of the TCA cycle (Fu et al., 2024b).

To further investigate the role of SOX in brain development, hippocampal neuronal cultures were generated from two-day-old mice. This approach allows for the cultivation of neuronal cultures for longer time periods, bypassing the 9.5-day survival limit.

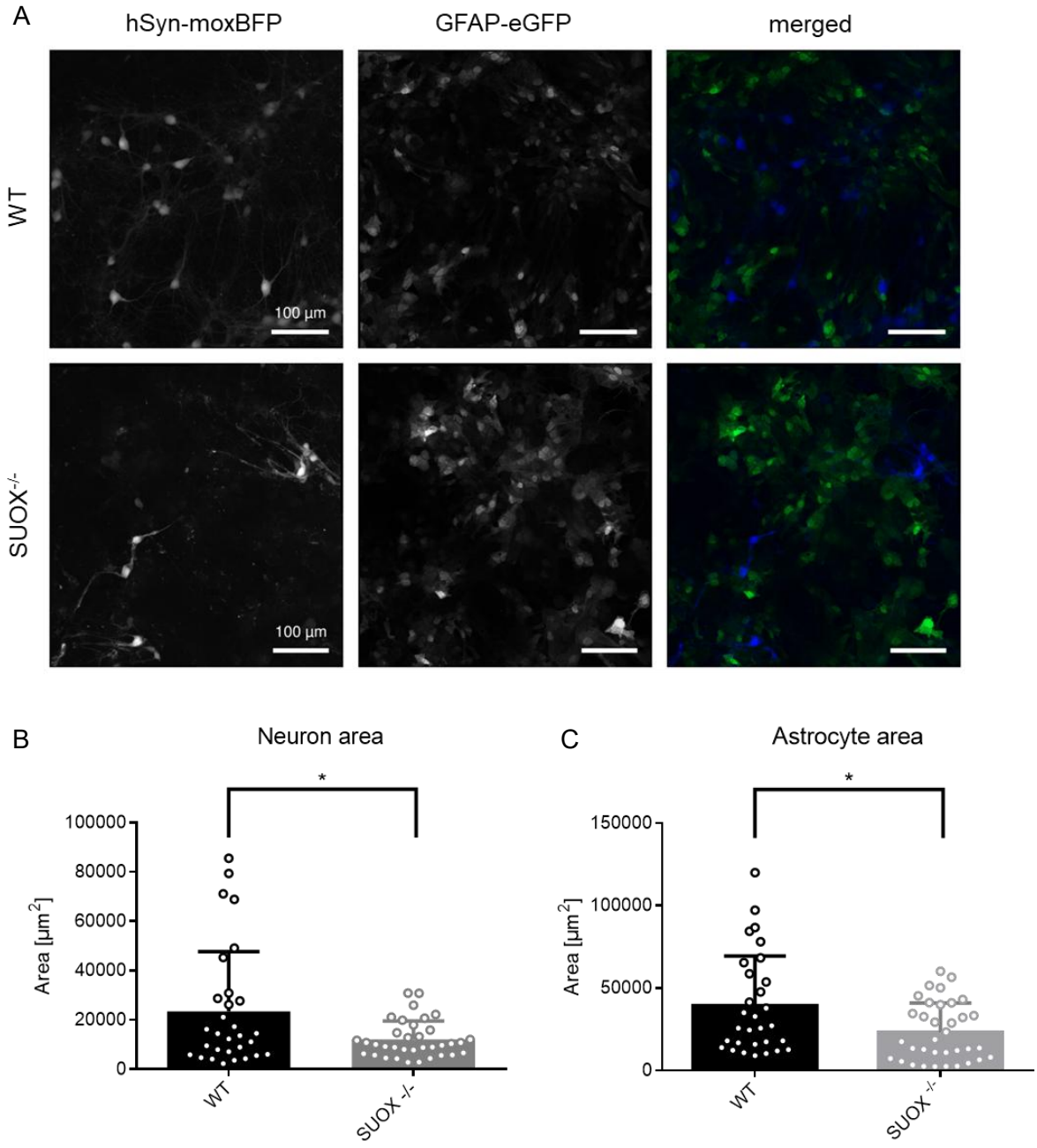

Figure 17: Analysis of area spanned by neurons and astrocytes in hippocampal neurons
Hippocampal cultures from WT and SUOX$^{-/-}$ P2 mice were transduced at DIV11 with hSyn-mox BFP and GFPA-eGFP constructs as cell fillers for neurons and astrocytes, respectively. At DIV14 cells were fixed and imaged. (A) Representative microscope images from tile scans from WT and SUOX$^{-/-}$ cultures. (B) Analysis of the neuron and astrocyte areas using automated ImageJ macros (n=2). Two-tailed unpaired student's t-test was performed as indicated. p-value: * < 0.05

As a first step to characterize these hippocampal neuronal cultures, their developmental states at 14 days in vitro (DIV) were analyzed. The generation of primary hippocampal cultures from mouse brains inherently results in co-cultures of neurons and astrocytes. To distinguish these cell types, Adeno-associated viruses were used to express monomeric oxygen-insensitive blue fluorescent protein (moxBFP) under the neuron-specific human synapsin (hSyn) promoter and enhanced green fluorescent protein (eGFP) under the astrocyte-specific glial fibrillary acidic protein (GFAP) promoter, effectively labeling neurons and astrocytes, respectively. Cultures were transduced at DIV11 and fixed for analysis at DIV14. Automated image quantification revealed a significant reduction in both neuronal network and astrocyte area (Figure 17 A-C). While it remains unclear whether these reductions resulted from impaired cell proliferation or increased cell death, these findings were consistent with the neurodegenerative phenotype observed in SOXD patients.

In SOXD patients, severe neurodegeneration is driven by SSC-mediated toxicity resulting in a cleavage of gephyrin and subsequent loss of inhibitory synapses (Kumar et al., 2019). To determine whether this pathological mechanism is also present in SOX-deficient hippocampal cultures, gephyrin cleavage was analyzed in cells maintained until DIV14-DIV23 using immunoblotting (Figure 18 A). Gephyrin cleavage occurs typically within the flexible C-domain that connects E- and G-domain (Kawasaki et al., 1997; Tyagarajan et al., 2011).

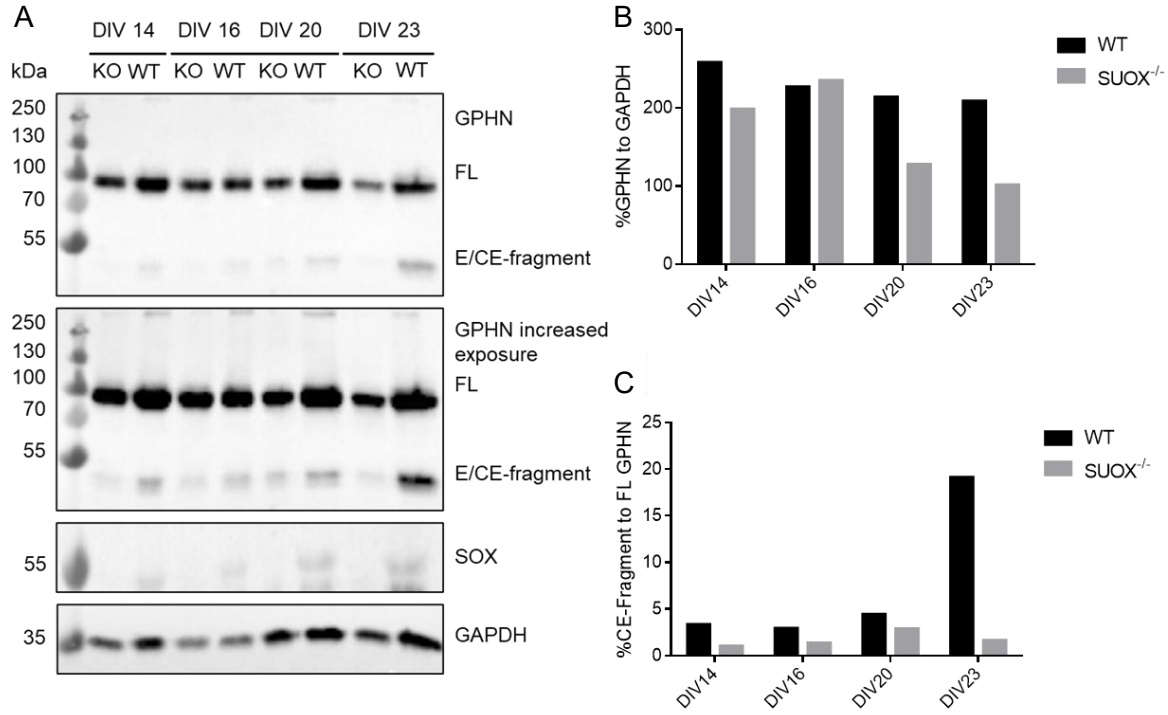

Figure 18: Time-dependent gephyrin degradation in hippocampal neurons
Hippocampal neurons from WT and SUOX$^{-/-}$ P2 mice were cultivated until DIV14-DIV23. (A) WB-based analysis of gephyrin degradation, using 50 µg of protein. GAPDH served as a loading control (n=1). (B) Evaluation of the combined band intensities of gephyrin and the E/CE-fragment normalized to the GAPDH signal. (C) Evaluation of the band intensity for the E/CE-fragment compared to the sum of full-length (FL) and E/CE-fragment intensities.

Here, full-length (FL) gephyrin and its cleavage product of E-domain (E) and E-domain with residual parts of the C-domain (CE) were analyzed. This quantitative analysis of gephyrin levels by western blot revealed a two-fold reduction in total gephyrin levels at DIV20 and DIV23 upon loss of SOX, with no change observed during earlier time points (Figure 18 B). In contrast to that, WT samples showed a two-fold increase in gephyrin degradation at early time points and a marked 12-fold increase at DIV23 (Figure 18 C). These findings are contradictory to the increased cleavage of gephyrin reported earlier (Kumar et al., 2019). In sum, SOX-deficient cultures developed decreased gephyrin levels over time. The absence of increased gephyrin cleavage in these cultures suggests a novel mechanism underlying these findings. However, it should be noted that this experiment was performed only once and further replicates are necessary to draw a final conclusion.

Previous studies demonstrated elevated sulfite levels in urine and plasma samples of both SOXD patients and SOX-deficient mice (Claerhout et al., 2018; Fu et al., 2024b). In the absence of a reducing environment, sulfite readily reacts with cystine to form the S-sulfonated form (SSC) (Kumar et al., 2019). Thus, SOX deficiency leads to increased SSC concentrations. Besides that, thiosulfate (SSO_3^{2-}), an intermediate of the H_2S oxidation pathway, was also shown to be elevated.

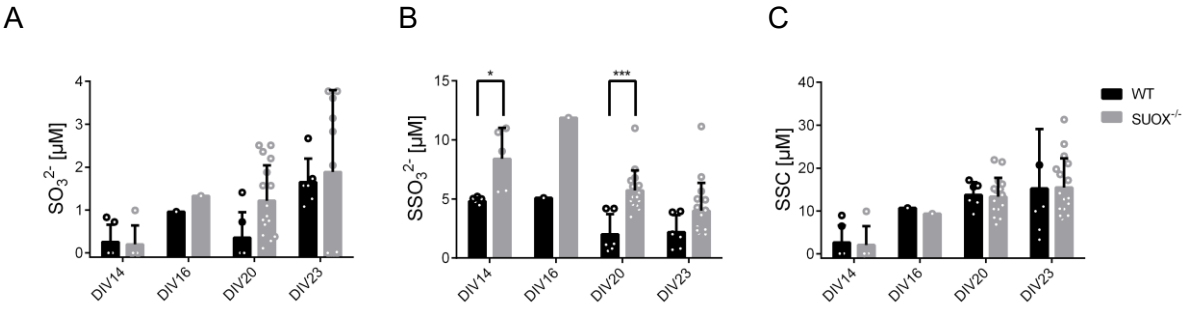

Figure 19: Time-dependent concentrations of sulfite, thiosulfate and SSC in the medium of hippocampal neurons
Hippocampal neurons from WT and SUOX$^{-/-}$ P2 mice were cultivated until DIV 14 (n=4), DIV 16 (n=1), DIV 20 (WT n=4, SUOX$^{-/-}$ n= 17) and DIV 23 (WT n=4, SUOX$^{-/-}$ n= 17). (A)-(C) Concentrations of sulfite (A), thiosulfate (B) and SSC (C) in the medium were determined by HPLC analysis. Two-way ANOVA with Sidak's post-hoc test was performed as indicated. p-value: ***< 0.001, * < 0.05.

To further characterize the generated murine hippocampal cultures in the previous experiment, it was examined whether the levels of sulfite, thiosulfate and SSC in the culture medium of hippocampal *SUOX*$^{-/-}$ neurons resemble the previous published findings. Time-dependent analysis revealed that sulfite concentrations remained low ranging from 0.5-4 µM SO_3^{2-} , increasing over time in both WT and SOX-deficient cultures, with no significant differences observed between genotypes (Figure 19 A). In contrast, SSO_3^{2-} concentrations steadily decreased over time, dropping from 8.5 µM to 4 µM in SOX-deficient cultures and from 5 µM to 2 µM in WT cultures (Figure 19 B). In line with previous reports, lack of sulfite oxidase

resulted in an increase in thiosulfate levels (Fu et al., 2024a). Finally, SSC concentrations increased over time, rising from 2 µM at DIV14 to 15 µM at DIV23, again with no significant changes between WT and SOX-deficient samples (Figure 19 C). While this finding contrasts with previous studies reporting elevated SSC in the absence of SOX, it aligns with the previous observation of absent gephyrin cleavage in these cultures (2.4). This suggests that the *in vitro* environment may influence the biochemical consequences of SOX deficiency differently than *in vivo* systems.

Although a reduction in the confluency of neurons and astrocytes in SOX-deficient cultures was observed, there were no corresponding increases in SSC concentrations or gephyrin cleavage. Thus, the underlying cause of the reduced cellular network remained elusive. Previously it was examined a diminished mitochondrial respiration in SOX-deficient MEFs, which may account for reported lower ATP levels observed during sulfite accumulation (Mellis et al., 2021; Zhang et al., 2004). Given the critical role of mitochondria in meeting the high energy demands during brain development, it was investigated whether mitochondrial respiration is similarly impaired in SOX-deficient murine hippocampal cultures. Thus, mitochondrial respiration was assessed at DIV14 using a Seahorse XFe96 analyzer (Figure 20). All measured states of mitochondrial respiration, basal, maximal and ATP-linked respiration, as well as the proton leak and the spare respiratory capacity were markedly reduced (~25%) in SOX-deficient cells compared to WT cells (Figure 20 B).

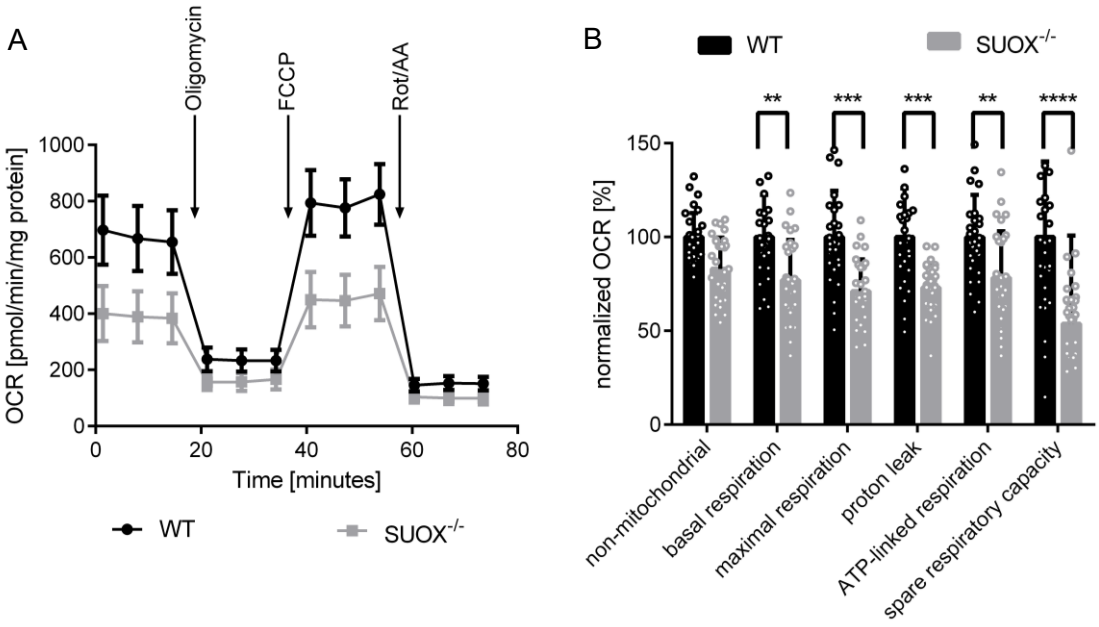

Figure 20: Mitochondrial respiration of DIV14 hippocampal neurons
Hippocampal neurons from P2 mice were cultivated until DIV14 and mitochondrial respiration as monitored using a Seahorse XFe96 Analyzer. (A) Representative graph of the oxygen consumption rate normalized to the amount of protein. Sequential injection of 2 µM oligomycin, 1 µM FCCP, 0.5 µM rotenone/antimycin A was performed (indicated by the arrows). Each dot represents n=6 technical replicates. (B) Evaluation of the OCR normalized to WT (n=3 biological replicates, n=6 technical replicates). Two-way ANOVA with Sidak's post-hoc test was performed as indicated. p-value: *** < 0.001, ** < 0.01

These findings indicate an impairment of mitochondrial energy metabolism, consistent with previous reports (Glänzel et al., 2024; Grings et al., 2014). This mitochondrial dysfunction might be the reason for the observed alterations in neuronal and astrocytic homeostasis (2.4). It is important to note that it cannot be distinguished between the specific contribution of neurons and astrocytes to the overall oxygen consumption.

2.5 Regulation of SOX activity

The previous sections focused on the role of SOX for mitochondrial function in different systems with regard to respiration and metabolism. Thereby the two different functions of SOX, sulfite oxidation and NO-production were distinguished. The obtained findings suggested that both functions are important for healthy mitochondria, in vitro, in cellulo and in vivo. This raises the need to further investigate regulation principles for SOX dual function to allow for treatment options in different disease contexts including SOXD.

Recently, the awareness for SOXD was raised by the identification of 15 novel pathogenic *SUOX* missense mutations (Kaczmarek et al., 2021). While the discovery of cPMP raised an effective treatment for MOCD type A, there is no therapy targeting the underlying molecular mechanism available (Schwarz et al., 2025; Touati et al., 2000). Therefore, modulating the regulation of SOX activity represents a promising strategy, especially for patients with variants exhibiting impaired SOX function which is based on impaired Moco binding (Bender et al., 2019a; Kaczmarek et al., 2022). The next chapters will focus on elucidating the molecular mechanisms that regulate SOX activity.

2.5.1 Regulation of SOX activity by MOCS1AB and molybdate

The recently characterized SOX patient variant R366H was shown to be deficient in Moco binding (Kaczmarek et al., 2022). Previous studies demonstrated that molybdate supplementation in both WT and patient fibroblasts expressing another Moco-binding deficient variant, G362S, led to a two-fold increase in SOX activity, likely due to enhanced Moco availability (Bender et al., 2019a). Since MOCS1A and MOCS1B catalyze the rate-limiting step of Moco biosynthesis, their overexpression is expected to increase cellular Moco levels (Hänzelmann et al., 2002). To further explore this hypothesis *SUOX*$^{-/-}$ FlpIn™ cells expressing either hSOX WT or the patient variant hSOX R366H were transfected with a MOCS1AB construct, enabling co-expression of MOCS1A and MOCS1B, in addition to molybdate supplementation (Figure 21).

Following the expression of the MOCS1 cDNA we found a significant increase in specific SOX activity for hSOX WT, from 111.0 ± 17.1 µM cyt *c* min^{-1} mg protein^{-1} to 343.6 ± 32.9 µM cyt *c* min^{-1} mg protein^{-1} (Figure 21 B). Even the specific SOX activity of the Moco-binding

deficient R366H variant increased from 6.8 ± 1.2 µM cyt *c*·min^{-1}·mg protein^{-1} to 18.4 ± 7.5 µM cyt *c*·min^{-1}·mg protein^{-1}. These results demonstrate that increasing Moco availability significantly enhanced SOX activity in both WT and even in the R366H variant, supporting the hypothesis that Moco supply is a key determinant of SOX function and harbors great potential to rescue Moco-deficient patient variants in SOXD.

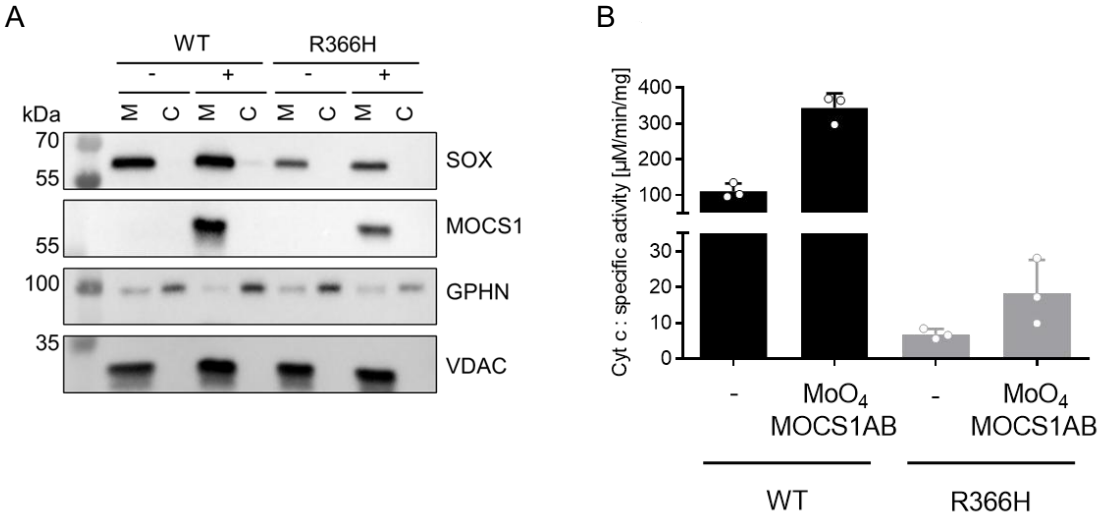

Figure 21: Expression and activity of hSOX WT and patient variant R366H
HSOX variants were stably expressed in FlpIn™ cells transiently expressing MOCS1AB and supplemented with molybdate. (A) Representative WB-based analysis of mitochondrial enrichment and MOCS1 expression. 20 µg mitochondria were used, VDAC served as mitochondrial marker and gephyrin as a cytosolic one. (B) Sulfite-dependent cyt c specific SOX activity of 30 µg enriched mitochondria (n=3).

2.5.2 Regulation of SOX activity by CLUH

SOX is a nuclear encoded enzyme, which is synthesized in a pre-mature form in the cytosol and undergoes a hierarchical maturation process upon translocation into the mitochondria (Klein and Schwarz, 2012). The mRNA binding protein CLUH was identified as an important protein in mitochondrial biogenesis, primarily by binding and regulating the translation and stability of various nuclear mRNAs encoding mitochondrial proteins (Gao et al., 2014; Pla-Martín et al., 2020; Schatton et al., 2017). Among these proteins, SOX was encoded by one of the mRNAs targeted by CLUH (Gao et al., 2014). This raised the question of whether SOX activity is influenced by CLUH, suggesting a link between CLUH expression and the regulation of SOX within the broader context of mitochondrial protein synthesis.

SOX expression levels were monitored first in livers from 8-week-old WT and *CLUH*$^{-/-}$ mice using immunoblotting. SOX expression appeared reduced upon loss of CLUH (Figure 22 A). As the CLUH antibody was raised against a human peptide sequence, no signal was obtained in mouse tissue (Figure 22). Consistently, a significant reduction in SOX activity was observed in *CLUH*$^{-/-}$ liver extracts compared to WT with 20.9 ± 3.5 µM cyt *c*·min^{-1}·mg protein^{-1} and 48.0 ± 3.0 µM cyt *c*·min^{-1}·mg protein^{-1}, respectively (Figure 22 B).

This data suggests that CLUH function is required for SOX activity.

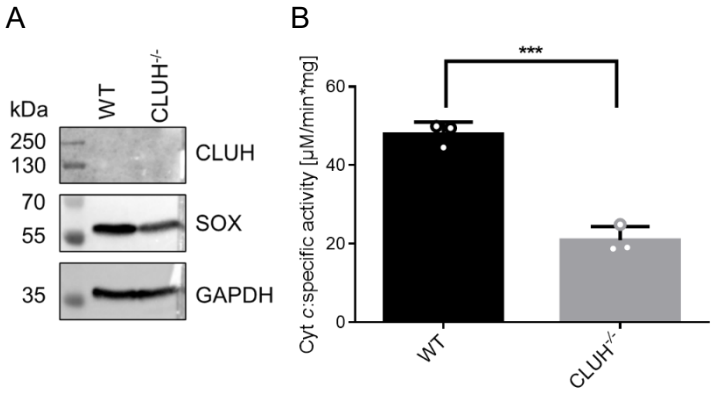

Figure 22: SOX expression and activity in CLUH$^{-/-}$ liver at eight weeks of age
(A) Representative WB-analysis of SOX expression. 25 µg lysate were used. (B) Sulfite-dependent cyt c specific SOX activity in 25 µg liver lysates (n=3 technical replicates). Two-tailed unpaired student's t-test was performed as indicated. p-value: ***< 0.001

Based on the previous findings this work aimed to further investigate the relationship between CLUH and SOX activity. Therefore, three cell lines were used: a) *CLUH*$^{-/-}$ FlpIn^{TM} cells (CLUH$^{-/-}$), b) WT FlpIn^{TM} cells overexpressing Flag-tagged CLUH (CLUH OE) and c) WT FlpIn^{TM} cells expressing the empty plasmid (mock). Immunoblot analysis confirmed successful overexpression in CLUH OE, its absence in *CLUH*$^{-/-}$ cells and the endogenous levels in the mock condition (Figure 23 A). The analysis of SOX activity revealed significant differences in these three conditions: First, *CLUH*$^{-/-}$ cells exhibited a three-fold decrease in SOX activity compared to mock cells with 4.7 ± 1.0 µM cyt c·min^{-1}·mg protein^{-1} and 12.2 ± 3.0 µM cyt *c*·min^{-1}·mg protein^{-1}, respectively (Figure 23 B). In contrast, cells overexpressing CLUH showed a marked increase in SOX activity to 19.1 ± 2.5 µM cyt *c*·min^{-1}·mg protein^{-1}.

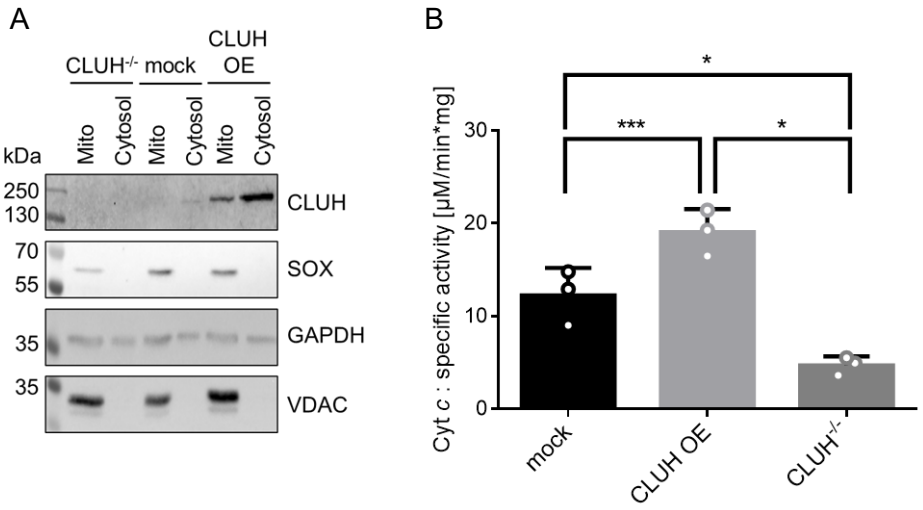

Figure 23: Impact of CLUH expression on SOX activity
Comparison of WT FlpIn^{TM} cells (mock), WT FlpIn^{TM} cells stably overexpressing CLUH for 72h (CLUH OE) and CLUH-deficient FlpIn^{TM} cells (CLUH$^{-/-}$) (A) Representative WB-based analysis of SOX and CLUH expression in enriched mitochondria. 30 µg were used and VDAC served as a mitochondrial marker and GAPDH as a cytosolic one. (B) Sulfite-dependent cyt c specific SOX activity of 30 µg enriched mitochondria (n=3). One-way ANOVA with Tukey post-hoc test was performed as indicated. p-value ***< 0.001, ** < 0.01, * < 0.05.

These findings are in line with the previously observed reduction of SOX activity in *CLUH*$^{-/-}$ liver. With this it was verified that SOX activity (and likely SOX expression) is dependent on CLUH expression levels.

In the previous two chapters the connection between CLUH expression and SOX activity was established. Next, these findings were applied to a disease context, aiming to rescue SOX activity of two previously described patient variants, hSOX R366H and hSOX G362S (Bender et al., 2019a; Kaczmarek et al., 2022). Both variants were shown to be unstable due to impaired Moco-binding, thus elevating expression levels could increase overall SOX activity.

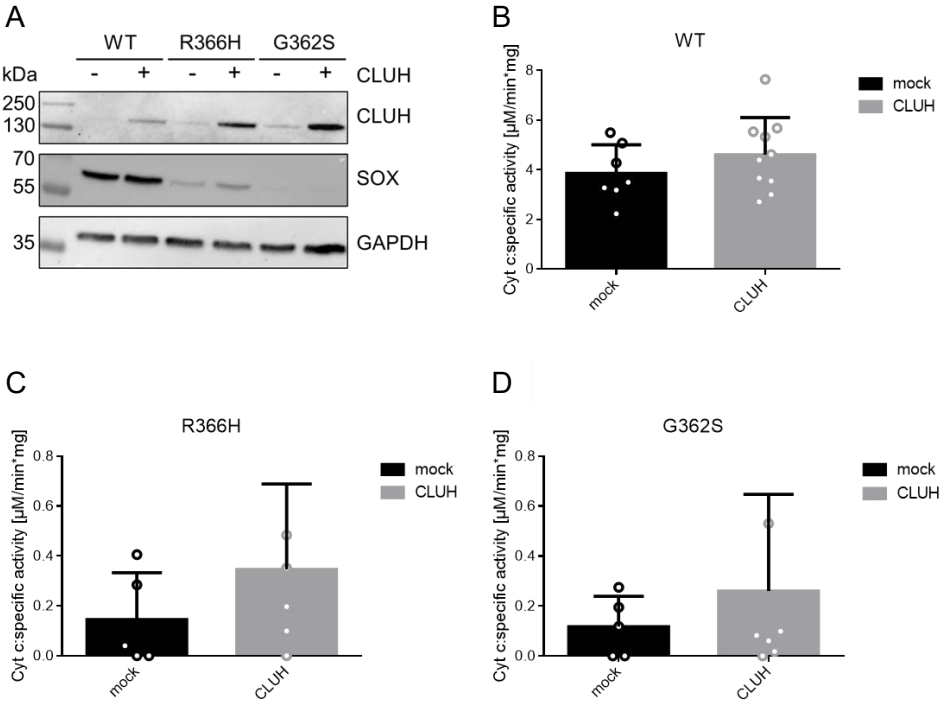

Figure 24: Impact of CLUH overexpression on SOX activity of hSOX WT and patient variants R366H and G362S
FlpIn^{TM} SUOX$^{-/-}$ cells stably expressing hSOX WT (WT), R366H (R366H) and G362S (G362S) were transiently transfected with CLUH (CLUH) or ctrl plasmid (mock) for 96h (A) Representative WB-based analysis of CLUH and SOX expression levels using GAPDH as loading control. 100 µg of protein were used. (B)-(C) Sulfite-dependent cyt c specific SOX activity of hSOX (B) WT (n=7 mock, n=10 CLUH), (C) R366H (n=5 mock, n=6 CLUH) and (D) G362S (n=5 mock, n=7 CLUH). 100 µg of protein were used.

Thus, *SUOX*$^{-/-}$ FlpIn^{TM} cells were used which either inducible stably express hSOX WT (WT), hSOX R366H (R366H) or hSOX G362S (G362S). Next, either Flag-tagged CLUH (CLUH) or empty Flag-tag plasmid (mock) were transiently transfected on top and expression performed for four days. Immunoblot analysis confirmed successful CLUH transfection and the previously reported markedly decreased SOX levels for both patient variants could be verified (Figure 24 A). Determining SOX activity in cells expressing hSOX WT revealed a non-significant increase from 3.9 ± 1.2 µM cyt *c*·min^{-1}·mg protein^{-1} in mock treated cells to 4.6 ± 1.5 µM cyt *c*·min^{-1}·mg protein^{-1} in CLUH-transfected cells (Figure 24 B). Similarly, both patient variants exhibited non-significant increases from 0.2 ± 0.2 µM cyt *c*·min^{-1}·mg protein^{-1} to 0.4 ± 0.4 µM

cyt *c*·min^{-1}·mg protein^{-1} and 0.2 ± 0.1 µM cyt *c*·min^{-1}·mg protein^{-1} to 0.3 ± 0.4 µM cyt *c*·min^{-1}·mg protein^{-1} for hSOX R366H and hSOX G362S, respectively (Figure 24 C, D).

In sum, in this experimental setup of transient transfection with CLUH, significant increases of SOX activity in any condition, as seen previously upon stable expression, could not be observed (3.6.2). A major issue of transient transfection might be the transfection efficiency indicating slightly unequal amounts of correctly expressing cells. Nonetheless, the tendency towards CLUH-mediated increases of SOX activity and expression appears again for both patient variants. This highlights the potential of CLUH as a regulator for SOX activity in the disease context of SOXD.

3 Discussion

This work shed light on the multifaceted role of SOX in mitochondrial respiration and NO metabolism, highlighting its involvement in both health and disease. Through a series of biochemical, cellular and *in vivo* studies it was demonstrated that SOX is more than just a detoxifying enzyme, but also plays a pivotal role in maintaining mitochondrial bioenergetics, supporting hypoxic adaptation and influencing tissue-specific pathophysiology.

3.1 SOX loss alters mitochondrial bioenergetics

Previous studies revealed a 10% contribution of SOX-dependent respiration towards total mitochondrial respiration (Kaczmarek, 2019). In addition, ATP levels in SOX-deficient cells were shown to be decreased under glucose-deprived conditions, indicating crucial role of SOX to maintain mitochondrial bioenergetics (Mellis et al., 2021). This study expands the view of SOX beyond its classical role in sulfite detoxification suggesting SOX serves as a regulator of mitochondrial bioenergetics across various tissues, including fibroblasts, liver and neurons.

Initial analyses in SOX-deficient mouse embryonic fibroblasts (MEFs) revealed impaired mitochondrial respiration (Figure 8). A significant reduction of 25% in basal OCR and ATP-linked respiration was observed, aligning with decreased ATP levels and mitochondrial membrane potential reported earlier in sulfite-accumulating cells (Mellis et al., 2021; Vincent et al., 2004; Zhang et al., 2004). Previously a sulfite-dependent contribution of ~10% was reported, attributed to the SOX-dependent reduction of cytochrome *c* (Kaczmarek, 2019). The reduction observed in this work exceeds this effect, suggesting a more systemic impact of SOX-deficiency on OXPHOS beyond funneling electrons to complex IV via cytochrome *c* reduction.

Further mechanistic insights were obtained via high-resolution respirometry of isolated mitochondria from SOX-deficient MEFs (Figure 9). These mitochondria exhibited a substantial reduction in oxygen consumption, particularly in response to ADP and succinate, indicating impaired activity of complexes II and V. Maximal respiratory capacity induced by FCCP was significantly diminished, confirming that the bioenergetic reserve was also compromised. Importantly, these defects were not attributable to loss of mitochondrial integrity, as shown by preserved response to cytochrome *c*.

To investigate whether structural deficits in respiratory complexes underlie these functional impairments BN-PAGE analysis was conducted (Figure S2). However, both BN-PAGE and subsequent Western blotting of enriched mitochondria revealed no consistent alterations in the assembly or steady-state levels of OXPHOS complexes between WT and SOX-deficient samples. The observed technical variability and limited resolution did not allow to draw a

reliable conclusion regarding respiratory complex formation. Thus, protein expression levels were analyzed alternatively using the more sensitive proteomic analysis, which also allows for broader protein expression profiling.

Proteomic profiling supported the functional data, identifying widespread downregulation of proteins involved in OXPHOS and the TCA cycle (Figure 11). Notably, 90 proteins related to ETC complexes,17 assembly factors and 10 proteins associated with OXPHOS were reduced. TCA cycle components - including PDH, MDH, CS, Aco, IDH, αKDH, SDH and FH - were similarly downregulated, highlighting a systemic impairment of mitochondrial energy metabolism in response to SOX loss. Particular proteomic changes will be discussed in more detail in the next chapters, including CoQ biosynthesis, respiratory complex assembly, TCA metabolism and glycolysis.

The data within this work showed that SOX-deficient mitochondria exhibit downregulation of several CoQ biosynthesis-related proteins, including Coq3, Coq5, Coq6, Coq8b, Coq9, and Coq10b (Figure 11, Table S1).Previous proteomic analyses of five knockout mouse strains deficient in essential factors required for mitochondrial DNA gene expression, leading to OXPHOS dysfunction, revealed a secondary CoQ deficiency in mammals (Kühl et al., 2017). Specifically, reduced levels of multiple proteins critical for CoQ biosynthesis were identified, including Coq3, Coq5, Coq6, Coq7, Coq8A, Coq9, and Coq10A. The authors proposed two potential underlying mechanisms. Either CoQ biosynthesis is actively downregulated to match the reduced demand from dysfunctional respiratory chain complexes, or OXPHOS impairment compromises inner mitochondrial membrane integrity, leading to destabilization of the CoQ biosynthetic complex. This suggests that the mitochondrial dysfunction resulting from SOX loss observed in this work may similarly impact CoQ biosynthesis, either through a regulatory feedback mechanism or through structural destabilization of membrane-associated biosynthetic machinery. Interestingly, CoQ levels were found to be increased in SOXD liver extracts (unpublished results, Fu et al.) This unexpected increase in CoQ levels in SOX-deficient liver may reflect tissue-specific compensatory mechanisms. One possibility is that post-translational regulation, such as decreased persulfidation of CoQ8B in SOXD, enhances the specific activity of the remaining biosynthetic machinery (Fu et al., 2024b). Alternatively, reduced respiratory chain activity could slow CoQ turnover, resulting in net accumulation. These hypotheses suggest that the regulation of CoQ homeostasis in response to mitochondrial dysfunction is more complex and may vary across tissues.

Interestingly, this study revealed that several members of the fas-activated serine/threonine kinase domain-containing (FASTKD) protein family were upregulated in SOX-deficient mitochondria (Table S4). These proteins have been implicated in supporting mitochondrial translation and respiratory complex assembly under stress conditions and their induction may

reflect a compensatory response to the bioenergetic and structural challenges posed by SOX deficiency (Jourdain et al., 2017; Ohkubo et al., 2021; Simarro et al., 2010).

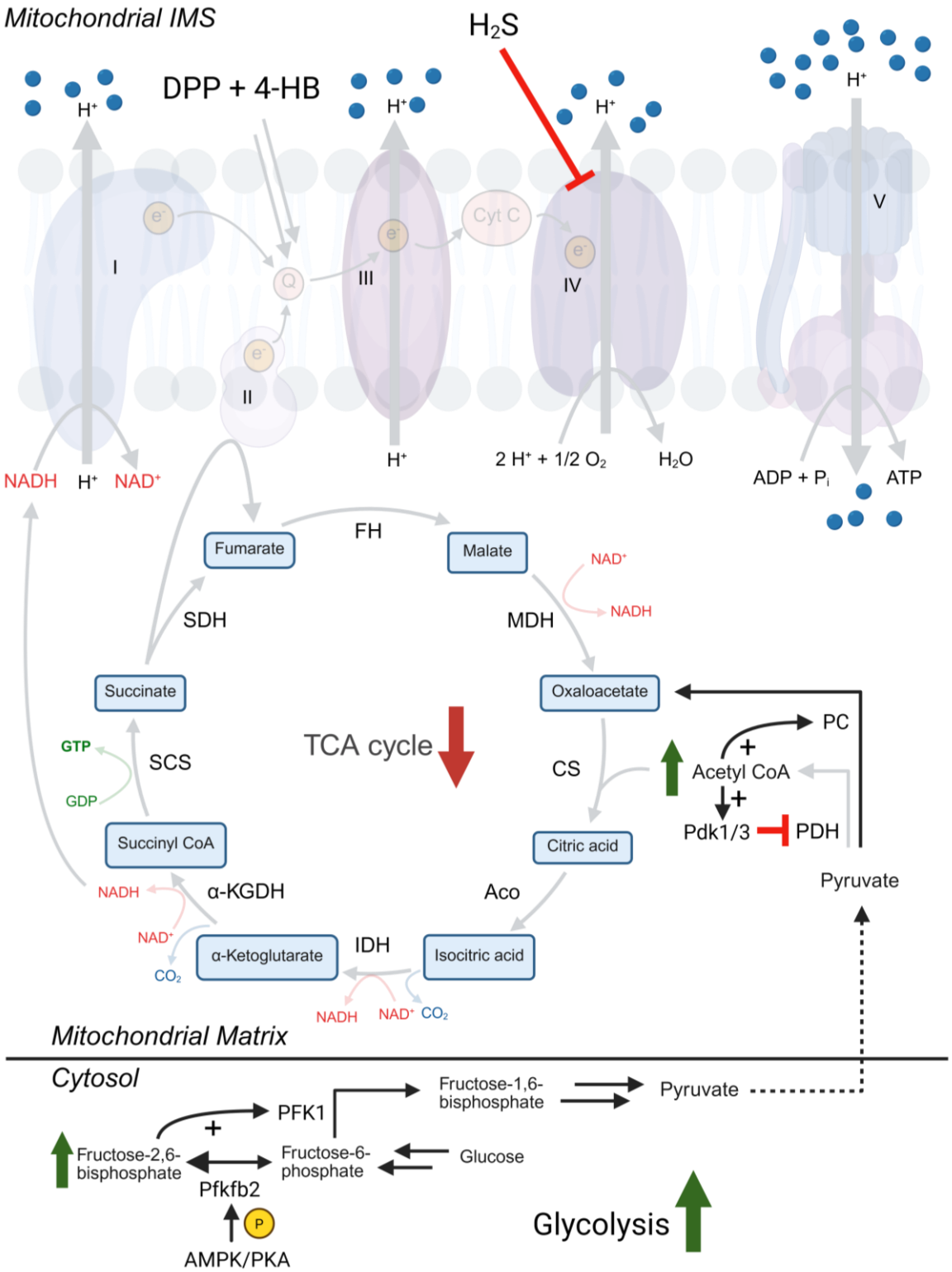

Figure 25: Metabolic rewiring in mitochondria upon loss of SOX.
Loss of SOX leads to H_2S-mediated inhibition of complex IV and downregulation of OXPHOS complexes, inducing a metabolic rewiring to meet cellular energy demands. AMPK/PKA-mediated phosphorylation of Pfkfb2 elevates fructose-2,6-bisphosphate, stimulating Pfk1 and enhancing glycolysis. Additionally, TCA cycle enzymes are downregulated by a yet unknown mechanism, resulting in Acetyl-CoA accumulation, activating Pdk1/3 and PC, inhibiting PDH and shifting pyruvate metabolism from oxidative decarboxylation to anaplerotic carboxylation to maintain TCA cycle flux. In parallel CoQ biosynthesis is downregulated in response to OXPHOS dysfunction.

In addition, Pdk1, Pdk3, and pyruvate carboxylase (PC) were found to be upregulated in SOX-deficient mitochondria (Figure 11, Table S1, Table S4). Both Pdk isoforms and PC are known to be activated in response to elevated acetyl-CoA levels, promoting a metabolic shift away from oxidative decarboxylation toward carboxylation of pyruvate to oxaloacetate (Jitrapakdee et al., 2008; Kim et al., 2006; Koh et al., 2022).

Specifically, Pdk1/3 phosphorylates and inhibits PDH, suppressing conversion of pyruvate into acetyl-CoA, while PC catalyzes the carboxylation of pyruvate into oxaloacetate to maintain TCA cycle flux. These co-regulated changes suggest that SOX-deficient mitochondria may accumulate acetyl-CoA, potentially due to reduced TCA turnover, thus triggering upregulation of both Pdk1/3 and PC as compensatory responses to preserve cycle activity.

Furthermore, a significant upregulation of Pfkfb2 was observed alongside its upstream regulatory kinases PKA (Prkar1a, Prkar2a, Prkar2b) and AMPK (Prkaa1) (Table S4, Table S5). Pfkfb2 is a bifunctional enzyme that governs levels of fructose-2,6-bisphosphate (Fru-2,6-P_2), a potent allosteric activator of glycolysis through its action on phosphofructokinase-1 (Ros and Schulze, 2013). Phosphorylation by PKA or AMPK at conserved C-terminal sites (e.g. Ser466/Ser483) shifts Pfkfb2 toward its kinase activity, boosting F2,6BP synthesis and enhancing glycolytic flux (Marsin et al., 2000; Pozuelo Rubio et al., 2003). These coordinated changes suggest an additional rescue mechanism of SOX-deficient cells, by upregulation of glycolysis to compensate for impaired OXPHOS.

To confirm that the observed mitochondrial impairment was not restricted to cultured fibroblasts, analyses were extended to liver mitochondria isolated from SOX-deficient mice. High-resolution respirometry of enriched hepatic mitochondria revealed a consistent – but due to limited data quantity - non-significant reduction of about 20% in oxygen consumption across all substrate conditions compared to wild-type controls (Figure 10). These findings suggest that the results observed in MEFs extend to *in vivo* conditions and SOX-dependent bioenergetic defects extend to metabolically active organs. Analysis of later time points than P2 (e.g. P6) might reveal more drastic changes, due to accumulated damage in tissues, as observed for enlarged alveolar spaces at P6 (Fu, 2023).

A similar respiratory phenotype was observed in primary hippocampal cultures from SOX-deficient mice. At DIV14, Seahorse-based analysis revealed a uniform reduction of about 25% in basal, maximal, ATP-linked respiration, and spare respiratory capacity (Figure 20). Given the brain's high energy demand-especially during neurodevelopment, these mitochondrial deficiencies likely contribute to the observed reductions in areas spanned by astrocyte and neuron (Figure 17), which will be discussed in a later section (3.5).

In summary, this work demonstrated impaired mitochondrial respiration *in organello*, *in cellulo* and *ex vivo.* In aggregate, this work demonstrated reductions of 20-25 % in basal, ATP-linked, and maximal respiration rates across fibroblasts, hepatocytes, and neurons, exceeding the expected impact raised by previous reports of direct SOX-mediated respiration (Kaczmarek, 2019). These functional deficits correlate with widespread proteomic downregulation of OXPHOS and TCA cycle components, revealing systemic mitochondrial impairment and metabolic reprogramming in the absence of SOX (Figure 25). This metabolic rewiring supports the observed metabolic switch in SOXD mice induced by the inhibition of complex IV by H_2S (Carballal et al., 2021; Fu et al., 2024b). Here, a reduction in complex IV activity was not observed, however the contribution of complex IV inhibition to the decreased basal respiration in SOX-deficient MEFs cannot be excluded (Figure 8). Furthermore, high resolution respiratory measurements with enriched mitochondria might be unsuitable to monitor H_2S-dependent complex IV inhibition considering the short life time of this impairment in cell-free systems of only 10-30 minutes (Borisov and Forte, 2021; Di Meo et al., 2011). In addition to the H_2S mediated metabolic rewiring, the elevated sulfite levels could exacerbate the mitochondrial dysfunction by inhibiting MDH and glutamate dehydrogenase (Grings et al., 2014; Zhang et al., 2004).

3.2 SOX-dependent nitrite reduction reduces mitochondrial respiration

The identification of SOX as a mitochondrial nitrite reductase opens new avenues in redox biology. Short-term nitrite and sulfite exposure experiments revealed that SOX-dependent NO production modulates mitochondrial spare respiratory capacity (Figure 13). Sulfite alone enhanced spare capacity in WT cells, but not in SOX-deficient MEFs. This effect was abolished by co-treatment with nitrite, showing opposing SOX-dependent effects of nitrite and sulfite treatments. This observation indicates that both functions of SOX, sulfite oxidation and nitrite reduction, respectively, reciprocally modulate mitochondrial respiration. In line with this, previous studies reported a reciprocal regulation of sulfite oxidation and nitrite reduction (Kaczmarek et al., 2019).

These findings suggest that SOX operates not only as a metabolic enzyme but also as a redox sensor, modulating mitochondrial dynamics in response to nitrite availability. The increase in spare respiratory capacity upon sulfite exposure is likely attributed to the increase of electron flow into the ETC through SOX-dependent cytochrome *c* reduction (Kaczmarek, 2019).

For nitrite reduction two principal mechanisms can be proposed. On the one hand, nitrite might compete with sulfite for the binding site within SOX, but previous reports showed that SOX has an about ten-fold higher affinity for sulfite and only prefers nitrite under hypoxic or low pH

conditions (Bender et al., 2019b; Kaczmarek et al., 2019; Wilson and Rajagopalan, 2004). Thus, a second explanation appears feasible targeting SOX-mediated NO-production which may involve multiple mechanisms. On the one hand, NO was shown to inhibit Aco2 and PDH, which result in reduced electron flow from the TCA cycle (Castro et al., 1998; Palmieri et al., 2020; Stadler et al., 1991; Yan et al., 2012). Particularly PDH was shown to be important for the regulation of the spare respiratory capacity in a complex II-mediated fashion (Pfleger et al., 2015). On the other hand, NO may directly inhibit complexes of the ETC. In the context of short-term NO exposure, reversible inhibition of complex IV is well-documented (Bolaños et al., 1994; Brown and Cooper, 1994; Clementi et al., 1998). However, in the present study, the NO-mediated effects on respiration only emerged upon ETC uncoupling, suggesting a modest degree of inhibition under basal conditions. While this experiment was based on short-term nitrite exposure, chronic NO exposure was also shown to inhibit mitochondrial respiration, mainly mediated by S-nitrosylation of ETC complexes (Ramachandran et al., 2004).

Long-term nitrite exposure experiments revealed only tendencies in changes of the OCR. In cells expressing functional human SOX, nitrite slightly reduced mitochondrial respiration, however changes did not reach the critical level of significance (Figure 14). The ability of rotenone to eliminate the respiration differences suggests a complex I mediated mechanism. This aligns with previous findings describing S-nitrosylation-mediated impairment of complex I during prolonged NO exposure (Bolaños et al., 1994; Clementi et al., 1998). Strikingly, SOX-deficient cells responded contrary to SOX expressing ones, with a modest, non-significant rise in oxygen consumption (Figure 14, Figure S5). This increase could originate from enhanced mitochondrial connectivity. In the absence of nitrite reduction by SOX, these cells were likely to accumulate higher nitrite levels, which may activate PKA to phosphorylate and inhibit Drp1 - particularly at Ser656. This inhibition would suppress mitochondrial fission and promote fusion, yielding elongated mitochondrial networks with increased respiratory capacity, as previously documented (Pride et al., 2014).

Taken together, the effects of short-term nitrite treatment are rather minor while long-term nitrite treatment only revealed tendencies. However, it is plausible that these mechanisms become more pronounced under hypoxic conditions, where SOX-dependent nitrite reduction is favored and NO production increases (Kaczmarek, 2019). Thus, the physiological relevance of SOX as a nitrite reductase may be most prominent during hypoxic stress, where its role in maintaining redox balance and tuning mitochondrial respiration could be critical. In this context, the reciprocal regulation of sulfite oxidation and nitrite reduction by SOX, along with their opposing effects on the ETC, may act as a metabolic switch in response to low oxygen levels or decreased pH (Figure 26). Under normal conditions SOX catalyzes sulfite oxidation, funneling electrons into the ETC and enhancing spare respiratory capacity. Conversely, under

hypoxic conditions such as during ischemia or if the pH in the IMS drops, potentially due to increased activity of ETC complexes I-III, nitrite reduction by SOX is favored. Thus, the sulfite oxidation function of SOX is inhibited and NO production increased, resulting in reduced mitochondrial respiration. During ischemia this switch may serve as a protective mechanism by limiting ROS generation upon reoxygenation (Abe et al., 2009; Granger and Kvietys, 2015). Similarly, under low pH conditions, the functional shift of SOX toward NO production may provide feedback inhibition of ETC complexes, thereby reducing ROS formation resulting from ETC overactivation.

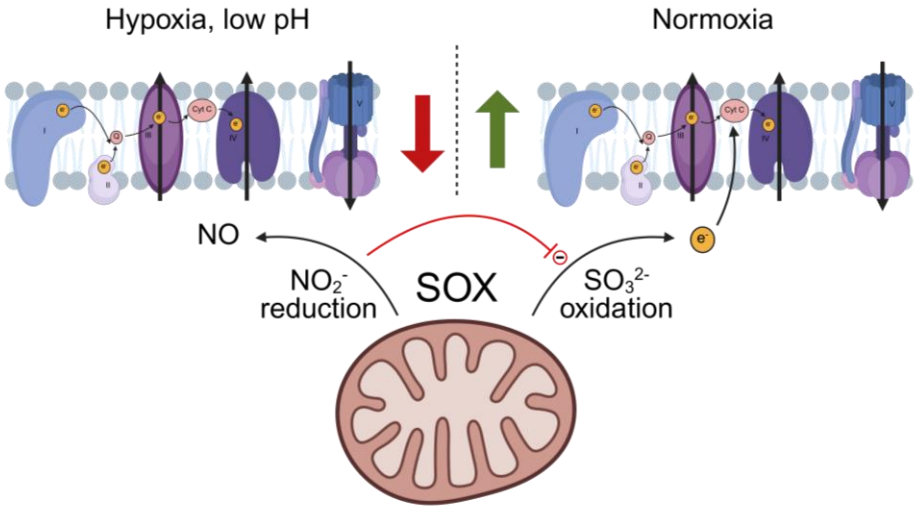

Figure 26: Reciprocal regulation of SOX function and its postulated influence on mitochondrial respiration.
Under normoxic conditions SOX-dependent sulfite oxidation promotes mitochondrial respiration by funneling electrons toward cytochrome *c*. In contrast, under hypoxic conditions or if the pH drops, nitrite reducting function of SOX is favored, decreasing mitochondrial respiration by a) inhibiting sulfite oxidation and b) inhibiting ETC complexes by NO production.

3.3 SOX loss alters extracellular matrix composition

While in human patients SOXD results in early childhood death due to severe neurodegeneration, these symptoms are absent in the recently development mouse model for SOXD and the main cause of death remains unclear (Fu et al., 2024b; Shih et al., 1977). Two known symptoms of these mice are enlarged alveolar spaces and a skin barrier defect (Fu et al., 2024b; Johannes, 2023). On the one hand, the reported enlarged alveolar airspaces were hypothesized to result from decreased ECM protein expression collagen I and III due to elevated sulfite levels (Fu, 2023). Since type I and III collagens compose the alveolar wall and alveolar septa, their reduction would directly compromise pulmonary structural integrity (Ito et al., 2019; Sobin et al., 1988). On the other hand, the mechanism underlying the skin barrier defect is yet unknown, but proper ECM integrity was shown to be crucial for intact skin

development and wound healing (Bhattacharjee et al., 2019; Bouwstra et al., 2021; Dong et al., 2025).

Interestingly, whole-cell proteome analysis within this work revealed that SOX deficiency also affected the ECM. In total 36 ECM-associated proteins were affected, 32 were downregulated and 4 were upregulated (Figure 12, Table S3). Importantly the ECM is a critical component of fibroblasts identity and function (Figure 12) (Frantz et al., 2010; Plikus et al., 2021).

SOX could influence ECM integrity at two stages. First, a mechanistic link between SOX activity and ECM regulation could be mediated through sulfate bioavailability and protein sulfation. Second, loss of SOX results in sulfite accumulation, which is known to disrupt disulfide bonds, which are crucial elements for ECM integrity.

Loss of SOX activity results in decreased sulfate levels. In turn, a decrease in PAPSS2 expression was identified, the key enzyme synthesizing PAPS, the universal sulfate donor for sulfation reactions (Dejima et al., 2006). Sulfation is essential for modifying proteoglycans such as syndecans and heparan sulfates, which are critical components for ECM organization, cell adhesion and growth factor signaling (Chapman et al., 2004; Ravikumar et al., 2020; Soares Da Costa et al., 2017). In line with this, sulfate containing proteoglycans such as syndecan-2 and versican were downregulated in SOX-deficient cells, suggesting impaired post-translational modification and ECM maturation.

Secondly, sulfite accumulation is known to chemically disrupt disulfide bonds, which are crucial for the structural integrity of ECM proteins, particularly collagens (Bächinger et al., 1980; Ilani et al., 2013). This is underlined by proteomic analyses revealing a marked reduction in the expression of disulfide-bond dependent collagen type I (Sharma et al., 2017), III (Boudko et al., 2008), V (Foidart et al., 1981) and XII (Chiquet et al., 2014). While direct data on collagen expression levels in fibroblasts is limited, studies on placental tissue demonstrate that type I and III collagens account for the majority of collagenous protein, while type V collagen contributes with approximately 20% (Foidart et al., 1981). Collagens I and III are the major structural components of the ECM, with collagen I forming thick densely packed fibrils providing tensile strength and collagen III demonstrating greater flexibility and elasticity (Singh et al., 2023). Collagen V regulates the nucleation and initial assembly of collagen fibrils, playing a critical role in controlling fibril diameter and organization (Wenstrup et al., 2004). Collagen XII belongs to the fibril-associated collagens with interrupted triple helices (FACIT) family and regulates the organization and mechanical properties of fibril bundles through its interaction with heterotypic fibrils (Gregory et al., 2024; Izu et al., 2011).

In sum, these findings indicate a downstream effect of SOX loss on ECM integrity due to sulfite accumulation. Since fibroblasts are the major cells responsible for ECM production and

turnover the results of this work are relevant to improve the understanding of the pathophysiology of SOX deficiency (Ito et al., 2019). The dual mechanism of impaired proteoglycan sulfation and disrupted collagen stability provides a comprehensive explanation for the observed ECM dysfunction and its potential contribution to the pulmonary pathology observed in SOX-deficient models. Furthermore, a contribution toward the observed skin barrier defect is likely. Nevertheless, further studies are required to decipher the complete consequences of reduced expression of ECM components in SOX-deficiency on ECM structure and function.

3.4 SOX is important to maintain cardiac function under stress conditions

In recent years the role of SOX as a nitrite reductase gained increased attention (Bender and Schwarz, 2018; Christie et al., 2023; Kaczmarek et al., 2019). Especially, the recent study on astrocytes shed light on SOX function during hypoxic vasodilation (Christie et al., 2023). While NOS enzymes are the classical source of NO during normoxic conditions, NOS activity is absent during hypoxia and alternative enzymatic pathways, including SOX, become critical to maintain NO levels. This work provides both, biochemical and physiological evidence supporting the relevance of SOX in this process, more specifically under stress conditions of HFpEF and PH, conditions under which NO bioavailability is impaired and vascular reactivity altered.

The HFpEF-PH mouse model, established through high-fat diet, NOS inhibition, and chronic hypoxia, enabled to study the contribution of SOX to NO-mediated vasodilation under conditions that mirror the human disease phenotype (Schiattarella et al., 2019). Consistent with literature, an increased SAP was observed in HFpEF mice and a pronounced hypoxia-induced increase was found in RVSP and fulton index, indicating pulmonary hypertension and right ventricular (RV) hypertrophy (Figure 15) (Gomez-Arroyo et al., 2012; Schiattarella et al., 2019; Zhang et al., 2022). While WT and *SUOX*$^{+/-}$ mice showed similar trends in RVSP elevation under PH or HFpEF-PH conditions, *SUOX*$^{+/-}$ mice uniquely exhibited a significantly greater fulton index under HFpEF-PH conditions. Interestingly, mice of both genotypes are stressed by increased RVSP, but the unique increase in *SUOX*$^{+/-}$ mice in fulton index suggests differences in the response to that stress. This finding points to an exacerbated RV hypertrophy and cardiac remodeling when SOX activity is partially compromised. The underlying mechanism could involve two different well known pathways involved in cardiac remodeling: the beta-adrenoceptor (β-AR) signaling pathway or the cGMP signaling pathway (Figure 27) (Numata and Takimoto, 2022; Ziolo et al., 2008).

First, challenging mice with HFpEF and PH activates the sympathetic nerve activity and induces the β-AR signaling pathway, which results in increased cardiac contraction and heart rate (Fu et al., 2012; Mak et al., 2012; Velez-Roa et al., 2004). While in WT mice, this pathway is balanced by NO signalling, the impaired NO signalling in $SUOX^{+/-}$ mice leads to overactivated β-AR signalling, which ultimately results in increased cardiac remodelling, indicated by the increased fulton index (Figure 15) (Fu et al., 2012; Ziolo et al., 2008).

Second, HFpEF and PH are associated with the activation of transforming growth factor-β (TGF-β), which results in cardiac fibrosis and remodelling (Kapur, 2011; Liu et al., 2017). The activation of guanylate-cyclase by NO, producing cGMP and thus activating protein kinase G (PKG) was shown to inhibit the TGF-β signalling pathway (Li et al., 2008; Numata and Takimoto, 2022). Since NO homeostasis is impaired in $SUOX^{+/-}$ mice, TGF-β signalling is dysregulated, resulting in the increased cardiac remodelling observed in these mice (Figure 15).

Both postulated mechanism are supported by the detected SOX expression in the heart in mice, as well as in humans (Kohl, 2019; Uhlén et al., 2015 (proteinatlas.org)). Notably, *$SUOX^{+/-}$* mice are phenotypically indistinguishable from their WT litter mates under normal baseline conditions, thus the results of this work likely underscore the importance of SOX-dependent nitrite reduction for hypoxic vasodilation. Future studies should focus on the postulated role of SOX in regulation of the TGF-β and β-AR signaling pathways. Furthermore, H/E staining of the heart could reveal further differences in tissue morphology. More specific staining such as Masson's trichrome or picrosirius red could help to visualize cardiac fibrosis in challenged SOX impaired mice. Here the studies should be expanded by using inducible and/or tissue specific SOX-deficient mice.

The results within this work support the view that SOX plays a protective and compensatory role under hypoxic conditions, where canonical NO production by NOS enzymes is absent. These observations are in line with previous reports highlighting the role of SOX for the cerebral blood flow during hypoxia and the favorable NO production under these conditions (Christie et al., 2023; Kaczmarek, 2019).

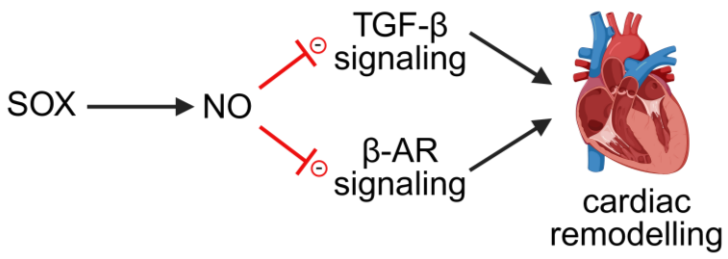

Figure 27: Postulated role for SOX in cardiac remodeling under hypoxic conditions.
Under hypoxic stress conditions, SOX-dependent NO production inhibits TGF-β and/or β-AR signaling, thus regulating cardiac remodeling.

To investigate the growing evidence that SOX is essential for vasodilation during hypoxic conditions, this study aimed to gain further insights into the underlying mechanisms. Previous reports hypothesized that cytochrome *c* may serve as an electron donor to SOX during brain hypoxia, thus an *in vitro* assay was established in this work to test this hypothesis (Christie et al., 2023). The concentration of SOX within the IMS was estimated to be about 50 µM, while for cytochrome *c* concentrations ranging from 0.5-1 mM are reported, thus the ratio used in this study with 50 µM SOX and 1.6 mM cytochrome *c* resembled physiological conditions (Efstathiou, 2016; Forman and Azzi, 1997; Pasdois et al., 2011). Spectroscopic analyses revealed that reduced cytochrome *c* could indeed partially reduce SOX, as indicated by a spectral shift through reduction of the heme center. With the partial reduction of about 30%, these results support the idea of a reverse electron transfer from cytochrome *c* to SOX. This hypothesis is further supported by the proposal of SOX accepting electrons from the ETC during mitochondrial stress such as during hypoxia. Notably, a full pre-reduction of cytochrome *c* was not achieved, thus the results likely underscore the potential of SOX reduction by cytochrome *c*.

In summary, this work provides both physiological and mechanistic evidence for the role of SOX in adaptation to hypoxic stress conditions by mediating cardioprotective under HFpEF-PH conditions. Future studies should explore full-body or tissue-specific inducible SOX knockout models to investigate the total contribution of SOX-dependent nitrite reduction during hypoxia.

3.5 SOX plays a key role for neuronal development

The characterization of SOX-deficient hippocampal neuronal cultures provides new insights into the pathophysiology of MoCD and SOXD, particularly with regard to brain development and neurodegeneration. This cell culture model allows to overcome the early postnatal lethality observed *in vivo* by extended *in vitro* cultivation, enabling the analysis of later developmental and metabolic events in SOXD (Fu et al., 2024b).

A key observation from the experiments performed was the significant reduction in both neuronal and astrocyte areas in *SUOX*$^{-/-}$ cultures (Figure 17). This reduction is consistent with the neurodevelopmental and neurodegenerative phenotypes observed in SOXD patients (Claerhout et al., 2018). With this an impaired neuronal phenotype was observed even of the murine SOXD model. Strikingly, within this work the pathomechanism causing neurodegeneration was absent in these neuronal cultures, suggesting a different, yet unknown, underlaying mechanism. Previously, neuronal impairments of SOXD were linked to SSC-mediated excitotoxicity hallmarked by increased SSC levels and gephyrin cleavage (Kumar et al., 2019). But this work showed a preliminary reduction in total gephyrin levels

instead of increased gephyrin cleavage in *SUOX*$^{-/-}$ cultures (Figure 18). In line with this absent gephyrin cleavage, no significant elevation in sulfite or SSC levels in *SUOX*$^{-/-}$ culture media compared to controls were found (Figure 19).

This discrepancy points to potential differences between sulfur metabolite-dependent pathogenicity of human patients (*in vivo*) and the used murine cell culture model (*in vitro*) suggesting SSC-independence. One explanation might be that *in vivo* brain-active SSC emerges either from the periphery or is sufficiently produced by the brain itself, which is excluded from isolated cell culture. However, since gephyrin is the main scaffolding protein at inhibitory synapses, the observed reduction of total gephyrin levels could be the result of decreased synapse formation in SOX-deficient cells, further supported by the decreased cell confluency (Figure 17) (Choii and Ko, 2015; Kirsch et al., 1993). In conclusion SOX-deficient neurons also showed impairments of gephyrin levels, although not raised by SSC-mediated cleavage.

Looking for an SSC-independent explanation for the observed neuronal impairments, further sulfur metabolites in the culture media as well as mitochondrial respiration were analyzed. Thiosulfate, the catabolic oxidation product of H_2S, was moderately elevated, supporting previous findings about H_2S accumulation in the absence of functional SOX (Fu et al., 2024b). One mode of action of elevated H_2S is the inhibition of cytochrome *c* oxidase (Tiranti et al., 2009). Importantly, the analysis revealed profound mitochondrial dysfunction in SOX-deficient hippocampal cultures, as demonstrated by significantly reduced mitochondrial respiration of about 25% (Figure 20). These findings are consistent with earlier observations within this work in SOX-deficient MEFs and suggest consistent mitochondrial impairment across various cell types.

Neurons exhibit exceptionally high energy demands, particularly during periods of synaptogenesis and network maturation, processes that are critically dependent on ATP production via OXPHOS (Chang et al., 2006; Herculano-Houzel, 2011; Shulman et al., 2004; Vergara et al., 2019; Zheng et al., 2016). Impairments in OXPHOS may serve as a primary driver of neurodevelopmental deficits in SOXD, independent of SSC-mediated toxicity. Instead, elevated H_2S levels may play a more prominent role, resembling the pathomechanisms observed in ethylmalonic encephalopathy (EE) or sulfide:quinone oxidoreductase deficiency (SQORD) (Kožich et al., 2022). Both diseases were reported with increases in H_2S levels. SQORD is characterized by mutations in the *SQOR* gene encoding the mitochondrial enzyme SQR, which oxidizes H_2S to persulfides (Jackson et al., 2012; Lagoutte et al., 2010).

In EE, mutations in the *ETHE1* gene, coding for the enzyme PDO which converts persulfides into thiols and sulfite, result in persulfide accumulation (Kabil and Banerjee, 2012). These persulfides are further metabolized by thiosulfate sulfurtransferase yielding thiosulfate. Both

disease are characterized by neurodegeneration and neurological symptoms such as psychomotor delay and spasticity (Friederich et al., 2020; Grings et al., 2020). In addition, both diseases share a marked reduction in complex IV activity, indicating impaired OXPHOS involvement in the pathomechanism. (Friederich et al., 2020; Sathe et al., 2021; Tiranti et al., 2009).

Broadly, OXPHOS dysfunction is a hallmark of numerous neurodevelopmental and neurodegenerative disorders, including leigh syndrome (Distelmaier et al., 2009; Ruhoy and Saneto, 2014), rett syndrome (Gibson et al., 2010; Kriaucionis et al., 2006), angelman syndrome (Su et al., 2011) and Alzheimer‘s disease (AD) (Rapoport, 2003; Sonsungsan et al., 2024). While the reduction of about 25% in mitochondrial respiration observed in this study is less severe than that reported in Leigh syndrome (about 65%) (Uittenbogaard et al., 2021), it closely mirrors the reductions observed in AD (about 20%) (Hatanpää et al., 1996; Maynard et al., 2015). These findings support the hypothesis that mitochondrial dysfunction contributes significantly to the neurodevelopmental abnormalities observed in SOXD.

Together, the findings of this work suggest that in hippocampal cultures, SOX deficiency predominantly affects mitochondrial function. The *in vitro* system provides a valuable tool to dissect early cellular and metabolic impairments and may represent an earlier stage of disease progression before toxic metabolite accumulation reaches neurotoxic thresholds. Nevertheless, the discrepancies between this cell culture model and previously reported findings *in vivo* underscore the need to consider both models in parallel or SOXD-inducible models to fully understand SOXD pathophysiology and allow for the development of therapeutic strategies.

3.6 Regulatory mechanisms modulating SOX activity and their therapeutical potential

As stated earlier, up to date, only MoCD type A can be treated with cPMP, with the only option to treat SOXD so far is to reduce the symptoms by dietary (Abe et al., 2021; Boles et al., 1993; Touati et al., 2000). Recent data suggest that treatment with glutathione disulfide (GSSG) and glutathione trisulfide (GSSSG) can extend the lifespan of SOXD mice by two and three days, respectively, offering a potential therapeutic strategy by targeting oxidative stress and sulfur metabolism (Fu et al., 2024a). The regulation of SOX activity represents an attractive target to develop therapeutic strategies for SOXD. Our findings highlight two independent but converging pathways that modulate SOX function. On the one hand, the elevation of Moco levels by increased Moco biosynthesis through MOCS1AB overexpression and molybdate supplementation. On the other hand, the post-transcriptional regulation of SOX expression via the mRNA-binding protein CLUH.

3.6.1 Moco availability is a limiting factor of SOX activity

In line with previous studies, we show that molybdate supplementation, in combination with MOCS1AB overexpression, significantly increases SOX activity in both WT and patient-derived R366H variant (Figure 21) (Bender et al., 2019a). This suggests that Moco biosynthesis and availability are key rate-limiting factors for SOX function. MOCS1A/B catalyze the first and rate-limiting step in Moco biosynthesis, thus their overexpression likely results in elevated Moco levels (Hänzelmann et al., 2002). The marked three-fold increase in activity for SOX WT and R366H variant supports the therapeutic potential of targeting Moco biosynthesis for patients with residual SOX activity. However, to date, the mechanisms regulating MOCS1A/B gene and protein expression remain unknown, which complicates potential therapeutic strategies. One possible approach to increase their protein levels is gene replacement therapy. This method could also be used to directly restore SOX expression. Therefore, targeting Moco biosynthesis via MOCS1A/B in combination with SOX supplementation, may improve therapeutic outcomes or provide an alternative when direct SOX targeting proves insufficient.

3.6.2 CLUH controls SOX protein activity

CLUH was identified as a post-transcriptional regulator of mitochondrial mRNAs, including SOX (Gao et al., 2014; Schatton et al., 2017). This study revealed its functional impact on SOX activity and expression (2.5.2). Loss of CLUH in mouse liver and FlpIn^{TM} cells leads to a substantial decrease in SOX activity, confirming a positive impact on SOX by CLUH (Figure 22, Figure 23). Consequently, CLUH overexpression increased SOX activity, suggesting that CLUH abundance directly influences the translation or stability of SOX mRNA and its subsequent mitochondrial localization or maturation. This is particular interesting for Moco-binding deficient SOX variants, since the absence of Moco results in degradation and thus decreased SOX activity. Importantly, Moco-binding deficient patient variants such as R366H and G362S showed non-significant but consistent increases in activity upon CLUH overexpression, which might be sufficient to improve SOXD conditions (Figure 24) (Bender et al., 2019a; Kaczmarek et al., 2022).

Although modest, these increases suggest that regulation of SOX on mRNA level by CLUH potentially supports residual SOX activity and highlights CLUH as a new potential target for therapeutical approaches. However, plasmids were used only containing the non-coding regions for hSOX variants expression, lacking the 3’ and 5’ untranslated regions (UTR). To date there is no known binding sequence of CLUH, but other studies revealed common binding motifs for RNA-binding proteins to be present in the 3’ UTR (Dassi et al., 2013; Plass et al., 2017). Thus, this work might be limited to indirect effects and underscores the potential of CLUH to restore SOX activity in patient variants. In addition, CLUH is known as a key regulator

of mRNA translation for a specific subset of mitochondrial proteins, particularly those involved in bioenergetic processes (Gao et al., 2014; Schatton et al., 2017). Since a reduction in mitochondrial bioenergetics in SOX-deficient cells was also observed, targeting CLUH could simultaneously address two mechanisms contributing to the pathogenesis of SOXD. On the one hand, targeting CLUH could improve mitochondrial bioenergetics by upregulating a subset of proteins involved in the mitochondrial metabolism. On the other hand, SOX activity could be improved, thus attenuating the decreased mitochondrial dysfunction upon loss of SOX activity.

In sum, our findings revealed two new therapeutic approaches to control SOX activity in SOXD. To date, SOXD treatments are limited to dietary sulfite restrictions (Schwarz et al., 2025; Touati et al., 2000). Targeting Moco supply and SOX translation via molybdate, which increases Moco availability, and MOCS1A/B or CLUH, respectively, offers approaches targeting the underlying mechanism (Bender et al., 2019a). A recent study by Kaczmarek et al. identified 15 new pathogenic SO missense variants, amongst these 7 exhibited residual SOX activity, highlighting the growing need for SOXD therapy and underlining the potential of the here described mechanism-based therapeutic approaches (Kaczmarek et al., 2021). However, there are still limitations of these approaches, since they only target SOX variants with deficient Moco-binding by either increasing their expression or increasing Moco availability. In contrast, other variants are not degraded but show normal expression levels and also exhibit unaltered Moco-binding. Nevertheless, further studies are required to validate these findings *in vivo*.

4 Conclusion and future perspectives

This work highlighted a multifaceted role of SOX in mammalian physiology beyond its canonical function in cysteine catabolism. Through a combination of biochemical, proteomic, and physiological analyses, it was demonstrated that SOX plays a pivotal role not only in sustaining mitochondrial bioenergetics but also in contributing to nitrite-dependent NO production, particularly under hypoxic conditions.

Loss of SOX function was shown to impair OXPHOS, alter mitochondrial proteome composition by downregulating OXPHOS and TCA cycle enzymes, and disrupt expression of extracellular matrix components, highlighting its critical involvement in cellular energy homeostasis and structural integrity. Based on the proteomic changes and impairment in mitochondrial dysfunction, this thesis provides a model of metabolic rewiring taking place in mitochondria upon loss of SOX. The observed defects in multiple tissues, including liver, heart, and hippocampal neurons, underscore the systemic relevance of SOX, providing broader understanding of the role of SOX for mitochondrial bioenergetics as well as the mechanisms underlying the observed mitochondrial dysfunction in SOXD.

Furthermore, the identification of cytochrome *c* as a putative electron donor for SOX under anaerobic conditions provides a mechanistic explanation for oxygen-independent NO production, with important implications for hypoxic stress adaptation, particularly in the context of HFpEF. Here loss of SOX-dependent NO production is suggested to result in malfunctional cardiac remodeling by impaired regulation of either ß-AR or TGF-β signaling or a combination of both. For the first time this underlines the physiological importance of SOX-dependent NO production.

Additionally, this work established a new SOX-deficient cell culture-based murine model system allowing the exploration of the neuronal phenotype observed in human SOXD patients, which is absent in $SUOX^{-/-}$ mice. SOX was found to be essential for proper neuronal and astrocytic development. Its loss led to impaired mitochondrial respiration in neuronal cultures, independent of SSC accumulation. Instead, the dysfunction is likely driven by H_2S-mediated impairment of OXPHOS, suggesting a contribution of mitochondrial dysfunction toward the neurodegeneration in SOXD patients.

Looking ahead, several open questions remain. The *in vivo* relevance of SOX-derived NO in tissues beyond the heart and in disease contexts beyond HFpEF warrants further investigation. The recently generated conditional SOX knockout mice offer an ideal tool to explore tissue-specific roles of SOX, enabling direct comparison with the heterozygous model used here. Additionally, the contribution of SOX to hypoxic signaling, vascular tone regulation, and

metabolic adaptation should be further studied, particularly by employing metabolic flux analyses to characterize the proposed metabolic rewiring observed in SOXD.

While this work identified CLUH as a target to increase SOX activity, the molecular basis of its post-transcriptional control remains unclear. Future studies should dissect the RNA-binding dynamics of CLUH and its specific interaction with SOX mRNA. Furthermore, possible mechanisms to regulate MOCS1 activity to tune Moco production and thus increase SOX activity should be addressed.

Moreover, given the striking impact of SOX deficiency on ECM composition, future research should address how SOX interplays with extracellular signaling and how the observed alterations in expression of ECM proteins expand to its structural integrity.

Finally, the deficits observed in neuronal and astrocytic development call for more detailed functional analyses. The established SOX-deficient hippocampal culture model provides a robust system for investigating mechanisms of neurodevelopmental impairment. By selectively ablating astrocytes (e.g., with L-alpha-aminoadipic acid) or neurons (e.g., with NMDA), future studies can determine the cell-type-specific contributions to impaired development and mitochondrial dysfunction.

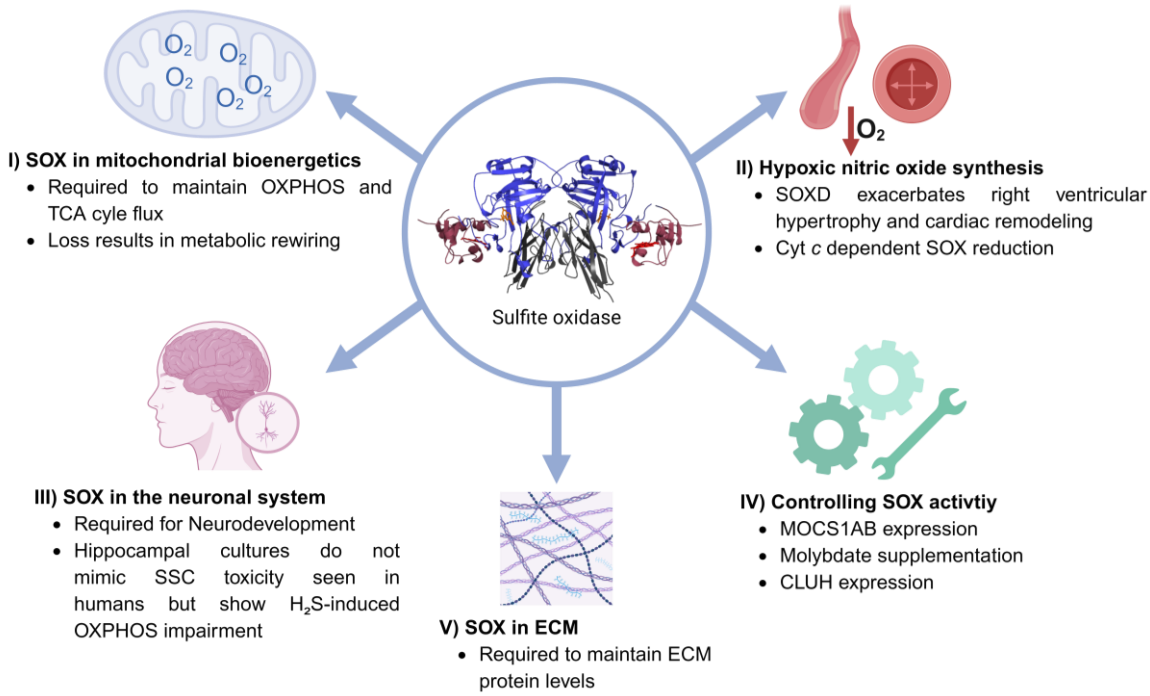

Figure 28: Multifaceted role of sulfite oxidase in cellular and physiological processes.
Sulfite oxidase was shown to be crucial for several cellular and physiology processes: I) Maintaining mitochondrial bioenergetics, II) Promoting cardiac remodeling under hypoxic stress conditions III) Mediating proper neuronal development and V) maintaining expression of ECM components. Furthermore, this work deciphered novel mechanism to control SOX activity, offering new therapeutic approaches for SOXD and related diseases.

In conclusion, this work establishes SOX as a central integrator of sulfur metabolism, mitochondrial energy production, and hypoxic NO signaling. These findings substantially broaden the functional landscape of SOX and provide a framework for targeted mechanistic and therapeutic exploration in both rare genetic disorders and common pathologies involving mitochondrial dysfunction.

5 Methods

5.1 Material

Organisms and cells

In this study different prokaryotic and eukaryotic cells and organisms were used. The different bacterial strains used for plasmid amplification and protein expression are listed in Table 1. The eukaryotic cells used for different biochemical and molecular biological approaches are listed in Table 2.

Table 1: E.coli strains used in this study

***E. coli* strain**	**genotype**	**purpose**	**reference**
NEB turbo	F´ *proA*$^{+}$*B*$^{+}$ *lacI*^{q} Δ*lacZ* M15/ *fhuA2* Δ*(lac-proAB) glnV gal R(zgb- 210::Tn10*)Tet^{S} *endA1 thi-1* Δ*(hsdS-mcrB)5*	Plasmid amplification	New England Biolabs
TP1004	Δ*(argF-lac)169* Δ*(fimB-fimE) 632 (::IS1)* Δ*(fruK-yeiR) 725 (fruA25)* F- Lambda- *[araD139]B/r deoC1 e14- flhD5301 gyrA219 non-9 rbsR22 relA1 rpsL150(strR)* Δ***mobAB::Kan***	Protein expression	(Palmer et al., 1996)

Table 2:Eukaryotic cells used in this study

cell type	**description**	**purpose**	**reference**
Flp-In™ T-REx™ 293	Human embryonic kidney cells withpFRT⁄lacZeo and pcDNA™6⁄TR stably integrated	protein expression, western blotting, activity assays	ThermoFisher Scientific
Flp-In T-Rex *SUOX*$^{-/-}$	Human embryonic kidney cells CRISPR/Cas9 nickase induced SO_KO	Protein expression, western blotting, activity assays, oxygen consumption experiments	Kaczmarek (University of Cologne)
Flp-In T-Rex *SUOX*$^{-/-}$ hSOX WT	Human embryonic kidney cells CRISPR/Cas9 nickase induced SO_KO, stably expressing hSOX WT	Protein expression, western blotting, activity assays, oxygen consumption experiments	Kaczmarek (University of Cologne)

Flp-In T-Rex *SUOX*$^{-/-}$ hSOX R366H	Human embryonic kidney cells CRISPR/Cas9 nickase induced SO_KO, stably expressing hSOX R366H	Protein expression, western blotting, activity assays	Kaczmarek (University of Cologne)
Flp-In T-Rex *SUOX*$^{-/-}$ hSOX G362S	Human embryonic kidney cells CRISPR/Cas9 nickase induced SO_KO, stably expressing hSOX G362S	Protein expression, western blotting, activity assays	Bender (University of Cologne)
Immortalized MEF	Mouse embryonic fibroblasts obtained from WT mice and immortalized by transfection with the SV40 virus	Protein expression, western blotting, oxygen consumption experiments	Mellis (University of Cologne)
Primary hippocampal neurons	Primary hippocampal neurons derived from P2 mice	oxygen consumption experiments, imaging	

Plasmids

Here we used different plasmids from different companies listed in Table 10.

Table 3: Empty plasmids used in this study.

plasmid	**resistance**	**promoter**	**affinity tag**	**company**
pQE80L	Amp	T5	His_6	Qiagen
pcDNA5.1	Amp	CMV	-	ThermoFisher
pAAV	Amp	GFAP		-
pAAV	Amp	hSyn		-

Antibodies

The different primary and secondary antibodies used in this study for western blotting are listed in Table 12.

Table 4: Antibodies used in this study.

antibody	dilution	company	article #
anti human sulfite oxidase	1:2000	Sigma-Aldrich	WH0006821M1
anti gephyrin (3B11)	1:50	(Smolinsky et al., 2008)	cell supernatant
anti VDAC	1:1000	abcam	AB15895
anti human CLUH	1:2000	Novus Biologicals	NB100-93306
anti Flag-tag	1:1000	Cell signaling	#14793
anti MOCS1	1:250	Sigma-Aldrich	HPA045783
anti GAPDH	1:5000	Sigma-Aldrich	G9545
anti NDUFA9	1:2000	Sigma-Aldrich	HPA073212
anti MTCO1	1:2000	Sigma-Aldrich	ZRB2574
anti SDHA	1:2000	Sigma-Aldrich	HPA041981
anti ATP5A1	1:2000	Sigma-Aldrich	SAB5700936
anti UQCRC1	1:2000	Sigma-Aldrich	SAB2702301
anti mouse IgG_HRP	1:10000	Santa Cruz	Sc2308
anti rabbit IgG_HRP	1:10000	Santa Cruz	Sc2054

5.2 Methods

5.2.1 Molecular biological methods

Plasmid amplification, purification and sequencing

Plasmid were amplified by transforming *E. coli* (DE3) turbo cells and cultivating o/n at 37 °C. Subsequently, 4 ml LB medium were supplemented with ampicillin (100 µg/ml) and inoculated with a transformed clone and grown at 37 °C o/n. The E.Z.N.A. plasmid DNA mini kit 1 (omega Bio-tek) was used to purify the plasmids according to the manufacturers manual. Sequencing was done via Sanger sequencing (Eurofins GATC).

5.2.2 Biochemical methods

Recombinant protein expression

In order to express recombinant N-terminal His6-tagged hSOX under the expression of the T5 promotor, TP1004 *E. coli* were transformed with pQE80L plasmids. Transformed bacteria were grown on LB agar plates supplemented with ampicillin (100 µg/ml) and cultivated o/n at 37 °C. Single colonies were selected and grown o/n at 37 °C with 111 rpm in 50 ml LB medium containing ampicillin. Next, 2 L LB medium supplemented with ampicillin and 500 µM sodium molybdate were inoculated with the pre-culture and grown at 37 °C with 90 rpm until mid-log

phase (OD_{600} = 0.5-0.6). Protein expression was induced by adding 125 µM isopropyl-ß-D-thiogalactopyranosid and allowed for 72 h at 18 °C and 90 rpm for 72 h.

Cell harvesting and disruption

First, cells were pelleted by centrifugation at 4000 x g at 4 °C for 20 min. The resulting pellet of 4 L culture were resuspended in 250 ml lysis buffer (50 mM Tris/Ac pH 8.0, 300 mM NaCl, 15 mM Imidazole). Cell lysis was started by addition of lysozyme and stirring for 30 min prior to freezing at -20 °C. After thawing the lysate was sonicated for two cycles of 1 min each with 49% amplitude. Lastly, cells were mechanically disrupted using an Emulsiflex-C5 high-pressure homogenizer (Avestin) at 1300 bar and 4 °C. Cell debris was pelleted by centrifugation at 50000 x g at 4 °C for 30 min. The supernatant containing the soluble recombinant proteins was collected and used for further purification.

Purification of recombinant human sulfite oxidase

To purify His_6-tagged proteins, Ni-NTA affinity chromatography was performed. Ni-NTA resin (5 mL per liter of culture medium) was equilibrated with 5 column volumes (CV) of lysis buffer. The supernatant containing the expressed proteins was added to the resin, and the suspension was gently stirred to allow binding. Unbound proteins and impurities were removed by washing the resin with 20 CV of Ni-NTA wash buffer (50 mM Tris-acetate, pH 8.0; 300 mM NaCl). Next, the resin was equilibrated with protein buffer (50 mM Tris/Ac pH 8.0, 30 mM NaCl) and bound proteins were cleaved off the column by incubating with GST-tagged PreScission Protease (2.5 mg/mL resin, provided by Marie Mohn, University of Cologne) for 1 h at RT. After elution, residual GST-tagged PreScission Protease was removed by passing the solution through a glutathione sepharose matrix (Machery&Nagel). The final eluate was concentrated using a 50 kDa molecular weight cutoff concentrator (Amicon). The protein solution was flash-frozen in liquid nitrogen and stored at -80 °C until further use.

Determination of protein concentration

The concentration of recombinant hSOX was determined by measuring the absorption of the heme Soret band at 413 nm in a photometer. For the calculation an extinction coefficient of ε = 113000 L/mol*cm was used. The protein concentrations of cell lysates and isolated mitochondria were determined via Bradford

The protein concentrations of crude extracts, isolated mitochondria and immunoprecipitation-enriched proteins was determined via Bradford in a 96-well plate –based format. The absorptions were compared to a BSA standard regression.

HPLC-based Form A analysis

To quantify Moco in recombinant SO variants, its oxidized fluorescent derivative, Form A, was measured. A protein sample containing 100 pmol (based on absorption at 413 nm) was diluted to a final volume of 140 µL in 100 mM Tris/HCl buffer (pH 7.2). The protein was mixed with an oxidation mix (17.5 µl 1.5%/2.0% I_2/KI solution mixed with 1.7 µl 37%HCl) and the reaction was incubated at RT o/n to oxidize Moco to Form A. Next, the reaction mixture was centrifuged for 5 min at 21380 x g, the supernatant was transferred to a fresh Eppendorf tube and mixed with freshly prepared 1% ascorbic acid. The pH was adjusted to 8.3 with 70 µl 1 M unbuffered Tris. 5 µl 1 M $MgCL_2$ were added and dephosphorylation of Form A was accomplished by addition of 0.5 µl alkaline phosphatase (Roche; 7500 U/ml) and incubation for 30 min at RT in the dark. The solution was centrifuged again for 10 minutes at maximum speed, and the supernatant was diluted 1:10 with deionized water (ddH_2O) in HPLC glass vials for analysis. Quantification of Form A was performed using a C18 reverse-phase column (XBridge™, 3.5 µm, 4.6 × 150 mm) connected to an Agilent 1200SL HPLC system. Methanol served as the organic phase for elution, with a flow rate of 2 mL/min. Detection was achieved by fluorescence measurement with excitation at 370 nm and emission at 450 nm. The retention time of Form A in the sample was compared to that of a Form A standard provided by Marie Mohn (University of Cologne) for accurate quantification.

HPLC-based measurement of sulfite and thiosulfate

Concentrations of sulfite and thiosulfate were determined using a modified version of the previously described protocol (Macabrey et al., 2022). Samples taken from the medium of P2 hippocampal Neurons at DIV14-DIV23 were stored at -20 °C until further use. After thawing the samples were centrifuged at 21130 x g for 10 min at 4 °C. 15 µl of the supernatant were mixed with 15 µl reaction buffer (160 mM HEPES pH 8.0, 16 mM EDTA), 15 µl acetonitrile and 3 µl 46 mM monobromobimane (mBBr) and incubated in the dark at RT for 30 min. The reaction was stopped by adding 30 µl methanesulfonic acid and incubation for 5 min at RT in the dark. Afterwards the samples were centrifuged at 21130 x g for 10 min at RT. 50 µl of the supernatant were diluted with 200 µl running buffer A(0.25% acetic acid pH 4.2) and transferred to an HPLC vial. Sulfite and thiosulfate concentrations were analyzed by injection of 10 µl into the HPLC on a C18 reversed-phase column (EC 250/3 NUCLEODUR C18 HTec, 5µm, MACHEREY-NAGEL) at 40 °C. The flow rate was set to 0.9 ml/min and a gradient of buffer A and B (100% methanol) according to Table 5 was applied.

Table 5: Gradient profile for the HPLC analysis of sulfite and thiosulfate

time [min]	buffer A [%]	buffer B [%]
0.0	85	15
0.75	85	15
2.65	77	23
5.43	67	33
6.03	63	37
8.06	55	45
8.44	35	65
8.82	0	100
11.34	0	100
11.72	85	15
15.0	85	15

Fluorescence spectroscopy was employed to detect sulfite and thiosulfate using an excitation at 380 nm and emission at 480 nm. The peaks were quantified by integration the peak areas and comparison with individual standards for each compound.

HPLC-based measurement of SSC

Concentration of SSC was determined as described previously (Jakubiczka-Smorag et al., 2016). Samples taken from the medium of P2 hippocampal Neurons at DIV14-DIV23 were stored at -20 °C until further use. After thawing the samples were centrifuged at 21130 x g for 10 min at 4 °C. 30 µl of the supernatant were mixed with 30 µl 200 mM Na_2CO_3/$NaHCO_3$ and 60 µl 10 mM 9-fluorenylmethyloxycarbonyl chloride (FMOC-Cl). After incubation for 20 min in the dark at RT, the reaction was stopped by addition of 10 µl amantadine-HCl and incubation for 5 min at RT. Subsequently, the samples were centrifuged by 21130 x g for 10 min at 4 °C and the supernatant was transferred to a glass HPLC vial. SSC was separated from other metabolites on a 250 x 3 mm 5 µm Nucleodur HTec C18 (Macherey-Nagel) column. 10 µl of the sample were injected and peaks were separated by the following running protocol (Table 1) with 50 mM Sodium formate, 0.05% trifluoroacetic acid pH 4.5 as buffer A and 100% methanol as buffer B.

Table 6: Gradient profile for the HPLC analysis of SSC

time [min]	buffer A [%]	buffer B [%]	flow rate [ml/min]
0.0	65	35	1
2.1	65	35	1
7.5	40	60	1
8.0	40	60	1
8.1	0	100	1
9.6	0	100	1
9.7	65	35	1.4
13.0	65	35	1.4
13.1	65	35	1
15.0	65	35	1

SSC eluted at 8.81 min and the peak area was quantified via absorbance at 265 nm.

SDS-Page

Proteins were separated according to their molecular weight by SDS-Page. First, proteins were denatured and reduced using 5X Laemmli buffer (50% glycerol, 3.5% SDS, 15% β-Mercaptoethanol, 0.02 µl Bromophenol blue) and heating to 95 °C for 5 min (Laemmli, 1970). Afterwards, discontinuous SDS-Page was performed using 10 or 12% acrylamide/bisacrylamide gels. Finally, protein gels were used for western blot analysis.

Western blot analysis

After SDS-PAGE the negatively charged proteins were transferred to a PVDF membrane by electroblotting using a semi-dry blotter (C.B.S. Scientific). The PVDF membrane was activated by incubation in 100% methanol for 1 min. The separating gel was equilibrated shortly in transfer buffer (25 mM Tris/HCl pH 8.8, 192 mM glycine, 10% methanol). Blotting was performed by applying a current according to the following equation: $current\,[mA] = \frac{number\ of\ gels\ x\ gel\ percentage\ x\ 11}{hours\ of\ blotting}$. Afterwards unspecific binding sites were blocked by incubation with 5% milk in TBS-T for 1 h at RT, followed by incubation with the primary antibody in 1% milk in TBS-T for 1 h at RT or at 4 °C o/n. Membranes were washed thrice in TBS-T for 10 min at RT. Next, membranes were incubated with the HRP-coupled secondary antibody in 1% milk in TBS-T. for 1 h at RT and subsequently washed as described before. After a final washing step with TBS for 10 min at RT, the membranes were covered with the chemiluminescent substrate (ThermoFisher Scientific). The detection of the HRP-derived signals was conducted by ChemiDoc MP (BioRad).

BN-PAGE

To analyse the supercomplex formation in mitochondrial fractions, 100 µg mitochondria isolated from SOX-deficient and WT MEFs were pelleted by centrifugation at 10.000 x g for 10 min at 4 °C. The mitochondrial pellets were then solubilized on ice for 15 min in a buffer containing 50 mM NaCl, 50 mM imidazole/HCl, 2 mM 6-aminohexanoic acid and 1 mM EDTA at pH 7.0 supplemented with 4% digitonin. Following solubilization samples were centrifuged for 30 min at 17.000 x g at 4 °C to remove insoluble material. The resulting supernatant was mixed with 25% glycerol and 2.5% loading dye (5% coomassie blue G-250 in 500 mM 6-aminhexanoic acid) before loading onto a 4-16% bis-acrylamid gradient gel (Sigma Aldrich). Electrophoretic separation was performed using NativePAGE conditions: initially, gels were run for 60 min at 150 V in dark blue cathode buffer (0.02% Coomassie Blue G-250, 50 mM tricine, 50 mM Bis-Tris, pH 6.8). Thereafter, the dark blue cathode buffer was replaced with light blue cathode buffer (0.002% Coomassie Blue G-250, 50 mM tricine, 50 mM Bis-Tris, pH 6.8), and electrophoresis was continued until the blue front reached the gel's end. Post-separation, gels were either fixed and stained using 10% acetic acid/20% methanol followed by destaining in 8% acetic acid, or proteins were transferred onto a polyvinylidene fluoride (PVDF) membrane using blotting buffer (50 mM tricine, 7.5 mM imidazole), as previously described (Western blot analysis).

Sulfite-dependent cytochrome *c* reduction

Sulfite-dependent SOX activity can be determined by following the reduction of the final electron acceptor cytochrome *c*. Upon starting the reaction with sulfite, the reduction of cytochrome *c* (ε 550 = 19630 L/mol*cm) can be monitored by measuring the absorption change at 550 nm in a Tecan Spark reader. The reaction took place in a final volume of 200 µl containing 50 µM porcine cytochrome *c* (Serva), 20 µg/ml catalase and 100 µg mitochondria in a 100 mM Tris/Ac pH 8.0 buffer system. For each experiment technical triplicates were used. Sulfite-dependent SOX activities were calculated by determining the initial velocities of the cytochrome *c* reduction subtracted by a buffer control sample lacking sulfite. In a final step, the SOX activities were normalized to the amount of protein used.

SOX reduction by cytochrome *c*

All procedures were carried out under anaerobic conditions using an anaerobic hood. First, cytochrome *c* was dissolved in storage buffer (20 mM NaCl, 50 mM Tris/Ac pH 8.0) and reduced by incubation with 100 mM Ascorbate for 10 min. Following reduction, excess ascorbate was removed using a PD10 desalting column (emp biotech) according to the manufacturers protocol, with storage buffer as the elution buffer. Next, 25 µM His-tagged SOX was mixed with 1.6 mM reduced or oxidized cytochrome *c* and incubated for 15 min. The SOX-

cytochrome *c* mixtures, as well as controls containing SOX or reduced cytochrome *c* alone, were added to 50 µl pre-equilibrated Ni-NTA slurry. Binding was allowed to proceed for 30 min at RT with head-over-end rotation. Afterward incubation, the slurry was collected by centrifugation for 1 min at 300 rpm. The supernatant was discarded, and the resin was washed five times with 200 µl Lysis buffer (300 mM NaCl, 50 mM Tris/Ac pH 8.0) to get rid of unbound proteins. Bound His-tagged SOX was eluted with 100 µl elution buffer (250 mM Imidazole, 300 mM NaCl, 50 mM Tris/Ac pH 8.0) and incubation for 5 min. Afterwards, the samples were centrifuged for 1 min at 300 rpm and the supernatant was transferred to new eppendorf tubes. Protein samples were then diluted with 100 µl 100 mM Tris/Ac pH 8.0, transferred to a quartz cuvette and sealed with parafilm to prevent autooxidation. UV-vis spectra were recorded using a Photometer (Perkin Elmer) and UV-vis lab software (version 4.1.0.).

5.2.3 Cell biological methods

Cultivation of mammalian cells

Human embryonic kindey (HEK) FlpIn™ cells and immortalized mouse embryonic fibroblasts (MEF) were grown as adherent monolayers in Dulbecco's Modified Eagle's Medium (DMEM) (Pan Biotech) supplemented with 2 mM glutamine (gibco™ by Life Technologies) and 10% fetal bovine serum (FBS, Pan Biotech) at 37 °C and 5% CO2. Cells were grown until confluent before detaching with Trypsin/EDTA and redistribution to new 10 or 15 cm dishes with either 10 or 15 ml fresh culture medium, respectively.

Transient transfection of mammalian cells

Transfection with PEI

For transfection with PEI, cells were grown until they reached 70-80% confluency on 10 cm dishes and the medium was replaced by 5 ml fresh cell culture medium. First, 1 ml DMEM without additives was incubated with 51.2 µl PEI (polyethylenimine, 1 mg/mL, diluted in H2O, pH 6.8) for 5 min at RT. Next, 12.8 µg plasmid DNA was added to the mixture followed by incubation for 20 min at RT, before the mixture was added dropwise to the cells. After 24 h 5 ml fresh cell culture medium were added to the cells and another 24-72 h later the cells were harvested as described earlier.

Transfection with GeneJuice

For transfection with GeneJuice (Novagen), cells were grown until they reached 70-80% confluency and the medium was changed. First, 500 µl DMEM without additives were incubated with 30 µl GeneJuice for 5 min. Next, 12 µg DNA was added followed by an

incubation of 15 min before the mixture was added dropwise to the cells. 48-96 h later the cells were harvested as described before.

Mitochondrial enrichment of murine livers

Murine livers were dissected from mice at 2 days after birth. Mitochondrial enrichment was conducted as described previously (Kucharská et al., 2000). Briefly, the wet weight of the livers was determined, and the tissues were minced in an ice-cold glass beaker containing ice-cold isolation medium (225 mM mannitol, 75 mM sucrose, 0.2 mM EDTA, 20 mM HEPES pH 7.4). The minced tissue was then suspended in 10 volumes of the same ice-cold isolation medium and homogenized with 8 strokes at 1000 rpm. The homogenate was diluted to achieve less than 10% tissue content (1 g liver to 20 ml homogenate) and centrifuged at 1000 x g for 10 minutes at 4 °C. The resulting supernatant was carefully transferred to a new tube and centrifuged again at 6200 x g for 10 minutes at 4 °C. After discarding the supernatant, the mitochondrial pellet was resuspended in isolation buffer for subsequent analyses.

Mitochondrial enrichment of mammalian cells

Cells were grown until confluency on 15 cm dishes and washed with 10 ml pre-warmed mito buffer (20 mM HEPES/NaOH pH 7.4, 220 mM mannitol, 70 mM sucrose, 1 mM EDTA). Afterwards cells were scraped off the plate using a cell scraper and homogenized using a teflon homogenizer (Sartorius) with 15 strokes at 1100 rpm at 4 °C. Centrifugation at 800 x g for 5 min at 4 °C pelleted cell debris and intact cells. The mitochondria containing supernatant was centrifuged for 15 min at 13000 x g and 4 °C. The mitochondrial fraction was washed 3 times with mito buffer by resuspending the pellet mitochondria and centrifugation at 13000 x g for 15 min at 4 °C. The final pellet was resuspended in 200 µl mito buffer or in case of the SOX activity assays in 100 mM Tris/Ac pH 8.0.

Harvesting of mammalian cells

Cell culture dishes were washed twice with warm PBS and the cells were scraped off the plate using a cell scraper and transferred into Eppendorf tubes. Following, the cell suspension was sonicated at 20% amplitude for 15 sec. Cell debris was removed by centrifugation at 21380 x g for 10 min at 4 °C.

Preparation and cultivation of primary hippocampal neurons

Primary hippocampal neurons were prepared from mice at day 2 of life. Mice were sacrificed by decapitation and hippocampi were isolated and stored in GBSS solution supplemented with 0.05% glucose until further use. The hippocampi were incubated in 1 ml Trypsin/EDTA solution for 30 min at 37 °C with multiple inversions in between. Next, trypsin was removed and the

hippocampi were washed thrice with 1 ml DMEM supplemented with 10% FBS. Following, the tissue was dissociated using a 1 ml syringe with 18 G cannula. Next, cells were pelleted by centrifugation at 400 x g for 5 min at RT. The supernatant was removed and the cell pelleted was resuspended in 1 ml NB (Neurobasal Medium, Gibco) medium supplemented with 1X B-27 (Gibco) 1X N-2 (Gibco), 1X Pen/Strep (Gibco) and 420 µM Glutamin. Subsequently, the cell number was determined using a Neubauer counting chamber and cells were seeded as needed for the individual approaches.

Respiratory measurements

Oxygraph respiration measurements

In order to monitor the oxygen consumption rates of Human embryonic kidney (HEK) FlpIn™ cells, immortalized mouse embryonic fibroblasts (MEF) or murine livers, intact mitochondria were enriched as described earlier. The Oxygraph-2k (Oroboros) was air-calibrated according to the manufacturers protocol prior to resuspending 100 or 25 µg mitochondria in 2.5 ml Miro5 buffer (0.5 mM EGTA, 20 mM Taurine, 3 mM $MgCl_2$, 110 mM Sucrose, 60 mM Potassium-Lactobionate, 10 mM KH_2PO_4, 20 mM HEPES, 1 mg/ml BSA, pH 7.1). First, Pyruvate and Malate, ADP, cytochrome *c* and Glutamate were sequentially injected. Saturating ADP concentrations stimulated oxidative phosphorylation and cytochrome *c* injection served as a control for mitochondrial membrane integrity. Pyruvate, Malate and Glutamate allowed to indirectly funnel electrons into complex I by generating NAHD. Next, succinate was added as substrate for complex II. Following, the uncoupling agent Carbonylcyanid-p-trifluormethoxyphenylhydrazon (FCCP) was titrated to monitor maximal respiration. Rotenone and antimycin A were added to block complex I and II respectively. Next, Ascorbate and N,N,N',N'-Tetramethyl-p-phenylenediamine dihydrochloride, (TMPD) were added and the chamber was opened for 20 min before closing and measuring complex IV activity. Finally, azide was added to block complex IV and completely abolished oxygen consumption. The obtained oxygen consumption rates were analyzed using the provided data analysis template (Oroboros Instruments GmbH) with correction for titration volume. Since the machine was freshly calibrated in between the experiments, one replicate obtained from hepatocytic mitochondria was corrected for an increased baseline.

Seahorse respiration measurements

The oxygen consumption rate of MEF and primary hippocampal neurons was measured using the Agilent Seahorse XFe96 Analyzer. For Primary hippocampal neurons, 40.000 cells/well were seeded on a poly-l-lysine (Sigma, PLL) coated 96 multi-well seahorse plate (Agilent) and grown until DIV 14. For MEF, 25.000 cells/well were seeded on a 96 multi-well seahorse plate

(Agilent) and grown for 1 day. Prior to the assay, the culture medium was removed and the cells were washed thrice 200 µl with ACSF medium (110 mM NaCl, 1.8 mM $CaCl_2$, 5.4 mM KCl, 0.8 mM $MgSO_4$, 0.92 mM KH_2PO_4, 20 mM HEPES, 10 mM glucose, 2 mM L-glutamine, 1 mM sodium pyruvate, pH 7.4). After the final washing step 200 µl ACSF medium were added to the cells. Afterwards the cell plate was incubated for 1 h in a non-CO_2 incubator at 37 °C for degassing before starting the assay. The sensor cartridge was hydrated on the day before the assay according to the manufacturers protocol. Each measurement consisted of 3 measurement cycles with 3 min of mixing and 3 min of measuring. First the baseline of oxygen consumption was measured. Next, in case of the MEFs medium or 20 µM Na_2SO_3 and/or 1 mM Nitrite were added. This step was skipped in case of the primary hippocampal neurons. Next, the sequential injection of 2 µM oligomycin, 1 µM FCCP and 0.5 µM rotenone and antimycin A was performed. To later on normalize the oxygen consumption rate to the cell numbers, the nuclei were stained by addition of 0.02 mg/mL Hoechst injected together with the mixture of rotenone and antimycin A and incubated for 20 min. After the assay, the Hoechst staining was monitored by using a Cytation 5 (Agilent).

Preparation of liver lysates

Fresh-frozen liver from $CLUH^{+/+}$ and $CLUH^{-/-}$ mice at the age of 8 weeks were obtained from AG Rugarli. Livers were thawed on ice and weighed. Next, 10 x volume lysis buffer (50 mM Tris/HCl, 300 mM NaCl, 5 mM EDTA, 5 mM DTT and 2 X complete EDTA-free protease inhibitor (Roche)) were added and the tissue was homogenized by hand using an ice-cold dounce homogenizer with 30 strokes. Afterwards, the homogenate was lysed by adding $1/10^{th}$ colume of 10% (w/v) 3-[(3-cholamidopropyl)dimethylammonio]-1-propanesulfonate (CHAPS) and overhead incubation at 4 °C for 60 min. Cell debris was pelleted by centrifugation at 21380 x g for 15 min at 4 °C and the supernatant was stored at -80 °C until further use.

Mass spectrometry

Cells were lysed in Urea Buffer (8 M Urea, 50 mM TEAB buffer, 1X EDTA-free complete protease inhibitor). Subsequently, cell suspension was sonicated and centrifuged for 15 min at 20.000 x g to remove cell debris. Afterwards the protein concentration was measured by Bradford. Mitochondria were enriched as described before (seeMitochondrial enrichment) and protein content was also determined by Bradford. For downstream tryptic digestion, 50 µg of total cell lysate protein and 100 µg of mitochondrial protein were used. First, proteins were reduced by addition of 5 mM DTT, followed by vortexing and incubation for 1 h at 25 °C. Free cysteine residues were then alkylated with 40 mM chloroacetamide (CAA) for 30 minutes in the dark. Samples were subsequently diluted with TEAB buffer to reduce the urea concentration to ≤ 2 M. Trypsin was added at an enzyme-to-substrate ratio of 1:75, and

digestion was carried out o/n at 25 °C. The next day, enzymatic digestion was stopped by acidifying the samples with formic acid to a final concentration of 1%. Peptides were purified using StageTips according to the CECAD Proteomics Facility protocol (Version 3.0, January 2024). Data was visualized using Instant Clue version 0.12.2 (Nolte et al., 2018).

Microscopy

In order to analyze the neuron and astrocyte areas, primary hippocampal neuronal cultures were prepared as described before and 75.000 cells/well were seeded onto poly L-lysine coated coverslips in a 24-well dish. After 11 days in vitro cells were transduced with AAV viruses pAAV-hSyn-moxBFP and pAAV-GFAP-eGFP and grown until DIV14. The cells were washed thrice with PBS and fixed by incubation with 4% paraformaldehyde (PFA) for 15 min at 4 °C. Afterwards, cells were washed thrice with PBS and the cover slips were mounted using Mowiol/Dabco. Microscopy images were acquired using a Leica TCS SP8 LIGHTNING upright confocal microscope with an HC PL APO CS2 63x/1.30 glycerol objective, HyD detectors and diode lasers with 405 (moxBFP) and 488 nm (eGFP). For image deconvolution the automated setting for “Mowiol” was used. Image were acquired using the LASX Navigator with stacks of 3 µm z-step size and tile scans of 12484x12680 526.59x534.86 microns. Previous macros were adapted for automated image analysis using ImageJ/FIJI 1.53t (Liebsch et al., 2023).

AAV production

Recombinant adeno-associated virus particles (AAV2/1) were generated in HEK293 cells and purified using PEG/NaCl precipitation, followed by chloroform extraction as described previously (Kimura et al., 2019). The viral titers were quantified using the Gel Green® (*Biotium*) protocol (Xu et al., 2020). The fluorescence was detected at 507 ± 5 nm excitation and 528 ± 5 nm emission using a plate reader equipped with monochromators (Tecan Spark).

5.2.4 Mice experiments

HFpEF and PH mouse model

Wildtype and *SUOX*$^{+/-}$ male C57BL/6NJ mice were challenged for heart failure with preserved ejection fraction according to the previously reported protocol (Schiattarella et al., 2019). Mice were either fed a chow or a high fat diet for 18 weeks. Additionally, nitric oxide synthases were inhibited using N-Nitro-L-arginine methylester (L-NAME, Sigma), inducing a state where NO production only depends on metal-dependent enzymes like SOX. This model for HFpEF was further modified by our collaborators from AG Rosenkranz to also induce PH by exposing mice to hypoxia (10% O_2) for the last 6 weeks. Systolic arterial pressure (SAP), right ventricular systolic pressure (RVSP) and the fulton index (RV/(LV+S)), representing the ratio between the

weight of the right ventricle to the weight of the left ventricle and septum, were determined as hallmarks for HFpEF and PH.

5.2.5 Statistical analysis

Figure illustration and statistical analysis were performed with GraphPad Prism 6. Statistical tests and the number of replicates are described in each figure legend. Data is displayed as mean ± standard deviation. Unpaired Student's *t*-test and multiple *t*-test were performed with a 95% significance level. 2-way ANOVA was performed with 95% significance level and Bonferroni or Sidak's post-hoc tests.

6 References

Abe, Y., Aihara, Y., Endo, W., Hasegawa, H., Ichida, K., Uematsu, M., Kure, S., 2021. The effect of dietary protein restriction in a case of molybdenum cofactor deficiency with *MOCS1* mutation. Mol. Genet. Metab. Rep. 26, 100716. https://doi.org/10.1016/j.ymgmr.2021.100716

Abe, Y., Hines, I., Zibari, G., Grisham, M.B., 2009. Hepatocellular Protection by Nitric Oxide or Nitrite in Ischemia and Reperfusion Injury. Arch. Biochem. Biophys. 484, 232–237. https://doi.org/10.1016/j.abb.2008.10.006

Adamus, J.P., Ruszczyńska, A., Wyczałkowska-Tomasik, A., 2024. Molybdenum's Role as an Essential Element in Enzymes Catabolizing Redox Reactions: A Review. Biomolecules 14, 869. https://doi.org/10.3390/biom14070869

Andrew, P.J., Mayer, B., 1999. Enzymatic function of nitric oxide synthases. Cardiovasc. Res. 43, 521–531. https://doi.org/10.1016/S0008-6363(99)00115-7

Arnold, W.P., Mittal, C.K., Katsuki, S., Murad, F., 1977. Nitric oxide activates guanylate cyclase and increases guanosine 3':5'-cyclic monophosphate levels in various tissue preparations. Proc. Natl. Acad. Sci. U. S. A. 74, 3203–3207.

Aziz, N., Jamil, R.T., 2025. Biochemistry, Xanthine Oxidase, in: StatPearls. StatPearls Publishing, Treasure Island (FL).

Bächinger, H.P., Bruckner, P., Timpl, R., Prockop, D.J., Engel, J., 1980. Folding Mechanism of the Triple Helix in Type-III Collagen and Type-III pN–Collagen. Eur. J. Biochem. 106, 619–632. https://doi.org/10.1111/j.1432-1033.1980.tb04610.x

Baliga, R.S., Milsom, A.B., Ghosh, S.M., Trinder, S.L., MacAllister, R.J., Ahluwalia, A., Hobbs, A.J., 2012. Dietary nitrate ameliorates pulmonary hypertension: cytoprotective role for endothelial nitric oxide synthase and xanthine oxidoreductase. Circulation 125, 2922–2932. https://doi.org/10.1161/CIRCULATIONAHA.112.100586

Basu, S., Azarova, N.A., Font, M.D., King, S.B., Hogg, N., Gladwin, M.T., Shiva, S., Kim-Shapiro, D.B., 2008. Nitrite reductase activity of cytochrome c. J. Biol. Chem. 283, 32590–32597. https://doi.org/10.1074/jbc.M806934200

Belaidi, A.A., Schwarz, G., 2013. Molybdenum Cofactor Deficiency: Metabolic Link Between Taurine and S-Sulfocysteine, in: El Idrissi, A., L'Amoreaux, W.J. (Eds.), Taurine 8. Springer, New York, NY, pp. 13–19. https://doi.org/10.1007/978-1-4614-6093-0_2

Bender, D., Kaczmarek, A.T., Kuester, S., Burlina, A.B., Schwarz, G., 2020. Oxygen and nitrite reduction by heme-deficient sulphite oxidase in a patient with mild sulphite oxidase deficiency. J. Inherit. Metab. Dis. 43, 748–757. https://doi.org/10.1002/jimd.12216

Bender, D., Kaczmarek, A.T., Santamaria-Araujo, J.A., Stueve, B., Waltz, S., Bartsch, D., Kurian, L., Cirak, S., Schwarz, G., 2019a. Impaired mitochondrial maturation of sulfite oxidase in a patient with severe sulfite oxidase deficiency. Hum. Mol. Genet. 28, 2885–2899. https://doi.org/10.1093/hmg/ddz109

Bender, D., Schwarz, G., 2018. Nitrite-dependent nitric oxide synthesis by molybdenum enzymes. FEBS Lett. 592, 2126–2139. https://doi.org/10.1002/1873-3468.13089

Bender, D., Tobias Kaczmarek, A., Niks, D., Hille, R., Schwarz, G., 2019b. Mechanism of nitrite-dependent NO synthesis by human sulfite oxidase. Biochem. J. 476, 1805–1815. https://doi.org/10.1042/BCJ20190143

Bhattacharjee, O., Ayyangar, U., Kurbet, A.S., Ashok, D., Raghavan, S., 2019. Unraveling the ECM-Immune Cell Crosstalk in Skin Diseases. Front. Cell Dev. Biol. 7. https://doi.org/10.3389/fcell.2019.00068

Bindoli, A., Cavallini, L., Rigobello, M.P., Coassin, M., Di Lisa, F., 1988. Modification of the xanthine-converting enzyme of perfused rat heart during ischemia and oxidative stress. Free Radic. Biol. Med. 4, 163–167. https://doi.org/10.1016/0891-5849(88)90024-X

Bittner, F., Oreb, M., Mendel, R.R., 2001. ABA3 Is a Molybdenum Cofactor Sulfurase Required for Activation of Aldehyde Oxidase and Xanthine Dehydrogenase in *Arabidopsis thaliana**. J. Biol. Chem. 276, 40381–40384. https://doi.org/10.1074/jbc.C100472200

Bolaños, J.P., Peuchen, S., Heales, S.J., Land, J.M., Clark, J.B., 1994. Nitric oxide-mediated inhibition of the mitochondrial respiratory chain in cultured astrocytes. J. Neurochem. 63, 910–916. https://doi.org/10.1046/j.1471-4159.1994.63030910.x

Boles, R.G., Ment, L.R., Meyn, M.S., Horwich, A.L., Kratz, L.E., Rinaldo, P., 1993. Short-term response to dietary therapy in molybdenum cofactor deficiency. Ann. Neurol. 34, 742–744. https://doi.org/10.1002/ana.410340520

Borisov, V.B., Forte, E., 2021. Impact of Hydrogen Sulfide on Mitochondrial and Bacterial Bioenergetics. Int. J. Mol. Sci. 22, 12688. https://doi.org/10.3390/ijms222312688

Boudko, S.P., Engel, J., Okuyama, K., Mizuno, K., Bächinger, H.P., Schumacher, M.A., 2008. Crystal Structure of Human Type III Collagen Gly991–Gly1032 Cystine Knot-containing Peptide Shows Both 7/2 and 10/3 Triple Helical Symmetries. J. Biol. Chem. 283, 32580–32589. https://doi.org/10.1074/jbc.m805394200

Bouwstra, J.A., Helder, R.W.J., El Ghalbzouri, A., 2021. Human skin equivalents: Impaired barrier function in relation to the lipid and protein properties of the stratum corneum. Adv. Drug Deliv. Rev. 175, 113802. https://doi.org/10.1016/j.addr.2021.05.012

Brondani, M., Ribeiro, R.T., Pinheiro, C.V., Hoffmann, C.I.H., Marcuzzo, M.B., Mohsen, A.-W., Wajner, M., Seminotti, B., Vockley, J., Leipnitz, G., 2025. Metformin restores mitochondrial bioenergetics and redox homeostasis through modulation of mitochondrial biogenesis and dynamics in patient derived cultured fibroblasts and an animal model of molybdenum cofactor deficiency. Biomed. Pharmacother. 187, 118123. https://doi.org/10.1016/j.biopha.2025.118123

Brown, G.C., 2007. Nitric oxide and mitochondria. Front. Biosci. J. Virtual Libr. 12, 1024–1033. https://doi.org/10.2741/2122

Brown, G.C., 1999. Nitric oxide and mitochondrial respiration. Biochim. Biophys. Acta BBA - Bioenerg. 1411, 351–369. https://doi.org/10.1016/S0005-2728(99)00025-0

Brown, G.C., Borutaite, V., 2004. Inhibition of mitochondrial respiratory complex I by nitric oxide, peroxynitrite and S-nitrosothiols. Biochim. Biophys. Acta BBA - Bioenerg., EBEC 2004 1658, 44–49. https://doi.org/10.1016/j.bbabio.2004.03.016

Brown, G.C., Cooper, C.E., 1994. Nanomolar concentrations of nitric oxide reversibly inhibit synaptosomal respiration by competing with oxygen at cytochrome oxidase. FEBS Lett. 356, 295–298. https://doi.org/10.1016/0014-5793(94)01290-3

Bryan, N.S., 2022. Nitric oxide deficiency is a primary driver of hypertension. Biochem. Pharmacol. 206, 115325. https://doi.org/10.1016/j.bcp.2022.115325

Carballal, S., Vitvitsky, V., Kumar, R., Hanna, D.A., Libiad, M., Gupta, A., Jones, J.W., Banerjee, R., 2021. Hydrogen sulfide stimulates lipid biogenesis from glutamine that is dependent on the mitochondrial NAD(P)H pool. J. Biol. Chem. 297, 100950. https://doi.org/10.1016/j.jbc.2021.100950

Carlström, M., Liu, M., Yang, T., Zollbrecht, C., Huang, L., Peleli, M., Borniquel, S., Kishikawa, H., Hezel, M., Persson, A.E.G., Weitzberg, E., Lundberg, J.O., 2015. Cross-talk Between Nitrate-Nitrite-NO and NO Synthase Pathways in Control of Vascular NO Homeostasis. Antioxid. Redox Signal. 23, 295–306. https://doi.org/10.1089/ars.2013.5481

Castro, L.A., Robalinho, R.L., Cayota, A., Meneghini, R., Radi, R., 1998. Nitric oxide and peroxynitrite-dependent aconitase inactivation and iron-regulatory protein-1 activation in mammalian fibroblasts. Arch. Biochem. Biophys. 359, 215–224. https://doi.org/10.1006/abbi.1998.0898

Cecco, E., Gladwin, M.T., Sparacino-Watkins, C., 2017. 29 - Oxygen Inhibits Nitrite Reduction to Nitric Oxide by the Molybdenum-Dependent mARC-2 Enzyme. Free Radic. Biol. Med., SfRBM 2017 SfRBM's 24th Annual Meeting Program and Abstracts November 29 - December 2, 2017 Hilton Baltimore Baltimore, MD USA 112, 34. https://doi.org/10.1016/j.freeradbiomed.2017.10.042

Chang, D.T.W., Honick, A.S., Reynolds, I.J., 2006. Mitochondrial Trafficking to Synapses in Cultured Primary Cortical Neurons. J. Neurosci. 26, 7035–7045. https://doi.org/10.1523/JNEUROSCI.1012-06.2006

Chapman, E., Best, M.D., Hanson, S.R., Wong, C.-H., 2004. Sulfotransferases: Structure, Mechanism, Biological Activity, Inhibition, and Synthetic Utility. Angew. Chem. Int. Ed. 43, 3526–3548. https://doi.org/10.1002/anie.200300631

Chiquet, M., Birk, D.E., Bönnemann, C.G., Koch, M., 2014. Molecules in Focus: Collagen XII: Protecting bone and muscle integrity by organizing collagen fibrils. Int. J. Biochem. Cell Biol. 53, 51–54. https://doi.org/10.1016/j.biocel.2014.04.020

Choii, G., Ko, J., 2015. Gephyrin: a central GABAergic synapse organizer. Exp. Mol. Med. 47, e158–e158. https://doi.org/10.1038/emm.2015.5

Christie, I.N., Theparambil, S.M., Braga, A., Doronin, M., Hosford, P.S., Brazhe, A., Mascarenhas, A., Nizari, S., Hadjihambi, A., Wells, J.A., Hobbs, A., Semyanov, A., Abramov, A.Y., Angelova, P.R., Gourine, A.V., 2023. Astrocytes produce nitric oxide via nitrite reduction in mitochondria to regulate cerebral blood flow during brain hypoxia. Cell Rep. 42, 113514. https://doi.org/10.1016/j.celrep.2023.113514

Ciociola, E., Dutta, T., Sasidharan, K., Kovooru, L., Noto, F.R., Pennisi, G., Petta, S., Mirarchi, A., Maurotti, S., Scopacasa, B., Tirinato, L., Candeloro, P., Henricsson, M., Lindén, D., Jamialahmadi, O., Pujia, A., Mancina, R.M., Romeo, S., 2025. Downregulation of the MARC1 p.A165 risk allele reduces hepatocyte lipid content by increasing beta-oxidation. Clin. Mol. Hepatol. 31, 445–459. https://doi.org/10.3350/cmh.2024.0642

Claerhout, H., Witters, P., Régal, L., Jansen, K., Van Hoestenberghe, M.-R., Breckpot, J., Vermeersch, P., 2018. Isolated sulfite oxidase deficiency. J. Inherit. Metab. Dis. 41, 101–108. https://doi.org/10.1007/s10545-017-0089-4

Cleeter, M.W., Cooper, J.M., Darley-Usmar, V.M., Moncada, S., Schapira, A.H., 1994. Reversible inhibition of cytochrome c oxidase, the terminal enzyme of the mitochondrial respiratory chain, by nitric oxide. Implications for neurodegenerative diseases. FEBS Lett. 345, 50–54. https://doi.org/10.1016/0014-5793(94)00424-2

Clementi, E., Brown, G.C., Feelisch, M., Moncada, S., 1998. Persistent inhibition of cell respiration by nitric oxide: Crucial role of S-nitrosylation of mitochondrial complex I and protective action of glutathione. Proc. Natl. Acad. Sci. U. S. A. 95, 7631–7636.

Coelho, C., Mahro, M., Trincão, J., Carvalho, A.T.P., Ramos, M.J., Terao, M., Garattini, E., Leimkühler, S., Romão, M.J., 2012. The First Mammalian Aldehyde Oxidase Crystal Structure. J. Biol. Chem. 287, 40690–40702. https://doi.org/10.1074/jbc.M112.390419

Cogliati, S., Cabrera-Alarcón, J.L., Enriquez, J.A., 2021. Regulation and functional role of the electron transport chain supercomplexes. Biochem. Soc. Trans. 49, 2655–2668. https://doi.org/10.1042/BST20210460

Cooper, C.E., Brown, G.C., 2008. The inhibition of mitochondrial cytochrome oxidase by the gases carbon monoxide, nitric oxide, hydrogen cyanide and hydrogen sulfide: chemical mechanism and physiological significance. J. Bioenerg. Biomembr. 40, 533–539. https://doi.org/10.1007/s10863-008-9166-6

Coyne, E.S., Nie, Y., Lee, D., Pandovski, S., Yang, T., Zhou, H., Rosahl, T.W., Carballo-Jane, E., Abdurrachim, D., Zhou, Yongqi, Hendra, C., Ali, A.A.B., Meyers, S., Blumenschein, W., Gongol, B., Liu, Y., Zhou, Yingjiang, Talukdar, S., 2025. Loss of mitochondrial amidoxime-reducing component 1 (mARC1) prevents disease progression by reducing fibrosis in multiple mouse models of chronic liver disease. Hepatol. Commun. 9, e0637. https://doi.org/10.1097/HC9.0000000000000637

Crane, B.R., Arvai, A.S., Gachhui, R., Wu, C., Ghosh, D.K., Getzoff, E.D., Stuehr, D.J., Tainer, J.A., 1997. The Structure of Nitric Oxide Synthase Oxygenase Domain and Inhibitor Complexes. Science 278, 425–431. https://doi.org/10.1126/science.278.5337.425

Dassi, E., Zuccotti, P., Leo, S., Provenzani, A., Assfalg, M., D'Onofrio, M., Riva, P., Quattrone, A., 2013. Hyper conserved elements in vertebrate mRNA 3′-UTRs reveal a translational network of RNA-binding proteins controlled by HuR. Nucleic Acids Res. 41, 3201–3216. https://doi.org/10.1093/nar/gkt017

Dauth, S., Grevesse, T., Pantazopoulos, H., Campbell, P.H., Maoz, B.M., Berretta, S., Parker, K.K., 2016. Extracellular Matrix Protein Expression Is Brain Region Dependent. J. Comp. Neurol. 524, 1309–1336. https://doi.org/10.1002/cne.23965

Dejanovic, B., Schwarz, G., 2014. Neuronal Nitric Oxide Synthase-Dependent S-Nitrosylation of Gephyrin Regulates Gephyrin Clustering at GABAergic Synapses. J. Neurosci. 34, 7763–7768. https://doi.org/10.1523/JNEUROSCI.0531-14.2014

Dejima, K., Seko, A., Yamashita, K., Gengyo-Ando, K., Mitani, S., Izumikawa, T., Kitagawa, H., Sugahara, K., Mizuguchi, S., Nomura, K., 2006. Essential Roles of 3′-Phosphoadenosine 5′-Phoshosulfate Synthase in Embryonic and Larval Development of the Nematode *Caenorhabditis elegans**. J. Biol. Chem. 281, 11431–11440. https://doi.org/10.1074/jbc.M601509200

Di Meo, I., Fagiolari, G., Prelle, A., Viscomi, C., Zeviani, M., Tiranti, V., 2011. Chronic Exposure to Sulfide Causes Accelerated Degradation of Cytochrome c Oxidase in Ethylmalonic Encephalopathy. Antioxid. Redox Signal. 15, 353–362. https://doi.org/10.1089/ars.2010.3520

Dikalov, S.I., Mayorov, V.I., Panov, A.V., 2017. Physiological Levels of Nitric Oxide Diminish Mitochondrial Superoxide. Potential Role of Mitochondrial Dinitrosyl Iron Complexes and Nitrosothiols. Front. Physiol. 8. https://doi.org/10.3389/fphys.2017.00907

Distelmaier, F., Koopman, W.J.H., van den Heuvel, L.P., Rodenburg, R.J., Mayatepek, E., Willems, P.H.G.M., Smeitink, J.A.M., 2009. Mitochondrial complex I deficiency: from organelle dysfunction to clinical disease. Brain 132, 833–842. https://doi.org/10.1093/brain/awp058

Divakaruni, A.S., Paradyse, A., Ferrick, D.A., Murphy, A.N., Jastroch, M., 2014. Chapter Sixteen - Analysis and Interpretation of Microplate-Based Oxygen Consumption and pH Data, in: Murphy, A.N., Chan, D.C. (Eds.), Methods in Enzymology, Mitochondrial Function. Academic Press, pp. 309–354. https://doi.org/10.1016/B978-0-12-801415-8.00016-3

Dong, X., Xiang, H., Li, Jiajia, Hao, A., Wang, H., Gou, Y., Li, A., Rahaman, S., Qiu, Y., Li, Jiahao, Mei, O., Zhong, J., You, W., Shen, G., Wu, X., Li, Jingjing, Shu, Y., Shi, L.L., Zhu, Y., Reid, R.R., He, T.-C., Fan, J., 2025. Dermal fibroblast-derived extracellular matrix (ECM) synergizes with keratinocytes in promoting re-epithelization and scarless healing of skin wounds: Towards optimized skin tissue engineering. Bioact. Mater. 47, 1–17. https://doi.org/10.1016/j.bioactmat.2024.12.030

Dyson, N., Khambata, R.S., Parakaw, T., Massimo, G., Khuat, N.H., Noor, A.A., Gee, L.C., Lim, I., Siddique, U., Sullivan, A.J., Ho, J.W., Rathod, K., Barnes, M.R., Cabrera, C.P., Ahluwalia, A., 2024. The nitrite reductase activity of xanthine oxidoreductase sustains cardiovascular health. https://doi.org/10.1101/2024.11.01.621390

Efstathiou, S., 2016. Identification and characterization of posttranslational modifications in murine sulfite oxidase.

Eh, M., Kaczmarek, A.T., Schwarz, G., Bender, D., 2022. Molecular mechanism of intramolecular electron transfer in dimeric sulfite oxidase. J. Biol. Chem. 298, 101668. https://doi.org/10.1016/j.jbc.2022.101668

Emdin, C.A., Haas, M.E., Khera, A.V., Aragam, K., Chaffin, M., Klarin, D., Hindy, G., Jiang, L., Wei, W.-Q., Feng, Q., Karjalainen, J., Havulinna, A., Kiiskinen, T., Bick, A., Ardissino, D., Wilson, J.G., Schunkert, H., McPherson, R., Watkins, H., Elosua, R., Bown, M.J., Samani, N.J., Baber, U., Erdmann, J., Gupta, N., Danesh, J., Saleheen, D., Chang, K.-M., Vujkovic, M., Voight, B., Damrauer, S., Lynch, J., Kaplan, D., Serper, M., Tsao, P., Mercader, J., Hanis, C., Daly, M., Denny, J., Gabriel, S., Kathiresan, S., 2020. A missense variant in Mitochondrial Amidoxime Reducing Component 1 gene and protection against liver disease. PLoS Genet. 16, e1008629. https://doi.org/10.1371/journal.pgen.1008629

Emdin, C.A., Haas, M.E., Khera, A.V., Aragam, K., Chaffin, M., Klarin, D., Hindy, G., Jiang, L., Wei, W.-Q., Feng, Q., Karjalainen, J., Havulinna, A., Kiiskinen, T., Bick, A., Ardissino, D., Wilson, J.G., Schunkert, H., McPherson, R., Watkins, H., Elosua, R., Bown, M.J., Samani, N.J., Baber, U., Erdmann, J., Gupta, N., Danesh, J., Saleheen, D., Chang, K.-M., Vujkovic, M., Voight, B., Damrauer, S., Lynch, J., Kaplan, D., Serper, M., Tsao, P., Program, M.V., Mercader, J., Hanis, C., Daly, M., Denny, J., Gabriel, S., Kathiresan, S., 2021. Correction: A missense variant in Mitochondrial Amidoxime Reducing Component 1 gene and protection against liver disease. PLoS Genet. 17, e1009503. https://doi.org/10.1371/journal.pgen.1009503

Emesh, S., Rapson, T.D., Rajapakshe, S.A., Kappler, U., Bernhardt, P.V., Tollin, G., Enemark, J.H., 2009. Intramolecular electron transfer in sulfite oxidizing enzymes: elucidating the role of a conserved active site arginine. Biochemistry 48, 2156–2163. https://doi.org/10.1021/bi801553q

Enroth, C., Eger, B.T., Okamoto, K., Nishino, Tomoko, Nishino, Takeshi, Pai, E.F., 2000. Crystal structures of bovine milk xanthine dehydrogenase and xanthine oxidase: Structure-based mechanism of conversion. Proc. Natl. Acad. Sci. U. S. A. 97, 10723–10728. https://doi.org/10.1073/pnas.97.20.10723

Erusalimsky, J.D., Moncada, S., 2007. Nitric Oxide and Mitochondrial Signaling. Arterioscler. Thromb. Vasc. Biol. 27, 2524–2531. https://doi.org/10.1161/ATVBAHA.107.151167

Faitg, J., Davey, T., Laws, R., Lawless, C., Tuppen, H., Fitton, E., Turnbull, D., Vincent, A.E., 2025. Mapping mitochondrial morphology and function: COX-SBFSEM reveals patterns in mitochondrial disease. Commun. Biol. 8, 24. https://doi.org/10.1038/s42003-024-07389-7

Farahani, Aryan, Farahani, Arman, Kashfi, K., Ghasemi, A., 2025. Inducible nitric oxide synthase (iNOS): More than an inducible enzyme? Rethinking the classification of NOS isoforms. Pharmacol. Res. 216, 107781. https://doi.org/10.1016/j.phrs.2025.107781

Feng, C., Kedia, R.V., Hazzard, J.T., Hurley, J.K., Tollin, G., Enemark, J.H., 2002. Effect of Solution Viscosity on Intramolecular Electron Transfer in Sulfite Oxidase. Biochemistry 41, 5816–5821. https://doi.org/10.1021/bi016059f

Feng, C., Wilson, H.L., Hurley, J.K., Hazzard, J.T., Tollin, G., Rajagopalan, K.V., Enemark, J.H., 2003. Essential Role of Conserved Arginine 160 in Intramolecular Electron Transfer in Human Sulfite Oxidase. Biochemistry 42, 12235–12242. https://doi.org/10.1021/bi0350194

Fischer, K., Barbier, G.G., Hecht, H.-J., Mendel, R.R., Campbell, W.H., Schwarz, G., 2005. Structural Basis of Eukaryotic Nitrate Reduction: Crystal Structures of the Nitrate Reductase Active Site. Plant Cell 17, 1167–1179. https://doi.org/10.1105/tpc.104.029694

Foidart, J.-M., Tryggvason, K., Gehron Robey, P., Liotta, L.A., Martin, G.R., 1981. Biosynthesis of Type IV and V (αA-αB) Collagens by Human Placenta. Coll. Relat. Res. 1, 137–150. https://doi.org/10.1016/S0174-173X(81)80016-7

Forman, H.J., Azzi, A., 1997. On the virtual existence of superoxide anions in mitochondria: thoughts regarding its role in pathophysiology. FASEB J. Off. Publ. Fed. Am. Soc. Exp. Biol. 11, 374–375. https://doi.org/10.1096/fasebj.11.5.9141504

Forner, F., Foster, L.J., Campanaro, S., Valle, G., Mann, M., 2006. Quantitative Proteomic Comparison of Rat Mitochondria from Muscle, Heart, and Liver *. Mol. Cell. Proteomics 5, 608–619. https://doi.org/10.1074/mcp.M500298-MCP200

Förstermann, U., Kleinert, H., 1995. Nitric oxide synthase: expression and expressional control of the three isoforms. Naunyn. Schmiedebergs Arch. Pharmacol. 352, 351–364. https://doi.org/10.1007/BF00172772

Förstermann, U., Sessa, W.C., 2012. Nitric oxide synthases: regulation and function. Eur. Heart J. 33, 829–837. https://doi.org/10.1093/eurheartj/ehr304

Frantz, C., Stewart, K.M., Weaver, V.M., 2010. The extracellular matrix at a glance. J. Cell Sci. 123, 4195–4200. https://doi.org/10.1242/jcs.023820

Friederich, M.W., Elias, A.F., Kuster, A., Laugwitz, L., Larson, A.A., Landry, A.P., Ellwood-Digel, L., Mirsky, D.M., Dimmock, D., Haven, J., Jiang, H., MacLean, K.N., Styren, K., Schoof, J., Goujon, L., Lefrancois, T., Friederich, M., Coughlin, C.R., Banerjee, R., Haack, T.B., Van Hove, J.L.K., 2020. Pathogenic variants in SQOR encoding sulfide:quinone oxidoreductase are a potentially treatable cause of Leigh disease. J. Inherit. Metab. Dis. 43, 1024–1036. https://doi.org/10.1002/jimd.12232

Friedman, J.R., Nunnari, J., 2014. Mitochondrial form and function. Nature 505, 335–343. https://doi.org/10.1038/nature12985

Fu, C.-Y., 2023. Metabolic Changes in Sulfite Oxidase Deficiency: Novel Pathomechanisms of Sulfite and Sulfides. Universität zu Köln.

Fu, C.-Y., Kohl, J.B., Liebsch, F., D'Andrea, D., Mai, M., Mellis, A.T., Kouroussis, E., Ditrói, T., Santamaria-Araujo, J.A., Yeo, S.Y., Endepols, H., Křížková, M., Kozich, V., Barayeu, U., Akaike, T., Hennermann, J.B., Nagy, P., Filipovic, M., Schwarz, G., 2024a. Sulfite oxidase deficiency causes persulfidation loss and H_2S release. bioRxiv 2024.03.13.584820. https://doi.org/10.1101/2024.03.13.584820

Fu, C.-Y., Kohl, J.B., Liebsch, F., D'Andrea, D., Mai, M., Mellis, A.T., Kouroussis, E., Ditrói, T., Santamaria-Araujo, J.A., Yeo, S.Y., Endepols, H., Křížková, M., Kozich, V., Barayeu, U., Akaike, T., Hennermann, J.B., Nagy, P., Filipovic, M., Schwarz, G., 2024b. Sulfite oxidase deficiency causes persulfidation loss and H2S release. bioRxiv 2024.03.13.584820. https://doi.org/10.1101/2024.03.13.584820

Fu, Y., Xiao, H., Zhang, Y., 2012. Beta-adrenoceptor signaling pathways mediate cardiac pathological remodeling. Front. Biosci.-Elite 4, 1625–1637. https://doi.org/10.2741/484

Furchgott, R.F., Zawadzki, J.V., 1980. The obligatory role of endothelial cells in the relaxation of arterial smooth muscle by acetylcholine. Nature 288, 373–376. https://doi.org/10.1038/288373a0

Gajula, S.N.R., Nathani ,Tanaaz Navin, Patil ,Rashmi Madhukar, Talari ,Sasikala, and Sonti, R., 2022. Aldehyde oxidase mediated drug metabolism: an underpredicted obstacle in drug discovery and development. Drug Metab. Rev. 54, 427–448. https://doi.org/10.1080/03602532.2022.2144879

Galante, L.L., Schwarzbauer, J.E., 2007. Requirements for sulfate transport and the diastrophic dysplasia sulfate transporter in fibronectin matrix assembly. J. Cell Biol. 179, 999–1009. https://doi.org/10.1083/jcb.200707150

Galkin, A., Moncada, S., 2007. S-nitrosation of mitochondrial complex I depends on its structural conformation. J. Biol. Chem. 282, 37448–37453. https://doi.org/10.1074/jbc.M707543200

Gao, J., Schatton, D., Martinelli, P., Hansen, H., Pla-Martin, D., Barth, E., Becker, C., Altmueller, J., Frommolt, P., Sardiello, M., Rugarli, E.I., 2014. CLUH regulates mitochondrial biogenesis by binding mRNAs of nuclear-encoded mitochondrial proteins. J. Cell Biol. 207, 213–223. https://doi.org/10.1083/jcb.201403129

Garcia, G.C., Bartol, T.M., Phan, S., Bushong, E.A., Perkins, G., Sejnowski, T.J., Ellisman, M.H., Skupin, A., 2019. Mitochondrial morphology provides a mechanism for energy buffering at synapses. Sci. Rep. 9, 18306. https://doi.org/10.1038/s41598-019-54159-1

Garthwaite, J., Charles, S.L., Chess-Williams, R., 1988. Endothelium-derived relaxing factor release on activation of NMDA receptors suggests role as intercellular messenger in the brain. Nature 336, 385–388. https://doi.org/10.1038/336385a0

Gibson, J.H., Slobedman, B., KN, H., Williamson, S.L., Minchenko, D., El-Osta, A., Stern, J.L., Christodoulou, J., 2010. Downstream targets of methyl CpG binding protein 2 and their abnormal expression in the frontal cortex of the human Rett syndrome brain. BMC Neurosci. 11, 53. https://doi.org/10.1186/1471-2202-11-53

Gladwin, M.T., Kim-Shapiro, D.B., 2008. The functional nitrite reductase activity of the heme-globins. Blood 112, 2636–2647. https://doi.org/10.1182/blood-2008-01-115261

Glancy, B., Kim, Y., Katti, P., Willingham, T.B., 2020. The Functional Impact of Mitochondrial Structure Across Subcellular Scales. Front. Physiol. 11. https://doi.org/10.3389/fphys.2020.541040

Glänzel, N.M., da Rosa-Junior, N.T., Signori, M.F., de Andrade Silveira, J., Pinheiro, C.V., Marcuzzo, M.B., Campos-Carraro, C., da Rosa Araujo, A.S., Schiöth, H.B., Wajner, M., Leipnitz, G., 2024. Increased ROS levels, antioxidant defense disturbances and bioenergetic disruption induced by thiosulfate administration in the brain of neonatal rats. Metab. Brain Dis. 40, 73. https://doi.org/10.1007/s11011-024-01510-9

Gomez-Arroyo, J., Saleem, S.J., Mizuno, S., Syed, A.A., Bogaard, H.J., Abbate, A., Taraseviciene-Stewart, L., Sung, Y., Kraskauskas, D., Farkas, D., Conrad, D.H., Nicolls, M.R., Voelkel, N.F., 2012. A brief overview of mouse models of pulmonary arterial hypertension: problems and prospects. Am. J. Physiol. - Lung Cell. Mol. Physiol. 302, L977–L991. https://doi.org/10.1152/ajplung.00362.2011

Granger, D.N., Kvietys, P.R., 2015. Reperfusion injury and reactive oxygen species: The evolution of a concept. Redox Biol. 6, 524–551. https://doi.org/10.1016/j.redox.2015.08.020

Gregory, C.A., Ma, J., Lomeli, S., 2024. The coordinated activities of collagen VI and XII in maintenance of tissue structure, function and repair: evidence for a physical interaction. Front. Mol. Biosci. 11. https://doi.org/10.3389/fmolb.2024.1376091

Grings, M., Moura, A.P., Amaral, A.U., Parmeggiani, B., Gasparotto, J., Moreira, J.C.F., Gelain, D.P., Wyse, A.T.S., Wajner, M., Leipnitz, G., 2014. Sulfite disrupts brain mitochondrial energy homeostasis and induces mitochondrial permeability transition pore opening *via* thiol group

modification. Biochim. Biophys. Acta BBA - Mol. Basis Dis. 1842, 1413–1422. https://doi.org/10.1016/j.bbadis.2014.04.022

Grings, M., Seminotti, B., Karunanidhi, A., Ghaloul-Gonzalez, L., Mohsen, A.-W., Wipf, P., Palmfeldt, J., Vockley, J., Leipnitz, G., 2019. ETHE1 and MOCS1 deficiencies: Disruption of mitochondrial bioenergetics, dynamics, redox homeostasis and endoplasmic reticulum-mitochondria crosstalk in patient fibroblasts. Sci. Rep. 9, 12651. https://doi.org/10.1038/s41598-019-49014-2

Grings, M., Wajner, M., Leipnitz, G., 2020. Mitochondrial Dysfunction and Redox Homeostasis Impairment as Pathomechanisms of Brain Damage in Ethylmalonic Encephalopathy: Insights from Animal and Human Studies. Cell. Mol. Neurobiol. 42, 565–575. https://doi.org/10.1007/s10571-020-00976-2

Guimier, A., Gordon, C.T., Godard, F., Ravenscroft, G., Oufadem, M., Vasnier, C., Rambaud, C., Nitschke, P., Bole-Feysot, C., Masson, C., Dauger, S., Longman, C., Laing, N.G., Kugener, B., Bonnet, D., Bouvagnet, P., Di Filippo, S., Probst, V., Redon, R., Charron, P., Rötig, A., Lyonnet, S., Dautant, A., de Pontual, L., di Rago, J.-P., Delahodde, A., Amiel, J., 2016. Biallelic PPA2 Mutations Cause Sudden Unexpected Cardiac Arrest in Infancy. Am. J. Hum. Genet. 99, 666–673. https://doi.org/10.1016/j.ajhg.2016.06.021

Guo, Y., Gao, Z., LaGory, E.L., Kristin, L.W., Gupte, J., Gong, Y., Rardin, M.J., Liu, T., Nguyen, T.T., Long, J., Hsu, Y.-H., Murray, J.K., Lade, J., Jackson, S., Zhang, J., 2024. Liver-specific mitochondrial amidoxime-reducing component 1 (Mtarc1) knockdown protects the liver from diet-induced MASH in multiple mouse models. Hepatol. Commun. 8, e0419. https://doi.org/10.1097/HC9.0000000000000419

Hänzelmann, P., Schwarz, G., Mendel, R.R., 2002. Functionality of Alternative Splice Forms of the First Enzymes Involved in Human Molybdenum Cofactor Biosynthesis*. J. Biol. Chem. 277, 18303–18312. https://doi.org/10.1074/jbc.M200947200

Hatanpää, K., Brady, D.R., Stoll, J., Rapoport, S.I., Chandrasekaran, K., 1996. Neuronal activity and early neurofibrillary tangles in Alzheimer's disease. Ann. Neurol. 40, 411–420. https://doi.org/10.1002/ana.410400310

Havemeyer, A., Bittner, F., Wollers, S., Mendel, R., Kunze, T., Clement, B., 2006. Identification of the missing component in the mitochondrial benzamidoxime prodrug-converting system as a novel molybdenum enzyme. J. Biol. Chem. 281, 34796–34802. https://doi.org/10.1074/jbc.M607697200

He, Y., Haque, M.M., Stuehr, D.J., Lu, H.P., 2015. Single-molecule spectroscopy reveals how calmodulin activates NO synthase by controlling its conformational fluctuation dynamics. Proc. Natl. Acad. Sci. 112, 11835–11840. https://doi.org/10.1073/pnas.1508829112

Herculano-Houzel, S., 2011. Scaling of Brain Metabolism with a Fixed Energy Budget per Neuron: Implications for Neuronal Activity, Plasticity and Evolution. PLoS ONE 6, e17514. https://doi.org/10.1371/journal.pone.0017514

Hess, D.T., Matsumoto, A., Kim, S.-O., Marshall, H.E., Stamler, J.S., 2005. Protein S-nitrosylation: purview and parameters. Nat. Rev. Mol. Cell Biol. 6, 150–166. https://doi.org/10.1038/nrm1569

Hildebrandt, T.M., Grieshaber, M.K., 2008. Three enzymatic activities catalyze the oxidation of sulfide to thiosulfate in mammalian and invertebrate mitochondria. FEBS J. 275, 3352–3361. https://doi.org/10.1111/j.1742-4658.2008.06482.x

Hille, R., Nishino, T., 1995. Flavoprotein structure and mechanism. 4. Xanthine oxidase and xanthine dehydrogenase. FASEB J. Off. Publ. Fed. Am. Soc. Exp. Biol. 9, 995–1003.

Hitosugi, T., Fan, J., Chung, T.-W., Lythgoe, K., Wang, X., Xie, J., Ge, Q., Gu, T.-L., Polakiewicz, R.D., Roesel, J.L., Chen, Z. (Georgia), Boggon, T.J., Lonial, S., Fu, H., Khuri, F.R., Kang, S., Chen, J., 2011. Tyrosine phosphorylation of mitochondrial pyruvate dehydrogenase kinase 1 is important for cancer metabolism. Mol. Cell 44, 864–877. https://doi.org/10.1016/j.molcel.2011.10.015

Ho, G.P.H., Selvakumar, B., Mukai, J., Hester, L.D., Wang, Y., Gogos, J.A., Snyder, S.H., 2011. S-Nitrosylation and S-Palmitoylation Reciprocally Regulate Synaptic Targeting of PSD-95. Neuron 71, 131–141. https://doi.org/10.1016/j.neuron.2011.05.033

Hock, M.B., Kralli, A., 2009. Transcriptional Control of Mitochondrial Biogenesis and Function. Annu. Rev. Physiol. 71, 177–203. https://doi.org/10.1146/annurev.physiol.010908.163119

Hord, N.G., Tang, Y., Bryan, N.S., 2009. Food sources of nitrates and nitrites: the physiologic context for potential health benefits2. Am. J. Clin. Nutr. 90, 1–10. https://doi.org/10.3945/ajcn.2008.27131

Huang, Z., Shiva, S., Kim-Shapiro, D.B., Patel, R.P., Ringwood, L.A., Irby, C.E., Huang, K.T., Ho, C., Hogg, N., Schechter, A.N., Gladwin, M.T., 2005. Enzymatic function of hemoglobin as a nitrite reductase that produces NO under allosteric control. J. Clin. Invest. 115, 2099–2107. https://doi.org/10.1172/JCI24650

Huxtable, R.J., 1992. Physiological actions of taurine. Physiol. Rev. 72, 101–163. https://doi.org/10.1152/physrev.1992.72.1.101

Ichida, K., Matsumura, T., Sakuma, R., Hosoya, T., Nishino, T., 2001. Mutation of human molybdenum cofactor sulfurase gene is responsible for classical xanthinuria type II. Biochem. Biophys. Res. Commun. 282, 1194–1200. https://doi.org/10.1006/bbrc.2001.4719

Iglesias, D.E., Bombicino, S.S., Valdez, L.B., Boveris, A., 2015. Nitric oxide interacts with mitochondrial complex III producing antimycin-like effects. Free Radic. Biol. Med. 89, 602–613. https://doi.org/10.1016/j.freeradbiomed.2015.08.024

Ignarro, L.J., Byrns, R.E., Buga, G.M., Wood, K.S., 1987. Endothelium-derived relaxing factor from pulmonary artery and vein possesses pharmacologic and chemical properties identical to those of nitric oxide radical. Circ. Res. 61, 866–879.

Ilani, T., Alon, A., Grossman, I., Horowitz, B., Kartvelishvily, E., Cohen, S.R., Fass, D., 2013. A Secreted Disulfide Catalyst Controls Extracellular Matrix Composition and Function. Science 341, 74–76. https://doi.org/10.1126/science.1238279

Islinger, M., Lüers, G.H., Li, K.W., Loos, M., Völkl, A., 2007. Rat liver peroxisomes after fibrate treatment. A survey using quantitative mass spectrometry. J. Biol. Chem. 282, 23055–23069. https://doi.org/10.1074/jbc.M610910200

Ito, J.T., Lourenço, J.D., Righetti, R.F., Tibério, I.F.L.C., Prado, C.M., Lopes, F.D.T.Q.S., 2019. Extracellular Matrix Component Remodeling in Respiratory Diseases: What Has Been Found in Clinical and Experimental Studies? Cells 8, 342. https://doi.org/10.3390/cells8040342

Izu, Y., Sun, M., Zwolanek, D., Veit, G., Williams, V., Cha, B., Jepsen, K.J., Koch, M., Birk, D.E., 2011. Type XII collagen regulates osteoblast polarity and communication during bone formation. J. Cell Biol. 193, 1115–1130. https://doi.org/10.1083/jcb.201010010

Jackson, M.R., Melideo, S.L., Jorns, M.S., 2012. Human sulfide:quinone oxidoreductase catalyzes the first step in hydrogen sulfide metabolism and produces a sulfane sulfur metabolite. Biochemistry 51, 6804–6815. https://doi.org/10.1021/bi300778t

Jakubiczka-Smorag, J., Santamaria-Araujo, J.A., Metz, I., Kumar, A., Hakroush, S., Brueck, W., Schwarz, G., Burfeind, P., Reiss, J., Smorag, L., 2016. Mouse model for molybdenum cofactor deficiency type B recapitulates the phenotype observed in molybdenum cofactor deficient patients. Hum. Genet. 135, 813–826. https://doi.org/10.1007/s00439-016-1676-4

Janik, M.K., Smyk, W., Kruk, B., Szczepankiewicz, B., Górnicka, B., Lebiedzińska-Arciszewska, M., Potes, Y., Simões, I.C.M., Weber, S.N., Lammert, F., Więckowski, M.R., Milkiewicz, P., Krawczyk, M., 2021. MARC1 p.A165T variant is associated with decreased markers of liver injury and enhanced antioxidant capacity in autoimmune hepatitis. Sci. Rep. 11, 24407. https://doi.org/10.1038/s41598-021-03521-3

Jitrapakdee, S., St Maurice, M., Rayment, I., Cleland, W.W., Wallace, J.C., Attwood, P.V., 2008. Structure, mechanism and regulation of pyruvate carboxylase. Biochem. J. 413, 369–387. https://doi.org/10.1042/BJ20080709

Johannes, L., 2023. Isolated sulfite oxidase deficiency in mice: potential treatment strategies and discovery of a novel dermal phenotype.

Johannes, L., Fu, C.-Y., Schwarz, G., 2022. Molybdenum Cofactor Deficiency in Humans. Molecules 27, 6896. https://doi.org/10.3390/molecules27206896

Johannsen, D.L., Ravussin, E., 2009. The role of mitochondria in health and disease. Curr. Opin. Pharmacol. 9, 780–786. https://doi.org/10.1016/j.coph.2009.09.002

Johnson, J.L., Hainline, B.E., Rajagopalan, K.V., Arison, B.H., 1984. The pterin component of the molybdenum cofactor. Structural characterization of two fluorescent derivatives. J. Biol. Chem. 259, 5414–5422. https://doi.org/10.1016/S0021-9258(18)91027-6

Johnson-Winters, K., Nordstrom, A.R., Emesh, S., Astashkin, A.V., Rajapakshe, A., Berry, R.E., Tollin, G., Enemark, J.H., 2010. Effects of interdomain tether length and flexibility on the kinetics of intramolecular electron transfer in human sulfite oxidase. Biochemistry 49, 1290–1296. https://doi.org/10.1021/bi9020296

Jourdain, A.A., Popow, J., de la Fuente, M.A., Martinou, J.-C., Anderson, P., Simarro, M., 2017. The FASTK family of proteins: emerging regulators of mitochondrial RNA biology. Nucleic Acids Res. 45, 10941–10947. https://doi.org/10.1093/nar/gkx772

Kabil, O., Banerjee, R., 2014. Enzymology of H2S Biogenesis, Decay and Signaling. Antioxid. Redox Signal. 20, 770–782. https://doi.org/10.1089/ars.2013.5339

Kabil, O., Banerjee, R., 2012. Characterization of Patient Mutations in Human Persulfide Dioxygenase (ETHE1) Involved in H2S Catabolism. J. Biol. Chem. 287, 44561–44567. https://doi.org/10.1074/jbc.M112.407411

Kaczmarek, A.T., 2019. Reaction mechanism and physiologic relevance of sulfite oxidase-dependent NO formation. Universität zu Köln.

Kaczmarek, A.T., Bahlmann, N., Thaqi, B., May, P., Schwarz, G., 2021. Machine learning-based identification and characterization of 15 novel pathogenic *SUOX* missense mutations. Mol. Genet. Metab. 134, 188–194. https://doi.org/10.1016/j.ymgme.2021.07.011

Kaczmarek, A.T., Bender, D., Gehling, T., Kohl, J.B., Daimagüler, H.-S., Santamaria-Araujo, J.A., Liebau, M.C., Koy, A., Cirak, S., Schwarz, G., 2022. A defect in molybdenum cofactor binding causes an attenuated form of sulfite oxidase deficiency. J. Inherit. Metab. Dis. 45, 169–182. https://doi.org/10.1002/jimd.12454

Kaczmarek, A.T., Strampraad, M.J.F., Hagedoorn, P.-L., Schwarz, G., 2019. Reciprocal regulation of sulfite oxidation and nitrite reduction by mitochondrial sulfite oxidase. Nitric Oxide 89, 22–31. https://doi.org/10.1016/j.niox.2019.04.004

Kapur, N.K., 2011. Transforming Growth Factor-β. Circ. Heart Fail. 4, 5–7. https://doi.org/10.1161/CIRCHEARTFAILURE.110.960054

Kaufholdt, D., Baillie, C.-K., Meinen, R., Mendel, R.R., Hänsch, R., 2017. The Molybdenum Cofactor Biosynthesis Network: In vivo Protein-Protein Interactions of an Actin Associated Multi-Protein Complex. Front. Plant Sci. 8. https://doi.org/10.3389/fpls.2017.01946

Kawasaki, B.T., Hoffman, K.B., Yamamoto, R.S., Bahr, B.A., 1997. Variants of the receptor/channel clustering molecule gephyrin in brain: distinct distribution patterns, developmental profiles, and proteolytic cleavage by calpain. J. Neurosci. Res. 49, 381–388.

Kim, J., Tchernyshyov, I., Semenza, G.L., Dang, C.V., 2006. HIF-1-mediated expression of pyruvate dehydrogenase kinase: A metabolic switch required for cellular adaptation to hypoxia. Cell Metab. 3, 177–185. https://doi.org/10.1016/j.cmet.2006.02.002

Kimura, H., 2014. Hydrogen Sulfide and Polysulfides as Biological Mediators. Molecules 19, 16146–16157. https://doi.org/10.3390/molecules191016146

Kimura, T., Ferran, B., Tsukahara, Y., Shang, Q., Desai, S., Fedoce, A., Pimentel, D.R., Luptak, I., Adachi, T., Ido, Y., Matsui, R., Bachschmid, M.M., 2019. Production of adeno-associated virus vectors for in vitro and in vivo applications. Sci. Rep. 9, 13601. https://doi.org/10.1038/s41598-019-49624-w

Kirsch, J., Wolters, I., Triller, A., Betz, H., 1993. Gephyrin antisense oligonucleotides prevent glycine receptor clustering in spinal neurons. Nature 366, 745–748. https://doi.org/10.1038/366745a0

Kisker, C., Schindelin, H., Pacheco, A., Wehbi, W.A., Garrett, R.M., Rajagopalan, K.V., Enemark, J.H., Rees, D.C., 1997. Molecular Basis of Sulfite Oxidase Deficiency from the Structure of Sulfite Oxidase. Cell 91, 973–983. https://doi.org/10.1016/S0092-8674(00)80488-2

Klein, J.M., Busch, J.D., Potting, C., Baker, M.J., Langer, T., Schwarz, G., 2012. The Mitochondrial Amidoxime-reducing Component (mARC1) Is a Novel Signal-anchored Protein of the Outer Mitochondrial Membrane. J. Biol. Chem. 287, 42795–42803. https://doi.org/10.1074/jbc.M112.419424

Klein, J.M., Schwarz, G., 2012. Cofactor-dependent maturation of mammalian sulfite oxidase links two mitochondrial import pathways. J. Cell Sci. 125, 4876–4885. https://doi.org/10.1242/jcs.110114

Kleinbongard, P., Dejam, A., Lauer, T., Jax, T., Kerber, S., Gharini, P., Balzer, J., Zotz, R.B., Scharf, R.E., Willers, R., Schechter, A.N., Feelisch, M., Kelm, M., 2006. Plasma nitrite concentrations reflect the degree of endothelial dysfunction in humans. Free Radic. Biol. Med. 40, 295–302. https://doi.org/10.1016/j.freeradbiomed.2005.08.025

Koh, J.-H., Pataky, M.W., Dasari, S., Klaus, K.A., Vuckovic, I., Ruegsegger, G.N., Kumar, A.P., Robinson, M.M., Nair, K.S., 2022. Enhancement of anaerobic glycolysis – a role of PGC-1α4 in resistance exercise. Nat. Commun. 13, 2324. https://doi.org/10.1038/s41467-022-30056-6

Kohl, J.B., 2019. A Novel Mouse Model of Sulfite Oxidase Deficiency: Pathological Changes in Cysteine and H2S Metabolism. Universität zu Köln, Köln.

Kondoh, H., Lleonart, M.E., Gil, J., Wang, J., Degan, P., Peters, G., Martinez, D., Carnero, A., Beach, D., 2005. Glycolytic enzymes can modulate cellular life span. Cancer Res. 65, 177–185.

Kožich, V., Schwahn, B.C., Sokolová, J., Křížková, M., Ditroi, T., Krijt, J., Khalil, Y., Křížek, T., Vaculíková-Fantlová, T., Stibůrková, B., Mills, P., Clayton, P., Barvíková, K., Blessing, H., Sykut-Cegielska, J., Dionisi-Vici, C., Gasperini, S., García-Cazorla, Á., Haack, T.B., Honzík, T., Ješina, P., Kuster, A., Laugwitz, L., Martinelli, D., Porta, F., Santer, R., Schwarz, G., Nagy, P., 2022. Human ultrarare genetic disorders of sulfur metabolism demonstrate redundancies in H2S homeostasis. Redox Biol. 58, 102517. https://doi.org/10.1016/j.redox.2022.102517

Kramer, S., Johnson, J., Ribeiro, A., Millington, D., Rajagopalan, K., 1987. The structure of the molybdenum cofactor. Characterization of di-(carboxamidomethyl)molybdopterin from sulfite oxidase and xanthine oxidase. J. Biol. Chem. 262, 16357–16363. https://doi.org/10.1016/S0021-9258(18)49263-0

Kriaucionis, S., Paterson, A., Curtis, J., Guy, J., MacLeod, N., Bird, A., 2006. Gene Expression Analysis Exposes Mitochondrial Abnormalities in a Mouse Model of Rett Syndrome. Mol. Cell. Biol. 26, 5033–5042. https://doi.org/10.1128/MCB.01665-05

Kubitza, C., Bittner, F., Ginsel, C., Havemeyer, A., Clement, B., Scheidig, A.J., 2018. Crystal structure of human mARC1 reveals its exceptional position among eukaryotic molybdenum enzymes. Proc. Natl. Acad. Sci. 115, 11958–11963. https://doi.org/10.1073/pnas.1808576115

Kucharská, J., Braunová, Z., Ulicná, O., Zlatos, L., Gvozdjáková, A., 2000. Deficit of coenzyme Q in heart and liver mitochondria of rats with streptozotocin-induced diabetes. Physiol. Res. 49, 411–418.

Kühl, I., Miranda, M., Atanassov, I., Kuznetsova, I., Hinze, Y., Mourier, A., Filipovska, A., Larsson, N.-G., 2017. Transcriptomic and proteomic landscape of mitochondrial dysfunction reveals secondary coenzyme Q deficiency in mammals. eLife 6, e30952. https://doi.org/10.7554/eLife.30952

Kumar, A., Dejanovic, B., Hetsch, F., Semtner, M., Fusca, D., Arjune, S., Santamaria-Araujo, J.A., Winkelmann, A., Ayton, S., Bush, A.I., Kloppenburg, P., Meier, J.C., Schwarz, G., Belaidi, A.A., 2019. S-sulfocysteine/NMDA receptor–dependent signaling underlies neurodegeneration in molybdenum cofactor deficiency. J. Clin. Invest. 127, 4365–4378. https://doi.org/10.1172/JCI89885

Laemmli, U.K., 1970. Cleavage of Structural Proteins during the Assembly of the Head of Bacteriophage T4. Nature 227, 680–685. https://doi.org/10.1038/227680a0

Lagoutte, E., Mimoun, S., Andriamihaja, M., Chaumontet, C., Blachier, F., Bouillaud, F., 2010. Oxidation of hydrogen sulfide remains a priority in mammalian cells and causes reverse electron transfer in colonocytes. Biochim. Biophys. Acta 1797, 1500–1511. https://doi.org/10.1016/j.bbabio.2010.04.004

Leo, F., Suvorava, T., Heuser, S.K., Li, J., LoBue, A., Barbarino, F., Piragine, E., Schneckmann, R., Hutzler, B., Good, M.E., Fernandez, B.O., Vornholz, L., Rogers, S., Doctor, A., Grandoch, M., Stegbauer, J., Weitzberg, E., Feelisch, M., Lundberg, J.O., Isakson, B.E., Kelm, M., Cortese-Krott, M.M., 2021. Red Blood Cell and Endothelial eNOS Independently Regulate Circulating Nitric Oxide Metabolites and Blood Pressure. Circulation 144, 870–889. https://doi.org/10.1161/CIRCULATIONAHA.120.049606

Li, H., Samouilov, A., Liu, X., Zweier, J.L., 2003. Characterization of the magnitude and kinetics of xanthine oxidase-catalyzed nitrate reduction: evaluation of its role in nitrite and nitric oxide generation in anoxic tissues. Biochemistry 42, 1150–1159. https://doi.org/10.1021/bi026385a

Li, L., Huang, J., Liu, Y., 2024. The extracellular matrix glycoprotein fibrillin-1 in health and disease. Front. Cell Dev. Biol. 11. https://doi.org/10.3389/fcell.2023.1302285

Li, P., Wang, D., Lucas, J., Oparil, S., Xing, D., Cao, X., Novak, L., Renfrow, M.B., Chen, Y.-F., 2008. Atrial Natriuretic Peptide Inhibits Transforming Growth Factor β–Induced Smad Signaling and Myofibroblast Transformation in Mouse Cardiac Fibroblasts. Circ. Res. 102, 185–192. https://doi.org/10.1161/CIRCRESAHA.107.157677

Li, X., Jiang, Y., Meisenhelder, J., Yang, W., Hawke, D.H., Zheng, Y., Xia, Y., Aldape, K., He, J., Hunter, T., Wang, L., Lu, Z., 2016. Mitochondria-translocated phosphoglycerate kinase 1 functions as a protein kinase to coordinate glycolysis and TCA cycle in tumorigenesis. Mol. Cell 61, 705–719. https://doi.org/10.1016/j.molcel.2016.02.009

Libiad, M., Yadav, P.K., Vitvitsky, V., Martinov, M., Banerjee, R., 2014. Organization of the Human Mitochondrial Hydrogen Sulfide Oxidation Pathway♦. J. Biol. Chem. 289, 30901–30910. https://doi.org/10.1074/jbc.M114.602664

Liebsch, F., Eggersmann, F.R., Merkler, Y., Kloppenburg, P., Schwarz, G., 2023. Automated Image Analysis Reveals Different Localization of Synaptic Gephyrin C4 Splice Variants. eNeuro 10, ENEURO.0102-22.2022. https://doi.org/10.1523/ENEURO.0102-22.2022

Lim, Y.J., Foo, T.C., Yeung, A.W.S., Tu, X., Ma, Y., Hawkins, C.L., Witting, P.K., Jameson, G.N.L., Terentis, A.C., Thomas, S.R., 2019. Human Indoleamine 2,3-Dioxygenase 1 Is an Efficient Mammalian Nitrite Reductase. Biochemistry 58, 974–986. https://doi.org/10.1021/acs.biochem.8b01231

Liu, G., Ma, C., Yang, H., Zhang, P.-Y., 2017. Transforming growth factor β and its role in heart disease (Review). Exp. Ther. Med. 13, 2123–2128. https://doi.org/10.3892/etm.2017.4246

Lundberg, J.O., 2012. Nitrate transport in salivary glands with implications for NO homeostasis. Proc. Natl. Acad. Sci. U. S. A. 109, 13144–13145. https://doi.org/10.1073/pnas.1210412109

Lundberg, J.O., Weitzberg, E., Gladwin, M.T., 2008. The nitrate–nitrite–nitric oxide pathway in physiology and therapeutics. Nat. Rev. Drug Discov. 7, 156–167. https://doi.org/10.1038/nrd2466

Lundberg, J.O., Weitzberg, E., Lundberg, J.M., Alving, K., 1994. Intragastric nitric oxide production in humans: measurements in expelled air. Gut 35, 1543–1546. https://doi.org/10.1136/gut.35.11.1543

Macabrey, D., Joniová, J., Gasser, Q., Bechelli, C., Longchamp, A., Urfer, S., Lambelet, M., Fu, C.-Y., Schwarz, G., Wagnières, G., Déglise, S., Allagnat, F., 2022. Sodium thiosulfate, a source of hydrogen sulfide, stimulates endothelial cell proliferation and neovascularization. Front. Cardiovasc. Med. 9, 965965. https://doi.org/10.3389/fcvm.2022.965965

Magalon, A., Mendel, R.R., 2015. Biosynthesis and Insertion of the Molybdenum Cofactor. EcoSal Plus 6, 10.1128/ecosalplus.ESP-0006–2013. https://doi.org/10.1128/ecosalplus.esp-0006-2013

Maia, L.B., Pereira, V., Mira, L., Moura, J.J.G., 2015. Nitrite Reductase Activity of Rat and Human Xanthine Oxidase, Xanthine Dehydrogenase, and Aldehyde Oxidase: Evaluation of

Their Contribution to NO Formation in Vivo. Biochemistry 54, 685–710. https://doi.org/10.1021/bi500987w

Mak, S., Witte, K.K., Al-Hesayen, A., Granton, J.J., Parker, J.D., 2012. Cardiac sympathetic activation in patients with pulmonary arterial hypertension. Am. J. Physiol.-Regul. Integr. Comp. Physiol. 302, R1153–R1157. https://doi.org/10.1152/ajpregu.00652.2011

Marcia, M., Ermler, U., Peng, G., Michel, H., 2010. A new structure-based classification of sulfide:quinone oxidoreductases. Proteins Struct. Funct. Bioinforma. 78, 1073–1083. https://doi.org/10.1002/prot.22665

Marsin, A.-S., Bertrand†, L., Rider, M.H., Deprez, J., Beauloye, C., Vincent‡, M.F., Berghe‡, G.V. den, Carling, D., Hue, L., 2000. Phosphorylation and activation of heart PFK-2 by AMPK has a role in the stimulation of glycolysis during ischaemia. Curr. Biol. 10, 1247–1255. https://doi.org/10.1016/S0960-9822(00)00742-9

Maynard, S., Hejl, A.-M., Dinh, T.-S.T., Keijzers, G., Hansen, Å.M., Desler, C., Moreno-Villanueva, M., Bürkle, A., Rasmussen, L.J., Waldemar, G., Bohr, V.A., 2015. Defective mitochondrial respiration, altered dNTP pools and reduced AP endonuclease 1 activity in peripheral blood mononuclear cells of Alzheimer's disease patients. Aging 7, 793–810. https://doi.org/10.18632/aging.100810

Mayr, S.J., Röper, J., Schwarz, G., 2020. Alternative splicing of the bicistronic gene molybdenum cofactor synthesis 1 (MOCS1) uncovers a novel mitochondrial protein maturation mechanism. J. Biol. Chem. 295, 3029–3039. https://doi.org/10.1074/jbc.RA119.010720

McFate, T., Mohyeldin, A., Lu, H., Thakar, J., Henriques, J., Halim, N.D., Wu, H., Schell, M.J., Tsang, T.M., Teahan, O., Zhou, S., Califano, J.A., Jeoung, N.H., Harris, R.A., Verma, A., 2008. Pyruvate Dehydrogenase Complex Activity Controls Metabolic and Malignant Phenotype in Cancer Cells. J. Biol. Chem. 283, 22700–22708. https://doi.org/10.1074/jbc.M801765200

Mellis, A.-T., Misko, A.L., Arjune, S., Liang, Y., Erdélyi, K., Ditrói, T., Kaczmarek, A.T., Nagy, P., Schwarz, G., 2020. The role of glutamate oxaloacetate transaminases in sulfite biosynthesis and H2S metabolism. Redox Biol. 38, 101800. https://doi.org/10.1016/j.redox.2020.101800

Mellis, A.-T., Roeper, J., Misko, A.L., Kohl, J., Schwarz, G., 2021. Sulfite Alters the Mitochondrial Network in Molybdenum Cofactor Deficiency. Front. Genet. 11. https://doi.org/10.3389/fgene.2020.594828

Mendel, R.R., 2013. The Molybdenum Cofactor. J. Biol. Chem. 288, 13165–13172. https://doi.org/10.1074/jbc.R113.455311

Mendel, R.R., Schwarz, G., 2011. Molybdenum cofactor biosynthesis in plants and humans. Coord. Chem. Rev., Molybdenum 255, 1145–1158. https://doi.org/10.1016/j.ccr.2011.01.054

Millar, T.M., Stevens, C.R., Benjamin, N., Eisenthal, R., Harrison, R., Blake, D.R., 1998. Xanthine oxidoreductase catalyses the reduction of nitrates and nitrite to nitric oxide under hypoxic conditions. FEBS Lett. 427, 225–228. https://doi.org/10.1016/S0014-5793(98)00430-X

Murphy, E., Ardehali, H., Balaban, R.S., DiLisa, F., Dorn, G.W., Kitsis, R.N., Otsu, K., Ping, P., Rizzuto, R., Sack, M.N., Wallace, D., Youle, R.J., on behalf of the American Heart Association Council on Basic Cardiovascular Sciences, Council on Clinical Cardiology, and Council on Functional Genomics and Translational Biology, 2016. Mitochondrial Function, Biology, and Role in Disease. Circ. Res. 118, 1960–1991. https://doi.org/10.1161/RES.0000000000000104

Nakamura, T., Lipton, S.A., 2010. Redox regulation of mitochondrial fission, protein misfolding, synaptic damage, and neuronal cell death: potential implications for Alzheimer's and Parkinson's diseases. Apoptosis 15, 1354–1363. https://doi.org/10.1007/s10495-010-0476-x

Nishino, Tomoko, Nishino, Takeshi, 1997. The Conversion from the Dehydrogenase Type to the Oxidase Type of Rat Liver Xanthine Dehydrogenase by Modification of Cysteine Residues with Fluorodinitrobenzene*. J. Biol. Chem. 272, 29859–29864. https://doi.org/10.1074/jbc.272.47.29859

Nolte, H., MacVicar, T.D., Tellkamp, F., Krüger, M., 2018. Instant Clue: A Software Suite for Interactive Data Visualization and Analysis. Sci. Rep. 8, 12648. https://doi.org/10.1038/s41598-018-31154-6

Numata, G., Takimoto, E., 2022. Cyclic GMP and PKG Signaling in Heart Failure. Front. Pharmacol. 13. https://doi.org/10.3389/fphar.2022.792798

Nunnari, J., Suomalainen, A., 2012. Mitochondria: In Sickness and in Health. Cell 148, 1145–1159. https://doi.org/10.1016/j.cell.2012.02.035

Oh, C., Nakamura, T., Zhang, X., Lipton, S.A., 2024. Redox regulation, protein S-nitrosylation, and synapse loss in Alzheimer's and related dementias. Neuron 112, 3823–3850. https://doi.org/10.1016/j.neuron.2024.10.013

Oh, C.-K., Sultan, A., Platzer, J., Dolatabadi, N., Soldner, F., McClatchy, D.B., Diedrich, J.K., Yates, J.R., Ambasudhan, R., Nakamura, T., Jaenisch, R., Lipton, S.A., 2017. S-Nitrosylation of PINK1 Attenuates PINK1/Parkin-Dependent Mitophagy in hiPSC-Based Parkinson's Disease Models. Cell Rep. 21, 2171–2182. https://doi.org/10.1016/j.celrep.2017.10.068

Ohkubo, A., Van Haute, L., Rudler, D.L., Stentenbach, M., Steiner, F.A., Rackham, O., Minczuk, M., Filipovska, A., Martinou, J.-C., 2021. The FASTK family proteins fine-tune mitochondrial RNA processing. PLoS Genet. 17, e1009873. https://doi.org/10.1371/journal.pgen.1009873

Okamoto, K., Matsumoto, K., Hille, R., Eger, B.T., Pai, E.F., Nishino, T., 2004. The crystal structure of xanthine oxidoreductase during catalysis: Implications for reaction mechanism and enzyme inhibition. Proc. Natl. Acad. Sci. 101, 7931–7936. https://doi.org/10.1073/pnas.0400973101

Ono, H., Ito, A., 1984. Transport of the Precursor for Sulfite Oxidase into Intermembrane Space of Liver Mitochondria: Characterization of Import and Processing Activities1. J. Biochem. (Tokyo) 95, 345–352. https://doi.org/10.1093/oxfordjournals.jbchem.a134614

Pacheco, A., Hazzard, J.T., Tollin, G., Enemark, J.H., 1999. The pH dependence of intramolecular electron transfer rates in sulfite oxidase at high and low anion concentrations. JBIC J. Biol. Inorg. Chem. 4, 390–401. https://doi.org/10.1007/s007750050325

Page, C.C., Moser, C.C., Chen, X., Dutton, P.L., 1999. Natural engineering principles of electron tunnelling in biological oxidation–reduction. Nature 402, 47–52. https://doi.org/10.1038/46972

Palmer, R.M.J., Ferrige, A.G., Moncada, S., 1987. Nitric oxide release accounts for the biological activity of endothelium-derived relaxing factor. Nature 327, 524–526. https://doi.org/10.1038/327524a0

Palmer, T., Santini, C.L., Iobbi-Nivol, C., Eaves, D.J., Boxer, D.H., Giordano, G., 1996. Involvement of the narJ and mob gene products in distinct steps in the biosynthesis of the molybdoenzyme nitrate reductase in Escherichia coli. Mol. Microbiol. 20, 875–884. https://doi.org/10.1111/j.1365-2958.1996.tb02525.x

Palmieri, E.M., Gonzalez-Cotto, M., Baseler, W.A., Davies, L.C., Ghesquière, B., Maio, N., Rice, C.M., Rouault, T.A., Cassel, T., Higashi, R.M., Lane, A.N., Fan, T.W.-M., Wink, D.A., McVicar, D.W., 2020. Nitric oxide orchestrates metabolic rewiring in M1 macrophages by targeting aconitase 2 and pyruvate dehydrogenase. Nat. Commun. 11, 698. https://doi.org/10.1038/s41467-020-14433-7

Pappas, G., Wilkinson, M.L., Gow, A.J., 2023. Nitric oxide regulation of cellular metabolism: Adaptive tuning of cellular energy. Nitric Oxide 131, 8–17. https://doi.org/10.1016/j.niox.2022.11.006

Paragas, E.M., Choughule, K., Jones, J.P., Barr, J.T., 2021. Enzyme Kinetics, Pharmacokinetics, and Inhibition of Aldehyde Oxidase, in: Nagar, S., Argikar, U.A., Tweedie,

D. (Eds.), Enzyme Kinetics in Drug Metabolism: Fundamentals and Applications. Springer US, New York, NY, pp. 257–284. https://doi.org/10.1007/978-1-0716-1554-6_10

Pasdois, P., Parker, J.E., Griffiths, E.J., Halestrap, A.P., 2011. The role of oxidized cytochrome c in regulating mitochondrial reactive oxygen species production and its perturbation in ischaemia. Biochem. J. 436, 493–505. https://doi.org/10.1042/BJ20101957

Paul, B.D., Snyder, S.H., 2018. Gasotransmitter hydrogen sulfide signaling in neuronal health and disease. Biochem. Pharmacol., The Role of Hydrogen Sulfide in Health and Disease 149, 101–109. https://doi.org/10.1016/j.bcp.2017.11.019

Paul, B.D., Snyder, S.H., 2012. H2S signalling through protein sulfhydration and beyond. Nat. Rev. Mol. Cell Biol. 13, 499–507. https://doi.org/10.1038/nrm3391

Perrelli, M.-G., Pagliaro, P., Penna, C., 2011. Ischemia/reperfusion injury and cardioprotective mechanisms: Role of mitochondria and reactive oxygen species. World J. Cardiol. 3, 186–200. https://doi.org/10.4330/wjc.v3.i6.186

Pfleger, J., He, M., Abdellatif, M., 2015. Mitochondrial complex II is a source of the reserve respiratory capacity that is regulated by metabolic sensors and promotes cell survival. Cell Death Dis. 6, e1835–e1835. https://doi.org/10.1038/cddis.2015.202

Pla-Martín, D., Schatton, D., Wiederstein, J.L., Marx, M., Khiati, S., Krüger, M., Rugarli, E.I., 2020. CLUH granules coordinate translation of mitochondrial proteins with mTORC1 signaling and mitophagy. EMBO J. 39, e102731. https://doi.org/10.15252/embj.2019102731

Plass, M., Rasmussen, S.H., Krogh, A., 2017. Highly accessible AU-rich regions in 3' untranslated regions are hotspots for binding of regulatory factors. PLoS Comput. Biol. 13, e1005460. https://doi.org/10.1371/journal.pcbi.1005460

Plikus, M.V., Wang, X., Sinha, S., Forte, E., Thompson, S.M., Herzog, E.L., Driskell, R.R., Rosenthal, N., Biernaskie, J., Horsley, V., 2021. Fibroblasts: origins, definitions, and functions in health and disease. Cell 184, 3852–3872. https://doi.org/10.1016/j.cell.2021.06.024

Poderoso, J.J., Carreras, M.C., Lisdero, C., Riobó, N., Schöpfer, F., Boveris, A., 1996. Nitric Oxide Inhibits Electron Transfer and Increases Superoxide Radical Production in Rat Heart Mitochondria and Submitochondrial Particles. Arch. Biochem. Biophys. 328, 85–92. https://doi.org/10.1006/abbi.1996.0146

Poderoso, J.J., Carreras, M.C., Schöpfer, F., Lisdero, C.L., Riobó, N.A., Giulivi, C., Boveris, A.D., Boveris, A., Cadenas, E., 1999. The reaction of nitric oxide with ubiquinol: kinetic properties and biological significance. Free Radic. Biol. Med. 26, 925–935. https://doi.org/10.1016/S0891-5849(98)00277-9

Porcelli, A.M., Ghelli, A., Zanna, C., Pinton, P., Rizzuto, R., Rugolo, M., 2005. pH difference across the outer mitochondrial membrane measured with a green fluorescent protein mutant. Biochem. Biophys. Res. Commun. 326, 799–804. https://doi.org/10.1016/j.bbrc.2004.11.105

Pozuelo Rubio, M., Peggie, M., Wong, B.H.C., Morrice, N., MacKintosh, C., 2003. 14-3-3s regulate fructose-2,6-bisphosphate levels by binding to PKB-phosphorylated cardiac fructose-2,6-bisphosphate kinase/phosphatase. EMBO J. 22, 3514–3523. https://doi.org/10.1093/emboj/cdg363

Pride, C.K., Mo, L., Quesnelle, K., Dagda, R.K., Murillo, D., Geary, L., Corey, C., Portella, R., Zharikov, S., St Croix, C., Maniar, S., Chu, C.T., K. H. Khoo, N., Shiva, S., 2014. Nitrite activates protein kinase A in normoxia to mediate mitochondrial fusion and tolerance to ischaemia/reperfusion. Cardiovasc. Res. 101, 57–68. https://doi.org/10.1093/cvr/cvt224

Prieto, I., Alarcón, C.R., García-Gómez, R., Berdún, R., Urgel, T., Portero, M., Pamplona, R., Martínez-Ruiz, A., Ruiz-Sanz, J.I., Ruiz-Larrea, M.B., Jove, M., Cerdán, S., Monsalve, M., 2019. Metabolic adaptations in spontaneously immortalized PGC-1α knock-out mouse embryonic fibroblasts increase their oncogenic potential. Redox Biol. 29, 101396. https://doi.org/10.1016/j.redox.2019.101396

Quintana-Cabrera, R., Scorrano, L., 2023. Determinants and outcomes of mitochondrial dynamics. Mol. Cell, Focus on mitochondria 83, 857–876. https://doi.org/10.1016/j.molcel.2023.02.012

Rafea, R., Siragusa, M., Fleming, I., 2025. The Ever-Expanding Influence of the Endothelial Nitric Oxide Synthase. Basic Clin. Pharmacol. Toxicol. 136, e70029. https://doi.org/10.1111/bcpt.70029

Rajapakshe, A., Astashkin, A.V., Klein, E.L., Reichmann, D., Mendel, R.R., Bittner, F., Enemark, J.H., 2011. Structural studies of the molybdenum center of mitochondrial amidoxime reducing component (mARC) by pulsed EPR spectroscopy and 17O-labeling. Biochemistry 50, 8813–8822. https://doi.org/10.1021/bi2005762

Ramachandran, A., Ceaser, E., Darley-Usmar, V.M., 2004. Chronic exposure to nitric oxide alters the free iron pool in endothelial cells: Role of mitochondrial respiratory complexes and heat shock proteins. Proc. Natl. Acad. Sci. 101, 384–389. https://doi.org/10.1073/pnas.0304653101

Rapoport, S.I., 2003. Coupled reductions in brain oxidative phosphorylation and synaptic function can be quantified and staged in the course of Alzheimer disease. Neurotox. Res. 5, 385–398. https://doi.org/10.1007/BF03033167

Rastogi, A., Joshi, P., Contreras, E., Gama, V., 2019. Remodeling of mitochondrial morphology and function: an emerging hallmark of cellular reprogramming. Cell Stress 3, 181–194. https://doi.org/10.15698/cst2019.06.189

Ravikumar, M., Smith, R.A.A., Nurcombe, V., Cool, S.M., 2020. Heparan Sulfate Proteoglycans: Key Mediators of Stem Cell Function. Front. Cell Dev. Biol. 8. https://doi.org/10.3389/fcell.2020.581213

Reeder, B.J., Deganutti, G., Ukeri, J., Atanasio, S., Svistunenko, D.A., Ronchetti, C., Mobarec, J.C., Welbourn, E., Asaju, J., Vos, M.H., Wilson, M.T., Reynolds, C.A., 2024. The circularly permuted globin domain of androglobin exhibits atypical heme stabilization and nitric oxide interaction. Chem. Sci. 15, 6738–6751. https://doi.org/10.1039/D4SC00953C

RIOBÓ, N.A., CLEMENTI, E., MELANI, M., BOVERIS, A., CADENAS, E., MONCADA, S., PODEROSO, J.J., 2001. Nitric oxide inhibits mitochondrial NADH:ubiquinone reductase activity through peroxynitrite formation. Biochem. J. 359, 139–145. https://doi.org/10.1042/bj3590139

Ripps, H., Shen, W., 2012. Review: Taurine: A “very essential” amino acid. Mol. Vis. 18, 2673–2686.

Rixen, S., Havemeyer, A., Tyl-Bielicka, A., Pysniak, K., Gajewska, M., Kulecka, M., Ostrowski, J., Mikula, M., Clement, B., 2019. Mitochondrial amidoxime-reducing component 2 (MARC2) has a significant role in N-reductive activity and energy metabolism. J. Biol. Chem. 294, 17593–17602. https://doi.org/10.1074/jbc.RA119.007606

Rixen, S., Indorf, P.M., Kubitza, C., Struwe, M.A., Klopp, C., Scheidig, A.J., Kunze, T., Clement, B., 2023. Reduction of Hydrogen Peroxide by Human Mitochondrial Amidoxime Reducing Component Enzymes. Mol. Basel Switz. 28, 6384. https://doi.org/10.3390/molecules28176384

Ros, S., Schulze, A., 2013. Balancing glycolytic flux: the role of 6-phosphofructo-2-kinase/fructose 2,6-bisphosphatases in cancer metabolism. Cancer Metab. 1, 8. https://doi.org/10.1186/2049-3002-1-8

Ruhoy, I.S., Saneto, R.P., 2014. The genetics of Leigh syndrome and its implications for clinical practice and risk management. Appl. Clin. Genet. 7, 221–234. https://doi.org/10.2147/TACG.S46176

Santamaria-Araujo, J.A., Fischer, B., Otte, T., Nimtz, M., Mendel, R.R., Wray, V., Schwarz, G., 2004. The tetrahydropyranopterin structure of the sulfur-free and metal-free molybdenum cofactor precursor. J. Biol. Chem. 279, 15994–15999. https://doi.org/10.1074/jbc.M311815200

Sathe, G., Deepha, S., Gayathri, N., Nagappa, M., Parayil Sankaran, B., Taly, A.B., Khanna, T., Pandey, A., Govindaraj, P., 2021. Ethylmalonic encephalopathy *ETHE1* p. D165H mutation alters the mitochondrial function in human skeletal muscle proteome. Mitochondrion 58, 64–71. https://doi.org/10.1016/j.mito.2021.02.011

Scarpulla, R.C., 2002. Transcriptional activators and coactivators in the nuclear control of mitochondrial function in mammalian cells. Gene, Papers presented at the International Meeting “Mitochondria:Evolution, Genomics, Homeostasis and Pathology”, Selva di Fasano (BR, Italy), 9-12 May 2001 286, 81–89. https://doi.org/10.1016/S0378-1119(01)00809-5

Schatton, D., Pla-Martin, D., Marx, M.-C., Hansen, H., Mourier, A., Nemazanyy, I., Pessia, A., Zentis, P., Corona, T., Kondylis, V., Barth, E., Schauss, A.C., Velagapudi, V., Rugarli, E.I., 2017. CLUH regulates mitochondrial metabolism by controlling translation and decay of target mRNAs. J. Cell Biol. 216, 675–693. https://doi.org/10.1083/jcb.201607019

Schiattarella, G.G., Altamirano, F., Tong, D., French, K.M., Villalobos, E., Kim, S.Y., Luo, X., Jiang, N., May, H.I., Wang, Z.V., Hill, T.M., Mammen, P.P.A., Huang, J., Lee, D.I., Hahn, V.S., Sharma, K., Kass, D.A., Lavandero, S., Gillette, T.G., Hill, J.A., 2019. Nitrosative stress drives heart failure with preserved ejection fraction. Nature 568, 351–356. https://doi.org/10.1038/s41586-019-1100-z

Schon, E.A., DiMauro, S., Hirano, M., 2012. Human mitochondrial DNA: roles of inherited and somatic mutations. Nat. Rev. Genet. 13, 878–890. https://doi.org/10.1038/nrg3275

Schrader, N., Fischer, K., Theis, K., Mendel, R.R., Schwarz, G., Kisker, C., 2003. The Crystal Structure of Plant Sulfite Oxidase Provides Insights into Sulfite Oxidation in Plants and Animals. Structure 11, 1251–1263. https://doi.org/10.1016/j.str.2003.09.001

Schwahn, B.C., Van Spronsen, F.J., Belaidi, A.A., Bowhay, S., Christodoulou, J., Derks, T.G., Hennermann, J.B., Jameson, E., König, K., McGregor, T.L., Font-Montgomery, E., Santamaria-Araujo, J.A., Santra, S., Vaidya, M., Vierzig, A., Wassmer, E., Weis, I., Wong, F.Y., Veldman, A., Schwarz, G., 2015. Efficacy and safety of cyclic pyranopterin monophosphate substitution in severe molybdenum cofactor deficiency type A: a prospective cohort study. Lancet Lond. Engl. 386, 1955–1963. https://doi.org/10.1016/S0140-6736(15)00124-5

Schwarz, G., Basel, D.G., Schwahn, B.C., Spiegel, R., Wong, F.Y., Bliss, R., Squires, L., 2025. Increased Survival in Patients With Molybdenum Cofactor Deficiency Type A Treated With Cyclic Pyranopterin Monophosphate. J. Inherit. Metab. Dis. 48, e70000. https://doi.org/10.1002/jimd.70000

Schwarz, G., Mendel, R.R., Ribbe, M.W., 2009. Molybdenum cofactors, enzymes and pathways. Nature 460, 839–847. https://doi.org/10.1038/nature08302

Sharma, U., Carrique, L., Vadon-Le Goff, S., Mariano, N., Georges, R.-N., Delolme, F., Koivunen, P., Myllyharju, J., Moali, C., Aghajari, N., Hulmes, D.J.S., 2017. Structural basis of homo- and heterotrimerization of collagen I. Nat. Commun. 8, 14671. https://doi.org/10.1038/ncomms14671

Shibuya, N., Tanaka, M., Yoshida, M., Ogasawara, Y., Togawa, T., Ishii, K., Kimura, H., 2009. 3-Mercaptopyruvate Sulfurtransferase Produces Hydrogen Sulfide and Bound Sulfane Sulfur in the Brain. Antioxid. Redox Signal. 11, 703–714. https://doi.org/10.1089/ars.2008.2253

Shih, V.E., Abroms, I.F., Johnson, J.L., Carney, M., Mandell, R., Robb, R.M., Cloherty, J.P., Rajagopalan, K.V., 1977. Sulfite Oxidase Deficiency. N. Engl. J. Med. 297, 1022–1028. https://doi.org/10.1056/NEJM197711102971902

Shiva, S., Brookes, P.S., Patel, R.P., Anderson, P.G., Darley-Usmar, V.M., 2001. Nitric oxide partitioning into mitochondrial membranes and the control of respiration at cytochrome c oxidase. Proc. Natl. Acad. Sci. U. S. A. 98, 7212–7217. https://doi.org/10.1073/pnas.131128898

Shiva, S., Sack, M.N., Greer, J.J., Duranski, M., Ringwood, L.A., Burwell, L., Wang, X., MacArthur, P.H., Shoja, A., Raghavachari, N., Calvert, J.W., Brookes, P.S., Lefer, D.J., Gladwin, M.T., 2007. Nitrite augments tolerance to ischemia/reperfusion injury via the modulation of mitochondrial electron transfer. J. Exp. Med. 204, 2089–2102. https://doi.org/10.1084/jem.20070198

Shulman, R.G., Rothman, D.L., Behar, K.L., Hyder, F., 2004. Energetic basis of brain activity: implications for neuroimaging. Trends Neurosci. 27, 489–495. https://doi.org/10.1016/j.tins.2004.06.005

Simarro, M., Gimenez-Cassina, A., Kedersha, N., Lazaro, J.-B., Adelmant, G.O., Marto, J.A., Rhee, K., Tisdale, S., Danial, N., Benarafa, C., Orduña, A., Anderson, P., 2010. FAST KINASE DOMAIN-CONTAINING PROTEIN 3 IS A MITOCHONDRIAL PROTEIN ESSENTIAL FOR CELLULAR RESPIRATION. Biochem. Biophys. Res. Commun. 401, 440–446. https://doi.org/10.1016/j.bbrc.2010.09.075

Singh, D., Rai, V., Agrawal, D.K., 2023. Regulation of Collagen I and Collagen III in Tissue Injury and Regeneration. Cardiol. Cardiovasc. Med. 7, 5–16. https://doi.org/10.26502/fccm.92920302

Smolinsky, B., Eichler, S., Buchmeier, S., Meier, J., Schwarz, G., 2008. Splice-specific Functions of Gephyrin in Molybdenum Cofactor Biosynthesis. J. Biol. Chem. 283, 17370–9. https://doi.org/10.1074/jbc.M800985200

Soares Da Costa, D., Reis, R.L., Pashkuleva, I., 2017. Sulfation of Glycosaminoglycans and Its Implications in Human Health and Disorders. Annu. Rev. Biomed. Eng. 19, 1–26. https://doi.org/10.1146/annurev-bioeng-071516-044610

Sobin, S.S., Fung, Y.C., Tremer, H.M., 1988. Collagen and elastin fibers in human pulmonary alveolar walls. J. Appl. Physiol. Bethesda Md 1985 64, 1659–1675. https://doi.org/10.1152/jappl.1988.64.4.1659

Sodhi, J.K., Wong, S., Kirkpatrick, D.S., Liu, L., Khojasteh, S.C., Hop, C.E.C.A., Barr, J.T., Jones, J.P., Halladay, J.S., 2015. A Novel Reaction Mediated by Human Aldehyde Oxidase: Amide Hydrolysis of GDC-0834. Drug Metab. Dispos. 43, 908–915. https://doi.org/10.1124/dmd.114.061804

Song, J., Herrmann, J.M., Becker, T., 2021. Quality control of the mitochondrial proteome. Nat. Rev. Mol. Cell Biol. 22, 54–70. https://doi.org/10.1038/s41580-020-00300-2

Sonsungsan, P., Aimauthon, S., Sriwichai, N., Namchaiw, P., 2024. Unveiling mitochondria as central components driving cognitive decline in alzheimer's disease through cross-transcriptomic analysis of hippocampus and entorhinal cortex microarray datasets. Heliyon 10, e39378. https://doi.org/10.1016/j.heliyon.2024.e39378

Sparacino-Watkins, C.E., Tejero, J., Sun, B., Gauthier, M.C., Thomas, J., Ragireddy, V., Merchant, B.A., Wang, J., Azarov, I., Basu, P., Gladwin, M.T., 2014. Nitrite Reductase and Nitric-oxide Synthase Activity of the Mitochondrial Molybdopterin Enzymes mARC1 and mARC2. J. Biol. Chem. 289, 10345–10358. https://doi.org/10.1074/jbc.M114.555177

Spatzal, T., Aksoyoglu, M., Zhang, L., Andrade, S.L.A., Schleicher, E., Weber, S., Rees, D.C., Einsle, O., 2011. Evidence for Interstitial Carbon in Nitrogenase FeMo Cofactor. Science 334, 940–940. https://doi.org/10.1126/science.1214025

Stadler, J., Billiar, T.R., Curran, R.D., Stuehr, D.J., Ochoa, J.B., Simmons, R.L., 1991. Effect of exogenous and endogenous nitric oxide on mitochondrial respiration of rat hepatocytes. Am. J. Physiol. 260, C910-916. https://doi.org/10.1152/ajpcell.1991.260.5.C910

Stamler, J.S., 1994. Redox signaling: nitrosylation and related target interactions of nitric oxide. Cell 78, 931–936.

Stein, B.W., Kirk, M.L., 2015. Electronic Structure Contributions to Reactivity in Xanthine Oxidase Family Enzymes. J. Biol. Inorg. Chem. JBIC Publ. Soc. Biol. Inorg. Chem. 20, 183–194. https://doi.org/10.1007/s00775-014-1212-8

Stipanuk, M.H., 2004. SULFUR AMINO ACID METABOLISM: Pathways for Production and Removal of Homocysteine and Cysteine. Annu. Rev. Nutr. 24, 539–577. https://doi.org/10.1146/annurev.nutr.24.012003.132418

Stomberski, C.T., Hess, D.T., Stamler, J.S., 2019. Protein S-Nitrosylation: Determinants of Specificity and Enzymatic Regulation of S-Nitrosothiol-Based Signaling. Antioxid. Redox Signal. 30, 1331–1351. https://doi.org/10.1089/ars.2017.7403

Strelevitz, T.J., Orozco, C.C., Obach, R.S., 2012. Hydralazine As a Selective Probe Inactivator of Aldehyde Oxidase in Human Hepatocytes: Estimation of the Contribution of Aldehyde Oxidase to Metabolic Clearance. Drug Metab. Dispos. 40, 1441–1448. https://doi.org/10.1124/dmd.112.045195

Struwe, M.A., Scheidig, A.J., Clement, B., 2023. The mitochondrial amidoxime reducing component—from prodrug-activation mechanism to drug-metabolizing enzyme and onward to drug target. J. Biol. Chem. 299, 105306. https://doi.org/10.1016/j.jbc.2023.105306

Stuehr, D.J., Wei, C.-C., Wang, Z., Hille, R., 2005. Exploring the redox reactions between heme and tetrahydrobiopterin in the nitric oxide synthases. Dalton Trans. 3427–3435. https://doi.org/10.1039/B506355H

Su, H., Fan, W., Coskun, P.E., Vesa, J., Gold, J.-A., Jiang, Y.-H., Potluri, P., Procaccio, V., Acab, A., Weiss, J.H., Wallace, D.C., Kimonis, V.E., 2011. Mitochondrial dysfunction in CA1 hippocampal neurons of the Ube3a deficient mouse model for Angelman syndrome. Neurosci. Lett. 487, 129–133. https://doi.org/10.1016/j.neulet.2009.06.079

Tábara, L.-C., Segawa, M., Prudent, J., 2025. Molecular mechanisms of mitochondrial dynamics. Nat. Rev. Mol. Cell Biol. 26, 123–146. https://doi.org/10.1038/s41580-024-00785-1

Tejero, J., Gladwin, M.T., 2014. The Globin Superfamily: Functions in Nitric Oxide Formation and Decay. Biol. Chem. 395, 631–639. https://doi.org/10.1515/hsz-2013-0289

Terao, M., Garattini, E., Romão, M.J., Leimkühler, S., 2020. Evolution, expression, and substrate specificities of aldehyde oxidase enzymes in eukaryotes. J. Biol. Chem. 295, 5377–5389. https://doi.org/10.1074/jbc.REV119.007741

Teschner, J., Lachmann, N., Schulze, J., Geisler, M., Selbach, K., Santamaria-Araujo, J., Balk, J., Mendel, R.R., Bittner, F., 2010. A novel role for Arabidopsis mitochondrial ABC transporter ATM3 in molybdenum cofactor biosynthesis. Plant Cell 22, 468–480. https://doi.org/10.1105/tpc.109.068478

Thibault, H.B., Kurtz, B., Raher, M.J., Shaik, R.S., Waxman, A., Derumeaux, G., Halpern, E.F., Bloch, K.D., Scherrer-Crosbie, M., 2010. Noninvasive Assessment of Murine Pulmonary

Arterial Pressure. Circ. Cardiovasc. Imaging 3, 157–163. https://doi.org/10.1161/CIRCIMAGING.109.887109

Tilokani, L., Nagashima, S., Paupe, V., Prudent, J., 2018. Mitochondrial dynamics: overview of molecular mechanisms. Essays Biochem. 62, 341–360. https://doi.org/10.1042/EBC20170104

Tiranti, V., Viscomi, C., Hildebrandt, T., Di Meo, I., Mineri, R., Tiveron, C., D Levitt, M., Prelle, A., Fagiolari, G., Rimoldi, M., Zeviani, M., 2009. Loss of ETHE1, a mitochondrial dioxygenase, causes fatal sulfide toxicity in ethylmalonic encephalopathy. Nat. Med. 15, 200–205. https://doi.org/10.1038/nm.1907

Touati, G., Rusthoven, E., Depondt, E., Dorche, C., Duran, M., Heron, B., Rabier, D., Russo, M., Saudubray, J.M., 2000. Dietary therapy in two patients with a mild form of sulphite oxidase deficiency. Evidence for clinical and biological improvement. J. Inherit. Metab. Dis. 23, 45–53. https://doi.org/10.1023/A:1005646813492

Tripatara, P., Patel, N.S.A., Webb, A., Rathod, K., Lecomte, F.M.J., Mazzon, E., Cuzzocrea, S., Yaqoob, M.M., Ahluwalia, A., Thiemermann, C., 2007. Nitrite-Derived Nitric Oxide Protects the Rat Kidney against Ischemia/Reperfusion Injury In Vivo: Role for Xanthine Oxidoreductase. J. Am. Soc. Nephrol. 18, 570. https://doi.org/10.1681/ASN.2006050450

Tyagarajan, S.K., Ghosh, H., Yévenes, G.E., Nikonenko, I., Ebeling, C., Schwerdel, C., Sidler, C., Zeilhofer, H.U., Gerrits, B., Muller, D., Fritschy, J.-M., 2011. Regulation of GABAergic synapse formation and plasticity by GSK3β-dependent phosphorylation of gephyrin. Proc. Natl. Acad. Sci. 108, 379–384. https://doi.org/10.1073/pnas.1011824108

Uhlén, M., Fagerberg, L., Hallström, B.M., Lindskog, C., Oksvold, P., Mardinoglu, A., Sivertsson, Å., Kampf, C., Sjöstedt, E., Asplund, A., Olsson, I., Edlund, K., Lundberg, E., Navani, S., Szigyarto, C.A.-K., Odeberg, J., Djureinovic, D., Takanen, J.O., Hober, S., Alm, T., Edqvist, P.-H., Berling, H., Tegel, H., Mulder, J., Rockberg, J., Nilsson, P., Schwenk, J.M., Hamsten, M., von Feilitzen, K., Forsberg, M., Persson, L., Johansson, F., Zwahlen, M., von Heijne, G., Nielsen, J., Pontén, F., 2015. Proteomics. Tissue-based map of the human proteome. Science 347, 1260419. https://doi.org/10.1126/science.1260419

Uittenbogaard, M., Sen, K., Whitehead, M., Brantner, C.A., Wang, Y., Wong, L.-J., Gropman, A., Chiaramello, A., 2021. Genetic and Mitochondrial Metabolic Analyses of an Atypical Form of Leigh Syndrome. Front. Cell Dev. Biol. 9, 767407. https://doi.org/10.3389/fcell.2021.767407

Umbrello, M., Dyson, A., Feelisch, M., Singer, M., 2013. The Key Role of Nitric Oxide in Hypoxia: Hypoxic Vasodilation and Energy Supply–Demand Matching. Antioxid. Redox Signal. 19, 1690–1710. https://doi.org/10.1089/ars.2012.4979

Unrug-Bielawska, K., Sandowska-Markiewicz, Z., Pyśniak, K., Piątkowska, M., Czarnowski, P., Goryca, K., Mróz, A., Żeber-Lubecka, N., Wójcik-Trechcińska, U., Bałabas, A., Dąbrowska, M., Surynt, P., Radkiewicz, M., Mikula, M., Ostrowski, J., 2025. Western Diet and fecal microbiota transplantation alter phenotypic, liver fatty acids, and gut metagenomics and metabolomics in Mtarc2 knockout mice. Genes Nutr. 20, 13. https://doi.org/10.1186/s12263-025-00772-x

Valdez∗, L.B., Iglesias, D.E., Bombicino, S.S., Boveris, A., 2012. Biochemical characterization of mitochondrial complex III inhibition by nitric oxide. Free Radic. Biol. Med., Society for Free Radical Research International 16th Biennial Meeting 53, S188–S189. https://doi.org/10.1016/j.freeradbiomed.2012.08.396

Velez-Roa, S., Ciarka, A., Najem, B., Vachiery, J.-L., Naeije, R., van de Borne, P., 2004. Increased Sympathetic Nerve Activity in Pulmonary Artery Hypertension. Circulation 110, 1308–1312. https://doi.org/10.1161/01.CIR.0000140724.90898.D3

Venema, R.C., Sayegh, H.S., Kent, J.D., Harrison, D.G., 1996. Identification, Characterization, and Comparison of the Calmodulin-binding Domains of the Endothelial and Inducible Nitric Oxide Synthases (∗). J. Biol. Chem. 271, 6435–6440. https://doi.org/10.1074/jbc.271.11.6435

Venkatesh, S., Ramachandran, A., Zachariah, A., Oommen, A., 2009. Mitochondrial ATP synthase inhibition and nitric oxide are involved in muscle weakness that occurs in acute exposure of rats to monocrotophos. Toxicol. Mech. Methods 19, 239–245. https://doi.org/10.1080/15376510802455354

Vergara, R.C., Jaramillo-Riveri, S., Luarte, A., Moënne-Loccoz, C., Fuentes, R., Couve, A., Maldonado, P.E., 2019. The Energy Homeostasis Principle: Neuronal Energy Regulation Drives Local Network Dynamics Generating Behavior. Front. Comput. Neurosci. 13, 49. https://doi.org/10.3389/fncom.2019.00049

Vincent, A.S., Lim, B.G., Tan, J., Whiteman, M., Cheung, N.S., Halliwell, B., Wong, K.P., 2004. Sulfite-mediated oxidative stress in kidney cells. Kidney Int. 65, 393–402. https://doi.org/10.1111/j.1523-1755.2004.00391.x

Wahl, B., Reichmann, D., Niks, D., Krompholz, N., Havemeyer, A., Clement, B., Messerschmidt, T., Rothkegel, M., Biester, H., Hille, R., Mendel, R.R., Bittner, F., 2010. Biochemical and Spectroscopic Characterization of the Human Mitochondrial Amidoxime Reducing Components hmARC-1 and hmARC-2 Suggests the Existence of a New Molybdenum Enzyme Family in Eukaryotes. J. Biol. Chem. 285, 37847–37859. https://doi.org/10.1074/jbc.M110.169532

Wainio, W.W., 1955. REACTIONS OF CYTOCHROME OXIDASE. J. Biol. Chem. 212, 723–733. https://doi.org/10.1016/S0021-9258(18)71011-9

Wallace, D.C., 2005. A Mitochondrial Paradigm of Metabolic and Degenerative Diseases, Aging, and Cancer: A Dawn for Evolutionary Medicine. Annu. Rev. Genet. 39, 359. https://doi.org/10.1146/annurev.genet.39.110304.095751

Wang, J., Krizowski, S., Fischer-Schrader, K., Niks, D., Tejero, J., Sparacino-Watkins, C., Wang, L., Ragireddy, V., Frizzell, S., Kelley, E.E., Zhang, Y., Basu, P., Hille, R., Schwarz, G., Gladwin, M.T., 2015. Sulfite Oxidase Catalyzes Single-Electron Transfer at Molybdenum Domain to Reduce Nitrite to Nitric Oxide. Antioxid. Redox Signal. 23, 283–294. https://doi.org/10.1089/ars.2013.5397

Wang, R., 2012. Physiological Implications of Hydrogen Sulfide: A Whiff Exploration That Blossomed. Physiol. Rev. 92, 791–896. https://doi.org/10.1152/physrev.00017.2011

Warnhoff, K., Hercher, T.W., Mendel, R.R., Ruvkun, G., 2021. Protein-bound molybdenum cofactor is bioavailable and rescues molybdenum cofactor-deficient C. elegans. Genes Dev. 35, 212–217. https://doi.org/10.1101/gad.345579.120

Warren, J.J., Mayer, J.M., 2010. The Thermochemical and Kinetic Properties of Ascorbate are Tuned by its Local Environment: Solution Chemistry and Biochemical Implications. J. Am. Chem. Soc. 132, 7784–7793. https://doi.org/10.1021/ja102337n

Webb, A., Bond, R., McLean, P., Uppal, R., Benjamin, N., Ahluwalia, A., 2004. Reduction of nitrite to nitric oxide during ischemia protects against myocardial ischemia–reperfusion damage. Proc. Natl. Acad. Sci. U. S. A. 101, 13683–13688. https://doi.org/10.1073/pnas.0402927101

Weber, J.-N., Minner-Meinen, R., Kaufholdt, D., 2023. The Mechanisms of Molybdate Distribution and Homeostasis with Special Focus on the Model Plant Arabidopsis thaliana. Molecules 29, 40. https://doi.org/10.3390/molecules29010040

Welter, R., Yu, L., Yu, C.-A., 1996. The Effects of Nitric Oxide on Electron Transport Complexes. Arch. Biochem. Biophys. 331, 9–14. https://doi.org/10.1006/abbi.1996.0276

Wenstrup, R.J., Florer, J.B., Brunskill, E.W., Bell, S.M., Chervoneva, I., Birk, D.E., 2004. Type V Collagen Controls the Initiation of Collagen Fibril Assembly*. J. Biol. Chem. 279, 53331–53337. https://doi.org/10.1074/jbc.M409622200

Wiese, S., Gronemeyer, T., Ofman, R., Kunze, M., Grou, C.P., Almeida, J.A., Eisenacher, M., Stephan, C., Hayen, H., Schollenberger, L., Korosec, T., Waterham, H.R., Schliebs, W., Erdmann, R., Berger, J., Meyer, H.E., Just, W., Azevedo, J.E., Wanders, R.J.A., Warscheid, B., 2007. Proteomics characterization of mouse kidney peroxisomes by tandem mass

spectrometry and protein correlation profiling. Mol. Cell. Proteomics MCP 6, 2045–2057. https://doi.org/10.1074/mcp.M700169-MCP200

Wilson, H.L., Rajagopalan, K.V., 2004. The Role of Tyrosine 343 in Substrate Binding and Catalysis by Human Sulfite Oxidase*. J. Biol. Chem. 279, 15105–15113. https://doi.org/10.1074/jbc.M314288200

Wink, D.A., Hines, H.B., Cheng, R.Y.S., Switzer, C.H., Flores-Santana, W., Vitek, M.P., Ridnour, L.A., Colton, C.A., 2011. Nitric oxide and redox mechanisms in the immune response. J. Leukoc. Biol. 89, 873–891. https://doi.org/10.1189/jlb.1010550

Wu, Y.N., Sudarshan, V.K., Zhu, S.C., Shao, Y.F., Kim, S.J., Zhang, Y.H., 2020. Functional interactions between complex I and complex II with nNOS in regulating cardiac mitochondrial activity in sham and hypertensive rat hearts. Pflugers Arch. 472, 1743–1755. https://doi.org/10.1007/s00424-020-02458-2

Xu, J., DeVries, S.H., Zhu, Y., 2020. Quantification of Adeno-Associated Virus with Safe Nucleic Acid Dyes. Hum. Gene Ther. 31, 1086–1099. https://doi.org/10.1089/hum.2020.063

Yan, L.-J., Liu, L., Forster, M.J., 2012. Reversible inactivation of dihydrolipoamide dehydrogenase by Angeli's salt. Sheng Wu Wu Li Hsueh Bao 28, 341–350.

Youle, R.J., van der Bliek, A.M., 2012. Mitochondrial Fission, Fusion, and Stress. Science 337, 1062–1065. https://doi.org/10.1126/science.1219855

Zhang, R., Hausladen, A., Qian, Z., Liao, X., Premont, R.T., Stamler, J.S., 2022. Hypoxic vasodilatory defect and pulmonary hypertension in mice lacking hemoglobin β-cysteine93 S-nitrosylation. JCI Insight 7, e155234. https://doi.org/10.1172/jci.insight.155234

Zhang, X., Vincent, A.S., Halliwell, B., Wong, K.P., 2004. A Mechanism of Sulfite Neurotoxicity DIRECT INHIBITION OF GLUTAMATE DEHYDROGENASE. J. Biol. Chem. 279, 43035–43045. https://doi.org/10.1074/jbc.M402759200

Zhang, Z., Naughton, D., Winyard, P.G., Benjamin, N., Blake, D.R., Symons, M.C., 1998. Generation of nitric oxide by a nitrite reductase activity of xanthine oxidase: a potential pathway for nitric oxide formation in the absence of nitric oxide synthase activity. Biochem. Biophys. Res. Commun. 249, 767–772. https://doi.org/10.1006/bbrc.1998.9226

Zheng, X., Boyer, L., Jin, M., Mertens, J., Kim, Y., Ma, L., Ma, L., Hamm, M., Gage, F.H., Hunter, T., 2016. Metabolic reprogramming during neuronal differentiation from aerobic glycolysis to neuronal oxidative phosphorylation. eLife 5, e13374. https://doi.org/10.7554/eLife.13374

Zhou, L., Zhu, D.-Y., 2009. Neuronal nitric oxide synthase: Structure, subcellular localization, regulation, and clinical implications. Nitric Oxide 20, 223–230. https://doi.org/10.1016/j.niox.2009.03.001

Ziolo, M.T., Kohr, M.J., Wang, H., 2008. Nitric Oxide Signaling and the Regulation of Myocardial Function. J. Mol. Cell. Cardiol. 45, 625–632. https://doi.org/10.1016/j.yjmcc.2008.07.015

7 Implementations in publications

Parts of this thesis were implemented into publications:

Figure 8:

Sulfite oxidase deficiency causes persulfidation loss and H2S release (under revision)

Chun-Yu Fu, Joshua B. Kohl, Filip Liebsch,, Davide D'Andrea, Tamás Ditrói, Seiryo Ogata, Franziska Neuser, Max Mai, Anna T. Mellis, Emilia Kouroussis, Masanobu Morita, Titus Gehling, José Angel Santamaria-Araujo, Sin Yuin Yeo, Heike Endepols, Michaela Křížková, Viktor Kozich, Marcus Krueger, Julia B. Hennermann, Uladzimir Barayeu, Takaaki Akaike, Peter Nagy, Milos Filipovic, Guenter Schwarz

Figure 21:

Kaczmarek AT, Bender D, Gehling T, Kohl JB, Daimagüler HS, Santamaria-Araujo JA, Liebau MC, Koy A, Cirak S, Schwarz G. **A defect in molybdenum cofactor binding causes an attenuated form of sulfite oxidase deficiency**. J Inherit Metab Dis. 2022 Mar;45(2):169-182. doi: 10.1002/jimd.12454. Epub 2021 Nov 24. PMID: 34741542.

8 Supplementary Data

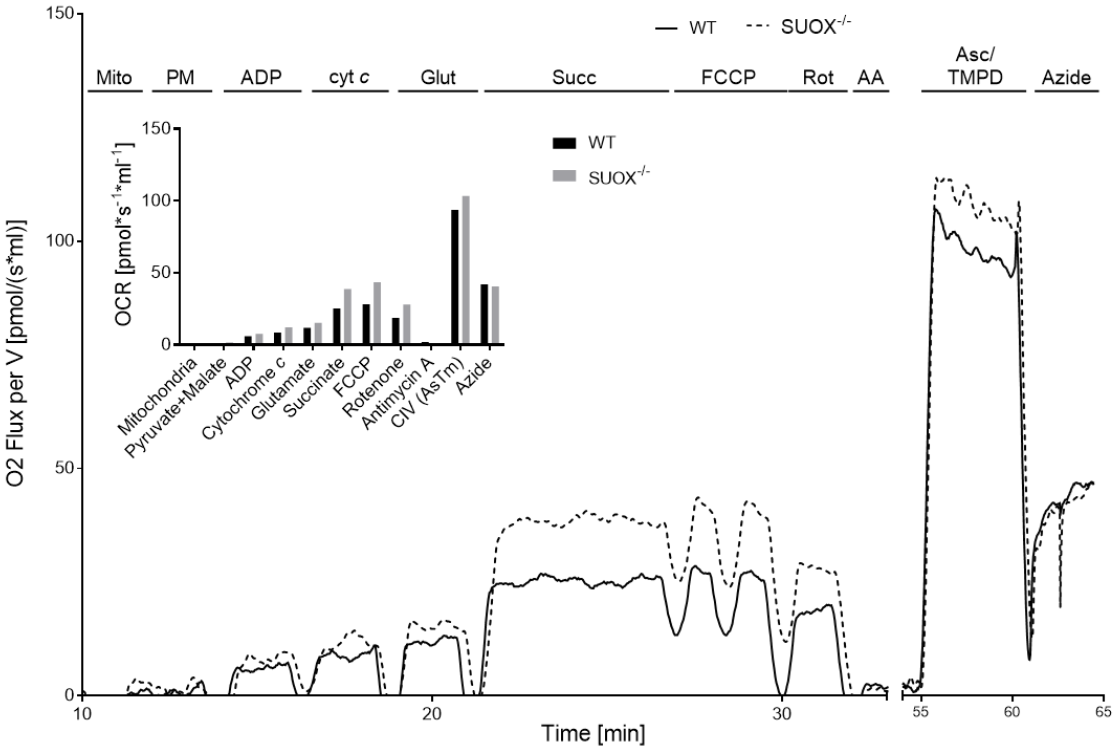

Figure S1: Respiration of enriched hepatocyte mitochondria from SUOX$^{-/-}$ and WT mice
Oxygraph measurements of enriched hepatocyte mitochondria of SUOX$^{-/-}$ and WT mice. Mito= mitochondria, PM = pyruvate + malate, cyt c = cytochrome c, Glut = glutamate, Succ = succinate, Rot = rotenone, AA = antimycine A, Asc = ascorbate. Inlet: Analysis of oxygen consumption traces after addition of various substrates (depicted) of enriched hepatocyte mitochondria from SUOX$^{-/-}$ (n=1) and WT mice. (n=1). 100 µg pure mitochondria were used. OCR was normalized to WT.

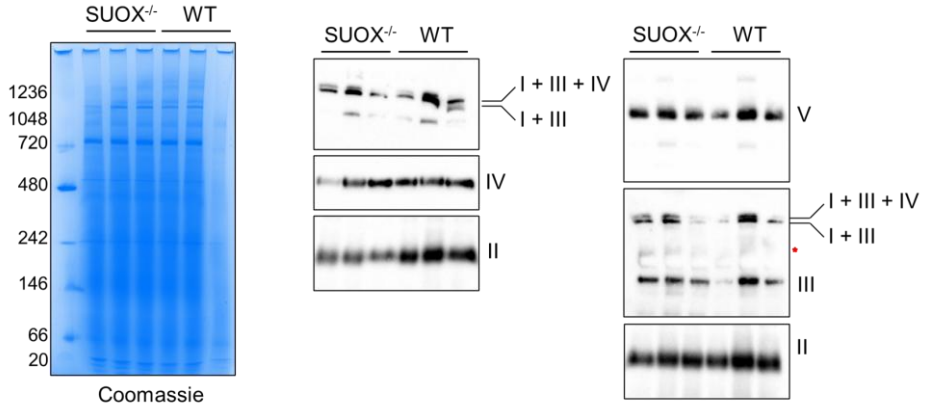

Figure S2: : BN-PAGE of mitochondria isolated from MEFs
30µg mitochondria were solubilized using digitonin and applied to a 4-12% polyacrylamide Bis-Tris gel. (A) Coomassie brilliant blue staining of BN-PAGE. (B) WB-based analysis of the expression of OXPHOS complexes. Unspecific bands indicated by a red star. Antibodies used to detect the different complexes: NDUFA9: complex I, SDHA: complex II, UQCRC1: complex III, MTCO1: complex IV, ATP5A1: complex V. Supercomplexes are labelled: I + III + IV and I + III.

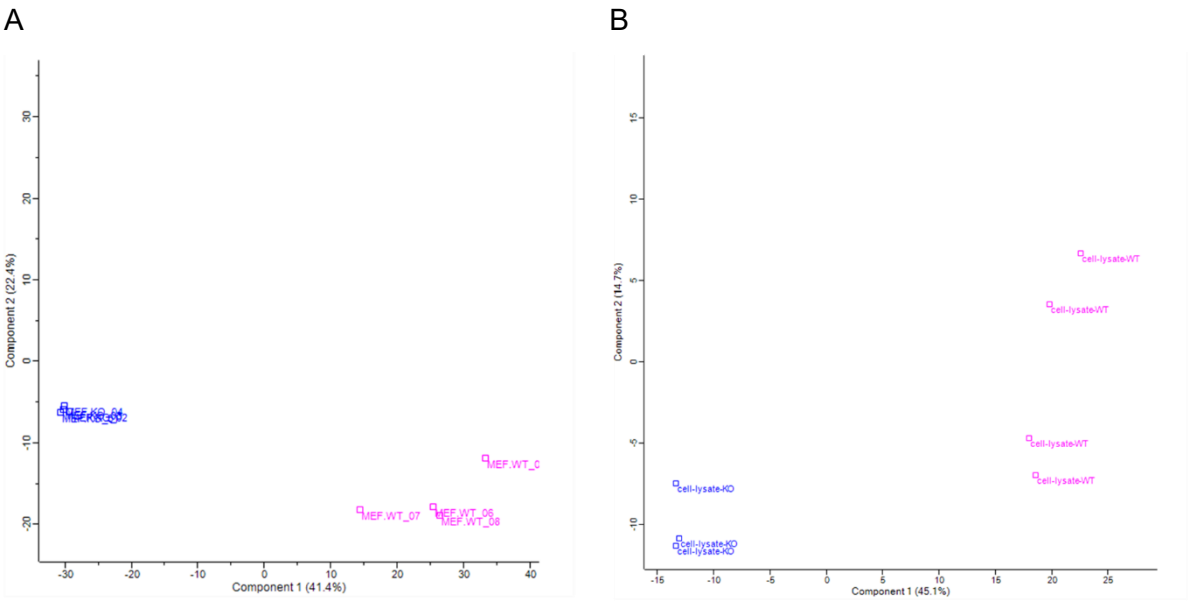

Figure S3: Principal component analysis of Mass spectrometry runs
(A) Mitochondria enriched from MEFs and (B) Whole cell lysates from MEFs

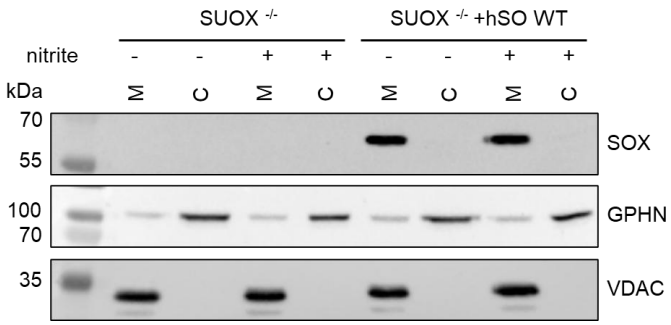

Figure S4: WB-based analysis of mitochondrial enrichment
Representative WB-based analysis of mitochondrial enrichment from nitrite treated FlpIn™ cells. 30 µg protein were used, gephyrin (GPHN) and VDAC served as cytosolic and mitochondrial markers, respectively.

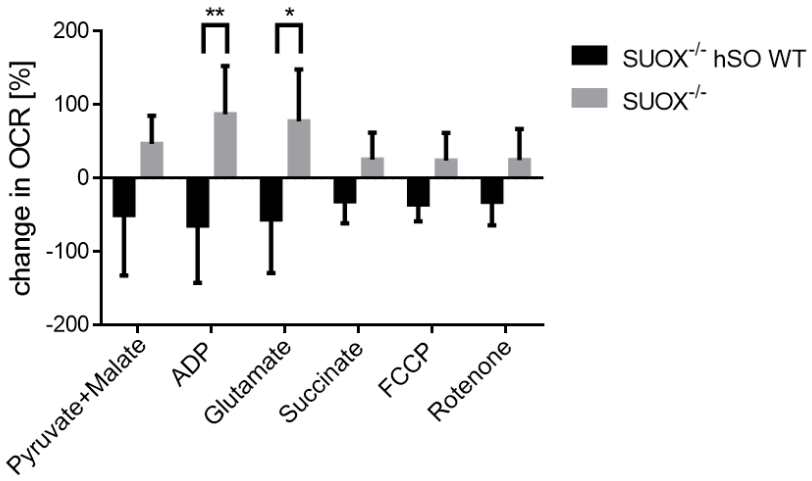

Figure S5: Contrary changes in OCR upon long-term nitrite exposure
Changes in the OCR of SUOX$^{-/-}$ cells and SUOX$^{-/-}$ cells expressing hSOWT (SUOX-/- + hSO WT) upon nitrite treatment with 50 µM nitrite for 72 h after addition of the indicated substrates, with a focus on physiological relevant mitochondrial respiration (leaving out OCR state after addition of OCR and the artificial complex IV activity). Two-way ANOVA with Sidak's post-hoc test was performed as indicated. p-value **< 0.01, * < 0.05

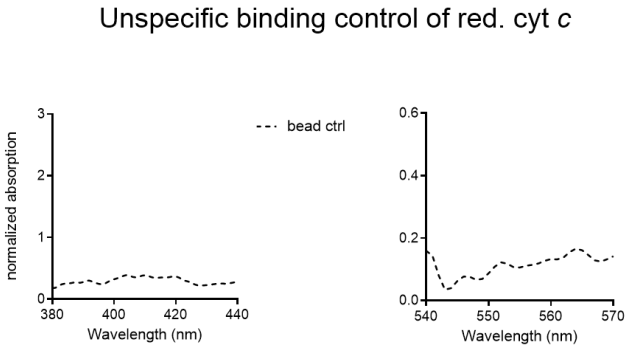

Figure S6: Unspecific binding control of reduced cytochrome c
Reduced cytochrome c was incubated Ni-NTA Agarose and subsequently washed several times prior to elution of bound proteins and evaluation by recording of an UV-Vis spectra.

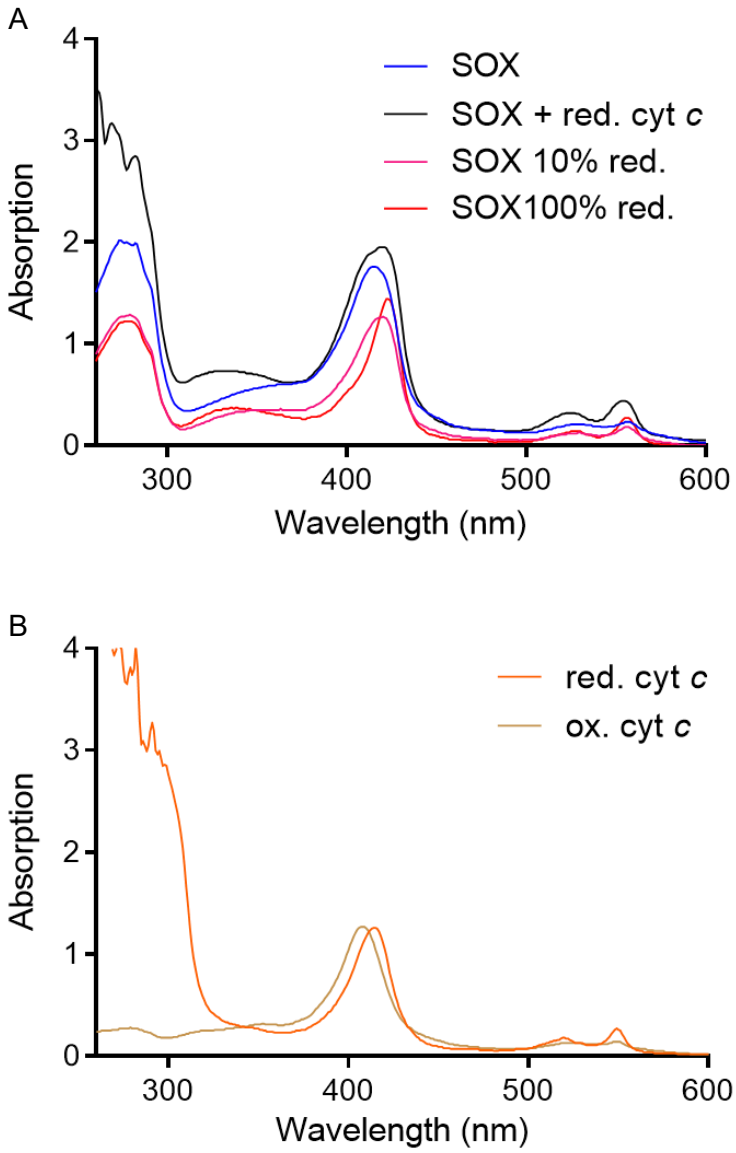

Figure S7: Full absorption spectra of SOX reduction by cytochrome *c*
Pre-reduced cytochrome c was incubated with SOX and afterwards removed by Ni-NTA purification of His-tagged SOX. Substochiometric and full reduction of SOX with sulfite served as an estimated quantification of cytochrome c mediated SOX reduction. Subsequently, Absorption spectra of (A) SOX, SOX incubated with cytochrome *c* and SOX reduced with substochiemtric or excess amounts of sulfite, (B) Oxidized and with ascorbate reduced cytochrome *c*

Table S1: Overview of downregulated proteins involved in OXPHOS

Protein Name	Part of OXPHOS
Acad9, Atpaf1, Atpaf2, Bcs1l, Coa3, Coa6, Coa7, Cox17, Cox20, Cox7a2l, Ndufaf1, Ndufaf2, Ndufaf3, Ndufaf4, Ndufaf8, Samm50, Sdhaf1, Timmdc1, Tmem126b, Uqcc1	Assembly factor
Atp6ap1, Coq10b, Coq3, Coq6, Coq9, Cox19, Hccs, Ppa2, Sco1, Sqor, Taco1	Associated
Ndufa2, Ndufa5, Ndufa6, Ndufa8, Ndufa9, Ndufa10, Ndufa11, Ndufa12, Ndufa13, Ndufb1, Ndufb2, Ndufb3, Ndufb4, Ndufb5, Ndufb7, Ndufb8, Ndufb9, Ndufb10, Ndufb11, Ndufc2, Ndufs1, Ndufs2, Ndufs3, Ndufs4, Ndufs5, Ndufs6, Ndufv1, Ndufv2, Ndufv3	Complex I
Sdha, Sdhb, Sdhc, Sdhd	Complex II
Cyc1, Uqcr10, Uqcrb, Uqcrc1, Uqcrc1, Uqcrc2, Uqcrfs1, Uqcrh, Uqcrq	Complex III
Cox4i1, Cox5b, Cox6a1, Cox6b1, Cox6c, Cox7a2, Cox7c, Mtco2, Ndufa4	Complex IV
Atp5f1a, Atp5f1b, Atp5f1c, Atp5f1e, Atp5me, Atp5mf, Atp5mg, Atp5mk, Atp5mpl, Atp5pb, Atp5pd, Atp5pf, Atp5po, Dmac2l, Mtatp8	Complex V

Table S2: Overview of downregulated proteins involved in TCA cycle

Protein Name	Part of TCA cycle
Cs	Citrate synthase
Dlst	Alpha-ketoglutarate dehydrogenase
Fh	Fumarate Hydratase
Glud1	Glutamate dehydrogenase
Idh2, Idh3a, Idh3g	Isocitrate dehydrogenase
Mdh2	Malate dehydrogenase
Pdha1, Pdhb, Pdhx	Pyruvate dehydrogenase
Pdk1, Pdk3	Pyruvate dehydrogenase kinase
Sdha, Sdhaf1, Sdhb, Sdhc, Sdhd	Succinate dehydrogenase
Aco2	Aconitase
Suclg2	Succinyl-CoA-synthetase

Table S3: Downregulated proteins associated with the ECM

Protein Name	ECM part
Col1a1, Col1a2, Col3a1, Col5a1, Col5a2, Col12a1,	Collagen
Aebp1 , Bgn, Ccn1, Efemp2, Fn1, Lox, Loxl1, P3h3, P4ha2, Pcolce, Sparc, Timp1, Tnc	Associated

Table S4: Significantly altered proteins detected in mitochondria from MEFs

UniProt ID	Genes	FC [log2]	q-value
Q5SUC9	*Sco1*	-5.70	0.000000
Q8R086	*Suox*	-5.60	0.000000
B1AXP6	*Tomm5*	-5.10	0.000000
Q9EPT5	*Slco2a1*	-4.69	0.000000
Q5SYH2	*Tmem199*	-4.51	0.000295
Q00977	*Gjb2*	-4.38	0.000000
P04104	*Krt1*	-4.19	0.000320
Q8K385	*FRRS1*	-4.17	0.000000
P30412	*Ppic*	-3.83	0.000561
Q61838	*Pzp*	-3.53	0.001655
P97493	*Txn2*	-3.44	0.000267
Q5XJY4	*Parl*	-3.36	0.000000
Q78IK2	*Atp5mk*	-3.11	0.000193
Q9D1R1	*Tmem126b*	-2.98	0.000416
Q8VDP6	*Cdipt*	-2.96	0.000257
Q9CQE1	*Nipsnap3b*	-2.94	0.000362
Q9DCC8	*Tomm20*	-2.94	0.000187
Q91V01	*Lpcat3*	-2.93	0.000615
Q8VCN5	*Cth*	-2.90	0.002000
Q91VC9	*Ghitm*	-2.81	0.000755
O54879	*Hmgb3*	-2.74	0.000251
Q2HXL6	*Edem3*	-2.66	0.000303
P41731	*Cd63*	-2.65	0.000997
Q9EQK7	*Icmt*	-2.61	0.000648
Q9CXV1	*Sdhd*	-2.53	0.000408
Q9CZX9	*Emc4*	-2.52	0.000273
Q05769	*Ptgs2*	-2.44	0.000844
P57787	*Slc16a3*	-2.43	0.001025
Q80V03	*Adck5*	-2.41	0.001333
P63166	*Sumo1*	-2.36	0.000554
Q80VP5	*Mtrfr*	-2.33	0.000693
Q9JLT4	*Txnrd2*	-2.33	0.000537
Q9WUR9	*Ak4*	-2.32	0.000000
P31786	*Dbi*	-2.31	0.000205
Q6ZWQ7	*Spcs3*	-2.27	0.003145
Q9Z0V8	*Timm17a*	-2.25	0.001699
Q8C5Q4	*Grsf1*	-2.20	0.001141
Q9CWD8	*Nubpl*	-2.15	0.000379
P61793	*Lpar1*	-2.11	0.000379
P28571	*Slc6a9*	-2.05	0.001426
P70403	*Cux1*	-2.04	0.000735
Q8CIF4	*Btd*	-2.02	0.002796
Q9D938	*Tmem160*	-2.02	0.001258
Q924D0	*Rtn4ip1*	-1.97	0.000245
Q9CPQ8	*Atp5mg*	-1.96	0.001938
Q3U3R4	*Lmf1*	-1.95	0.004551
P82349	*Sgcb*	-1.90	0.000378
Q9CZB0	*Sdhc*	-1.90	0.000827
P61804	*Dad1*	-1.90	0.001097
Q8R480	*Nup85*	-1.85	0.004330
O88653	*Lamtor3*	-1.84	0.016545
Q9CQX2	*Cyb5b*	-1.83	0.001824
O35459	*Ech1*	-1.81	0.005167
Q8BPE4	*Tmem177*	-1.81	0.000818
Q8K1C0	*Angel2*	-1.80	0.000951
Q5H8C4	*Vps13a*	-1.78	0.006851
P49962	*Srp9*	-1.77	0.000265
P17665	*Cox7c*	-1.75	0.000855
Q06185	*Atp5me*	-1.75	0.002067
Q4VAE3	*Tmem65*	-1.73	0.003530
Q99KR7	*Ppif*	-1.73	0.001968
P82347	*Sgcd*	-1.68	0.001570
Q3U6U5	*Gtpbp6*	-1.67	0.000371
Q9JHU9	*Isyna1*	-1.66	0.001143
P56135	*Atp5mf*	-1.65	0.001378
Q9D7E4		-1.63	0.002164
Q8R180	*Ero1a*	-1.61	0.001305
P48771	*Cox7a2*	-1.60	0.000320
Q99JT1	*Gatb*	-1.58	0.000850
P62743	*Ap2s1*	-1.57	0.004565
Q8BTW8	*Cdk5rap1*	-1.55	0.004998
O35658	*C1qbp*	-1.55	0.001265
Q8CI78	*Rmnd1*	-1.55	0.000817
Q3U2U7	*Mettl17*	-1.54	0.000385
P12265	*Gusb*	-1.54	0.001590
P70671	*Irf3*	-1.51	0.009218
Q6PE15	*Abhd10*	-1.51	0.001494
Q91WK1	*Spryd4*	-1.51	0.001192
Q6GQT1	*A2m*	-1.50	0.040940
P52927	*Hmga2*	-1.50	0.000544
Q9D6U8	*Fam162a*	-1.47	0.001363
Q9WTQ8	*Timm23*	-1.47	0.001088
Q8VE38	*Oxnad1*	-1.46	0.001722
Q62425	*Ndufa4*	-1.46	0.001078
Q9DCJ7	*Aurkaip1*	-1.45	0.009010
P56213	*Gfer*	-1.45	0.000761
Q9CQ19	*Myl9*	-1.44	0.005314
Q99JY8	*Plpp3*	-1.44	0.006045
Q3U276	*Sdhaf1*	-1.43	0.000738
P49070	*Camlg*	-1.43	0.016350

UniProt ID	Genes	FC [log2]	q-value
Q8R2R1	*Pomt1*	-1.43	0.001425
P02535	*Krt10*	-1.42	0.000492
Q8VCA6	*Tmem161a*	-1.41	0.002734
O88398	*Avil*	-1.39	0.000217
P51912	*Slc1a5*	-1.39	0.000709
O35943	*Fxn*	-1.38	0.000579
O55022	*Pgrmc1*	-1.38	0.001292
Q9CR67	*Tmem33*	-1.38	0.000810
P05202	*Got2*	-1.36	0.001319
Q9Z0J0	*Npc2*	-1.36	0.000653
B5X0E4	*Abcb5*	-1.35	0.016902
O08734	*Bak1*	-1.34	0.000646
Q8K009	*Aldh1l2*	-1.34	0.001531
Q8BXV2	*Bri3bp*	-1.34	0.000461
Q9CQU3	*Rer1*	-1.34	0.000912
Q505D7	*Opa3*	-1.34	0.000954
Q8K1Z0	*Coq9*	-1.34	0.000347
Q3UMR5	*Mcu*	1.33	0.001348
Q9D8Y1	*Tmem126a*	-1.33	0.000608
Q5NCF2	*Trappc1*	-1.32	0.013365
Q3THF9	*Coq10b*	-1.32	0.000184
Q921N7	*Tmem70*	-1.32	0.001117
Q9D8M4	*Rpl7l1*	-1.32	0.006532
Q99LB2	*Dhrs4*	-1.31	0.001051
Q8BUY5	*Timmdc1*	-1.31	0.000685
P53986	*Slc16a1*	-1.30	0.000373
P62806	*H4c1*	-1.30	0.000626
Q811I0	*Atpaf1*	-1.28	0.000832
Q9ERD7	*Tubb3*	-1.28	0.018874
Q9CQ92	*Fis1*	-1.28	0.000261
Q8JZS9	*Mrpl48*	-1.27	0.000593
Q9CR62	*Slc25a11*	-1.26	0.000939
Q61749	*Eif2b4*	-1.26	0.025018
Q9D7N6	*Mrpl30*	-1.25	0.032280
Q9ERR7	*Selenof*	-1.25	0.000765
Q9D8B4	*Ndufa11*	-1.24	0.000404
Q8C167	*Prepl*	-1.24	0.003252
Q3U4G3	*Xxylt1*	-1.23	0.000484
Q8BHL4	*Gprc5a*	-1.23	0.024256
Q3UFY8	*Trmt10c*	-1.23	0.000905
A2ADA5	*Pusl1*	-1.22	0.000611
O88322	*Nid2*	-1.22	0.001159
Q9CQB5	*Cisd2*	-1.22	0.000569
Q8BMG8	*Slc25a32*	-1.22	0.000477
Q8VEM8	*Slc25a3*	-1.22	0.000574
Q3UUI3	*Them4*	-1.22	0.003143

UniProt ID	Genes	FC [log2]	q-value
Q9CZN7	*Shmt2*	-1.21	0.000992
Q9CRD0	*Ociad1*	-1.20	0.000599
Q8BWH0	*Slc38a7*	-1.20	0.007301
Q9CPQ3	*Tomm22*	-1.19	0.000338
Q9DB73	*Cyb5r1*	-1.19	0.000366
Q8K215	*Lyrm4*	-1.18	0.000309
Q8R1I1	*Uqcr10*	-1.18	0.000488
Q63918	*Cavin2*	-1.18	0.000577
Q9CQV6	*Map1lc3b*	-1.17	0.034321
P28301	*Lox*	-1.17	0.000899
P29391	*Ftl1*	-1.17	0.000961
Q8K1J6	*Trnt1*	-1.16	0.001069
Q6GV12	*Kdsr*	-1.15	0.025210
Q9CQW0	*Emc6*	-1.15	0.000190
Q3TBW2	*Mrpl10*	-1.14	0.000725
Q9EPK6	*Sil1*	-1.14	0.036169
Q8CCM6	*Timm21*	-1.14	0.000392
Q9QXX4	*Slc25a13*	-1.14	0.000816
P49312	*Hnrnpa1*	-1.13	0.000325
Q91YU8	*Ppan*	-1.12	0.021764
P58021	*Tm9sf2*	-1.12	0.000486
Q9Z2Z6	*Slc25a20*	-1.12	0.000298
Q9CZE3	*Rab32*	-1.11	0.008647
Q8BGX2	*Timm29*	-1.11	0.000426
Q3UHB1	*Nt5dc3*	-1.11	0.000413
Q9D338	*Mrpl19*	-1.10	0.000805
P60603	*Romo1*	-1.10	0.000198
P06802	*Enpp1*	-1.10	0.000537
P17047	*Lamp2*	-1.10	0.000335
P56379	*Atp5mpl*	-1.10	0.000853
Q9DCB8	*Isca2*	-1.09	0.000713
O70401	*Tspan6*	-1.09	0.000314
Q9JKY0	*Cnot9*	-1.09	0.027329
P56394	*Cox17*	-1.09	0.000552
P49817	*Cav1*	-1.09	0.000247
Q8CBE3	*Wdr37*	-1.08	0.000356
Q9D1L0	*Chchd2*	-1.08	0.000334
Q99KK9	*Hars2*	-1.08	0.000539
P51881	*Slc25a5*	-1.08	0.000508
Q9QZ23	*Nfu1*	-1.08	0.000317
Q9CZP5	*Bcs1l*	-1.08	0.000734
Q9QYR9	*Acot2*	-1.07	0.000554
Q3V3R1	*Mthfd1l*	-1.07	0.000770
Q9DCV4	*Rmdn1*	-1.07	0.000582
P36552	*Cpox*	-1.07	0.000674
Q9CQV1	*Pam16*	-1.07	0.000821

UniProt ID	Genes	FC [log2]	q-value
Q78IK4	*Apool*	-1.07	0.000405
Q99J56	*Derl1*	-1.07	0.000185
Q9CQ85	*Timm22*	-1.06	0.000738
Q8BH86	*Dglucy*	-1.06	0.000431
Q8BKE6	*Cyp20a1*	-1.06	0.000525
P16460	*Ass1*	-1.06	0.000528
Q91W98	*Slc15a4*	-1.06	0.000401
Q91YM4	*Tbrg4*	-1.06	0.000482
Q8VCM4	*Lipt1*	-1.05	0.021590
Q9D6M3	*Slc25a22*	-1.04	0.000340
Q9D125	*Mrps25*	-1.04	0.000532
P48962	*Slc25a4*	-1.03	0.000448
Q8BH97	*Rcn3*	-1.03	0.000247
Q9ER88	*Dap3*	-1.02	0.000681
Q8BK08	*Tmem11*	-1.02	0.000464
Q9CRA5	*Golph3*	-1.02	0.020722
Q9WTR6	*Slc7a11*	-1.02	0.029233
P58742	*Aaas*	-1.01	0.000388
Q9DBE9	*Ftsj3*	-1.01	0.015327
Q8VCL2	*Sco2*	-1.01	0.000386
Q80Y14	*Glrx5*	-1.01	0.000355
Q3UQ84	*Tars2*	-1.01	0.000523
Q9CRA7	*Dmac2l*	-1.01	0.000197
Q8CEE7	*Rdh13*	-1.01	0.000519
Q9CQA6	*Chchd1*	-1.00	0.000332
Q6PDY2	*Ado*	-1.00	0.000206
P40630	*Tfam*	-1.00	0.000510
P0DN34	*Ndufb1*	-1.00	0.000351
Q9Z0V7	*Timm17b*	-0.99	0.000229
Q99LV7	*Pigx*	-0.99	0.000268
Q80YD1	*Supv3l1*	-0.99	0.000571
Q924L1	*Letmd1*	-0.99	0.000348
Q8K199	*Cmc2*	-0.98	0.000211
Q9CY50	*Ssr1*	-0.98	0.000220
Q9D880	*Timm50*	-0.98	0.000313
O08992	*Sdcbp*	-0.97	0.000234
Q8C7E7	*Stbd1*	-0.97	0.000279
Q99M04	*Lias*	-0.97	0.000620
Q7TMF3	*Ndufa12*	-0.97	0.000200
P38647	*Hspa9*	-0.97	0.000419
Q9CQV5	*Mrps24*	-0.97	0.000326
Q91VA6	*Poldip2*	-0.97	0.000678
Q9D1B9	*Mrpl28*	-0.97	0.000429
P46978	*Stt3a*	-0.96	0.000403
Q9D1P0	*Mrpl13*	-0.96	0.000512
Q9CQE3	*Mrps17*	-0.96	0.000319

UniProt ID	Genes	FC [log2]	q-value
Q3U186	*Rars2*	-0.96	0.000515
Q8JZY4	*Prorp*	-0.96	0.000258
P58064	*Mrps6*	-0.95	0.000377
Q9DCW4	*Etfb*	-0.95	0.000596
Q7TPD2	*Fam185a*	-0.95	0.000559
Q80Y81	*Elac2*	-0.94	0.000343
Q9DCZ4	*Apoo*	-0.94	0.000336
Q9QX60	*Dguok*	-0.94	0.041575
O88736	*Hsd17b7*	-0.94	0.034641
Q499X9	*Mars2*	-0.94	0.000459
Q8BYL4	*Yars2*	-0.93	0.000498
P20108	*Prdx3*	-0.93	0.000451
P67984	*Rpl22*	-0.93	0.000349
Q9CZ83	*Mrpl55*	-0.93	0.000203
Q9D1C3	*Pyurf*	-0.92	0.001389
Q8VHI3	*Pofut2*	-0.92	0.000301
Q71RI9	*Kyat3*	-0.92	0.000367
Q6ZPU9	*Kifbp*	-0.92	0.001505
Q9CXJ1	*Ears2*	-0.92	0.000435
Q80TF3	*Pcdh19*	-0.92	0.000353
Q99J47	*Dhrs7b*	-0.92	0.000456
Q9CXW2	*Mrps22*	-0.92	0.000444
Q8BPM0	*Daam1*	-0.92	0.000239
P01942	*Hba*	-0.91	0.000235
Q9CQF0	*Mrpl11*	-0.91	0.000530
Q8BH04	*Pck2*	-0.91	0.000370
Q5SSK3	*Tefm*	-0.91	0.000323
Q8BJZ4	*Mrps35*	-0.91	0.000357
Q8BGK6	*Slc7a6*	-0.90	0.026898
Q9CQV7	*Dnajc19*	-0.90	0.000243
Q8CGK3	*Lonp1*	-0.90	0.000471
Q64133	*Maoa*	-0.90	0.000453
Q8R4N0	*Clybl*	-0.90	0.000297
Q9JIM1	*Slc29a1*	-0.90	0.000231
Q921X9	*Pdia5*	-0.90	0.000443
Q9DCX2	*Atp5pd*	-0.89	0.000383
Q8JZU2	*Slc25a1*	-0.89	0.000285
Q8BWT1	*Acaa2*	-0.89	0.000330
Q9CQL4	*Mrpl20*	-0.89	0.000494
B7ZMP1	*Xpnpep3*	-0.89	0.000369
Q9JJA4	*Wdr12*	-0.89	0.026899
Q9JI39	*Abcb10*	-0.88	0.000327
Q9D1N9	*Mrpl21*	-0.88	0.000297
Q8VHE0	*Sec63*	-0.88	0.000342
Q91YJ5	*Mtif2*	-0.88	0.000214
Q8R2Y8	*Ptrh2*	-0.88	0.000316

UniProt ID	Genes	FC [log2]	q-value
Q921L3	*Tmco1*	-0.88	0.000228
Q922E6	*Fastkd2*	-0.87	0.000296
Q924T2	*Mrps2*	-0.87	0.000251
Q9DCU6	*Mrpl4*	-0.87	0.000376
Q3TYS2	*Cybc1*	-0.87	0.000262
Q9CQ45	*Nenf*	-0.86	0.000254
Q8VBZ3	*Clptm1*	-0.86	0.000200
P57759	*Erp29*	-0.85	0.000264
Q8BXQ2	*Pigt*	-0.85	0.000315
Q8C7K6	*Pcyox1l*	-0.85	0.000188
Q60870	*Reep5*	-0.85	0.001835
O88783	*F5*	-0.85	0.000233
Q8K0C8	*Cox19*	-0.85	0.034401
Q61733	*Mrps31*	-0.85	0.000193
P09671	*Sod2*	-0.84	0.000221
Q9JJG9	*Noa1*	-0.84	0.000308
Q8BU88	*Mrpl22*	-0.84	0.000221
Q9R112	*Sqor*	-0.84	0.000305
Q99K23	*Ufsp2*	-0.84	0.000267
Q9CQZ5	*Ndufa6*	-0.84	0.000228
Q99N94	*Mrpl9*	-0.83	0.000329
Q8R3K3	*Ptcd2*	-0.83	0.000213
Q9DAT5	*Trmu*	-0.83	0.000199
Q7TMV3	*Fastkd5*	-0.83	0.000369
Q9JHP7	*Poglut2*	-0.83	0.000343
Q91YT0	*Ndufv1*	-0.83	0.000328
Q9D273	*Mmab*	-0.83	0.000260
Q9CYR0	*Ssbp1*	-0.83	0.000690
Q8R3Q6	*Mix23*	-0.83	0.000244
P68037	*Ube2l3*	-0.83	0.000271
Q9D7N3	*Mrps9*	-0.83	0.000248
P50171	*Hsd17b8*	-0.82	0.000228
P62071	*Rras2*	-0.82	0.000201
Q9CQN1	*Trap1*	-0.82	0.000385
Q566J8	*Coq8b*	-0.82	0.000350
Q9CZN8	*Qrsl1*	-0.82	0.000216
Q8BGA9	*Oxa1l*	-0.82	0.000266
Q9ERI6	*Rdh14*	-0.82	0.000265
Q9CPW2	*Fdx2*	-0.82	0.000260
Q9DCT2	*Ndufs3*	-0.82	0.000238
Q8BFR5	*Tufm*	-0.82	0.000203
Q3UVK0	*Ermp1*	-0.82	0.000375
Q8CD10	*Micu2*	-0.81	0.000274
Q9D0D3	*Mtpap*	-0.81	0.000269
Q922Q4	*Pycr2*	-0.81	0.000536
P62073	*Timm10*	-0.81	0.000277

UniProt ID	Genes	FC [log2]	q-value
P43024	*Cox6a1*	-0.81	0.000455
Q9DAM5	*Slc25a19*	-0.81	0.000275
O35857	*Timm44*	-0.81	0.000292
Q8BHE8	*Maip1*	-0.81	0.000218
P21995	*Emb*	-0.81	0.000219
P29341	*Pabpc1*	-0.81	0.000306
Q9JIY5	*Htra2*	-0.81	0.000268
Q9CQL5	*Mrpl18*	-0.81	0.000291
P48036	*Anxa5*	-0.80	0.000216
Q80VD1	*Fam98b*	-0.80	0.000266
Q8BQZ5	*Cpsf4*	-0.80	0.032655
Q60597	*Ogdh*	-0.80	0.000279
Q3U2A8	*Vars2*	-0.79	0.000272
Q80X85	*Mrps7*	-0.79	0.000344
Q9JJL8	*Sars2*	-0.79	0.000193
O55125	*Nipsnap1*	-0.79	0.000237
Q9CQ54	*Ndufc2*	-0.79	0.000240
Q9ES97	*Rtn3*	-0.79	0.000254
Q9CR68	*Uqcrfs1*	-0.79	0.000257
Q9QYF1	*Rdh11*	-0.79	0.000239
Q791V5	*Mtch2*	-0.79	0.000242
Q8C3X2	*Ccdc90b*	-0.79	0.000895
P09405	*Ncl*	-0.79	0.000253
P63158	*Hmgb1*	-0.79	0.000255
Q8BH59	*Slc25a12*	-0.79	0.000282
Q03145	*Epha2*	-0.78	0.000217
Q5U458	*Dnajc11*	-0.78	0.000325
Q99LP6	*Grpel1*	-0.78	0.000240
Q6GQT9	*Nomo1*	-0.78	0.000254
Q8BYW9	*Eogt*	-0.78	0.000204
Q3TZM9	*Alg11*	-0.78	0.000290
Q9CZU4	*Eral1*	-0.77	0.000253
Q921S7	*Mrpl37*	-0.77	0.000204
Q9Z2I0	*Letm1*	-0.77	0.000236
P51175	*Ppox*	-0.77	0.000185
Q99M87	*Dnaja3*	-0.77	0.000278
Q80UU9	*Pgrmc2*	-0.77	0.000225
Q91VM9	*Ppa2*	-0.77	0.000273
Q9CYA0	*Creld2*	-0.77	0.000194
Q8VCM8	*Ncln*	-0.77	0.000255
Q9D1Q4	*Dpm3*	-0.77	0.001357
Q9D6K5	*Synj2bp*	-0.77	0.000215
Q99N93	*Mrpl16*	-0.77	0.000200
P29758	*Oat*	-0.77	0.000231
Q810S1	*Mcub*	-0.76	0.000207
P56695	*Wfs1*	-0.76	0.000242

UniProt ID	Genes	FC [log2]	q-value
P23242	*Gja1*	-0.76	0.000212
Q9EQI8	*Mrpl46*	-0.76	0.000190
Q8R143	*Pttg1ip*	-0.76	0.000506
Q8BK72	*Mrps27*	-0.76	0.000209
Q9CWX2	*Ndufaf1*	-0.76	0.000248
Q9R0X4	*Acot9*	-0.76	0.000203
P16110	*Lgals3*	-0.76	0.000284
Q9JIZ9	*Plscr3*	-0.76	0.000285
Q9D7J4	*Cox20*	-0.76	0.000269
Q8BX10	*Pgam5*	-0.76	0.000228
Q5ND52	*Mrm3*	-0.75	0.000236
Q9CWG8	*Ndufaf7*	-0.75	0.000212
Q8CB44	*Gramd4*	-0.74	0.014776
P17225	*Ptbp1*	-0.74	0.000264
Q8BGH2	*Samm50*	-0.74	0.000251
Q8BIP0	*Dars2*	-0.74	0.000240
Q8CIC2	*Nup42*	-0.74	0.013367
Q9WTK3	*Gpaa1*	-0.74	0.000204
Q9DCM0	*Ethe1*	-0.74	0.000230
P18155	*Mthfd2*	-0.74	0.000259
Q14CH7	*Aars2*	-0.74	0.000201
Q812F8	*Mgat4b*	-0.74	0.000281
Q99J23	*Ghdc*	-0.74	0.000396
Q66GT5	*Ptpmt1*	-0.74	0.000277
Q8R5J9	*Arl6ip5*	-0.73	0.000889
Q99P65	*Slc29a3*	-0.73	0.004993
Q3TTY5	*Krt2*	-0.73	0.000383
Q60930	*Vdac2*	-0.73	0.000231
Q8K273	*Mmgt1*	-0.73	0.000392
O35435	*Dhodh*	-0.73	0.000270
Q9CXC3	*Mgme1*	-0.73	0.000190
Q925I1	*Atad3*	-0.72	0.000241
Q8JZN5	*Acad9*	-0.72	0.000250
Q9ERS2	*Ndufa13*	-0.72	0.000368
Q9JKL4	*Ndufaf3*	-0.72	0.000651
Q6PD26	*Pigs*	-0.72	0.000278
Q9D0Q7	*Mrpl45*	-0.72	0.000245
O54724	*Cavin1*	-0.72	0.000263
Q8BTS4	*Nup54*	-0.72	0.000311
Q922R8	*Pdia6*	-0.72	0.000275
B9EJ86	*Osbpl8*	-0.72	0.000282
P52875	*Tmem165*	-0.72	0.000866
Q6PB66	*Lrpprc*	-0.71	0.000227
Q03265	*Atp5f1a*	-0.71	0.000218
Q91WS0	*Cisd1*	-0.71	0.000895
Q8CFI5	*Pars2*	-0.71	0.000254

UniProt ID	Genes	FC [log2]	q-value
Q9DBG6	*Rpn2*	-0.71	0.000189
P63038	*Hspd1*	-0.71	0.000201
O08749	*Dld*	-0.71	0.000186
Q3TLP5	*Echdc2*	-0.71	0.000233
Q8CAK1	*Iba57*	-0.71	0.000278
P62774	*Mtpn*	-0.71	0.000243
Q9D1H6	*Ndufaf4*	-0.71	0.000841
P50544	*Acadvl*	-0.71	0.000226
Q9CYW4	*Hdhd3*	-0.70	0.000263
Q9DBE8	*Alg2*	-0.70	0.000258
Q8BH55	*Thnsl1*	-0.70	0.000236
Q9WUR2	*Eci2*	-0.70	0.000543
Q9CQY5	*Magt1*	-0.70	0.001162
Q9CY73	*Mrpl44*	-0.70	0.000202
Q9DB77	*Uqcrc2*	-0.70	0.000260
Q9CR24	*Nudt8*	-0.70	0.000248
Q60932	*Vdac1*	-0.70	0.000265
Q99JB2	*Stoml2*	-0.70	0.000231
Q8VBT0	*Tmx1*	-0.70	0.000395
P26443	*Glud1*	-0.70	0.000266
Q99N96	*Mrpl1*	-0.69	0.000257
Q9Z110	*Aldh18a1*	-0.69	0.000195
Q3TMX7	*Qsox2*	-0.69	0.000263
Q91YP0	*L2hgdh*	-0.69	0.000208
Q9JIK9	*Mrps34*	-0.69	0.000206
Q8K1R3	*Pnpt1*	-0.69	0.000266
Q99N89	*Mrpl43*	-0.69	0.000234
Q9D2V8	*Mfsd10*	-0.68	0.000512
Q9CWT6	*Ddx28*	-0.68	0.000266
Q9DC71	*Mrps15*	-0.68	0.000268
Q91ZN5	*Slc35b2*	-0.68	0.000551
Q61586	*Gpam*	-0.68	0.000408
O35972	*Mrpl23*	-0.68	0.000249
Q6ZWN5	*Rps9*	-0.67	0.000233
Q8K013	*Gtpbp10*	-0.67	0.000259
Q9CQH3	*Ndufb5*	-0.67	0.000406
Q8K4F5	*Abhd11*	-0.67	0.000265
Q9DCS9	*Ndufb10*	-0.67	0.000742
Q8BHF7	*Pgs1*	-0.67	0.000195
Q9R0P6	*Sec11a*	-0.67	0.000367
O08715	*Akap1*	-0.67	0.000371
Q8VE22	*Mrps23*	-0.67	0.000229
Q80XN0	*Bdh1*	-0.67	0.000385
O35682	*Myadm*	-0.67	0.000982
Q9CWU2	*Zdhhc13*	-0.66	0.000252
P59017	*Bcl2l13*	-0.66	0.000375

UniProt ID	Genes	FC [log2]	q-value
Q8VEG4	*Exd2*	-0.66	0.000406
Q91ZA3	*Pcca*	-0.66	0.000267
Q9WV98	*Timm9*	-0.66	0.000188
Q3UDW8	*Hgsnat*	-0.66	0.000504
Q99MZ7	*Pecr*	-0.66	0.000311
Q3TIU4	*Pde12*	-0.66	0.000261
Q8BYB9	*Poglut1*	-0.66	0.000243
Q61234	*Snta1*	-0.66	0.000370
Q60760	*Grb10*	-0.66	0.000186
Q91ZV0	*Mia2*	-0.65	0.000247
P62301	*Rps13*	-0.65	0.000367
Q91VR2	*Atp5f1c*	-0.65	0.000274
Q9JI99	*Sgpp1*	-0.65	0.000498
Q8C0D5	*Efl1*	-0.65	0.001834
P61620	*Sec61a1*	-0.65	0.003660
Q3TJZ6	*Fam98a*	-0.65	0.002028
Q9CQX8	*Mrps36*	-0.65	0.000541
Q9QX47	*Son*	-0.65	0.021689
Q923Z3	*Mto1*	-0.65	0.000409
Q8BFP9	*Pdk1*	-0.65	0.000247
Q62426	*Cstb*	-0.65	0.000280
Q8VE37	*Rcc1*	-0.65	0.000284
P97930	*Dtymk*	-0.65	0.000374
Q9CR60	*Golt1b*	-0.65	0.005423
Q9D855	*Uqcrb*	-0.64	0.000500
P99027	*Rplp2*	-0.64	0.000687
Q8K2B3	*Sdha*	-0.64	0.000274
Q3UM83	*Klrg2*	-0.64	0.000389
P58281	*Opa1*	-0.64	0.000207
Q8BK67	*Rcc2*	-0.64	0.000271
P35282	*Rab21*	-0.64	0.000280
O35129	*Phb2*	-0.64	0.000406
Q99N87	*Mrps5*	-0.64	0.000247
Q8VDC0	*Lars2*	-0.64	0.000369
Q3ULF4	*Spg7*	-0.64	0.000262
P11930	*Nudt19*	-0.64	0.000410
Q9D2R8	*Mrps33*	-0.64	0.000376
Q80WJ7	*Mtdh*	-0.64	0.000456
P08113	*Hsp90b1*	-0.63	0.000402
Q8VE95		-0.63	0.000500
Q8BXZ1	*Tmx3*	-0.63	0.000249
Q9DC61	*Pmpca*	-0.63	0.000239
O54734	*Ddost*	-0.63	0.000552
Q3UHH8	*Gxylt1*	-0.63	0.000952
Q9CYF5	*Rcc1l*	-0.63	0.000228
Q3URE1	*Acsf3*	-0.63	0.000260

UniProt ID	Genes	FC-[log2]	q-value
Q8VEB4	*Pla2g15*	-0.63	0.000535
Q8CAQ8	*Immt*	-0.63	0.000250
P19783	*Cox4i1*	-0.62	0.000281
Q8BIJ6	*Iars2*	-0.62	0.000267
Q923K4	*Gtpbp3*	-0.62	0.001084
O35887	*Calu*	-0.62	0.000545
Q3TZZ7	*Esyt2*	-0.62	0.000263
P62746	*Rhob*	-0.62	0.000364
P22315	*Fech*	-0.62	0.000259
P27046	*Man2a1*	-0.62	0.000236
Q61102	*Abcb7*	-0.62	0.000250
Q8JZQ2	*Afg3l2*	-0.62	0.000279
Q9D051	*Pdhb*	-0.62	0.000409
Q3UN02	*Lclat1*	-0.62	0.000653
Q8BSF4	*Pisd*	-0.62	0.000400
Q99N91	*Mrpl34*	-0.62	0.000398
Q80ZM8	*Crls1*	-0.61	0.000614
Q80ZD3	*Slc26a11*	-0.61	0.000994
Q9D2G2	*Dlst*	0.61	0.000391
Q9CPU2	*Ndufb2*	-0.61	0.000252
P53395	*Dbt*	-0.61	0.000252
Q9JKF7	*Mrpl39*	-0.61	0.000253
Q9CQP0	*Mrpl33*	-0.61	0.000260
Q9JKN1	*Slc30a7*	-0.61	0.000648
P14211	*Calr*	-0.61	0.000497
Q8BWY3	*Etf1*	-0.61	0.000509
Q9CXR1	*Dhrs7*	-0.61	0.000617
Q9CYN9	*Atp6ap2*	-0.61	0.000262
Q9CQF8	*Mrpl57*	-0.61	0.000263
Q9CXI0	*Coq5*	-0.61	0.000987
Q9CQC7	*Ndufb4*	-0.61	0.000256
Q8CIW5	*Twnk*	-0.60	0.006856
Q9Z1J3	*Nfs1*	-0.60	0.000279
Q8CFX1	*H6pd*	-0.60	0.000268
Q8JZM0	*Tfb1m*	-0.60	0.000371
Q8BW00	*Ptrh1*	-0.60	0.002951
Q9CZW5	*Tomm70*	-0.60	0.000748
Q8R404	*Micos13*	-0.60	0.000728
Q9CXT8	*Pmpcb*	-0.60	0.000238
P55302	*Lrpap1*	-0.60	0.000543
Q5SS80	*Dhrs13*	-0.60	0.000253
Q91X21	*Kiaa2013*	-0.60	0.000387
Q9DCA2	*Mrps11*	-0.60	0.000556
Q99KV1	*Dnajb11*	-0.59	0.000730
Q9D1I6	*Mrpl14*	-0.59	0.000255
Q9D8P4	*Mrpl17*	-0.59	0.000733

UniProt ID	Genes	FC [log2]	q-value
Q9DC51	*Gnai3*	-0.59	0.000848
O88967	*Yme1l1*	-0.59	0.000270
P03930	*Mtatp8*	-0.59	0.000509
P00405	*Mtco2*	-0.59	0.001976
Q8C3X8	*Lmf2*	-0.59	0.000551
Q9CXT7	*Tmem192*	-0.59	0.000864
O09174	*Amacr*	-0.59	0.000382
Q9JKB1	*Uchl3*	-0.59	0.000863
Q8VDT9	*Mrpl50*	-0.59	0.000251
P52825	*Cpt2*	-0.59	0.000404
Q9CPR5	*Mrpl15*	-0.59	0.000256
Q8BX90	*Fndc3a*	-0.59	0.000823
Q8BMK4	*Ckap4*	-0.59	0.000252
Q8CBY0	*Gatc*	-0.59	0.000232
Q8R0X7	*Sgpl1*	-0.59	0.000258
Q9R1Q7	*Plp2*	-0.58	0.000820
Q8VEK0	*Tmem30a*	-0.58	0.000881
O08528	*Hk2*	-0.58	0.000229
O88848	*Arl6*	-0.58	0.001140
Q61578	*Fdxr*	-0.58	0.000288
Q8BJU9	*Mtrf1l*	-0.58	0.000254
Q8K0D5	*Gfm1*	-0.58	0.000397
Q8BTV1	*Tusc3*	-0.58	0.002477
Q9D5T0	*Atad1*	-0.58	0.000276
Q9Z0L8	*Ggh*	-0.58	0.000903
Q8R3F5	*Mcat*	-0.58	0.000408
Q922Q8	*Lrrc59*	-0.58	0.000268
Q9D8S9	*Bola1*	-0.58	0.000749
Q5SXY1	*Specc1*	-0.58	0.000873
Q80ZS3	*Mrps26*	-0.58	0.000383
P26645	*Marcks*	-0.58	0.006090
Q9DCJ5	*Ndufa8*	-0.57	0.000407
Q91VT4	*Cbr4*	-0.57	0.000549
Q9CZ42	*Naxd*	-0.57	0.000253
Q99JR1	*Sfxn1*	-0.57	0.000254
Q3URS9	*Ccdc51*	-0.57	0.000539
Q9JKW0	*Arl6ip1*	-0.57	0.000876
Q9CZR8	*Tsfm*	-0.57	0.003703
P97792	*Cxadr*	-0.57	0.000515
P13595	*Ncam1*	-0.57	0.000379
Q9CPT4	*Mydgf*	-0.57	0.001114
Q99MN9	*Pccb*	-0.57	0.000250
Q9D172	*Gatd3*	-0.56	0.000260
Q6P3B9	*Rbfa*	-0.56	0.000455
Q9CY16	*Mrps28*	-0.56	0.000786
Q8R035	*Mrpl58*	-0.56	0.000256

UniProt ID	Genes	FC [log2]	q-value
P62245	*Rps15a*	-0.56	0.000255
Q9D0M3	*Cyc1*	-0.56	0.000255
Q9R1B9	*Slit2*	-0.56	0.000250
Q9EPR2	*Pla2g12a*	-0.56	0.015993
P50427	*Sts*	-0.56	0.000551
Q99KR8	*Fuca2*	-0.56	0.001114
Q9CZ57	*Nsun4*	-0.56	0.000504
Q9DB20	*Atp5po*	-0.56	0.000688
Q99J99	*Mpst*	-0.56	0.000380
Q8C5H8	*Nadk2*	-0.56	0.000533
Q920A7	*Afg3l1*	-0.56	0.000269
P35564	*Canx*	-0.56	0.001390
Q9ERE7	*Mesd*	-0.56	0.000878
Q8K0Z7	*Taco1*	-0.56	0.000754
Q8VBW1	*Slc6a8*	-0.55	0.001477
Q8C2E4	*Ptcd1*	-0.55	0.000542
Q9EP72	*Emc7*	-0.55	0.000690
P56382	*Atp5f1e*	-0.55	0.003586
Q9DB15	*Mrpl12*	-0.55	0.000499
D3Z7Q2	*Smim20*	-0.55	0.011636
Q7TMS5	*Abcg2*	-0.55	0.000538
Q9D1H8	*Mrpl53*	-0.55	0.000894
Q3KNM2	*Marchf5*	-0.55	0.000874
O35680	*Mrps12*	-0.55	0.001107
P11276	*Fn1*	-0.55	0.000378
P53994	*Rab2a*	-0.55	0.000855
Q8K2M0	*Mrpl38*	-0.55	0.000742
Q8C7X2	*Emc1*	-0.55	0.000552
Q9D6K9	*Cers5*	-0.55	0.000876
Q8R0G7	*Spns1*	-0.55	0.000391
P62908	*Rps3*	-0.55	0.000650
P19221	*F2*	-0.55	0.000995
Q9CQ06	*Mrpl24*	-0.54	0.000557
P97450	*Atp5pf*	-0.54	0.000368
Q91WD5	*Ndufs2*	-0.54	0.000859
Q9EQG7	*Enpp5*	-0.54	0.000743
Q9JIA7	*Sphk2*	-0.54	0.013979
Q8R1S0	*Coq6*	-0.54	0.000692
Q9EPS3	*Glce*	-0.54	0.000740
D3Z7P3	*Gls*	-0.54	0.000554
Q99LC5	*Etfa*	-0.54	0.000249
Q8BG51	*Rhot1*	-0.54	0.000564
P06795	*Abcb1b*	-0.53	0.000845
Q9WV96	*Timm10b*	-0.53	0.000728
Q99LY9	*Ndufs5*	-0.53	0.000378
Q8CC88	*Vwa8*	-0.53	0.000388

UniProt ID	Genes	FC [log2]	q-value
Q99KS2	*Ngrn*	-0.53	0.000555
Q3TDN2	*Faf2*	-0.53	0.000394
D3YZG8	*Mthfd2l*	-0.53	0.000556
Q61555	*Fbn2*	-0.53	0.000456
P47758	*Srprb*	-0.53	0.000500
Q8BGT5	*Gpt2*	-0.53	0.001085
Q6P5B0	*Rrp12*	-0.53	0.000898
Q9D0G0	*Mrps30*	-0.53	0.000901
Q9D2R6	*Coa3*	-0.53	0.000899
Q9CPY7	*Lap3*	-0.53	0.000405
Q9Z2I8	*Suclg2*	-0.53	0.000862
Q9QZH6	*Ecsit*	-0.53	0.000381
Q8BP92	*Rcn2*	-0.53	0.000845
Q91WG3	*Trub2*	-0.53	0.001102
O08756	*Hsd17b10*	-0.53	0.000555
O35454	*Clcn6*	-0.52	0.001448
Q922W5	*Pycr1*	-0.52	0.007032
Q6P3A8	*Bckdhb*	-0.52	0.000540
Q80WW9	*Ddrgk1*	-0.52	0.003150
P62855	*Rps26*	-0.52	0.000854
Q99KI0	*Aco2*	-0.52	0.000513
O88384	*Vti1b*	-0.52	0.000555
Q8BK30	*Ndufv3*	-0.52	0.002372
Q9Z2I9	*Sucla2*	-0.52	0.000879
Q9CQQ7	*Atp5pb*	-0.52	0.007705
P70372	*Elavl1*	-0.52	0.004541
Q8BI84	*Mia3*	-0.52	0.000554
Q9QYA2	*Tomm40*	-0.51	0.005126
Q8BMF4	*Dlat*	-0.51	0.000531
Q99KE1	*Me2*	-0.51	0.000560
P47740	*Aldh3a2*	-0.51	0.000549
O70572	*Smpd2*	-0.51	0.000502
Q99N95	*Mrpl3*	-0.51	0.000613
Q8BGD8	*Coa6*	-0.51	0.001392
Q8C3X4	*Guf1*	-0.51	0.000652
Q9EQ80	*Nif3l1*	-0.51	0.001102
P37804	*Tagln*	-0.51	0.000970
Q9CR88	*Mrps14*	-0.50	0.001147
P16546	*Sptan1*	-0.50	0.000826
Q9Z2Q5	*Mrpl40*	-0.50	0.007504
Q9DCN2	*Cyb5r3*	-0.50	0.003392
Q80U63	*Mfn2*	-0.50	0.000729
P02469	*Lamb1*	-0.50	0.000554
Q91YX5	*Lpgat1*	-0.50	0.001104
Q9DC69	*Ndufa9*	-0.50	0.000882
Q8VCB1	*Ndc1*	-0.50	0.001147

UniProt ID	Genes	FC [log2]	q-value
B1AZA5	*Tmem245*	-0.50	0.000832
O55028	*Bckdk*	-0.50	0.000563
Q8BMD8	*Slc25a24*	-0.50	0.000948
P62075	*Timm13*	-0.50	0.006217
Q91ZW2	*Pofut1*	-0.50	0.001112
O54825	*Bysl*	-0.50	0.001001
P42125	*Eci1*	-0.50	0.001086
Q9CQ40	*Mrpl49*	-0.50	0.000691
Q14AI6	*Rpusd3*	-0.50	0.001101
Q8R216	*Sirt4*	-0.50	0.000989
Q8BMS4	*Coq3*	-0.50	0.000884
P47802	*Mtx1*	-0.50	0.000539
Q9CR59	*Gadd45gip1*	-0.50	0.000544
P14131	*Rps16*	-0.50	0.000865
P99028	*Uqcrh*	-0.49	0.000849
P20029	*Hspa5*	-0.49	0.000740
Q8BGC4	*Ptgr3*	-0.49	0.000691
P51174	*Acadl*	-0.49	0.000886
Q9CPQ1	*Cox6c*	-0.49	0.001389
Q9CWU6	*Uqcc1*	-0.49	0.000924
Q8K2B0	*P3h4*	-0.49	0.001304
Q99JY4	*Trabd*	-0.49	0.000887
Q9ERU9	*Ranbp2*	-0.49	0.000861
P47738	*Aldh2*	-0.49	0.000731
O88441	*Mtx2*	-0.49	0.000884
Q9CQA3	*Sdhb*	-0.49	0.003333
O09111	*Ndufb11*	-0.49	0.003023
Q91YY4	*Atpaf2*	-0.48	0.002455
Q9JHS4	*Clpx*	-0.48	0.000862
Q99LI2	*Clcc1*	-0.48	0.001113
Q8R3H7	*Hs2st1*	-0.48	0.001362
Q9D7A8	*Armc1*	-0.48	0.000983
Q9D773	*Mrpl2*	-0.48	0.001156
Q9D6S7	*Mrrf*	-0.48	0.003166
Q8R2Q4	*Gfm2*	-0.48	0.000733
Q8VEH8	*Erlec1*	-0.48	0.001122
Q8QZS1	*Hibch*	-0.48	0.000871
Q9ESW4	*Agk*	-0.48	0.000831
E9Q236	*Abcc4*	-0.48	0.000826
Q60931	*Vdac3*	-0.48	0.000553
P35486	*Pdha1*	-0.48	0.000744
P56480	*Atp5f1b*	-0.48	0.000979
Q8VDM4	*Psmd2*	-0.48	0.001711
P19324	*Serpinh1*	-0.48	0.001002
Q9CQ62	*Decr1*	-0.47	0.001607
P97807	*Fh*	-0.47	0.003526

UniProt ID	Genes	FC [log2]	q-value
P10605	*Ctsb*	-0.47	0.000839
Q9D6Z1	*Nop56*	-0.47	0.000732
Q8K411	*Pitrm1*	-0.47	0.000899
Q9QXT0	*Cnpy2*	-0.47	0.001356
Q9CQS4	*Slc25a46*	-0.47	0.000897
P09103	*P4hb*	-0.47	0.000872
Q64735	*Cr1l*	-0.47	0.001093
Q3TC33	*Ccdc127*	-0.47	0.000978
Q9DCS3	*Mecr*	-0.47	0.000993
A2AMZ4	*Ndufaf8*	-0.47	0.013497
Q8R0F8	*Fahd1*	-0.47	0.000818
Q9JHW2	*Nit2*	-0.47	0.001005
Q3UM18	*Lsg1*	-0.47	0.000858
P14069	*S100a6*	-0.47	0.000900
P62077	*Timm8b*	-0.47	0.000983
Q9DCL4	*Mettl15*	-0.47	0.010487
Q6P5E4	*Uggt1*	-0.47	0.000647
Q9D0I4	*Stx17*	-0.47	0.000729
P61358	*Rpl27*	-0.47	0.000892
Q8VDK1	*Nit1*	-0.47	0.000878
Q9CWE0	*Mtfr1l*	-0.47	0.000903
Q4PJX1	*Odr4*	-0.47	0.000889
Q9ET30	*Tm9sf3*	-0.47	0.000538
O35704	*Sptlc1*	-0.47	0.003899
Q99P88	*Nup155*	-0.46	0.000738
O55126	*Nipsnap2*	-0.46	0.001193
Q9DBH5	*Lman2*	-0.46	0.001511
Q60751	*Igf1r*	-0.46	0.001100
Q8CG70	*P3h3*	-0.46	0.001356
Q64433	*Hspe1*	-0.46	0.001117
Q8BG05	*Hnrnpa3*	-0.46	0.004642
Q61387	*Cox7a2l*	-0.46	0.000950
P14115	*Rpl27a*	-0.46	0.000972
Q9CQP3	*Chchd5*	-0.46	0.007547
Q9Z0X1	*Aifm1*	-0.46	0.000871
Q6ZQI3	*Mlec*	-0.46	0.001951
Q9CXZ1	*Ndufs4*	-0.46	0.001954
P52503	*Ndufs6*	-0.45	0.000898
Q8K2K6	*Agfg1*	-0.45	0.001804
Q8VDL4	*Adpgk*	-0.45	0.000747
Q99P72	*Rtn4*	-0.45	0.001841
O35855	*Bcat2*	-0.45	0.001975
Q4FK66	*Prpf38a*	-0.45	0.004691
Q99LM2	*Cdk5rap3*	-0.45	0.002367
P67778	*Phb1*	-0.45	0.001111
P30681	*Hmgb2*	-0.45	0.000906

UniProt ID	Genes	FC [log2]	q-value
Q05186	*Rcn1*	-0.45	0.001661
Q32NY4	*Cnnm3*	-0.44	0.004027
Q8CCJ3	*Ufl1*	-0.44	0.000875
Q8R0F3	*Sumf1*	-0.44	0.001092
Q8BKZ9	*Pdhx*	-0.44	0.000786
Q62186	*Ssr4*	-0.44	0.000840
Q4U2R1	*Herc2*	-0.44	0.017736
Q923X4	*Glrx2*	-0.44	0.001504
Q61425	*Hadh*	-0.44	0.003004
Q9ESL4	*Map3k20*	-0.44	0.001166
Q9CYK1	*Wars2*	-0.44	0.004858
B1AR13	*Cisd3*	-0.44	0.000981
Q922P9	*Glyr1*	-0.44	0.002976
P38060	*Hmgcl*	-0.44	0.000878
Q8R3J4	*Mterf3*	-0.44	0.002830
S4R2K0	*Pdf*	-0.44	0.001121
O35874	*Slc1a4*	-0.43	0.012821
Q9DBL1	*Acadsb*	-0.43	0.001083
Q9CWX4	*Rpusd4*	-0.43	0.006528
Q9WV55	*Vapa*	-0.43	0.010556
Q8K4X7	*Agpat4*	-0.43	0.009223
O88983	*Stx8*	-0.43	0.000900
Q8BKF1	*Polrmt*	-0.43	0.009148
Q8VCW8	*Acsf2*	-0.43	0.000890
Q9CZU6	*Cs*	-0.43	0.002139
Q9CQ69	*Uqcrq*	-0.43	0.006320
P58044	*Idi1*	-0.43	0.004497
Q5IRJ6	*Slc30a9*	-0.43	0.001084
O35639	*Anxa3*	-0.43	0.001832
Q9CZ13	*Uqcrc1*	-0.43	0.000893
O54967	*Tnk2*	-0.43	0.004035
Q9R1Q9	*Atp6ap1*	-0.43	0.008880
Q9DC23	*Dnajc10*	-0.43	0.001160
Q921H9	*Coa7*	-0.42	0.000899
O35379	*Abcc1*	-0.42	0.001263
Q99LB7	*Sardh*	-0.42	0.000844
Q8CCH2	*Nhlrc3*	-0.42	0.001886
O88425	*Nme6*	-0.42	0.001120
E2JF22	*Piezo1*	-0.42	0.001258
O70503	*Hsd17b12*	-0.42	0.001393
P35821	*Ptpn1*	-0.42	0.001161
Q8R2R6	*Mtg1*	-0.42	0.003394
Q64314	*Cd34*	-0.42	0.004113
P42567	*Eps15*	-0.42	0.002400
Q6ZWV7	*Rpl35*	-0.41	0.001264
Q61029	*Tmpo*	-0.41	0.001885

UniProt ID	Genes	FC [log2]	q-value
P10107	*Anxa1*	-0.41	0.000838
A2ASZ8	*Slc25a25*	-0.41	0.009244
Q8BH95	*Echs1*	-0.41	0.002370
Q59J78	*Ndufaf2*	-0.41	0.002074
Q9D6J5	*Ndufb8*	-0.41	0.002473
Q64516	*Gk*	-0.41	0.002401
Q9D0S9	*Hint2*	-0.41	0.003901
O54950	*Prkag1*	-0.41	0.001364
Q8BHN3	*Ganab*	-0.41	0.003247
Q80UM7	*Mogs*	-0.41	0.001259
P39688	*Fyn*	-0.41	0.005011
P55012	*Slc12a2*	-0.41	0.003248
Q9CQN7	*Mrpl41*	-0.41	0.003584
Q9EPE9	*Atp13a1*	-0.41	0.001154
Q91XV3	*Basp1*	-0.41	0.035197
Q9CQZ6	*Ndufb3*	-0.40	0.005040
Q920A5	*Scpep1*	-0.40	0.008588
P99029	*Prdx5*	-0.40	0.000988
Q8C172	*Cers6*	-0.40	0.006067
P19536	*Cox5b*	-0.40	0.024908
Q9D6J6	*Ndufv2*	-0.40	0.004940
Q9WV84	*Nme4*	-0.40	0.015453
Q91W53	*Golga7*	-0.40	0.002186
Q9CXY1	*Tmem175*	-0.40	0.010888
Q99L13	*Hibadh*	-0.40	0.004332
Q9D379	*Ephx1*	-0.40	0.004048
Q3UZ39	*Lrrfip1*	-0.40	0.011070
P52196	*Tst*	-0.40	0.000972
Q9CXI5	*Manf*	-0.40	0.002398
A2AUM9	*Cep152*	-0.40	0.038287
Q9CQJ8	*Ndufb9*	-0.40	0.001950
Q8K2Y7	*Mrpl47*	-0.39	0.006482
Q9QZD8	*Slc25a10*	-0.39	0.003259
Q9D8E6	*Rpl4*	-0.39	0.002109
Q91YW3	*Dnajc3*	-0.39	0.001165
P51807	*Dynlt1*	-0.39	0.005511
P10852	*Slc3a2*	-0.39	0.003191
P53702	*Hccs*	-0.39	0.011583
Q9CQS8	*Sec61b*	-0.39	0.030835
Q9D7P6	*Iscu*	-0.39	0.026469
Q91YQ5	*Rpn1*	-0.39	0.002474
P32507	*Nectin2*	-0.39	0.008662
P14824	*Anxa6*	-0.39	0.003925
Q9Z0W3	*Nup160*	-0.39	0.004809
Q6A0D4	*Rftn1*	-0.39	0.002546
Q14C51	*Ptcd3*	-0.39	0.015093

UniProt ID	Genes	FC [log2]	q-value
P62960	*Ybx1*	-0.39	0.019076
Q3TXS7	*Psmd1*	-0.39	0.003524
Q8BSY0	*Asph*	-0.39	0.000980
P45952	*Acadm*	-0.39	0.001453
Q61738	*Itga7*	-0.39	0.003975
P14148	*Rpl7*	-0.39	0.002182
O88792	*F11r*	-0.39	0.009489
Q99N84	*Mrps18b*	-0.39	0.002910
Q6PGN1	*Erfe*	-0.38	0.010018
Q8R502	*Lrrc8c*	-0.38	0.004841
Q61263	*Soat1*	-0.38	0.013273
Q04519	*Smpd1*	-0.38	0.003334
Q8BHS6	*Armcx3*	-0.38	0.002691
Q5SV80	*Myo19*	-0.38	0.007709
P31266	*Rbpj*	-0.38	0.006786
O08917	*Flot1*	-0.38	0.002183
P28665	*Mug1*	-0.38	0.011625
P84091	*Ap2m1*	-0.38	0.003255
P58059	*Mrps21*	-0.38	0.012430
Q8K248	*Hpdl*	-0.38	0.002162
Q8VCX5	*Micu1*	-0.38	0.004543
P20444	*Prkca*	-0.38	0.003532
P11438	*Lamp1*	-0.38	0.004833
Q91XD7	*Creld1*	-0.38	0.038616
Q60715	*P4ha1*	-0.38	0.001449
Q9D7B6	*Acad8*	-0.38	0.003537
Q9CPY1	*Mrpl51*	-0.37	0.001909
Q9EPB5	*Serhl*	-0.37	0.002136
Q7TPR4	*Actn1*	-0.37	0.002402
Q60738	*Slc30a1*	-0.37	0.003979
Q9CQV4	*Retreg3*	-0.37	0.017376
Q8BYM8	*Cars2*	-0.37	0.002978
Q64008	*Rab34*	-0.37	0.012095
Q01768	*Nme2*	-0.37	0.008918
Q9DB25	*Alg5*	-0.37	0.002496
Q9R0A0	*Pex14*	-0.37	0.002351
Q9D024	*Ccdc47*	-0.37	0.012053
Q91VD9	*Ndufs1*	-0.37	0.002689
P51410	*Rpl9*	-0.37	0.012655
Q8BTM8	*Flna*	-0.37	0.004844
P81117	*Nucb2*	-0.36	0.011620
Q8C547	*Heatr5b*	-0.36	0.012778
Q8BHB4	*Wdr3*	-0.36	0.008897
O54962	*Banf1*	-0.36	0.004286
P32921	*Wars1*	-0.36	0.003027
P09528	*Fth1*	-0.36	0.005104

UniProt ID	Genes	FC [log2]	q-value
O70325	*Gpx4*	-0.36	0.013371
Q9CXF4	*Tbc1d15*	-0.36	0.004666
Q9DBF1	*Aldh7a1*	-0.36	0.002454
Q9D0L7	*Armc10*	-0.36	0.004846
Q99LC3	*Ndufa10*	-0.36	0.006107
Q8BMS1	*Hadha*	-0.36	0.003792
Q922B2	*Dars1*	-0.36	0.004046
Q3TBT3	*Sting1*	-0.36	0.002931
Q9DC37	*Mfsd1*	-0.36	0.035591
P62889	*Rpl30*	-0.35	0.006296
Q80W54	*Zmpste24*	-0.35	0.006691
Q8BHC1	*Rab39b*	-0.35	0.008407
Q91VN4	*Chchd6*	-0.35	0.004284
Q6A058	*Armcx2*	-0.35	0.012085
Q9CPP6	*Ndufa5*	-0.35	0.004937
P01029	*C4b*	-0.35	0.003126
Q3U7R1	*Esyt1*	-0.35	0.004091
O09005	*Degs1*	-0.35	0.012568
Q99N92	*Mrpl27*	-0.35	0.009071
Q99LJ1	*Fuca1*	-0.35	0.007019
P08249	*Mdh2*	-0.35	0.003536
Q921T2	*Tor1aip1*	-0.35	0.003085
G5E829	*Atp2b1*	-0.35	0.004282
Q91Z53	*Grhpr*	-0.35	0.004476
Q9R0Q7	*Ptges3*	-0.35	0.006904
P19182	*Ifrd1*	-0.35	0.021582
O88396	*Grpel2*	-0.35	0.012995
Q8BLN5	*Lss*	-0.35	0.002072
Q9QZQ8	*Macroh2a1*	-0.34	0.005672
O88455	*Dhcr7*	-0.34	0.007287
P14869	*Rplp0*	-0.34	0.005016
Q9DBS1	*Tmem43*	-0.34	0.004116
Q9Z204	*Hnrnpc*	-0.34	0.004851
Q91Z92	*B3galt6*	-0.34	0.016433
Q9WTP6	*Ak2*	-0.34	0.010007
Q9QXB9	*Drg2*	-0.34	0.005593
Q921I6	*Sh3bp4*	-0.34	0.009863
P61021	*Rab5b*	-0.34	0.010538
P62270	*Rps18*	-0.33	0.003308
Q9CSU0	*Rprd1b*	-0.33	0.016218
Q9JIG8	*Praf2*	-0.33	0.004618
Q9CQ75	*Ndufa2*	-0.33	0.007291
Q9D1M7	*Fkbp11*	-0.33	0.008810
A2APY7	*Ndufaf5*	-0.33	0.009651
Q91WM2	*Hdhd5*	-0.33	0.004478
Q9DCF9	*Ssr3*	-0.33	0.006980

UniProt ID	Genes	FC [log2]	q-value
Q9JIK5	*Ddx21*	-0.33	0.004935
Q80V26	*Bpnt2*	-0.33	0.009453
Q91V12	*Acot7*	-0.33	0.009067
Q9EQ20	*Aldh6a1*	-0.33	0.003973
P50136	*Bckdha*	-0.33	0.007304
P57784	*Snrpa1*	-0.33	0.008893
Q922H2	*Pdk3*	-0.32	0.004037
Q8VHX6	*Flnc*	-0.32	0.008844
Q07417	*Acads*	-0.32	0.012864
Q9CYN2	*Spcs2*	-0.32	0.020247
P21619	*Lmnb2*	-0.32	0.018567
Q9CR61	*Ndufb7*	-0.32	0.026326
Q8R2U0	*Seh1l*	-0.32	0.009530
P62858	*Rps28*	-0.32	0.021530
Q9CRD2	*Emc2*	-0.32	0.012100
Q8BM55	*Tmem214*	-0.32	0.009699
Q9CQE8	*RTRAF*	-0.32	0.014544
Q8BH79	*Ano10*	-0.32	0.024275
P17427	*Ap2a2*	-0.32	0.004644
O70378	*Emc8*	-0.31	0.007016
P06797	*Ctsl*	-0.31	0.013636
Q8BKC5	*Ipo5*	-0.31	0.007790
Q99N85	*Mrps18a*	-0.31	0.015075
P62897	*Cycs*	-0.31	0.009448
Q9CY27	*Tecr*	-0.31	0.012487
O35344	*Kpna3*	-0.31	0.013372
Q9CXY9	*Pigk*	-0.31	0.037193
Q9CXY6	*Ilf2*	-0.31	0.015363
Q9D0I9	*Rars1*	-0.31	0.009850
P61089	*Ube2n*	-0.30	0.020111
Q5SWD9	*Tsr1*	-0.30	0.012560
P54071	*Idh2*	-0.30	0.006907
Q62167	*Ddx3x*	-0.30	0.016198
Q9Z2L6	*Minpp1*	-0.30	0.017477
O70152	*Dpm1*	-0.30	0.013349
Q8K370	*Acad10*	-0.30	0.012392
Q8BVU5	*Nudt9*	-0.30	0.009279
Q2TPA8	*Hsdl2*	-0.30	0.010023
G5E8V9	*Arfip1*	-0.30	0.015673
Q9CPW9	*Metap1d*	-0.30	0.017846
Q7TT37	*Elp1*	-0.29	0.009868
Q9R1J0	*Nsdhl*	-0.29	0.019555
P70404	*Idh3g*	-0.29	0.011574
Q9D162	*Ccdc167*	-0.29	0.028028
Q9D6R2	*Idh3a*	-0.29	0.019822
Q99MB2	*Mtfr1*	-0.29	0.008801

UniProt ID	Genes	FC [log2]	q-value
P48678	*Lmna*	-0.28	0.011857
Q3UJU9	*Rmdn3*	-0.28	0.013462
Q9D898	*Arpc5l*	-0.28	0.014278
Q9D7S7	*Rpl22l1*	-0.28	0.020874
Q8BMJ2	*Lars1*	-0.28	0.013361
Q60649	*Clpb*	-0.28	0.018942
P68040	*Rack1*	-0.28	0.017670
Q3TQB2	*Foxred1*	-0.28	0.017720
Q91W90	*Txndc5*	-0.28	0.012322
P03975	*Iap*	-0.28	0.017721
Q8BTX9	*Hsdl1*	-0.28	0.015667
Q5XG73	*Acbd5*	-0.28	0.019298
Q6PCP5	*Mff*	-0.28	0.026920
Q921G7	*Etfdh*	-0.28	0.013930
Q9CZL5	*Pcbd2*	-0.27	0.017713
Q9WUQ2	*Preb*	-0.27	0.015376
Q02819	*Nucb1*	-0.27	0.010414
Q8CHT0	*Aldh4a1*	-0.27	0.016454
Q8VI75	*Ipo4*	-0.27	0.013963
P55096	*Abcd3*	-0.27	0.012079
Q91VX9	*Tmem168*	-0.27	0.022468
Q8VEH3	*Arl8a*	-0.27	0.024290
Q99LR1	*Abhd12*	-0.27	0.017617
Q6ZPR5	*Smpd4*	-0.27	0.012737
Q9EST5	*Anp32b*	-0.26	0.027620
O35448	*Ppt2*	-0.26	0.021262
Q8BHT6	*B3glct*	-0.26	0.024725
Q8BTY2	*Slc4a7*	-0.26	0.021538
Q8C163	*Exog*	-0.26	0.015261
Q8BLF1	*Nceh1*	-0.26	0.015255
Q9CQW1	*Ykt6*	-0.26	0.019909
Q3UMC0	*Afg2a*	-0.26	0.015335
Q9D8S4	*Rexo2*	-0.26	0.013486
Q9DAU1	*Cnpy3*	-0.26	0.025076
P63325	*Rps10*	-0.26	0.031419
Q91XL3	*Uxs1*	-0.26	0.024198
Q60759	*Gcdh*	-0.26	0.015357
Q5SW19	*Cluh*	-0.26	0.029774
Q9JJ80	*Rpf2*	-0.26	0.044929
Q60716	*P4ha2*	-0.25	0.021672
Q9Z2G6	*Sel1l*	-0.25	0.029661
P56391	*Cox6b1*	-0.25	0.020655
Q3U9G9	*Lbr*	-0.25	0.046733
Q8BU33	*Ilvbl*	-0.25	0.040146
Q9ERN0	*Scamp2*	-0.25	0.026891
Q8C080	*Snx16*	-0.25	0.016203

UniProt ID	Genes	FC [log2]	q-value
Q8BX17	*Gemin5*	-0.25	0.021706
Q9D8T7	*Slirp*	-0.25	0.025035
Q9CPV4	*Glod4*	-0.25	0.023906
Q8CIF6	*Sidt2*	-0.25	0.041398
Q8R127	*Sccpdh*	-0.25	0.025981
A6H611	*Mipep*	-0.25	0.026336
P24369	*Ppib*	-0.25	0.045665
Q9CPX7	*Mrps16*	-0.25	0.034833
Q5SWU9	*Acaca*	-0.25	0.024478
Q7TQ95	*Lnpk*	-0.25	0.022505
P61022	*Chp1*	-0.24	0.040131
Q8CI95	*Osbpl11*	-0.24	0.017730
Q8BFR4	*Gns*	-0.24	0.021480
Q9QXZ0	*Macf1*	-0.24	0.021557
Q8K0C4	*Cyp51a1*	-0.24	0.021957
P35979	*Rpl12*	-0.24	0.026879
Q8BG15	*Ctdspl2*	-0.24	0.032847
Q5SF07	*Igf2bp2*	-0.24	0.023195
Q8R4R6	*Nup35*	-0.24	0.040488
Q8BQ47	*Cnpy4*	-0.24	0.026821
Q91ZW3	*Smarca5*	-0.24	0.025173
Q9D404	*Oxsm*	-0.24	0.035820
Q91WC0	*Setd3*	-0.23	0.041627
O08709	*Prdx6*	-0.23	0.038066
Q60668	*Hnrnpd*	-0.23	0.037053
Q70FJ1	*Akap9*	-0.23	0.034020
Q91YP2	*Nln*	-0.23	0.018615
P83882	*Rpl36a*	-0.23	0.032311
Q8JZR0	*Acsl5*	-0.23	0.027699
Q91WN1	*Dnajc9*	-0.23	0.026200
P97742	*Cpt1a*	-0.23	0.028539
Q6PGH1	*Bud31*	-0.23	0.035807
Q9CZD3	*Gars1*	-0.22	0.041509
P70271	*Pdlim4*	-0.22	0.047445
Q811U4	*Mfn1*	-0.22	0.028318
P16332	*Mmut*	-0.22	0.030416
Q64521	*Gpd2*	-0.22	0.021698
P62242	*Rps8*	-0.22	0.024917
P14685	*Psmd3*	-0.22	0.027710
Q8VE99	*Ccdc115*	-0.22	0.035924
P51660	*Hsd17b4*	-0.22	0.028049
Q62261	*Sptbn1*	-0.21	0.026306
O55234	*Psmb5*	-0.21	0.045631
P12970	*Rpl7a*	-0.21	0.046421
Q6PFD9	*Nup98*	-0.21	0.029691
P61164	*Actr1a*	-0.20	0.038570

UniProt ID	Genes	FC [log2]	q-value
Q9DBG3	*Ap2b1*	-0.20	0.027134
Q91VR5	*Ddx1*	-0.20	0.040721
Q8C407	*Yipf4*	-0.20	0.047820
Q99PU8	*Dhx30*	-0.20	0.032436
Q99LC9	*Pex6*	-0.20	0.046117
Q62095	*Ddx3y*	-0.19	0.047089
Q8JZN7	*Rhot2*	-0.19	0.048415
Q9QZW0	*Atp11c*	-0.19	0.045768
Q8K297	*Colgalt1*	-0.19	0.045890
Q80X90	*Flnb*	-0.19	0.046868
P37040	*Por*	-0.18	0.043104
P62274	*Rps29*	0.19	0.046546
E9Q634	*Myo1e*	0.19	0.047196
Q8K4Q8	*Colec12*	0.19	0.047010
Q9R0E1	*Plod3*	0.19	0.034628
Q3UW53	*Niban1*	0.19	0.043772
Q9Z2W0	*Dnpep*	0.19	0.047210
Q60875	*Arhgef2*	0.20	0.045115
Q9D1J3	*Sarnp*	0.20	0.037554
P28352	*Apex1*	0.20	0.047192
P31324	*Prkar2b*	0.21	0.036390
Q8VEK3	*Hnrnpu*	0.21	0.040037
Q8CGY8	*Ogt*	0.21	0.046160
P46935	*Nedd4*	0.21	0.043440
Q9JM14	*Nt5c*	0.21	0.048680
Q9JK81	*Myg1*	0.21	0.029011
Q99MN1	*Kars1*	0.21	0.028089
P28474	*Adh5*	0.22	0.049506
O08583	*Alyref*	0.22	0.047152
P49717	*Mcm4*	0.22	0.032323
P61226	*Rap2b*	0.22	0.034862
P35922	*Fmr1*	0.22	0.030532
Q8CCB4	*Vps53*	0.22	0.036171
Q9DAK9	*Phpt1*	0.22	0.039737
O89001	*Cpd*	0.22	0.036763
A2AT37	*Upf2*	0.22	0.027975
Q9JHR7	*Ide*	0.22	0.031959
Q8BZ98	*Dnm3*	0.22	0.034686
P17182	*Eno1*	0.22	0.035173
O54998	*Fkbp7*	0.22	0.040609
A2AWA9	*Rabgap1*	0.22	0.024265
Q6PGG2	*Gmip*	0.22	0.026889
P97434	*Mprip*	0.22	0.028419
Q1HFZ0	*Nsun2*	0.22	0.045410
Q91YT8	*Tmem63a*	0.22	0.043023
Q9CZX7	*Pip4p2*	0.22	0.034623

UniProt ID	Genes	FC [log2]	q-value
P07901	*Hsp90aa1*	0.22	0.028265
Q4VA53	*Pds5b*	0.23	0.046241
Q8VE10	*Naa40*	0.23	0.044478
Q60854	*Serpinb6*	0.23	0.041373
P97471	*Smad4*	0.23	0.047712
Q6PGB6	*Naa50*	0.23	0.031499
Q501J7	*Phactr4*	0.23	0.048063
O35465	*Fkbp8*	0.23	0.022442
P20060	*Hexb*	0.23	0.028397
P70227	*Itpr3*	0.23	0.022452
Q9JIX0	*Eny2*	0.23	0.025067
Q62371	*Ddr2*	0.23	0.033076
Q5XF89	*Atp13a3*	0.23	0.021254
P68368	*Tuba4a*	0.23	0.047602
Q99KY4	*Gak*	0.23	0.036182
Q5U4D8	*Slc5a6*	0.23	0.042955
P52760	*Rida*	0.23	0.048838
Q8CFD4	*Snx8*	0.23	0.021184
O09131	*Gsto1*	0.24	0.025736
Q6PE01	*Snrnp40*	0.24	0.020762
Q9DCI9	*Mrpl32*	0.24	0.044607
Q9CR89	*Ergic2*	0.24	0.018168
P99026	*Psmb4*	0.24	0.040156
O88487	*Dync1i2*	0.24	0.020599
Q8K3H0	*Appl1*	0.24	0.021537
Q8BVU0	*Lrch3*	0.24	0.024459
P97315	*Csrp1*	0.24	0.031480
P46460	*Nsf*	0.24	0.015239
Q9JLB2	*Pals1*	0.24	0.024142
Q62422	*Ostf1*	0.24	0.026441
Q62446	*Fkbp3*	0.24	0.025132
P61202	*Cops2*	0.24	0.022053
Q80Z96	*Vangl1*	0.24	0.047488
Q9CYL5	*Glipr2*	0.24	0.019444
P55194	*Sh3bp1*	0.24	0.027119
P10493	*Nid1*	0.24	0.023249
P28798	*Grn*	0.24	0.031891
Q8BP48	*Metap1*	0.24	0.017370
Q3UMF0	*Cobll1*	0.24	0.023343
Q9R0P5	*Dstn*	0.24	0.028182
P11103	*Parp1*	0.25	0.025200
Q9D8B3	*Chmp4b*	0.25	0.046309
P52432	*Polr1c*	0.25	0.022581
A2BH40	*Arid1a*	0.25	0.040612
Q9D662	*Sec23b*	0.25	0.019457
Q61210	*Arhgef1*	0.25	0.021548

UniProt ID	Genes	FC [log2]	q-value
P56812	*Pdcd5*	0.25	0.015328
A2APB8	*Tpx2*	0.25	0.017691
P41216	*Acsl1*	0.25	0.020071
Q640N2	*Arl13b*	0.25	0.043588
Q6KAR6	*Exoc3*	0.25	0.028038
P29533	*Vcam1*	0.25	0.021538
Q99MR3	*Slc12a9*	0.25	0.025701
P97348	*Rhod*	0.25	0.027926
O88685	*Psmc3*	0.25	0.032424
Q99LC8	*Eif2b1*	0.25	0.026907
Q9WVG6	*Carm1*	0.25	0.017699
Q3THS6	*Mat2a*	0.25	0.021680
Q00262	*Stx2*	0.25	0.048883
Q9JMA1	*Usp14*	0.26	0.026627
P02468	*Lamc1*	0.26	0.021528
Q9Z2X1	*Hnrnpf*	0.26	0.018935
Q9D2Y4	*Mlkl*	0.26	0.021698
O70293	*Grk6*	0.26	0.025986
Q7M759	*Abhd17b*	0.26	0.028489
Q8BT60	*Cpne3*	0.26	0.016210
P32233	*Drg1*	0.26	0.016663
Q9D4H1	*Exoc2*	0.26	0.018366
Q69ZZ9	*Macf1*	0.26	0.021948
Q640N1	*Aebp1*	0.26	0.026688
Q91WQ3	*Yars1*	0.26	0.020136
Q810D6	*Grwd1*	0.26	0.025163
Q6A0A9	*FAM120A*	0.26	0.026910
Q8BWZ3	*Naa25*	0.26	0.020126
Q64324	*Stxbp2*	0.26	0.013492
Q3UIA2	*Arhgap17*	0.26	0.012732
Q9ET22	*Dpp7*	0.26	0.013344
Q8CI51	*Pdlim5*	0.26	0.013519
P40124	*Cap1*	0.27	0.017723
P58771	*Tpm1*	0.27	0.014885
P62754	*Rps6*	0.27	0.043066
Q9D0B0	*Srsf9*	0.27	0.023747
Q61703	*Itih2*	0.27	0.019452
Q99LX0	*Park7*	0.27	0.041468
Q99M31	*Hspa14*	0.27	0.015377
Q9EQK5	*Mvp*	0.27	0.014581
P60766	*Cdc42*	0.27	0.023516
P23116	*Eif3a*	0.27	0.016780
F8VPK0	*Skic3*	0.27	0.015111
Q8BRN9	*Cc2d1b*	0.27	0.028408
Q91Z67	*Srgap2*	0.28	0.017185
Q8BGT1	*Flrt3*	0.28	0.034326

UniProt ID	Genes	FC [log2]	q-value
Q9D0M1	*Prpsap1*	0.28	0.020120
Q810B6	*Ankfy1*	0.28	0.009859
Q9CWJ9	*Atic*	0.28	0.008994
Q99LN9	*Dohh*	0.28	0.011608
P51859	*Hdgf*	0.28	0.011873
Q61490	*Alcam*	0.28	0.021088
Q9D2R0	*Aacs*	0.28	0.015339
Q9R1Z8	*Sorbs3*	0.28	0.017197
Q8BGR6	*Arl15*	0.28	0.013303
Q8R1A4	*Dock7*	0.28	0.010346
Q6P6L0	*Filip1l*	0.28	0.015334
Q8VCH8	*Ubxn4*	0.28	0.033204
Q6ZWX6	*Eif2s1*	0.28	0.020128
Q3TVI8	*Pbxip1*	0.28	0.011717
E9Q5C9	*Nolc1*	0.28	0.011848
Q9CX34	*Sugt1*	0.28	0.021706
P23780	*Glb1*	0.28	0.014820
Q8VHK9	*Dhx36*	0.28	0.014284
Q8C129	*Lnpep*	0.28	0.011631
Q9D7X3	*Dusp3*	0.28	0.013463
Q05920	*Pc*	0.29	0.009695
Q78PY7	*Snd1*	0.29	0.010492
Q9DBS9	*Osbpl3*	0.29	0.012351
O70309	*Itgb5*	0.29	0.009152
Q9CY66	*Gar1*	0.29	0.018958
Q9WV68	*Decr2*	0.29	0.023898
Q5KU39	*Vps41*	0.29	0.015762
Q00PI9	*Hnrnpul2*	0.29	0.018303
Q9CW03	*Smc3*	0.29	0.022063
Q9Z1X4	*Ilf3*	0.29	0.013195
Q61584	*Fxr1*	0.29	0.012257
O88532	*Zfr*	0.29	0.028297
Q9ERB0	*Snap29*	0.29	0.008905
Q3UVL4	*Vps51*	0.29	0.017859
Q68FL4	*Ahcyl2*	0.29	0.018786
Q9CXW3	*Cacybp*	0.29	0.010874
Q8CIB5	*Fermt2*	0.29	0.009485
O08808	*Diaph1*	0.29	0.010238
Q91V41	*Rab14*	0.29	0.010418
O88543	*Cops3*	0.29	0.013184
P61979	*Hnrnpk*	0.29	0.009094
P68510	*Ywhah*	0.29	0.014590
P97429	*Anxa4*	0.30	0.009802
Q8VE70	*Pdcd10*	0.30	0.023961
P55937	*Golga3*	0.30	0.015014
Q64727	*Vcl*	0.30	0.024469

UniProt ID	Genes	FC [log2]	q-value
P22777	*Serpine1*	0.30	0.011867
Q3V0J1	*Tmem237*	0.30	0.021547
P25976	*Ubtf*	0.30	0.009197
Q3UU96	*Cdc42bpa*	0.30	0.011500
P20664	*Prim1*	0.30	0.025869
Q9Z0L0	*Tpbg*	0.30	0.011065
Q60737	*Csnk2a1*	0.30	0.007419
P70336	*Rock2*	0.30	0.008836
Q7TPC1	*Cdsn*	0.30	0.017156
Q7TT50	*Cdc42bpb*	0.30	0.008612
P07091	*S100a4*	0.30	0.012089
Q61035	*Hars1*	0.30	0.011700
P54276	*Msh6*	0.30	0.010883
Q61879	*Myh10*	0.30	0.006866
P97384	*Anxa11*	0.30	0.012074
Q99PG2	*Ogfr*	0.31	0.008222
Q3UPH7	*Arhgef40*	0.31	0.010392
Q6ZQ88	*Kdm1a*	0.31	0.028158
Q9WV60	*Gsk3b*	0.31	0.013456
Q9CPX6	*Atg3*	0.31	0.011569
Q6PA06	*Atl2*	0.31	0.012436
Q921Q7	*Rin1*	0.31	0.010466
P48759	*Ptx3*	0.31	0.046394
P06745	*Gpi*	0.31	0.009079
Q9R0Y5	*Ak1*	0.31	0.009797
O09159	*Man2b1*	0.31	0.008094
P07724	*Alb*	0.31	0.026415
Q9R0B9	*Plod2*	0.31	0.014219
P55258	*Rab8a*	0.31	0.036442
Q9EPL0	*Xylt2*	0.31	0.010703
Q6AW69	*Cgnl1*	0.31	0.030639
Q9CWZ7	*Napg*	0.31	0.007857
Q6PAM1	*Txlna*	0.31	0.021530
Q9R0L6	*Pcm1*	0.31	0.048176
Q99KH8	*Stk24*	0.31	0.007197
P62313	*Lsm6*	0.31	0.011060
Q9EPU0	*Upf1*	0.31	0.005946
Q811D0	*Dlg1*	0.31	0.010729
P62874	*Gnb1*	0.31	0.011481
Q8C7R4	*Uba6*	0.31	0.016669
Q9CQE7	*Ergic3*	0.32	0.028478
Q8VH51	*Rbm39*	0.32	0.006793
Q3V1L4	*Nt5c2*	0.32	0.010193
P98083	*Shc1*	0.32	0.017260
P50247	*Ahcy*	0.32	0.013189
Q8CCN5	*Bcas3*	0.32	0.014076

UniProt ID	Genes	FC [log2]	q-value
P0C0A3	*Chmp6*	0.32	0.021627
Q8BUR4	*Dock1*	0.32	0.011468
P24547	*Impdh2*	0.32	0.005565
Q9Z130	*Hnrnpdl*	0.32	0.012042
Q63850	*Nup62*	0.32	0.039407
B2RXC1	*Trappc11*	0.32	0.020754
F6ZDS4	*Tpr*	0.32	0.012084
Q99LD4	*Gps1*	0.32	0.018651
Q3TPX4	*Exoc5*	0.32	0.007316
Q8VCT3	*Rnpep*	0.32	0.012035
Q9EQC5	*Scyl1*	0.32	0.013188
P10711	*Tcea1*	0.32	0.033267
Q6Q477	*Atp2b4*	0.32	0.012270
Q64737	*Gart*	0.32	0.006488
Q8BVI4	*Qdpr*	0.32	0.026405
Q8BG81	*Poldip3*	0.32	0.008658
Q9JII6	*Akr1a1*	0.32	0.005882
Q8K2Z4	*Ncapd2*	0.32	0.004735
Q99LJ0	*Cttnbp2nl*	0.32	0.009235
Q6PGC1	*Dhx29*	0.32	0.013486
G5E870	*Trip12*	0.32	0.006110
Q11011	*Npepps*	0.32	0.004278
Q8BTW3	*Exosc6*	0.33	0.022628
P70257	*Nfix*	0.33	0.008072
Q9Z1G3	*Atp6v1c1*	0.33	0.004273
O35691	*Pnn*	0.33	0.009690
Q9EQH2	*Erap1*	0.33	0.011928
Q8C1B7	*Septin11*	0.33	0.006796
Q60847	*Col12a1*	0.33	0.004996
O88545	*Cops6*	0.33	0.013480
Q9JLQ0	*Cd2ap*	0.33	0.005922
P21107	*Tpm3*	0.33	0.005880
Q9CWS0	*Ddah1*	0.33	0.007768
Q9Z0R4	*Itsn1*	0.33	0.017714
O35657	*Neu1*	0.33	0.011436
Q61655	*Ddx19a*	0.33	0.012263
Q9Z1T1	*Ap3b1*	0.33	0.004480
Q99M28	*Rnps1*	0.33	0.036147
Q91WM3	*Rrp9*	0.33	0.010776
Q9DCR2	*Ap3s1*	0.33	0.008633
Q9ESX5	*Dkc1*	0.33	0.011125
P53995	*Anapc1*	0.33	0.017684
Q8BJY1	*Psmd5*	0.33	0.004334
Q3U0V1	*Khsrp*	0.33	0.005925
P70699	*Gaa*	0.33	0.007764
Q8R2T8	*Gtf3c5*	0.33	0.013376

UniProt ID	Genes	FC [log2]	q-value
Q80U72	*Scrib*	0.33	0.003727
P42208	*Septin2*	0.33	0.003897
P02340	*Tp53*	0.33	0.005128
Q6ZQ29	*Taok2*	0.33	0.027886
P61161	*Actr2*	0.33	0.005949
Q91VU0	*Fam3c*	0.33	0.011853
Q8R307	*Vps18*	0.33	0.007953
Q8CF89	*Tab1*	0.33	0.007604
P47964	*Rpl36*	0.34	0.040644
Q00623	*Apoa1*	0.34	0.005035
Q62376	*Snrnp70*	0.34	0.016205
Q571I9	*Aldh16a1*	0.34	0.014646
Q9JKC8	*Ap3m1*	0.34	0.005048
Q8VC85	*Lsm1*	0.34	0.003729
Q7TMQ7	*Wdr91*	0.34	0.006869
Q921W0	*Chmp1a*	0.34	0.040141
P34884	*Mif*	0.34	0.010012
P63085	*Mapk1*	0.34	0.002349
Q8BY89	*Slc44a2*	0.34	0.012899
Q9D1G2	*Pmvk*	0.34	0.004942
Q8BJW6	*Eif2a*	0.34	0.005822
O35250	*Exoc7*	0.34	0.007294
B9EJR8	*Dnaaf5*	0.34	0.027443
Q8BVL3	*Snx17*	0.34	0.005415
O54784	*Dapk3*	0.34	0.005421
P70362	*Ufd1*	0.35	0.010533
P26039	*Tln1*	0.35	0.004495
Q9WTZ1	*Rnf7*	0.35	0.018950
Q8C1Y8	*Ccz1*	0.35	0.006859
Q9CU62	*Smc1a*	0.35	0.002032
Q80U78	*Pum1*	0.35	0.009227
Q9EQH3	*Vps35*	0.35	0.004663
Q3B7Z2	*Osbp*	0.35	0.003958
Q9QZF2	*Gpc1*	0.35	0.004500
Q9Z0G0	*Gipc1*	0.35	0.003254
P15116	*Cdh2*	0.35	0.003165
Q9WVL3	*Slc12a7*	0.35	0.004044
Q60770	*Stxbp3*	0.35	0.003006
Q9CYG7	*Tomm34*	0.35	0.003312
P40336	*Vps26a*	0.36	0.012555
Q8C2E7	*Washc5*	0.36	0.003288
Q6PGH2	*Jpt2*	0.36	0.004558
Q9CQ79	*Txndc9*	0.36	0.007081
Q8VCE9	*Plekhh3*	0.36	0.004493
O88448	*Klc2*	0.36	0.004549
P62983	*Rps27a*	0.36	0.007458

UniProt ID	Genes	FC [log2]	q-value
P62880	*Gnb2*	0.36	0.009306
Q9ES74	*Nek7*	0.36	0.021678
P07607	*Tyms*	0.36	0.005033
Q922J3	*Clip1*	0.36	0.009854
Q2NL51	*Gsk3a*	0.36	0.001744
Q9Z1M8	*Ik*	0.36	0.004668
P63276	*Rps17*	0.36	0.021039
Q6P5F7	*Ttyh3*	0.36	0.004056
Q8BLU0	*Flrt2*	0.36	0.002828
Q9JKY5	*Hip1r*	0.36	0.003149
Q78ZA7	*Nap1l4*	0.36	0.012340
P61924	*Copz1*	0.36	0.001956
Q9R0E2	*Plod1*	0.36	0.001654
Q7TNC4	*Luc7l2*	0.37	0.003310
P63321	*Rala*	0.37	0.003361
Q8JZZ7	*Adgrl2*	0.37	0.006535
B1AY13	*Usp24*	0.37	0.004093
O35295	*Purb*	0.37	0.010573
Q8CHT3	*Ints5*	0.37	0.013362
Q61543	*Glg1*	0.37	0.001974
P26041	*Msn*	0.37	0.013088
Q8K0B2	*Lmbrd1*	0.37	0.014891
P36916	*Gnl1*	0.37	0.004075
Q9D281	*Fam114a1*	0.37	0.002797
P63028	*Tpt1*	0.37	0.016000
O35075	*Vps26c*	0.37	0.009863
Q8K2J0	*Plcd3*	0.37	0.004033
Q99KP6	*Prpf19*	0.37	0.002011
Q920B9	*Supt16h*	0.37	0.006522
Q62074	*Prkci*	0.37	0.002217
Q05793	*Hspg2*	0.37	0.001361
Q9DBU0	*Tm9sf1*	0.37	0.005109
P35285	*Rab22a*	0.37	0.007029
Q6PFR5	*Tra2a*	0.37	0.011421
Q99LL5	*Pwp1*	0.37	0.001451
Q921E2	*Rab31*	0.37	0.018212
P18760	*Cfl1*	0.37	0.007308
Q6IRU5	*Cltb*	0.37	0.006525
Q9CZX0	*Elp3*	0.37	0.001455
Q61191	*Hcfc1*	0.37	0.001360
Q9WUM4	*Coro1c*	0.37	0.002974
Q3UJB9	*Edc4*	0.37	0.001607
Q9D2N9	*Vps33a*	0.37	0.003420
Q6P8I4	*Pcnp*	0.37	0.010878
Q501J6	*Ddx17*	0.37	0.001833
Q921H8	*Acaa1a*	0.38	0.025161

UniProt ID	Genes	FC [log2]	q-value
P62137	*Ppp1ca*	0.38	0.003257
Q9D832	*Dnajb4*	0.38	0.015197
Q8BHL5	*Elmo2*	0.38	0.002827
Q9Z1G4	*Atp6v0a1*	0.38	0.003127
Q60790	*Rasa3*	0.38	0.001952
Q8K4Z5	*Sf3a1*	0.38	0.004425
O70589	*Cask*	0.38	0.001146
Q9JMG1	*Edf1*	0.38	0.005131
P07214	*Sparc*	0.38	0.004300
P19096	*Fasn*	0.38	0.001838
Q6P1F6	*Ppp2r2a*	0.38	0.012304
Q9DCD0	*Pgd*	0.38	0.002029
Q9DCH4	*Eif3f*	0.38	0.003170
Q9D1M0	*Sec13*	0.38	0.009014
Q80XR2	*Atp2c1*	0.38	0.010320
Q8CIE6	*Copa*	0.38	0.001477
B1AVY7	*Kif16b*	0.38	0.003895
Q9QZ06	*Tollip*	0.38	0.002397
P14152	*Mdh1*	0.38	0.003977
P62309	*Snrpg*	0.38	0.015322
Q99MI1	*Erc1*	0.38	0.008289
P47753	*Capza1*	0.38	0.003124
Q99JB8	*Pacsin3*	0.38	0.003025
Q06138	*Cab39*	0.38	0.002799
P25206	*Mcm3*	0.39	0.001836
Q99JR8	*Smarcd2*	0.39	0.005902
Q9DBY1	*Syvn1*	0.39	0.012249
Q9QZB7	*Actr10*	0.39	0.005406
Q8C8U0	*Ppfibp1*	0.39	0.013474
Q9WUD1	*Stub1*	0.39	0.004693
Q9D0R4	*Ddx56*	0.39	0.004553
O08784	*Tcof1*	0.39	0.011495
Q9ESZ8	*Gtf2i*	0.39	0.002252
Q8CFQ3	*Aqr*	0.39	0.008312
Q924M7	*Mpi*	0.39	0.003705
Q6IRU2	*Tpm4*	0.39	0.012339
P58802	*Tbc1d10a*	0.39	0.004556
Q8VDZ4	*Zdhhc5*	0.39	0.002404
Q8CG47	*Smc4*	0.39	0.001475
Q99J45	*Nrbp1*	0.40	0.007204
P14094	*Atp1b1*	0.40	0.008788
O08579	*Emd*	0.40	0.002033
Q3UQ28	*Pxdn*	0.40	0.001657
Q61206	*Pafah1b2*	0.40	0.001743
P67871	*Csnk2b*	0.40	0.003147
O89051	*Itm2b*	0.40	0.007629

UniProt ID	Genes	FC [log2]	q-value
Q8K2T1	*Nmral1*	0.40	0.004029
Q05D44	*Eif5b*	0.40	0.001255
Q9ERK4	*Cse1l*	0.40	0.011603
Q9EPK2	*Rp2*	0.40	0.004560
P54754	*Ephb3*	0.40	0.002371
Q8K1N2	*Phldb2*	0.40	0.011722
P26369	*U2af2*	0.40	0.002138
Q91YR7	*Prpf6*	0.40	0.001660
Q62136	*Ptpn21*	0.40	0.004031
P26043	*Rdx*	0.40	0.007035
Q01853	*Vcp*	0.40	0.003396
O55106	*Strn*	0.40	0.003189
Q62470	*Itga3*	0.41	0.000999
Q9ER00	*Stx12*	0.41	0.012069
Q69ZN7	*Myof*	0.41	0.000974
Q61239	*Fnta*	0.41	0.019052
Q9D1M4	*Eef1e1*	0.41	0.025913
Q80Y17	*Llgl1*	0.41	0.000950
Q99KN9	*Clint1*	0.41	0.007843
Q6PDH0	*Phldb1*	0.41	0.001391
Q61686	*Cbx5*	0.41	0.013473
Q60838	*Dvl2*	0.41	0.013355
Q569Z6	*Thrap3*	0.41	0.001140
Q61103	*Dpf2*	0.41	0.009239
Q9D1K2	*Atp6v1f*	0.41	0.008651
Q9Z160	*Cog1*	0.42	0.001652
O88544	*Cops4*	0.42	0.004546
O70591	*Pfdn2*	0.42	0.001839
Q8BX70	*Vps13c*	0.42	0.001355
Q8R060	*Zwilch*	0.42	0.010212
P27546	*Map4*	0.42	0.016216
P23591	*Gfus*	0.42	0.006538
Q07076	*Anxa7*	0.42	0.003290
Q99NB9	*Sf3b1*	0.42	0.001098
Q3USZ8	*Dipk2a*	0.42	0.026597
Q920E5	*Fdps*	0.42	0.001365
Q9Z0P4	*Palm*	0.42	0.001359
Q9Z1Q9	*Vars1*	0.42	0.001117
P50431	*Shmt1*	0.42	0.001143
O70194	*Eif3d*	0.42	0.000894
Q7TSC1	*Prrc2a*	0.42	0.001957
P40142	*Tkt*	0.42	0.001367
Q9DAW6	*Prpf4*	0.42	0.001109
Q99KB8	*Hagh*	0.42	0.009444
Q9D0R8	*Lsm12*	0.42	0.001509
P70297	*Stam*	0.42	0.002973

UniProt ID	Genes	FC [log2]	q-value
Q9Z2N8	*Actl6a*	0.42	0.001511
Q8CGB3	*Uaca*	0.42	0.001363
Q8CIV8	*Tbce*	0.42	0.023352
Q8CBY8	*Dctn4*	0.42	0.002770
B2RY56	*Rbm25*	0.42	0.003539
P98203	*Arvcf*	0.42	0.004849
Q8C3Y4	*Kntc1*	0.43	0.012244
P60229	*Eif3e*	0.43	0.001256
Q9D1C8	*Vps28*	0.43	0.001158
Q9Z2Q6	*Septin5*	0.43	0.000900
Q6PB44	*Ptpn23*	0.43	0.005030
Q8BIQ5	*Cstf2*	0.43	0.001153
Q9Z0S1	*Bpnt1*	0.43	0.001449
Q9CSN1	*Snw1*	0.43	0.000839
P11440	*Cdk1*	0.43	0.001192
Q99JR5	*Tinagl1*	0.43	0.004567
Q3U2P1	*Sec24a*	0.43	0.006872
Q9WUL7	*Arl3*	0.43	0.001360
P05064	*Aldoa*	0.43	0.001261
Q80WQ2	*Vac14*	0.43	0.012344
Q99J62	*Rfc4*	0.43	0.003707
Q9EP71	*Rai14*	0.43	0.000879
Q8C561	*Lmbrd2*	0.43	0.004562
Q9D287	*Bcas2*	0.43	0.001636
Q61699	*Hsph1*	0.43	0.000995
Q61656	*Ddx5*	0.44	0.000836
Q5SUR0	*Pfas*	0.44	0.001977
Q64449	*Mrc2*	0.44	0.000835
Q99KD5	*Unc45a*	0.44	0.000896
Q8BHL3	*Tbc1d10b*	0.44	0.011641
Q07832	*Plk1*	0.44	0.001031
Q8BMA6	*Srp68*	0.44	0.010409
Q9D7G0	*Prps1*	0.44	0.002524
Q8BX02	*Kank2*	0.44	0.000885
B2RY04	*Dock5*	0.44	0.002662
P61514	*Rpl37a*	0.44	0.017383
Q9D1G1	*Rab1b*	0.44	0.004839
Q9QZD9	*Eif3i*	0.44	0.000902
Q922S8	*Kif2c*	0.44	0.001163
Q9QYC7	*Ggcx*	0.44	0.001710
P99024	*Tubb5*	0.44	0.001105
Q9D7B7	*Gpx8*	0.44	0.000846
P70335	*Rock1*	0.44	0.001119
Q8CIN4	*Pak2*	0.44	0.001095
Q00993	*Axl*	0.44	0.001095
A2AR02	*Ppig*	0.44	0.001506

UniProt ID	Genes	FC [log2]	q-value
P57724	*Pcbp4*	0.44	0.006532
Q6PGF7	*Exoc8*	0.45	0.001108
Q91VH2	*Snx9*	0.45	0.001368
Q8CGU1	*Calcoco1*	0.45	0.014575
Q6P9R1	*Ddx51*	0.45	0.030682
Q8BRT1	*Clasp2*	0.45	0.005596
P35585	*Ap1m1*	0.45	0.000869
P46662	*Nf2*	0.45	0.024979
A6X935	*Itih4*	0.45	0.017729
Q922V4	*Plrg1*	0.45	0.002322
Q91YE6	*Ipo9*	0.45	0.003329
Q9DCL9	*Paics*	0.45	0.001082
Q5SNZ0	*Ccdc88a*	0.45	0.008806
Q01279	*Egfr*	0.45	0.002030
Q8BH57	*Wdr48*	0.45	0.001155
P47811	*Mapk14*	0.45	0.015370
P39749	*Fen1*	0.45	0.000994
Q99J77	*Nans*	0.45	0.000904
Q9EQQ9	*Oga*	0.45	0.005799
P97496	*Smarcc1*	0.46	0.000836
Q5FWI3	*Cemip2*	0.46	0.000842
P11688	*Itga5*	0.46	0.000748
Q9Z0R6	*Itsn2*	0.46	0.013476
Q922Y1	*Ubxn1*	0.46	0.000867
P50429	*Arsb*	0.46	0.000894
Q9Z1R2	*Bag6*	0.46	0.000865
Q8C166	*Cpne1*	0.46	0.000973
O55023	*Impa1*	0.46	0.000755
Q8VDN2	*Atp1a1*	0.46	0.000823
O54988	*Slk*	0.46	0.000905
Q61090	*Fzd7*	0.46	0.001160
Q3UMB9	*Washc4*	0.46	0.000741
Q9JIH2	*Nup50*	0.46	0.001837
Q60749	*Khdrbs1*	0.46	0.021295
P08074	*Cbr2*	0.46	0.006954
P70168	*Kpnb1*	0.46	0.001655
P20352	*F3*	0.46	0.001164
Q9Z2A0	*Pdpk1*	0.46	0.005038
Q61550	*Rad21*	0.46	0.001159
O88811	*Stam2*	0.46	0.000985
P60335	*Pcbp1*	0.46	0.001953
P50428	*Arsa*	0.46	0.000947
Q6PAR5	*Gapvd1*	0.47	0.000821
P24860	*Ccnb1*	0.47	0.003129
O08788	*Dctn1*	0.47	0.000736
P27601	*Gna13*	0.47	0.000843

UniProt ID	Genes	FC [log2]	q-value
Q920L1	*Fads1*	0.47	0.000820
Q8BH69	*Sephs1*	0.47	0.001087
Q9CQ43	*Dut*	0.47	0.002137
P56212	*Arpp19*	0.47	0.000952
P34022	*Ranbp1*	0.47	0.000694
P26883	*Fkbp1a*	0.47	0.006485
P70296	*Pebp1*	0.47	0.001099
O35405	*Pld3*	0.47	0.001106
Q8BGT6	*Micall1*	0.47	0.002181
P26638	*Sars1*	0.47	0.000860
Q61753	*Phgdh*	0.47	0.000561
A2AAE1	*Bltp1*	0.47	0.047275
O54916	*Reps1*	0.47	0.006478
Q9CYI4	*Luc7l*	0.48	0.001262
P00375	*Dhfr*	0.48	0.000732
Q9WVA3	*Bub3*	0.48	0.000981
P97393	*Arhgap5*	0.48	0.001254
Q8K2P7	*Slc38a1*	0.48	0.034560
Q6P069	*Sri*	0.48	0.001088
Q5DTX6	*Jcad*	0.48	0.004054
Q8VD65	*Pik3r4*	0.48	0.000969
Q9DBC7	*Prkar1a*	0.48	0.000908
Q922H4	*Gmppa*	0.48	0.001394
Q8CHG3	*Gcc2*	0.48	0.003168
Q80U49	*Cep170b*	0.48	0.012345
B2RXS4	*Plxnb2*	0.48	0.000560
P50518	*Atp6v1e1*	0.48	0.004423
G3X8U3	*QNG1*	0.48	0.008394
Q8BRV5	*Kiaa1671*	0.48	0.004118
Q3UDE2	*Ttll12*	0.48	0.000750
Q6NZC7	*Sec23ip*	0.48	0.001142
A2AGT5	*Ckap5*	0.48	0.000382
Q62356	*Fstl1*	0.48	0.001454
Q9ER72	*Cars1*	0.49	0.000685
Q60865	*Caprin1*	0.49	0.000880
Q5XJY5	*Arcn1*	0.49	0.000616
Q9CW46	*Raver1*	0.49	0.000873
Q91ZU6	*Dst*	0.49	0.004588
O54984	*Get3*	0.49	0.000656
O70318	*Epb41l2*	0.49	0.000996
Q9JIW9	*Ralb*	0.49	0.001089
Q9CZ30	*Ola1*	0.49	0.000860
Q8BJU0	*Sgta*	0.49	0.000837
O55128	*Sap18*	0.49	0.000654
Q9WVD4	*Clcn5*	0.49	0.005509
Q8VE97	*Srsf4*	0.49	0.025837

UniProt ID	Genes	FC [log2]	q-value
P97855	*G3bp1*	0.49	0.001606
P49025	*Cit*	0.49	0.000891
Q4VAA2	*Cdv3*	0.49	0.000997
Q05512	*Mark2*	0.49	0.002185
Q9D0T1	*Snu13*	0.49	0.000840
P62307	*Snrpf*	0.49	0.005919
Q9Z1F9	*Uba2*	0.49	0.005418
P97797	*Sirpa*	0.49	0.000897
P59325	*Eif5*	0.50	0.000613
Q8CH72	*Trim32*	0.50	0.000894
Q80U35	*Arhgef17*	0.50	0.000834
Q60692	*Psmb6*	0.50	0.000907
O54941	*Smarce1*	0.50	0.000971
Q9CY64	*Blvra*	0.50	0.000893
Q8K124	*Plekho2*	0.50	0.000539
Q91WC9	*Daglb*	0.50	0.000883
P49718	*Mcm5*	0.50	0.001001
Q64213	*Sf1*	0.50	0.002368
Q03963	*Eif2ak2*	0.50	0.000686
Q9QYB1	*Clic4*	0.50	0.003853
Q8K019	*Bclaf1*	0.50	0.000906
Q3UGS4	*Mcrip1*	0.50	0.000457
A2AF47	*Dock11*	0.50	0.000554
Q9R1C7	*Prpf40a*	0.50	0.007100
A2A7S8	*Kiaa1522*	0.50	0.001662
P70398	*Usp9x*	0.50	0.000877
P97287	*Mcl1*	0.51	0.010622
Q9JHJ0	*Tmod3*	0.51	0.000537
O88746	*Tom1*	0.51	0.000651
Q4PZA2	*Ece1*	0.51	0.000843
O08600	*Endog*	0.51	0.001005
Q9CQI3	*Gmfb*	0.51	0.000757
Q9WUM3	*Coro1b*	0.51	0.000744
Q921M7	*Cyrib*	0.51	0.001510
Q8VC70	*Rbms2*	0.51	0.000741
Q3THK7	*Gmps*	0.51	0.000534
P22935	*Crabp2*	0.51	0.003261
Q6PDM2	*Srsf1*	0.51	0.000501
Q3TJD7	*Pdlim7*	0.51	0.000949
Q8BTH8	*Csnk1g1*	0.51	0.000615
Q02053	*Uba1*	0.51	0.000534
P62814	*Atp6v1b2*	0.51	0.000514
Q8BVE3	*Atp6v1h*	0.51	0.000546
Q61881	*Mcm7*	0.52	0.000553
Q7TMY8	*Huwe1*	0.52	0.000558
Q9CQ73	*Pkp2*	0.52	0.000859

UniProt ID	Genes	FC [log2]	q-value
Q91YI4	*Arrb2*	0.52	0.000618
Q8CJ53	*Trip10*	0.52	0.001122
Q8C0M0	*Wdr59*	0.52	0.017907
Q6P8X1	*Snx6*	0.52	0.000509
Q921F4	*Hnrnpll*	0.52	0.013177
Q9Z1Z2	*Strap*	0.52	0.000655
P50516	*Atp6v1a*	0.52	0.000512
Q8CES0	*Naa30*	0.52	0.009035
Q9D8X2	*Ccdc124*	0.52	0.000851
P97314	*Csrp2*	0.52	0.000749
Q64331	*Myo6*	0.52	0.000756
O70492	*Snx3*	0.52	0.000533
P62141	*Ppp1cb*	0.53	0.002180
Q571E4	*Galns*	0.53	0.000454
O88502	*Pde8a*	0.53	0.000559
P62484	*Abi2*	0.53	0.000851
P27661	*H2ax*	0.53	0.004591
Q01320	*Top2a*	0.53	0.000496
P63001	*Rac1*	0.53	0.006885
Q76LS9	*Mindy1*	0.53	0.001958
O55222	*Ilk*	0.53	0.000902
Q9JK48	*Sh3glb1*	0.53	0.000396
P12367	*Prkar2a*	0.53	0.000532
Q64430	*Atp7a*	0.53	0.000852
Q8R1F1	*Niban2*	0.53	0.000254
Q8VDC1	*Fyco1*	0.53	0.000975
Q9CQT1	*Mri1*	0.53	0.001116
Q61235	*Sntb2*	0.53	0.000381
P33174	*Kif4*	0.53	0.000557
P35123	*Usp4*	0.53	0.000852
Q6P1B1	*Xpnpep1*	0.54	0.000506
P17918	*Pcna*	0.54	0.000504
Q9EPJ9	*Arfgap1*	0.54	0.000553
Q9D5V5	*Cul5*	0.54	0.000387
P32883	*Kras*	0.54	0.013175
Q8C0E2	*Vps26b*	0.54	0.000977
Q8BGQ7	*Aars1*	0.54	0.000905
Q99K70	*Rragc*	0.54	0.015217
Q920Q4	*Vps16*	0.54	0.000855
Q9CPW4	*Arpc5*	0.54	0.000650
P97465	*Dok1*	0.54	0.000758
O88738	*Birc6*	0.54	0.000563
Q01149	*Col1a2*	0.54	0.000856
O55131	*Septin7*	0.54	0.000535
P24270	*Cat*	0.54	0.000251
P84089	*Erh*	0.54	0.001157

UniProt ID	Genes	FC [log2]	q-value
Q60676	*Ppp5c*	0.54	0.001091
Q3UPF5	*Zc3hav1*	0.55	0.000374
Q8CGE9	*Rgs12*	0.55	0.000953
Q8BTJ4	*Enpp4*	0.55	0.000403
Q9CYZ2	*Tpd52l2*	0.55	0.000947
P56399	*Usp5*	0.55	0.000455
Q9R0G8	*Nrk*	0.55	0.000541
P47857	*Pfkm*	0.55	0.001658
Q8BTI8	*Srrm2*	0.55	0.000868
O35239	*Ptpn9*	0.55	0.000656
Q8VHG2	*Amot*	0.55	0.001358
Q91ZX7	*Lrp1*	0.56	0.000246
Q3UPL0	*Sec31a*	0.56	0.000249
Q8BJ05	*Zc3h14*	0.56	0.017192
Q99NH0	*Ankrd17*	0.56	0.002035
P35601	*Rfc1*	0.56	0.000366
Q9JKX6	*Nudt5*	0.56	0.000980
Q91W86	*Vps11*	0.56	0.000312
O35350	*Capn1*	0.56	0.001165
Q8R3P2	*Dtx2*	0.56	0.000654
Q8BY71	*Hat1*	0.56	0.000389
Q9QUM9	*Psma6*	0.56	0.000392
Q9DBR1	*Xrn2*	0.56	0.000379
Q9WV92	*Epb41l3*	0.56	0.000502
P47757	*Capzb*	0.56	0.000978
O89086	*Rbm3*	0.56	0.000558
Q0GNC1	*Inf2*	0.56	0.000404
Q5EG47	*Prkaa1*	0.57	0.000499
P52480	*Pkm*	0.57	0.000264
P97390	*Vps45*	0.57	0.000745
P28271	*Aco1*	0.57	0.000278
Q00612	*G6pdx*	0.57	0.000507
Q9CQC8	*Spg21*	0.57	0.000386
Q3UH60	*Dip2b*	0.57	0.000511
Q7TMB8	*Cyfip1*	0.57	0.000532
Q3TWN3	*Cnnm2*	0.57	0.000386
P20152	*Vim*	0.57	0.000389
Q8VDU0	*Gpsm2*	0.57	0.000501
P97371	*Psme1*	0.57	0.002034
P97333	*Nrp1*	0.57	0.000381
P97310	*Mcm2*	0.57	0.000544
Q9JLB0	*Pals2*	0.57	0.000273
Q9CQ88	*Tspan31*	0.57	0.011356
Q99KJ8	*Dctn2*	0.57	0.000411
Q6ZQ73	*Cand2*	0.57	0.000737
P24668	*M6pr*	0.57	0.005014

UniProt ID	Genes	FC [log2]	q-value
Q99NH2	*Pard3*	0.57	0.000657
Q9D0N7	*Chaf1b*	0.57	0.000897
Q8CGB6	*Tns2*	0.57	0.000386
Q8C0Z1	*Fam234a*	0.57	0.000235
P63101	*Ywhaz*	0.58	0.001260
Q8BTW9	*Pak4*	0.58	0.000882
Q9ET54	*Palld*	0.58	0.000255
Q8CHI8	*Ep400*	0.58	0.000925
Q99KW3	*Triobp*	0.58	0.000227
Q6Y7W8	*Gigyf2*	0.58	0.000553
Q6ZPE2	*Sbf1*	0.58	0.000392
Q9CR00	*Psmd9*	0.58	0.000410
P11157	*Rrm2*	0.58	0.001111
P39053	*Dnm1*	0.58	0.000372
Q9Z0H1	*Wdr46*	0.58	0.000737
Q9D0F9	*Pgm1*	0.58	0.000400
P28653	*Bgn*	0.58	0.000401
P48722	*Hspa4l*	0.58	0.000273
P45376	*Akr1b1*	0.58	0.000286
Q62193	*Rpa2*	0.58	0.001088
Q6EDY6	*Carmil1*	0.58	0.000275
Q9CW79	*Golga1*	0.58	0.000822
Q9QXE0	*Hacl1*	0.58	0.009905
P28658	*Atxn10*	0.59	0.000869
P35951	*Ldlr*	0.59	0.000370
Q62388	*Atm*	0.59	0.001103
Q3UQN2	*Fcho2*	0.59	0.000551
Q924C6	*Loxl4*	0.59	0.000394
Q9DBJ1	*Pgam1*	0.59	0.000250
P46664	*Adss2*	0.59	0.000248
P54763	*Ephb2*	0.59	0.000393
P15532	*Nme1*	0.59	0.001104
P35831	*Ptpn12*	0.59	0.000833
P17751	*Tpi1*	0.59	0.000265
P52293	*Kpna2*	0.59	0.000403
Q3UE37	*Ube2z*	0.59	0.004025
Q8BQM4	*Heatr3*	0.59	0.004042
Q8BXC6	*Commd2*	0.59	0.000652
Q9Z1N5	*Ddx39b*	0.59	0.001003
Q9WVK4	*Ehd1*	0.59	0.000374
E9Q7G0	*Numa1*	0.59	0.000514
Q91VX2	*Ubap2*	0.60	0.000689
O09172	*Gclm*	0.60	0.000270
Q9D868	*Ppih*	0.60	0.000971
Q9CWK8	*Snx2*	0.60	0.000287
Q9Z2U1	*Psma5*	0.60	0.000271

UniProt ID	Genes	FC [log2]	q-value
Q9D0A3	*Arpin*	0.60	0.000257
Q9JM76	*Arpc3*	0.60	0.001653
Q810A7	*Ddx42*	0.60	0.000649
Q99KQ4	*Nampt*	0.60	0.000407
P08122	*Col4a2*	0.60	0.000550
P13864	*Dnmt1*	0.61	0.000262
Q9DD03	*Rab13*	0.61	0.000616
O09044	*Snap23*	0.61	0.000550
Q9CR39	*Wdr45b*	0.61	0.000503
Q99LB0	*Dnttip1*	0.61	0.043038
P43275	*H1-1*	0.61	0.000227
Q8BH43	*Wasf2*	0.61	0.000263
Q921C5	*Bicd2*	0.61	0.000545
P50543	*S100a11*	0.61	0.000258
Q8BFZ3	*Actbl2*	0.61	0.001745
O88342	*Wdr1*	0.61	0.000241
Q9Z0M5	*Lipa*	0.61	0.000837
P51855	*Gss*	0.61	0.000754
Q99PP7	*Trim33*	0.61	0.000380
P97311	*Mcm6*	0.61	0.000247
Q9Z138	*Ror2*	0.61	0.000397
Q9Z1Y4	*Trip6*	0.61	0.000230
P63037	*Dnaja1*	0.62	0.000383
Q8K4M5	*Commd1*	0.62	0.001452
P06801	*Me1*	0.62	0.000373
Q8BT07	*Cep55*	0.62	0.000375
Q63844	*Mapk3*	0.62	0.000365
Q3TLH4	*Prrc2c*	0.62	0.000402
Q9QYF9	*Ndrg3*	0.62	0.000405
P84104	*Srsf3*	0.62	0.000264
Q9DC50	*Crot*	0.62	0.000276
Q80UG5	*Septin9*	0.62	0.000246
Q60972	*Rbbp4*	0.62	0.000736
Q8C863	*Itch*	0.62	0.000261
Q9R190	*Mta2*	0.62	0.000289
Q7TQI3	*Otub1*	0.62	0.000284
Q9D3E6	*Stag1*	0.62	0.014261
P52332	*Jak1*	0.62	0.000249
Q9ESY9	*Ifi30*	0.63	0.005825
Q8K2I4	*Manba*	0.63	0.001093
Q91ZR2	*Snx18*	0.63	0.000391
Q99K28	*Arfgap2*	0.63	0.000244
Q99JP6	*Homer3*	0.63	0.000246
Q8VD75	*Hip1*	0.63	0.000261
P47754	*Capza2*	0.63	0.000246
Q7TPH6	*Mycbp2*	0.63	0.000534

UniProt ID	Genes	FC [log2]	q-value
P97298	*Serpinf1*	0.63	0.000647
P70399	*Tp53bp1*	0.63	0.001423
Q9D823	*Rpl37*	0.63	0.008672
Q80YX1	*Tnc*	0.63	0.000546
Q9CR16	*Ppid*	0.63	0.000231
E9Q5G3	*Kif23*	0.63	0.000277
P30416	*Fkbp4*	0.63	0.000186
P18654	*Rps6ka3*	0.64	0.000746
P62962	*Pfn1*	0.64	0.000751
P22892	*Ap1g1*	0.64	0.001659
Q62465	*Vat1*	0.64	0.000457
O70311	*Nmt2*	0.64	0.000886
Q8BGD6	*Slc38a9*	0.64	0.002832
Q62087	*Pon3*	0.64	0.000540
P61971	*Nutf2*	0.64	0.000897
Q62419	*Sh3gl1*	0.64	0.000373
Q9CXP8	*Gng10*	0.64	0.000368
Q8VEE4	*Rpa1*	0.64	0.000879
Q9CYR6	*Pgm3*	0.64	0.000547
O70305	*Atxn2*	0.64	0.000395
P62320	*Snrpd3*	0.64	0.000373
P08752	*Gnai2*	0.64	0.000400
O35841	*Api5*	0.64	0.000253
O88844	*Idh1*	0.65	0.000274
Q60605	*Myl6*	0.65	0.000731
Q9Z0P5	*Twf2*	0.65	0.000388
Q7TMY4	*Thoc7*	0.65	0.001083
Q91VW5	*Golga4*	0.65	0.001255
P28867	*Prkcd*	0.65	0.000259
Q9R1P4	*Psma1*	0.65	0.000380
Q80XC3	*Usp6nl*	0.65	0.000245
Q9R117	*Tyk2*	0.65	0.000248
Q80VJ3	*Dnph1*	0.65	0.001455
Q8VHR5	*Gatad2b*	0.65	0.000824
Q61398	*Pcolce*	0.66	0.000372
Q8VDF2	*Uhrf1*	0.66	0.000229
O89110	*Casp8*	0.66	0.000747
P63280	*Ube2i*	0.66	0.000827
P70175	*Dlg3*	0.66	0.001145
Q922D4	*Ppp6r3*	0.66	0.000410
Q9CZY3	*Ube2v1*	0.66	0.000846
Q5F2E7	*Nufip2*	0.66	0.004856
Q8BGF6	*Elmod2*	0.66	0.001004
Q99KK7	*Dpp3*	0.66	0.000286
Q9Z0Y1	*Dctn3*	0.66	0.000377
Q9JHL1	*Nherf2*	0.66	0.000183
Q91W92	*Cdc42ep1*	0.66	0.000658
Q9D892	*Itpa*	0.66	0.000655
Q8R5A3	*Apbb1ip*	0.66	0.000364
Q80XQ2	*Tbc1d5*	0.66	0.000283
Q9CQ60	*Pgls*	0.66	0.000253
P18406	*Ccn1*	0.66	0.000232
Q61937	*Npm1*	0.66	0.000895
P98197	*Atp11a*	0.67	0.000272
P11087	*Col1a1*	0.67	0.000234
Q8BRG8	*Tmem209*	0.67	0.007426
Q8R422	*Cd109*	0.67	0.000197
Q8K1S3	*Unc5b*	0.67	0.000184
Q9WU62	*Incenp*	0.67	0.009549
Q8C650	*Septin10*	0.67	0.000365
P07141	*Csf1*	0.67	0.000264
Q9CZ44	*Nsfl1c*	0.67	0.000283
Q61391	*Mme*	0.67	0.000365
Q8CIH9	*Ppat*	0.67	0.000189
P11531	*Dmd*	0.67	0.001097
Q8K2F8	*Lsm14a*	0.68	0.011706
O88839	*Adam15*	0.68	0.000272
Q58A65	*Spag9*	0.68	0.003528
Q8K2J7	*Rell1*	0.68	0.000510
Q80X50	*Ubap2l*	0.68	0.000260
Q9Z1Z0	*Uso1*	0.68	0.000220
Q6P9P6	*Kif11*	0.68	0.000212
Q921I2	*Klhdc4*	0.68	0.002352
Q99ME2	*Wdr6*	0.68	0.000252
Q8VDD8	*Washc1*	0.68	0.000258
Q9Z0R9	*Fads2*	0.68	0.000245
P83741	*Wnk1*	0.69	0.000261
Q8VCM3	*Zfyve21*	0.69	0.012019
Q9WTQ5	*Akap12*	0.69	0.000198
Q07113	*Igf2r*	0.69	0.000227
Q9CPU0	*Glo1*	0.69	0.000247
Q9D8U8	*Snx5*	0.69	0.000240
Q8BGZ4	*Cdc23*	0.69	0.048642
Q8K2Q0	*Commd9*	0.69	0.000514
P37913	*Lig1*	0.69	0.000281
P11499	*Hsp90ab1*	0.69	0.000222
Q61112	*Sdf4*	0.69	0.047235
Q61171	*Prdx2*	0.69	0.000188
Q76MZ3	*Ppp2r1a*	0.69	0.000653
P09411	*Pgk1*	0.69	0.000285
Q99K01	*Pdxdc1*	0.69	0.000390
Q80ZW2	*Them6*	0.70	0.000498

UniProt ID	Genes	FC [log2]	q-value
Q9WVE8	*Pacsin2*	0.70	0.000257
Q9R008	*Mvk*	0.70	0.000267
Q8BGD9	*Eif4b*	0.70	0.000854
Q9CQR6	*Ppp6c*	0.70	0.000246
P63024	*Vamp3*	0.70	0.003250
Q3UEB3	*Puf60*	0.70	0.000505
Q68FH0	*Pkp4*	0.70	0.000256
P28667	*Marcksl1*	0.70	0.000247
O70433	*Fhl2*	0.70	0.000234
P59222	*Scarf2*	0.70	0.000412
Q8BGS0	*Mak16*	0.70	0.036556
O08738	*Casp6*	0.70	0.000211
Q9QYJ0	*Dnaja2*	0.70	0.000508
P58871	*Tnks1bp1*	0.70	0.000235
Q9Z103	*Adnp*	0.71	0.000290
Q3U1J4	*Ddb1*	0.71	0.000195
Q91YD9	*Wasl*	0.71	0.000864
Q923D5	*Wbp11*	0.71	0.000819
Q60855	*Ripk1*	0.71	0.000507
Q8K2Y9	*Ccm2*	0.71	0.000289
P23198	*Cbx3*	0.71	0.000196
Q80TM9	*Nisch*	0.71	0.000210
Q2YDW2	*Msto1*	0.71	0.000252
Q8R4U7	*Luzp1*	0.71	0.000263
Q8R146	*Apeh*	0.71	0.000191
Q99MR6	*Srrt*	0.71	0.000232
P35235	*Ptpn11*	0.71	0.000208
Q80W68	*Kirrel1*	0.72	0.000194
Q3UFK8	*Frmd8*	0.72	0.000245
Q6PGL7	*Washc2*	0.72	0.000229
O70458	*Osmr*	0.72	0.000264
Q9QYY8	*Spast*	0.72	0.000269
P35441	*Thbs1*	0.72	0.000264
P51432	*Plcb3*	0.72	0.000218
Q8VDP3	*Mical1*	0.72	0.000562
Q9JKF6	*Nectin1*	0.72	0.000310
O09061	*Psmb1*	0.72	0.004856
P54116	*Stom*	0.72	0.000246
Q62418	*Dbnl*	0.72	0.000197
Q05CL8	*Larp7*	0.72	0.034781
Q60598	*Cttn*	0.72	0.000367
P10404		0.73	0.000193
Q8K0C9	*Gmds*	0.73	0.000242
Q04207	*Rela*	0.73	0.000185
Q8CAY6	*Acat2*	0.73	0.000262
Q6P9Q6	*Fkbp15*	0.73	0.000192

UniProt ID	Genes	FC [log2]	q-value
Q99KN2	*Ciao1*	0.73	0.000881
P61982	*Ywhag*	0.73	0.000536
P51125	*Cast*	0.73	0.000388
Q99KC8	*Vwa5a*	0.73	0.000288
Q99PT1	*Arhgdia*	0.73	0.000395
L0N7N1	*Kif14*	0.73	0.000457
Q9Z0U1	*Tjp2*	0.73	0.000194
Q9R1T2	*Sae1*	0.73	0.001635
P70460	*Vasp*	0.73	0.000273
Q8CJG0	*Ago2*	0.74	0.006977
Q62203	*Sf3a2*	0.74	0.001144
Q3UHH1	*Zswim8*	0.74	0.019062
Q922E4	*Pcyt2*	0.74	0.042748
Q9JLV5	*Cul3*	0.74	0.000230
P48193	*Epb41*	0.74	0.000241
P21126	*Ubl4a*	0.74	0.000237
O35900	*Lsm2*	0.74	0.000256
Q00493	*Cpe*	0.74	0.036593
Q64311	*Ntan1*	0.74	0.026843
P97801	*Smn1*	0.74	0.000984
P45377	*Akr1b8*	0.74	0.000269
Q6RHR9	*Magi1*	0.74	0.000269
Q8BFW7	*Lpp*	0.74	0.000271
E9PVX6	*Mki67*	0.74	0.000289
P13808	*Slc4a2*	0.74	0.000202
Q4JIM5	*Abl2*	0.74	0.034509
Q8R1U1	*Cog4*	0.75	0.044920
O70310	*Nmt1*	0.75	0.000215
Q8CDJ8	*Ston1*	0.75	0.000280
Q91W39	*Ncoa5*	0.75	0.001233
Q7TPS5	*C2cd5*	0.75	0.011862
Q63829	*Commd3*	0.75	0.000308
Q8K2V1	*Ppp4r1*	0.75	0.000261
Q99L47	*St13*	0.75	0.000257
Q8R4C2	*Rufy2*	0.75	0.000184
Q6ZPJ3	*Ube2o*	0.76	0.000223
P05622	*Pdgfrb*	0.76	0.000287
P70349	*Hint1*	0.76	0.000268
Q00560	*Il6st*	0.76	0.000249
P57680	*Evc*	0.76	0.000235
Q9ESJ4	*Nckipsd*	0.76	0.000385
Q9EQP2	*Ehd4*	0.76	0.000265
Q5SSZ5	*Tns3*	0.76	0.000213
O88207	*Col5a1*	0.76	0.000287
O88520	*Shoc2*	0.76	0.000221
A2AI08	*Tprn*	0.77	0.000255

UniProt ID	Genes	FC [log2]	q-value
P58404	*Strn4*	0.77	0.000547
Q8K298	*Anln*	0.77	0.000241
Q9JIG7	*Ccdc22*	0.77	0.000352
Q9WTX5	*Skp1*	0.77	0.000251
Q8VDP4	*Ccar2*	0.77	0.000284
Q8BWW9	*Pkn2*	0.77	0.000285
Q91W40	*Klc3*	0.77	0.039094
Q99MD9	*Nasp*	0.77	0.000241
Q80WC7	*Agfg2*	0.78	0.000259
P16254	*Srp14*	0.78	0.027568
Q03173	*Enah*	0.78	0.000247
P46062	*Sipa1*	0.78	0.000277
O08553	*Dpysl2*	0.78	0.000268
O88413	*Tulp3*	0.78	0.000242
Q8CI08	*Slain2*	0.78	0.000205
P70255	*Nfic*	0.78	0.013183
Q9CQC6	*Bzw1*	0.78	0.000244
P18052	*Ptpra*	0.78	0.000219
Q8CI94	*Pygb*	0.78	0.000270
Q9CX84	*Rgs19*	0.78	0.000279
Q9QZ88	*Vps29*	0.78	0.000199
O70435	*Psma3*	0.78	0.000618
Q6PDQ2	*Chd4*	0.78	0.000311
Q4VAA7	*Snx33*	0.78	0.031374
Q8CHP8	*Pgp*	0.79	0.000290
Q3UHJ0	*Aak1*	0.79	0.000246
Q923B1	*Dbr1*	0.79	0.001110
Q8VC03	*Eml3*	0.79	0.012425
Q99ML4	*Dipk1b*	0.79	0.000870
Q9DBN5	*Lonp2*	0.80	0.000237
Q9Z2D8	*Mbd3*	0.80	0.000825
D3YYU8	*Obsl1*	0.80	0.000263
Q8CGC6	*Rbm28*	0.80	0.012090
Q8BQ30	*Ppp1r18*	0.80	0.000250
Q80YV3	*Trrap*	0.80	0.021939
A2AAY5	*Sh3pxd2b*	0.80	0.000256
Q80TH2	*Erbin*	0.80	0.000234
O88291	*Znf326*	0.80	0.000378
Q61292	*Lamb2*	0.80	0.000307
P62843	*Rps15*	0.80	0.008390
P41241	*Csk*	0.81	0.000399
Q91ZJ5	*Ugp2*	0.81	0.000245
Q8VBT9	*Aspscr1*	0.81	0.000834
Q61081	*Cdc37*	0.81	0.000261
P70677	*Casp3*	0.81	0.000248
Q9QY06	*Myo9b*	0.81	0.000246

UniProt ID	Genes	FC [log2]	q-value
Q61602	*Gli3*	0.81	0.000888
Q8K1E6	*Alkbh3*	0.81	0.000270
Q6KCD5	*Nipbl*	0.81	0.021001
Q9QZM0	*Ubqln2*	0.81	0.000404
Q9Z108	*Stau1*	0.81	0.000257
Q9D8S3	*Arfgap3*	0.81	0.000256
Q62433	*Ndrg1*	0.82	0.000542
Q9R059	*Fhl3*	0.82	0.000226
Q9D4J7	*Phf6*	0.82	0.007423
O89079	*Cope*	0.82	0.000244
Q68FF6	*Git1*	0.82	0.000287
O08599	*Stxbp1*	0.82	0.000312
Q91V92	*Acly*	0.82	0.000259
P27641	*Xrcc5*	0.82	0.000282
O09106	*Hdac1*	0.83	0.001394
Q9DC11	*Plxdc2*	0.83	0.000240
Q5NCE8	*Mrs2*	0.83	0.047076
Q9QXA5	*Lsm4*	0.83	0.000253
Q6KAU4	*Mvb12b*	0.83	0.000229
Q91XY4	*Pcdhga4*	0.83	0.000243
Q9QWY8	*Asap1*	0.83	0.000892
P42227	*Stat3*	0.83	0.000237
Q6VVW5	*Npr2*	0.83	0.000230
Q61164	*Ctcf*	0.83	0.000241
P19157	*Gstp1*	0.83	0.000310
P54761	*Ephb4*	0.83	0.000312
Q61687	*Atrx*	0.84	0.005009
Q99M54	*Cdca3*	0.84	0.000239
Q9DCC4	*Pycr3*	0.84	0.000189
Q9DBT5	*Ampd2*	0.84	0.000259
P28660	*Nckap1*	0.84	0.000515
E9Q7M2	*Tsc22d2*	0.84	0.000687
O55201	*Supt5h*	0.84	0.001082
P70202	*Lxn*	0.84	0.000234
P97379	*G3bp2*	0.84	0.000384
Q8VE98	*Cd276*	0.84	0.000186
Q0VGY8	*Tanc1*	0.84	0.000265
P63017	*Hspa8*	0.84	0.000238
Q61037	*Tsc2*	0.84	0.000401
Q61598	*Gdi2*	0.84	0.000252
Q3TJ91	*Llgl2*	0.85	0.000238
A2A699	*Fam171a2*	0.85	0.000248
Q9QY73	*Tmem59*	0.85	0.000206
Q3UHD6	*Snx27*	0.85	0.000341
P50396	*Gdi1*	0.85	0.000289
Q8BFQ8	*Gatd1*	0.85	0.000223

UniProt ID	Genes	FC [log2]	q-value
Q3TWW8	*Srsf6*	0.85	0.000395
P59997	*Kdm2a*	0.86	0.000857
Q8R1X6	*Spart*	0.86	0.000238
P54728	*Rad23b*	0.86	0.046705
Q9QZQ1	*Afdn*	0.86	0.000311
Q8R366	*Igsf8*	0.86	0.000428
Q64514	*Tpp2*	0.86	0.000415
Q9ER38	*Tor3a*	0.87	0.030367
Q6A4J8	*Usp7*	0.87	0.017363
Q80U87	*Usp8*	0.87	0.000276
Q6PAJ1	*Bcr*	0.87	0.012649
Q99LI8	*Hgs*	0.87	0.000202
Q8CHP5	*Pym1*	0.87	0.020100
P01901	*H2-K1*	0.87	0.000552
Q01341	*Adcy6*	0.87	0.000243
O89026	*Robo1*	0.88	0.000302
Q9D8B7	*Jam3*	0.88	0.000187
Q8CBW3	*Abi1*	0.88	0.000198
Q91YJ2	*Snx4*	0.88	0.000290
Q99MK8	*Grk2*	0.88	0.000321
Q9QYJ3	*Dnajb1*	0.88	0.000225
Q80VQ1	*Lrrc1*	0.88	0.000251
Q61553	*Fscn1*	0.88	0.000316
Q3TIV5	*Zc3h15*	0.88	0.000384
Q9CY18	*Snx7*	0.88	0.000258
Q8VE73	*Cul7*	0.88	0.000274
P60670	*Nploc4*	0.89	0.000286
Q9JJC6	*Rilpl1*	0.89	0.000276
E9Q912	*Rap1gds1*	0.89	0.000411
Q8C0E3	*Trim47*	0.89	0.000418
Q60864	*Stip1*	0.89	0.000197
Q921W4	*Cryzl1*	0.89	0.000255
Q64105	*Spr*	0.89	0.000236
Q99K41	*Emilin1*	0.89	0.000397
P53810	*Pitpna*	0.89	0.000402
O70493	*Snx12*	0.89	0.000359
Q91VJ2	*Cavin3*	0.90	0.000399
Q9ER73	*Elp4*	0.90	0.000304
P83940	*Eloc*	0.90	0.000242
P42232	*Stat5b*	0.90	0.000354
P70195	*Psmb7*	0.90	0.000822
P28828	*Ptprm*	0.90	0.000224
Q9WTX6	*Cul1*	0.90	0.000322
Q9QYC0	*Add1*	0.90	0.000251
Q3TN34	*Micall2*	0.90	0.000230
Q8BFQ4	*Wdr82*	0.91	0.001090

UniProt ID	Genes	FC [log2]	q-value
Q9WVM1	*Racgap1*	0.91	0.000280
Q80SZ7	*Gng5*	0.91	0.000867
Q91XC0	*Ajuba*	0.91	0.014596
Q8CH25	*Sltm*	0.92	0.035619
P81122	*Irs2*	0.92	0.001366
Q8VCF1	*Cant1*	0.92	0.017021
Q9ES00	*Ube4b*	0.92	0.022949
Q6R891	*Ppp1r9b*	0.92	0.000534
Q8C3W1		0.93	0.000233
A2ASQ1	*Agrn*	0.93	0.008218
Q9Z2X8	*Keap1*	0.93	0.000211
Q8CHH9	*Septin8*	0.93	0.000481
P26040	*Ezr*	0.93	0.000268
Q61508	*Ecm1*	0.93	0.000331
P60882	*Megf8*	0.93	0.000293
O35516	*Notch2*	0.93	0.000389
Q8VIK5	*Pear1*	0.93	0.000561
Q91VW3	*Sh3bgrl3*	0.94	0.000262
Q9EQG9	*Cert1*	0.94	0.000896
P17742	*Ppia*	0.94	0.000283
Q9WV80	*Snx1*	0.94	0.000517
S4R1M9	*Osbpl10*	0.94	0.000264
Q8BVG4	*Dpp9*	0.94	0.004338
Q99JW4	*Lims1*	0.94	0.000358
Q69ZS7	*Hbs1l*	0.94	0.034713
Q9QUR7	*Pin1*	0.94	0.000252
Q3ULJ0	*Gpd1l*	0.94	0.017854
Q61810	*Ltbp3*	0.94	0.000261
Q3TDD9	*Ppp1r21*	0.95	0.000214
Q3TYX3	*Smyd5*	0.95	0.005867
Q6P9Q4	*Fhod1*	0.95	0.000267
Q9QYI3	*Dnajc7*	0.95	0.000556
Q8R1T1	*Chmp7*	0.95	0.000849
Q8CJ26	*Nradd*	0.95	0.000470
Q9CY57	*Chtop*	0.96	0.001003
Q8R574	*Prpsap2*	0.96	0.020156
Q9CS42	*Prps2*	0.96	0.000399
Q61712	*Dnajc1*	0.96	0.028920
P02463	*Col4a1*	0.96	0.000521
Q9WVJ9	*Efemp2*	0.96	0.000372
Q8BZW8	*Nhlrc2*	0.96	0.000617
Q02248	*Ctnnb1*	0.97	0.000566
Q9CQR2	*Rps21*	0.97	0.000394
Q8CHY6	*Gatad2a*	0.97	0.000235
P83870	*Phf5a*	0.97	0.000199
Q66JT1	*Lrrc8e*	0.98	0.000363

UniProt ID	Genes	FC [log2]	q-value
P21460	*Cst3*	0.98	0.000272
Q3UDR8	*Yipf3*	0.98	0.000559
Q8BKX1	*Baiap2*	0.98	0.000454
P48410	*Abcd1*	0.98	0.000380
P16858	*Gapdh*	0.98	0.000257
Q60596	*Xrcc1*	0.98	0.000614
Q3TMW1	*Ccdc102a*	0.98	0.000270
P26231	*Ctnna1*	0.98	0.000590
Q9WVA4	*Tagln2*	0.98	0.000271
Q9QYK7	*Rnf11*	0.99	0.019541
Q99K51	*Pls3*	0.99	0.000282
P70290	*Mpp1*	0.99	0.000382
Q9CQX4	*Pclaf*	0.99	0.000548
Q91ZE0	*Tmlhe*	0.99	0.000400
Q3UFY7	*Nt5c3b*	0.99	0.000222
Q68FH4	*Galk2*	0.99	0.020319
Q8BKG3	*Ptk7*	0.99	0.000642
P31938	*Map2k1*	0.99	0.000300
Q9D0W5	*Ppil1*	0.99	0.000735
Q99MJ9	*Ddx50*	1.00	0.017372
Q9D706	*Rpap3*	1.00	0.000277
P97447	*Fhl1*	1.00	0.000332
Q8VED2	*Bloc1s4*	1.00	0.014686
Q61205	*Pafah1b3*	1.00	0.000244
Q5ND34	*Wdr81*	1.00	0.000249
Q60710	*Samhd1*	1.01	0.000756
Q9D1E6	*Tbcb*	1.01	0.007840
Q9WU84	*Ccs*	1.01	0.014587
P61759	*Vbp1*	1.02	0.000267
P97372	*Psme2*	1.02	0.000391
Q9Z0M6	*Adgre5*	1.02	0.000500
Q8BUK6	*Hook3*	1.02	0.000546
Q8VHY0	*Cspg4*	1.02	0.000660
Q8R317	*Ubqln1*	1.03	0.000412
Q6DID3	*Scaf8*	1.03	0.004275
O54774	*Ap3d1*	1.03	0.000230
B2RUR8	*Otud7b*	1.03	0.007454
Q8CI59	*Steap3*	1.03	0.000506
Q8K1N4	*Spats2*	1.03	0.000825
O35375	*Nrp2*	1.03	0.000496
Q8VHK1	*Caskin2*	1.03	0.000602
Q8BMQ8	*Mon1b*	1.03	0.021687
P49722	*Psma2*	1.03	0.000215
Q9CQT2	*Rbm7*	1.04	0.008542
E9Q555	*Rnf213*	1.04	0.000649
O35316	*Slc6a6*	1.04	0.000368

UniProt ID	Genes	FC [log2]	q-value
Q8K012	*Fnbp1l*	1.04	0.008863
Q91V64	*Isoc1*	1.04	0.006862
E9PY46	*Ift140*	1.04	0.001578
Q9D8N0	*Eef1g*	1.05	0.000701
Q9R045	*Angptl2*	1.05	0.011933
Q9D964	*Gatm*	1.05	0.000258
P97873	*Loxl1*	1.05	0.000623
P23249	*Mov10*	1.05	0.000475
Q62384	*Zpr1*	1.06	0.000227
Q5F2L2	*Fut10*	1.06	0.013469
Q02788	*Col6a2*	1.06	0.000585
Q9JHW4	*Eefsec*	1.06	0.004336
Q9WVM3	*Anapc7*	1.06	0.012756
P52734	*Fgd1*	1.06	0.000873
Q9QXS6	*Dbn1*	1.07	0.000257
Q91VK1	*Bzw2*	1.07	0.040494
Q9JLV1	*Bag3*	1.07	0.000390
Q9QYB5	*Add3*	1.07	0.000286
O35566	*Cd151*	1.08	0.000497
Q9QUI0	*Rhoa*	1.08	0.000497
P70429	*Evl*	1.08	0.012264
Q7TMF2	*Eri1*	1.08	0.010312
Q9D8Y0	*Efhd2*	1.08	0.000504
Q62165	*Dag1*	1.08	0.000663
P18653	*Rps6ka1*	1.08	0.000508
Q71FD7	*Fblim1*	1.09	0.000423
O70400	*Pdlim1*	1.09	0.000752
P30999	*Ctnnd1*	1.09	0.001016
O08915	*Aip*	1.09	0.000693
Q6PIU9		1.10	0.000588
Q9WV91	*Ptgfrn*	1.10	0.000849
Q8R4H2	*Arhgef12*	1.10	0.000281
Q8BHK9	*Ercc6l*	1.10	0.000780
P97432	*Nbr1*	1.10	0.008840
Q9D2V7	*Coro7*	1.11	0.000305
P40237	*Cd82*	1.12	0.000360
Q91WB7	*Ubtd1*	1.12	0.000636
Q3TW96	*Uap1l1*	1.12	0.000800
Q9Z2H5	*Epb41l1*	1.12	0.000408
Q91VR8	*Brk1*	1.13	0.000213
Q8CGA0	*Ppm1f*	1.13	0.012858
Q9EPK7	*Xpo7*	1.13	0.000848
O35326	*Srsf5*	1.13	0.000192
Q9JM13	*Rabgef1*	1.14	0.020108
A2ALU4	*Shroom2*	1.14	0.000564
Q8BIE6	*Frmd4a*	1.14	0.002253

UniProt ID	Genes	FC [log2]	q-value
Q8R2Y2	*Mcam*	1.14	0.000502
P98192	*Gnpat*	1.14	0.021304
Q8K1G2	*Evc2*	1.14	0.000548
P54227	*Stmn1*	1.15	0.000743
P70268	*Pkn1*	1.15	0.000689
P29387	*Gnb4*	1.15	0.000270
Q71LX4	*Tln2*	1.15	0.000394
Q9Z175	*Loxl3*	1.15	0.000248
Q8BWP8	*B4gat1*	1.15	0.000987
Q9DBV4	*Mxra8*	1.15	0.001138
Q921M4	*Golga2*	1.15	0.001127
Q8K2D3	*Edc3*	1.15	0.005653
Q8C9B9	*Dido1*	1.16	0.000887
Q9Z0P7	*Sufu*	1.16	0.000300
Q8K4J6	*Mrtfa*	1.16	0.002498
Q8R3V5	*Sh3glb2*	1.16	0.000670
P33611	*Pola2*	1.16	0.004350
Q6ZPF4	*Fmnl3*	1.16	0.000697
Q8BM86	*Lhfpl6*	1.16	0.002475
Q8R2U4	*Ntmt1*	1.17	0.004015
P70441	*Nherf1*	1.17	0.000729
Q8BIK4	*Dock9*	1.17	0.019336
Q78HU3	*Mvb12a*	1.17	0.011619
Q7TQK5	*Ccdc93*	1.17	0.000617
Q8R3B1	*Plcd1*	1.17	0.000861
Q569Z5	*Ddx46*	1.18	0.000775
P47226	*Tes*	1.18	0.000919
Q80Y56	*Rbsn*	1.18	0.000551
Q8R105	*Vps37c*	1.18	0.024192
Q91YM2	*Arhgap35*	1.18	0.004853
D3YX43	*Vsig10*	1.18	0.000407
Q8VI36	*Pxn*	1.19	0.000629
P34152	*Ptk2*	1.19	0.009576
O54956	*Pole2*	1.19	0.005885
Q64669	*Nqo1*	1.19	0.000191
P32067	*Ssb*	1.19	0.041575
Q8CHC4	*Synj1*	1.20	0.007297
Q68FE6	*Ripor1*	1.20	0.000984
Q3V1H1	*Ckap2*	1.20	0.001262
Q7TNP2	*Ppp2r1b*	1.20	0.006983
P07742	*Rrm1*	1.20	0.000437
Q02257	*Jup*	1.20	0.000705
Q6P9S7	*Galnt10*	1.20	0.020062
Q80TS3	*Adgrl3*	1.21	0.000239
P97798	*Neo1*	1.21	0.001228
Q9Z1R4	*D17h6s53e*	1.21	0.002073

UniProt ID	Genes	FC [log2]	q-value
Q3UUG6	*Tbc1d24*	1.21	0.014098
O70126	*Aurkb*	1.21	0.009231
Q8CFE2	*Hpf1*	1.21	0.000899
P18608	*Hmgn1*	1.22	0.000649
Q9JJK2	*Lancl2*	1.22	0.004280
P46938	*Yap1*	1.22	0.000216
O35381	*Anp32a*	1.22	0.014213
P35761	*Ttk*	1.22	0.000292
Q9JIP6	*Fzd2*	1.23	0.000886
Q9DBG5	*Plin3*	1.23	0.000838
Q8BJH1	*Zc2hc1a*	1.23	0.004040
Q8K4G5	*Ablim1*	1.23	0.000318
P62996	*Tra2b*	1.23	0.033691
Q924K8	*Mta3*	1.24	0.001365
Q8BHL7	*Cdc42se1*	1.24	0.000262
Q99M51	*Nck1*	1.25	0.012663
P57776	*Eef1d*	1.25	0.000614
Q9CQS2	*Nop10*	1.26	0.003582
Q8BKC8	*Pi4kb*	1.26	0.000932
Q8BG60	*Txnip*	1.26	0.000721
P62311	*Lsm3*	1.26	0.021929
P62627	*Dynlrb1*	1.27	0.000466
Q8C181	*Mbnl2*	1.27	0.000299
O55098	*Stk10*	1.27	0.000365
Q9QXD8	*Limd1*	1.28	0.001008
Q9JLQ2	*Git2*	1.28	0.000434
Q8VC04	*Tmem106a*	1.28	0.013201
O35309	*Nmi*	1.28	0.000656
Q99LD8	*Ddah2*	1.28	0.001459
Q810U5	*Ccdc50*	1.28	0.001508
Q8BG26	*Rusc1*	1.30	0.000892
P10287	*Cdh3*	1.30	0.000969
Q8BHZ4	*Znf592*	1.30	0.013001
Q922U1	*Prpf3*	1.30	0.006790
Q80YS6	*Afap1*	1.30	0.000266
Q9ERR1	*Ndel1*	1.31	0.004298
Q9CQV8	*Ywhab*	1.31	0.001033
Q08288	*Lyar*	1.31	0.003880
P53690	*Mmp14*	1.31	0.001181
Q9DCD5	*Tjap1*	1.31	0.001194
Q8QZV7	*IntS13*	1.32	0.001119
O35621	*Pmm1*	1.32	0.008901
Q61249	*Igbp1*	1.32	0.013359
Q8R570	*Snap47*	1.32	0.000619
Q5SUF2	*Luc7l3*	1.32	0.000267
Q8BTZ7	*Gmppb*	1.32	0.001424

UniProt ID	Genes	FC [log2]	q-value
P68372	*Tubb4b*	1.32	0.000396
P58466	*Ctdsp1*	1.32	0.013107
P70424	*Erbb2*	1.32	0.001393
Q60949	*Tbc1d1*	1.32	0.000420
P04925	*Prnp*	1.33	0.000411
Q8BLX7	*Col16a1*	1.33	0.001090
Q9DAW9	*Cnn3*	1.33	0.000248
Q80TE0	*Rpap1*	1.33	0.000734
Q9Z0H8	*Clip2*	1.34	0.000986
Q04857	*Col6a1*	1.35	0.001253
Q0P678	*Zc3h18*	1.35	0.000223
Q80T21	*Adamtsl4*	1.36	0.000747
Q7TNV0	*Dek*	1.36	0.000633
Q01705	*Notch1*	1.36	0.011075
Q8R3C0	*Mcmbp*	1.36	0.012079
Q62523	*Zyx*	1.37	0.000346
Q9R1T4	*Septin6*	1.37	0.001107
Q9CWL8	*Ctnnbl1*	1.37	0.000541
A2A432	*Cul4b*	1.38	0.000266
P48774	*Gstm5*	1.38	0.000496
P16330	*Cnp*	1.39	0.000867
Q9WTL7	*Lypla2*	1.39	0.009845
Q8BZ20	*Parp12*	1.39	0.000231
Q9WV34	*Mpp2*	1.39	0.000790
Q8CFV4	*Nrn1*	1.40	0.004095
Q60575	*Kif1b*	1.40	0.001086
Q9CQ26	*Stambp*	1.40	0.001978
O70583	*Mid1*	1.40	0.000503
Q8R550	*Sh3kbp1*	1.40	0.003083
Q9WTR5	*Cdh13*	1.41	0.001797
Q8VCG3	*Wdr74*	1.41	0.003699
A2A5R2	*Arfgef2*	1.41	0.007200
Q6PEB6	*Mob4*	1.41	0.012048
Q9CZ04	*Cops7a*	1.42	0.000874
P70697	*Urod*	1.42	0.001637
Q9CT10	*Ranbp3*	1.43	0.001145
Q9CZT5	*Vasn*	1.43	0.000490
Q9Z1Q5	*Clic1*	1.43	0.001425
Q99KG3	*Rbm10*	1.44	0.001118
Q69ZH9	*Arhgap23*	1.44	0.000366
P52795	*Efnb1*	1.44	0.022055
Q69Z38	*Peak1*	1.44	0.000842
Q921L5	*Cog2*	1.45	0.000376
Q62393	*Tpd52*	1.45	0.000857
P70303	*Ctps2*	1.45	0.008361
P10630	*Eif4a2*	1.46	0.016239
Q9R207	*Nbn*	1.46	0.001450
Q91YD6	*Vill*	1.47	0.001278
Q9EQY0	*Ern1*	1.47	0.001099
Q8R0S2	*Iqsec1*	1.48	0.001060
Q9D5V6	*Syap1*	1.48	0.004206
Q61792	*Lasp1*	1.49	0.001676
Q08024	*Cbfb*	1.49	0.009075
P17515	*Cxcl10*	1.50	0.000505
P84084	*Arf5*	1.50	0.000974
Q8BGB5	*Limd2*	1.51	0.000441
P14602	*Hspb1*	1.51	0.001148
Q6VN19	*Ranbp10*	1.51	0.001170
Q9DBH0	*Wwp2*	1.51	0.001507
Q61074	*Ppm1g*	1.51	0.000273
Q9EPQ8	*Tcf20*	1.52	0.000260
Q8CG79	*Tp53bp2*	1.52	0.000371
O70251	*Eef1b*	1.52	0.001442
Q810A3	*Ttc9c*	1.53	0.000384
Q99L28	*Rsl24d1*	1.53	0.001084
Q9Z2D3	*Gsdme*	1.53	0.000333
P0DOV2	*Ifi204*	1.53	0.001042
Q8R1M0	*Hmces*	1.54	0.000269
Q9QWF0	*Chaf1a*	1.54	0.001476
P20357	*Map2*	1.54	0.000745
P62317	*Snrpd2*	1.54	0.015317
Q07797	*Lgals3bp*	1.55	0.000947
Q9R233	*Tapbp*	1.55	0.001216
O35646	*Capn6*	1.55	0.001476
Q60631	*Grb2*	1.56	0.000256
Q3UA16	*Spc25*	1.57	0.000234
Q9CR23	*Tmem9*	1.57	0.000440
P40240	*Cd9*	1.57	0.000337
A3KGV1	*Odf2*	1.57	0.000271
Q6ZQA6	*Igsf3*	1.58	0.000549
Q6P5E6	*Gga2*	1.59	0.000833
Q9QYH6	*Maged1*	1.59	0.000226
Q9D4H8	*Cul2*	1.59	0.001842
Q9DBR4	*Apbb2*	1.60	0.000398
Q8VHH5	*Agap3*	1.60	0.000689
Q99K90	*Tab2*	1.60	0.000545
Q91YE3	*Egln1*	1.60	0.000479
Q8BKI2	*Tnrc6b*	1.60	0.000510
P62835	*Rap1a*	1.60	0.014624
Q9CPN8	*Igf2bp3*	1.60	0.001653
Q8BFR6	*Zfand1*	1.61	0.000890
Q8QZX2	*Haus3*	1.61	0.003701

UniProt ID	Genes	FC [log2]	q-value
Q9ESD7	*Dysf*	1.62	0.001746
Q8BGF3	*Dnaaf10*	1.62	0.000294
Q6DFV3	*Arhgap21*	1.62	0.000422
Q6DFW5	*Atp11b*	1.63	0.001094
P51655	*Gpc4*	1.64	0.001240
Q62130	*Ptpn14*	1.64	0.000248
Q9D7E3	*Ovca2*	1.64	0.005106
Q8BHL8	*Psmf1*	1.65	0.003534
Q8BXK8	*Agap1*	1.65	0.000985
Q4VAC9	*Plekhg3*	1.65	0.001084
Q80TQ2	*Cyld*	1.67	0.001656
Q8VBW6	*Nae1*	1.67	0.000895
Q8VE88	*Fam114a2*	1.69	0.000207
O08543	*Efna5*	1.69	0.001097
P58022	*Loxl2*	1.70	0.000238
Q6VH22	*Ift172*	1.70	0.001771
Q61151	*Ppp2r5e*	1.70	0.000237
Q61469	*Plpp1*	1.70	0.009750
O54890	*Itgb3*	1.71	0.000345
Q8K2V6	*Ipo11*	1.71	0.000266
A2APV2	*Fmnl2*	1.71	0.001610
Q9ER81	*Tor1aip2*	1.71	0.000209
Q922P8	*Tmem132a*	1.72	0.001851
Q8BGS1	*Epb41l5*	1.73	0.001109
P97479	*Myo7a*	1.74	0.001106
Q8K274	*Fn3krp*	1.75	0.001512
Q9CR26	*Vta1*	1.76	0.011149
Q62036	*Cep131*	1.77	0.000208
Q6PEV3	*Wipf2*	1.77	0.000473
Q9JJ11	*Tacc3*	1.77	0.000219
Q8BH15	*Cnot10*	1.80	0.000272
P97825	*Jpt1*	1.80	0.000667
Q8C170	*Myo9a*	1.82	0.000281
D3YZP9	*Ccdc6*	1.82	0.001746
Q9ES28	*Arhgef7*	1.83	0.000949
P16092	*Fgfr1*	1.84	0.000717
Q8CIE4	*Parp10*	1.86	0.000409
Q7TPM1	*Prrc2b*	1.87	0.000390
Q8C5L3	*Cnot2*	1.88	0.001096
Q1W617	*Shroom4*	1.88	0.000196
P53996	*Cnbp*	1.89	0.001000
Q8CGC4	*Lsm14b*	1.92	0.000756
Q8K207		1.92	0.000976
P01887	*B2m*	1.93	0.000449
Q99KN1	*Arrdc1*	1.94	0.000976
Q62159	*Rhoc*	1.94	0.010307

UniProt ID	Genes	FC [log2]	q-value
Q61140	*Bcar1*	1.97	0.000425
Q9QUN7	*Tlr2*	1.97	0.001550
Q80UP5	*Ankrd13a*	1.97	0.000998
Q8K245	*Uvrag*	1.98	0.000237
Q9Z2V5	*Hdac6*	1.98	0.000283
Q8R2Q8	*Bst2*	1.98	0.001908
O88572	*Lrp6*	1.98	0.000564
Q9D818	*Sapcd2*	1.99	0.002033
Q9EQJ9	*Magi3*	2.01	0.000209
P97494	*Gclc*	2.01	0.000397
Q3UHA3	*Spg11*	2.01	0.000251
E1U8D0	*Soga1*	2.01	0.001155
P61079	*Ube2d3*	2.01	0.001632
Q6Q899	*Rigi*	2.01	0.000000
Q8BIW1	*Prune1*	2.02	0.000511
P62984	*Uba52*	2.03	0.000339
Q8CAS9	*Parp9*	2.03	0.000000
Q61545	*Ewsr1*	2.05	0.000739
Q9JK84	*Pard6g*	2.06	0.000225
Q8BWS5	*Gprin3*	2.09	0.000000
Q05895	*Thbs3*	2.10	0.000276
Q7TNE3	*Spag7*	2.10	0.000438
Q9CWM4	*Pfdn1*	2.10	0.000831
Q3TGF2	*Fam107b*	2.11	0.000432
O35654	*Pold2*	2.12	0.000468
Q9DAR7	*Dcps*	2.12	0.000249
Q61730	*Il1rap*	2.13	0.000000
Q9JI10	*Stk3*	2.14	0.000258
P58389	*Ptpa*	2.16	0.000384
Q60973	*Rbbp7*	2.19	0.000562
P21958	*Tap1*	2.20	0.000228
Q9ET26	*Rnf114*	2.21	0.000795
Q922B9	*Itprid2*	2.21	0.000196
Q8BTI7	*Ankrd52*	2.21	0.000271
Q3V4B5	*Commd6*	2.22	0.000393
Q3UYV9	*Ncbp1*	2.23	0.000258
Q5DU25	*Iqsec2*	2.23	0.000949
Q9WVF7	*Pole*	2.25	0.001158
Q9Z1D1	*Eif3g*	2.27	0.000446
P59672	*Anks1a*	2.27	0.000324
Q9Z315	*Sart1*	2.28	0.000249
Q9D753	*Exosc8*	2.29	0.000288
Q9R118	*Htra1*	2.29	0.000000
Q9ERV1	*Mkrn2*	2.31	0.000187
O08746	*Matn2*	2.31	0.000210
O88712	*Ctbp1*	2.31	0.000271

UniProt ID	Genes	FC [log2]	q-value
Q8CJ27	*Aspm*	2.31	0.000000
B0V2N1	*Ptprs*	2.32	0.000000
Q9D5R2	*Wdr20*	2.32	0.000976
Q9Z2F2	*Oasl2*	2.32	0.000000
Q99N57	*Raf1*	2.34	0.000000
Q9EQW7	*Kif13a*	2.36	0.001000
P10649	*Gstm1*	2.36	0.000227
Q9JJV2	*Pfn2*	2.38	0.000288
P39429	*Traf2*	2.39	0.000192
Q8BIA4	*Fbxw8*	2.39	0.000295
Q3TFQ1	*Spryd7*	2.39	0.000692
Q06335	*Aplp2*	2.40	0.000847
Q9DCG9	*Trmt112*	2.40	0.003725
P97329	*Kif20a*	2.40	0.000000
Q9D1C1	*Ube2c*	2.41	0.000302
Q9CPP0	*Npm3*	2.42	0.000252
O35134	*Polr1a*	2.46	0.000000
Q6Y685	*Tacc1*	2.46	0.000275
Q99MU3	*Adar*	2.48	0.000999
Q5NBU8	*Xaf1*	2.49	0.000000
Q9R062	*Gyg1*	2.49	0.000282
Q9D7S9	*Chmp5*	2.52	0.000561
Q6A070	*Togaram1*	2.54	0.000262
Q9QXK7	*Cpsf3*	2.56	0.000000
E9PVD3	*Dchs1*	2.57	0.001257
P36371	*Tap2*	2.58	0.000000
Q6QI06	*Rictor*	2.58	0.000000
Q80Y98	*Ddhd2*	2.59	0.000000
Q8JZV7	*Amdhd2*	2.59	0.000284
Q9Z1S0	*Bub1b*	2.60	0.000879
P70261	*Pald1*	2.62	0.000286
Q9Z2C4	*Mtmr1*	2.62	0.000000
Q9QXK3	*Copg2*	2.67	0.000000
Q66JX5	*Cep43*	2.67	0.000246
Q3TC93	*Hs1bp3*	2.67	0.000191
Q9JKV5	*Scamp4*	2.69	0.001162
Q9DC28	*Csnk1d*	2.71	0.000253
Q9QZB9	*Dctn5*	2.74	0.000205
A6H8H2	*Dennd4c*	2.75	0.001879
O70161	*Pip5k1c*	2.75	0.000000
Q9DBG9	*Tax1bp3*	2.77	0.000190
Q9JK92	*Hspb8*	2.78	0.000900
Q8BNY6	*Ncs1*	2.78	0.001409
P08121	*Col3a1*	2.79	0.000605
P36993	*Ppm1b*	2.80	0.000000
Q62241	*Snrpc*	2.82	0.000370

UniProt ID	Genes	FC [log2]	q-value
Q8K1I7	*Wipf1*	2.87	0.000254
Q99LT0	*Dpy30*	2.88	0.000688
Q8R5M8	*Cadm1*	2.89	0.000000
P70275	*Sema3e*	2.90	0.000000
P97822	*Anp32e*	2.90	0.000000
Q8BQ89	*Lix1l*	2.92	0.000458
Q64339	*Isg15*	2.93	0.000233
Q9DCE9	*Igtp*	2.96	0.000463
P61622	*Itga11*	2.97	0.000000
Q76N33	*Stambpl1*	2.97	0.000232
Q91W18	*Tdrd3*	3.00	0.000398
Q9CQI6	*Cotl1*	3.04	0.000785
Q8K1A6	*Cc2d1a*	3.04	0.000224
O08573	*Lgals9*	3.06	0.000000
Q3U5Q7	*Cmpk2*	3.09	0.000000
Q91XE8	*Tmem205*	3.09	0.000000
Q3UJD6	*Usp19*	3.16	0.000000
Q91V98	*Cd248*	3.21	0.001204
Q01721	*Gas1*	3.21	0.000000
P97864	*Casp7*	3.23	0.000232
Q8VI94	*Oasl1*	3.23	0.000000
Q8BJU2	*Tspan9*	3.29	0.000185
P62892	*Rpl39*	3.34	0.003331
P22682	*Cbl*	3.40	0.000000
Q8R1S9	*Slc38a4*	3.41	0.000925
Q8VCR7	*Abhd14b*	3.46	0.000639
A0A140LIF8	*Irgm2*	3.47	0.000000
P52793	*Efna1*	3.49	0.000000
Q9Z2M7	*Pmm2*	3.49	0.000000
O35188	*Cx3cl1*	3.49	0.000000
P11928	*Oas1a*	3.56	0.000000
P97299	*Sfrp2*	3.61	0.000000
Q9D8N2	*Dennd10*	3.68	0.000188
Q2PZL6	*Fat4*	3.77	0.000000
P61588	*Rnd3*	3.84	0.000000
Q9QZE7	*Tsnax*	3.86	0.000000
Q9EPK8	*Trpv4*	3.93	0.000000
P42225	*Stat1*	4.06	0.000000
P48428	*Tbca*	4.16	0.000364
Q9R087	*Gpc6*	4.29	0.000000
P15864	*H1-2*	4.31	0.000000
P01899	*H2-D1*	4.33	0.000513
Q9D8C4	*Ifi35*	4.39	0.000000
Q64282	*Ifit1*	4.62	0.000000
Q8BSN9	*Fastkd3*	5.03	0.000000
Q80UW2	*Fbxo2*	5.06	0.000000

UniProt ID	Genes	FC [log2]	q-value
Q99P91	*Gpnmb*	5.36	0.000000
O88952	*Lin7c*	6.84	0.000000

Table S5: Significantly altered proteins detected in MEFs

Uniprot ID	Genes	FC [log2]	q-value
O70456	*Sfn*	-4.41	0.005195
P43407	*Sdc2*	-3.82	0.000000
Q8R086	*Suox*	-3.70	0.000000
P28301	*Lox*	-3.50	0.000000
O88428	*Papss2*	-3.48	0.000000
P20352	*F3*	-3.03	0.000000
Q61555	*Fbn2*	-2.80	0.000000
Q3V1M1	*Igsf10*	-2.76	0.000000
Q9DCT8	*Crip2*	-2.60	0.000000
Q8BH86	*Dglucy*	-2.57	0.000000
Q8K120	*Nfatc4*	-2.56	0.000000
P08121	*Col3a1*	-2.50	0.000000
O88322	*Nid2*	-2.39	0.000000
Q01149	*Col1a2*	-2.35	0.000000
P82347	*Sgcd*	-2.33	0.000000
O35640	*Anxa8*	-2.31	0.000000
P82343	*Renbp*	-2.30	0.000000
Q9CQ19	*Myl9*	-2.30	0.002000
P23242	*Gja1*	-2.30	0.000000
Q8R4R6	*Nup35*	-2.29	0.021971
P11862	*Gas2*	-2.26	0.000000
E9Q4P1	*Wdfy1*	-2.25	0.002818
Q8K007	*Sulf1*	-2.24	0.002952
Q9D0J4	*Arl2*	-2.18	0.012206
Q9CQU5	*Zwint*	-2.18	0.014076
P11087	*Col1a1*	-2.17	0.000000
Q61599	*Arhgdib*	-2.13	0.000000
Q9R1B9	*Slit2*	-2.10	0.000000
Q9CY50	*Ssr1*	-2.10	0.043364
Q8BZ98	*Dnm3*	-1.95	0.031079
P16125	*Ldhb*	-1.94	0.001297
P70271	*Pdlim4*	-1.88	0.000000
Q62059	*Vcan*	-1.78	0.004222
O88207	*Col5a1*	-1.77	0.000000
P27090	*Tgfb2*	-1.72	0.004727
P29391	*Ftl1*	-1.70	0.022767
Q8VDQ1	*Ptgr2*	-1.68	0.021642
Q80TF3	*Pcdh19*	-1.67	0.002105
Q8BW00	*Ptrh1*	-1.65	0.022444
Q8CG70	*P3h3*	-1.64	0.003915
Q64364	*Cdkn2a*	-1.64	0.002884
P18406	*Ccn1*	-1.60	0.004677
Q62219	*Tgfb1i1*	-1.60	0.004537
P26645	*Marcks*	-1.59	0.004327
P62965	*Crabp1*	-1.58	0.003111

Uniprot ID	Genes	FC [log2]	q-value
Q9JJX6	*P2rx4*	-1.57	0.030470
Q07231	*Zscan21*	-1.56	0.043409
Q8R2G6	*Ccdc80*	-1.54	0.004938
Q9WUR9	*Ak4*	-1.52	0.004077
O55242	*Sigmar1*	-1.51	0.041960
Q9QYR6	*Map1a*	-1.51	0.004417
Q08509	*Eps8*	-1.50	0.004643
P49817	*Cav1*	-1.50	0.005067
P16460	*Ass1*	-1.45	0.004240
P97929	*Brca2*	-1.42	0.006965
Q8K0Q5	*Arhgap18*	-1.40	0.004406
Q8BX90	*Fndc3a*	-1.39	0.024109
Q80UJ7	*Rab3gap1*	-1.39	0.005479
Q8BH97	*Rcn3*	-1.38	0.013815
Q99LB2	*Dhrs4*	-1.38	0.004444
Q2PZL6	*Fat4*	-1.36	0.006805
Q60847	*Col12a1*	-1.36	0.004750
Q08879	*Fbln1*	-1.35	0.005241
Q61703	*Itih2*	-1.34	0.017903
P15327	*Bpgm*	-1.31	0.005128
P21995	*Emb*	-1.30	0.007461
P52927	*Hmga2*	-1.29	0.006884
Q63918	*Cavin2*	-1.28	0.005405
Q9JLM8	*Dclk1*	-1.27	0.020819
P12032	*Timp1*	-1.26	0.013946
Q61398	*Pcolce*	-1.26	0.004878
Q3U962	*Col5a2*	-1.24	0.005333
Q9D379	*Ephx1*	-1.21	0.009853
Q9JHU9	*Isyna1*	-1.20	0.009391
Q8CG19	*Ltbp1*	-1.19	0.009495
Q70IV5	*Synm*	-1.19	0.011875
O54724	*Cavin1*	-1.19	0.009600
P24452	*Capg*	-1.18	0.022525
P37889	*Fbln2*	-1.13	0.015214
Q01279	*Egfr*	-1.12	0.014214
O35375	*Nrp2*	-1.11	0.016959
Q62356	*Fstl1*	-1.11	0.014678
Q8BH64	*Ehd2*	-1.11	0.013688
P07091	*S100a4*	-1.10	0.013020
P11276	*Fn1*	-1.09	0.013944
Q9QUH0	*Glrx*	-1.09	0.036464
P37804	*Tagln*	-1.09	0.024880
Q9CWR0	*Arhgef25*	-1.09	0.022043
Q60760	*Grb10*	-1.09	0.016820
P53798	*Fdft1*	-1.08	0.021684

Uniprot ID	Genes	FC [log2]	q-value
Q91VJ2	*Cavin3*	-1.08	0.015967
P48759	*Ptx3*	-1.07	0.024715
P15626	*Gstm2*	-1.06	0.036216
P28653	*Bgn*	-1.06	0.018049
Q61554	*Fbn1*	-1.05	0.021054
Q08091	*Cnn1*	-1.05	0.024077
Q8K4Q8	*Colec12*	-1.04	0.022371
Q9DC11	*Plxdc2*	-1.03	0.023946
Q921V5	*Mgat2*	-1.00	0.035946
Q9WVJ9	*Efemp2*	-0.99	0.029046
Q3UW53	*Niban1*	-0.99	0.022759
Q6NSR8	*Npepl1*	-0.98	0.025274
Q8BR92	*Palm2*	-0.97	0.026141
O70433	*Fhl2*	-0.96	0.030508
P52800	*Efnb2*	-0.96	0.026452
Q921X9	*Pdia5*	-0.96	0.025291
Q6DID7	*Wls*	-0.96	0.027581
P58774	*Tpm2*	-0.95	0.029211
P05622	*Pdgfrb*	-0.94	0.025976
Q8R1F6	*Hid1*	-0.93	0.026296
Q8K009	*Aldh1l2*	-0.93	0.029453
Q9CZT5	*Vasn*	-0.92	0.030674
Q60716	*P4ha2*	-0.92	0.026771
Q9R257	*Hebp1*	-0.92	0.031553
P27046	*Man2a1*	-0.91	0.031366
Q99LJ7	*Rcbtb2*	-0.90	0.043865
P55012	*Slc12a2*	-0.90	0.031714
P04117	*Fabp4*	-0.90	0.031522
Q8VCN5	*Cth*	-0.89	0.034789
Q9ET54	*Palld*	-0.89	0.031000
Q9QYR9	*Acot2*	-0.88	0.036269
Q3TIR3	*Ric8a*	-0.88	0.035324
Q9CQE1	*Nipsnap3b*	-0.87	0.041792
Q9D9V3	*Echdc1*	-0.86	0.032947
Q8BMG7	*Rab3gap2*	-0.86	0.034009
P14824	*Anxa6*	-0.85	0.032746
P63013	*Prrx1*	-0.84	0.035236
Q8CI51	*Pdlim5*	-0.84	0.032736
P35569	*Irs1*	-0.84	0.039950
P97873	*Loxl1*	-0.84	0.037844
Q8VHI3	*Pofut2*	-0.84	0.041371
O35459	*Ech1*	-0.82	0.045919
Q3U4G3	*Xxylt1*	-0.82	0.041556
Q80XI3	*Eif4g3*	-0.82	0.041371
P35441	*Thbs1*	-0.81	0.043276
P07214	*Sparc*	-0.81	0.036996

Uniprot ID	Genes	FC [log2]	q-value
Q69ZR2	*Hectd1*	-0.80	0.037105
Q8BWT1	*Acaa2*	-0.80	0.045778
Q80YX1	*Tnc*	-0.80	0.047716
Q9CPX6	*Atg3*	-0.80	0.044197
P62746	*Rhob*	-0.79	0.043356
Q9D281	*Fam114a1*	-0.79	0.041441
P20357	*Map2*	-0.78	0.041564
Q640N1	*Aebp1*	-0.78	0.043169
Q9QZL0	*Ripk3*	-0.77	0.043415
Q9EPR5	*Sorcs2*	-0.74	0.045511
Q9JLV6	*Pnkp*	-0.74	0.045842
Q9Z2H5	*Epb41l1*	0.76	0.046167
E9PVX6	*Mki67*	0.77	0.043191
P97494	*Gclc*	0.78	0.043305
Q9WU62	*Incenp*	0.80	0.036673
Q07797	*Lgals3bp*	0.81	0.046277
Q9QYL7	*Abt1*	0.81	0.039851
P30276	*Ccnb2*	0.82	0.046007
Q64516	*Gk*	0.82	0.041708
Q91W36	*Usp3*	0.82	0.046000
O35657	*Neu1*	0.83	0.039492
P97329	*Kif20a*	0.84	0.037966
Q9R233	*Tapbp*	0.84	0.045550
Q8CAS9	*Parp9*	0.85	0.039378
Q6PR54	*Rif1*	0.85	0.039660
Q99MU3	*Adar*	0.85	0.033048
Q80TR8	*Dcaf1*	0.86	0.033869
Q6Q899	*Rigi*	0.88	0.031337
Q9Z1S0	*Bub1b*	0.89	0.031877
Q8CE90	*Map2k7*	0.90	0.038130
O70126	*Aurkb*	0.90	0.036511
Q80WE4	*Kif20b*	0.91	0.043194
Q9JHL1	*Slc9a3r2*	0.93	0.031680
Q8K330	*Ssh3*	0.93	0.045502
Q8BWP8	*B4gat1*	0.93	0.043109
Q91WC9	*Daglb*	0.94	0.033963
A2AHC3	*Camsap1*	0.94	0.043850
Q01320	*Top2a*	0.95	0.024234
Q8BY02	*Nkrf*	0.96	0.031737
A2ASQ1	*Agrn*	0.97	0.030733
Q80Y19	*Arhgap11a*	0.97	0.031500
Q9JJV2	*Pfn2*	0.97	0.034323
Q9ERH4	*Nusap1*	0.99	0.030807
Q6P9P6	*Kif11*	1.02	0.021168
Q91VL8	*Terf2ip*	1.02	0.025436
Q149F1	*Rpusd2*	1.02	0.036836

Uniprot ID	Genes	FC [log2]	q-value
P10287	*Cdh3*	1.03	0.020947
Q8BP00	*Iqcb1*	1.06	0.046543
Q9CQ73	*Pkp2*	1.06	0.027885
P53564	*Cux1*	1.07	0.025132
Q62394	*Znf185*	1.07	0.044552
P0DOV2	*Ifi204*	1.08	0.025150
Q61179	*Irf9*	1.09	0.026611
O35955	*Psmb10*	1.09	0.032789
E9Q555	*Rnf213*	1.11	0.013829
Q9JJX7	*Tdp2*	1.11	0.045912
Q9CQR4	*Acot13*	1.14	0.030905
Q8R5H6	*Wasf1*	1.14	0.031471
O35646	*Capn6*	1.15	0.012893
Q91ZE0	*Tmlhe*	1.16	0.024349
Q8BWF0	*Aldh5a1*	1.18	0.041541
Q61823	*Pdcd4*	1.18	0.021576
Q9Z179	*Shcbp1*	1.19	0.014089
E1U8D0	*Soga1*	1.21	0.026400
P01887	*B2m*	1.22	0.027792
Q8BG60	*Txnip*	1.23	0.012082
Q8R2Q8	*Bst2*	1.23	0.004819
O08573	*Lgals9*	1.23	0.014897
Q3U182	*Crtc2*	1.26	0.025448
Q9QWH1	*Phc2*	1.29	0.038129
Q6P8M1	*Tatdn1*	1.30	0.047644
Q6A037	*N4bp1*	1.31	0.029618
Q3UDK1	*Trafd1*	1.32	0.005263
Q8CIG9	*Fbxl8*	1.34	0.032952
Q80YQ8	*Rmnd5a*	1.35	0.029785
Q8VE10	*Naa40*	1.35	0.027135
Q9WV34	*Mpp2*	1.36	0.024392
Q9JJ48	*Zc3h8*	1.36	0.031839
Q9D902	*Gtf2e2*	1.40	0.044030
Q8R2Y2	*Mcam*	1.40	0.004471
Q8C0P0	*Mastl*	1.41	0.009290
Q8R5F7	*Ifih1*	1.41	0.004825
Q9CZC8	*Scrn1*	1.42	0.031856
Q64314	*Cd34*	1.45	0.020656
Q61107	*Gbp4*	1.45	0.039453
Q9EPB5	*Serhl*	1.46	0.018784
Q0VBD2	*Mcm10*	1.47	0.005714
P58158	*B3gat3*	1.47	0.013965
A2ALU4	*Shroom2*	1.48	0.004157
Q8K248	*Hpdl*	1.52	0.013962
Q14AX6	*Cdk12*	1.53	0.024553
Q9D8C4	*Ifi35*	1.53	0.030836

Uniprot ID	Genes	FC [log2]	q-value
P23906	*Irf2*	1.55	0.015832
Q9CZ82	*Med18*	1.57	0.032117
Q9WUR2	*Eci2*	1.62	0.020892
Q8BHE1	*Gemin8*	1.62	0.022601
B2RRD7	*Brpf1*	1.63	0.012080
Q06335	*Aplp2*	1.67	0.005000
Q62086	*Pon2*	1.67	0.040017
Q9D1Q4	*Dpm3*	1.68	0.030637
Q9Z1R4	*D17h6s53e*	1.69	0.004606
Q9DCL8	*Ppp1r2*	1.70	0.041496
Q8BTX9	*Hsdl1*	1.70	0.039325
Q8K2L8	*Trappc12*	1.71	0.030952
Q9Z0M5	*Lipa*	1.73	0.032891
Q9Z2E1	*Mbd2*	1.75	0.007545
Q8K1I7	*Wipf1*	1.76	0.025605
Q9DB50	*Ap1s2*	1.79	0.009957
Q8CBB9	*Rsad2*	1.80	0.015085
Q8CFH6	*Sik2*	1.80	0.005153
Q64345	*Ifit3*	1.81	0.004984
Q3UIR3	*Dtx3l*	1.82	0.003043
Q9CPN8	*Igf2bp3*	1.84	0.000000
Q99JI6	*Rap1b*	1.86	0.039950
Q9ER80	*Rtp4*	1.88	0.000000
Q8VI94	*Oasl1*	1.89	0.000000
Q62087	*Pon3*	1.92	0.013564
Q80ZW2	*Them6*	1.93	0.002051
O35566	*Cd151*	1.93	0.031370
P49615	*Cdk5*	2.02	0.005063
Q8K400	*Stxbp5*	2.05	0.022620
Q9D1I2	*Card19*	2.05	0.011960
O35309	*Nmi*	2.07	0.000000
O08715	*Akap1*	2.08	0.034028
Q8BHF7	*Pgs1*	2.10	0.019873
Q64282	*Ifit1*	2.11	0.000000
P28063	*Psmb8*	2.13	0.004343
Q64112	*Ifit2*	2.14	0.004561
Q3U5Q7	*Cmpk2*	2.19	0.000000
Q8K1E6	*Alkbh3*	2.23	0.000000
P14602	*Hspb1*	2.25	0.000000
O54826	*Mllt10*	2.33	0.011960
P62743	*Ap2s1*	2.34	0.025342
Q9CQ10	*Chmp3*	2.35	0.030839
Q9WVQ0	*Pmfbp1*	2.47	0.021482
O35963	*Rab33b*	2.50	0.021324
Q9D964	*Gatm*	2.55	0.003024
Q6Y5D8	*Arhgap10*	2.67	0.000000

Uniprot ID	Genes	FC [log2]	q-value
Q9CQ90		2.71	0.000000
Q810J8	*Zfyve1*	2.90	0.004282
Q8C551	*Rad51ap1*	2.94	0.004903
P70265	*Pfkfb2*	3.00	0.041626
Q9Z265	*Chek2*	3.11	0.000000
Q9Z2F2	*Oasl2*	3.17	0.000000
A2AUY4	*Baz2b*	3.38	0.004000
Q61508	*Ecm1*	3.41	0.000000

Table S6: Mitochondrial proteins detected by whole-cell mass spectrometry

Uniprot ID	Genes	FC [log2]	q-value
Q8R086	*Suox*	-3.70	0.000000
Q8BH86	*Dglucy*	-2.57	0.000000
Q9D0J4	*Arl2*	-2.18	0.012206
P16125	*Ldhb*	-1.94	0.001297
Q8BW00	*Ptrh1*	-1.65	0.022444
Q9WUR9	*Ak4*	-1.52	0.004077
Q99LB2	*Dhrs4*	-1.38	0.004444
P97478	*Coq7*	-0.93	0.132741
Q8K009	*Aldh1l2*	-0.93	0.029453
Q9R257	*Hebp1*	-0.92	0.031553
Q9QYR9	*Acot2*	-0.88	0.036269
Q9CZ57	*Nsun4*	-0.88	0.111496
Q9CQE1	*Nipsnap3b*	-0.87	0.041792
Q9D9V3	*Echdc1*	-0.86	0.032947
O35459	*Ech1*	-0.82	0.045919
Q8BWT1	*Acaa2*	-0.80	0.045778
Q5IRJ6	*Slc30a9*	-0.74	0.120921
Q9D6U8	*Fam162a*	-0.60	0.088104
Q8VCL2	*Sco2*	-0.59	0.087762
P29758	*Oat*	-0.57	0.084042
Q9JIA7	*Sphk2*	-0.55	0.101400
Q64133	*Maoa*	-0.54	0.094715
Q9CQ75	*Ndufa2*	-0.54	0.123007
Q9CPQ1	*Cox6c*	-0.52	0.142973
Q8BW75	*Maob*	-0.52	0.109829
Q8K1C0	*Angel2*	-0.50	0.247661
Q8CD10	*Micu2*	-0.50	0.114314
Q9Z2G9	*Htatip2*	-0.49	0.168028
Q9JIZ9	*Plscr3*	-0.46	0.129644
Q9CYW4	*Hdhd3*	-0.46	0.142883
Q9D8S4	*Rexo2*	-0.45	0.139495
Q8K354	*Cbr3*	-0.44	0.142718
Q9DCW4	*Etfb*	-0.43	0.139398
Q8K215	*Lyrm4*	-0.43	0.143151
Q9D1L0	*Chchd2*	-0.43	0.151292
Q8BVU5	*Nudt9*	-0.43	0.137537
P11930	*Nudt19*	-0.42	0.154295
P97363	*Sptlc2*	-0.42	0.145023
Q8BH04	*Pck2*	-0.42	0.147914
P35290	*Rab24*	-0.39	0.226673
Q8BHS6	*Armcx3*	-0.39	0.153025
Q8K4X7	*Agpat4*	-0.39	0.165390
Q9CZN7	*Shmt2*	-0.38	0.154223
Q9D273	*Mmab*	-0.38	0.180045
Q8JZU2	*Slc25a1*	-0.37	0.168116
Q3V3R1	*Mthfd1l*	-0.37	0.167793
Q499X9	*Mars2*	-0.35	0.188509
Q99LC5	*Etfa*	-0.35	0.171210
Q9DBF1	*Aldh7a1*	-0.35	0.183086
Q3UMR5	*Mcu*	-0.35	0.173631
Q9CQV1	*Pam16*	-0.34	0.374231
O55028	*Bckdk*	-0.33	0.193065
P47199	*Cryz*	-0.32	0.186976
Q9R112	*Sqor*	-0.32	0.191903
Q8VCX5	*Micu1*	-0.32	0.195311
Q64373	*Bcl2l1*	-0.32	0.196718
Q91Z53	*Grhpr*	-0.30	0.201338
P58044	*Idi1*	-0.30	0.197489
P97742	*Cpt1a*	-0.30	0.201052
Q8CHT0	*Aldh4a1*	-0.30	0.194473
Q9D8Y1	*Tmem126a*	-0.29	0.207393
Q8R2Y8	*Ptrh2*	-0.29	0.208292
Q99L04	*Dhrs1*	-0.29	0.216476
Q9CZ42	*Naxd*	-0.29	0.215653
Q99LC3	*Ndufa10*	-0.28	0.219542
Q3TBW2	*Mrpl10*	-0.28	0.236079
Q91XL9	*Osbpl1a*	-0.28	0.207877
Q9JI39	*Abcb10*	-0.28	0.213895
P97287	*Mcl1*	-0.27	0.222255
Q60597	*Ogdh*	-0.27	0.209290
Q8C3X2	*Ccdc90b*	-0.27	0.222038
Q922Q4	*Pycr2*	-0.27	0.233283
Q924L1	*Letmd1*	-0.26	0.345653
Q9D8B4	*Ndufa11*	-0.25	0.234834
Q9JJL8	*Sars2*	-0.25	0.234491
Q9D7B6	*Acad8*	-0.25	0.233840
Q8BJZ4	*Mrps35*	-0.25	0.309804
P56380	*Nudt2*	-0.24	0.235988
Q91VM9	*Ppa2*	-0.24	0.235771
P62897	*Cycs*	-0.24	0.237430
Q60649	*Clpb*	-0.24	0.381466
Q8R1I1	*Uqcr10*	-0.24	0.268641
Q9DCT2	*Ndufs3*	-0.24	0.241522
P97386	*Lig3*	-0.24	0.239537
P32020	*Scp2*	-0.23	0.270782
Q07813	*Bax*	-0.23	0.288168
Q3TIU4	*Pde12*	-0.23	0.253238
Q80Y14	*Glrx5*	-0.21	0.287525
P54071	*Idh2*	-0.21	0.268882
Q80YD1	*Supv3l1*	-0.20	0.312277

Uniprot ID	Genes	FC [log2]	q-value
Q99JB2	*Stoml2*	-0.20	0.290722
Q9JIK9	*Mrps34*	-0.20	0.307234
Q91YT0	*Ndufv1*	-0.19	0.294713
P38647	*Hspa9*	-0.19	0.300388
Q80U63	*Mfn2*	-0.19	0.310464
Q9CQN1	*Trap1*	-0.19	0.297271
P51660	*Hsd17b4*	-0.18	0.304969
Q9CQ92	*Fis1*	-0.18	0.310453
P28352	*Apex1*	-0.18	0.313371
Q9DCC8	*Tomm20*	-0.18	0.333337
Q9EQ80	*Nif3l1*	-0.18	0.317900
Q9EQ20	*Aldh6a1*	-0.17	0.350900
Q9EQI8	*Mrpl46*	-0.17	0.329968
Q99KK9	*Hars2*	-0.17	0.329959
Q9D1N9	*Mrpl21*	-0.17	0.384511
Q9QYA2	*Tomm40*	-0.17	0.345135
O89110	*Casp8*	-0.17	0.329931
Q9JMH6	*Txnrd1*	-0.17	0.325628
Q80Y81	*Elac2*	-0.17	0.343139
P52825	*Cpt2*	-0.16	0.347246
Q811I0	*Atpaf1*	-0.16	0.384461
Q9D6K5	*Synj2bp*	-0.16	0.354177
Q9D2G2	*Dlst*	-0.16	0.364641
Q91WK1	*Spryd4*	-0.16	0.365742
P40630	*Tfam*	-0.16	0.368165
Q9D0D3	*Mtpap*	-0.15	0.381000
Q9CQS4	*Slc25a46*	-0.15	0.393179
Q91XF0	*Pnpo*	-0.15	0.388658
Q99LB7	*Sardh*	-0.15	0.393102
Q91YM4	*Tbrg4*	-0.15	0.382770
Q99J47	*Dhrs7b*	-0.15	0.382001
Q9QXX4	*Slc25a13*	-0.14	0.378640
Q5SWU9	*Acaca*	-0.14	0.383700
Q8CGK3	*Lonp1*	-0.14	0.399366
Q9CQ54	*Ndufc2*	-0.14	0.400427
Q7TMF3	*Ndufa12*	-0.14	0.423033
Q8VEM8	*Slc25a3*	-0.14	0.419084
Q9CQH3	*Ndufb5*	-0.13	0.438911
Q9CQC7	*Ndufb4*	-0.13	0.437239
Q3UQ84	*Tars2*	-0.13	0.448414
Q9DC69	*Ndufa9*	-0.12	0.447130
Q9CZL5	*Pcbd2*	-0.12	0.449836
Q9DCM0	*Ethe1*	-0.12	0.455671
Q91V61	*Sfxn3*	-0.12	0.451278
P22315	*Fech*	-0.12	0.459949
Q62425	*Ndufa4*	-0.12	0.480563

Uniprot ID	Genes	FC [log2]	q-value
Q9CR62	*Slc25a11*	-0.12	0.467358
Q9D0L7	*Armc10*	-0.12	0.461443
P97432	*Nbr1*	-0.12	0.468757
Q9CPY1	*Mrpl51*	-0.12	0.546156
Q8R4N0	*Clybl*	-0.12	0.505001
Q3TLP5	*Echdc2*	-0.11	0.498981
P19096	*Fasn*	-0.11	0.472214
Q8CEE7	*Rdh13*	-0.11	0.540445
P47740	*Aldh3a2*	-0.11	0.526189
Q9CQ62	*Decr1*	-0.11	0.526078
Q3U5F4	*Yrdc*	-0.11	0.505928
Q9CRD0	*Ociad1*	-0.10	0.525240
Q8BYL4	*Yars2*	-0.10	0.525284
P36552	*Cpox*	-0.10	0.529456
Q8JZS9	*Mrpl48*	-0.10	0.557089
Q3UHB1	*Nt5dc3*	-0.09	0.549365
Q8R2Q4	*Gfm2*	-0.09	0.600065
P26443	*Glud1*	-0.09	0.559912
P45952	*Acadm*	-0.09	0.558485
Q8K1M6	*Dnm1l*	-0.09	0.554853
Q91VD9	*Ndufs1*	-0.09	0.561081
Q9D6J6	*Ndufv2*	-0.09	0.599852
Q9CZR8	*Tsfm*	-0.08	0.651218
Q8BFR5	*Tufm*	-0.08	0.613608
Q8K2B3	*Sdha*	-0.08	0.615374
Q9CRA5	*Golph3*	-0.08	0.652508
Q9WV96	*Timm10b*	-0.07	0.704979
Q8BK08	*Tmem11*	-0.07	0.637995
P50544	*Acadvl*	-0.07	0.643581
P38060	*Hmgcl*	-0.07	0.688955
P99029	*Prdx5*	-0.07	0.650240
Q9CPR5	*Mrpl15*	-0.07	0.669105
P21300	*Akr1b7*	-0.07	0.681103
P56391	*Cox6b1*	-0.07	0.686458
P51175	*Ppox*	-0.07	0.678342
Q9DCN2	*Cyb5r3*	-0.07	0.674571
P09528	*Fth1*	-0.07	0.678390
Q8BJU9	*Mtrf1l*	-0.06	0.708124
Q9D1P0	*Mrpl13*	-0.06	0.730429
Q8BFP9	*Pdk1*	-0.05	0.734295
Q9D880	*Timm50*	-0.05	0.727287
Q9CQZ5	*Ndufa6*	-0.05	0.747314
Q9CQZ6	*Ndufb3*	-0.05	0.760569
Q60932	*Vdac1*	-0.05	0.749347
Q99KE1	*Me2*	-0.05	0.745300
Q5U458	*Dnajc11*	-0.05	0.754345

Uniprot ID	Genes	FC [log2]	q-value
Q8VCW8	*Acsf2*	-0.05	0.761833
Q920E5	*Fdps*	-0.05	0.762983
O70325	*Gpx4*	-0.04	0.773879
Q91WD5	*Ndufs2*	-0.04	0.807872
Q60930	*Vdac2*	-0.04	0.804508
Q9JHW2	*Nit2*	-0.04	0.823129
Q8CC88	*Vwa8*	-0.03	0.820539
Q99LX0	*Park7*	-0.03	0.829819
Q9ERB0	*Snap29*	-0.03	0.852085
Q9CZU6	*Cs*	-0.03	0.844797
Q9DBL1	*Acadsb*	-0.03	0.845104
Q9CPX7	*Mrps16*	-0.03	0.849995
O35658	*C1qbp*	-0.03	0.877426
Q8K1J6	*Trnt1*	-0.03	0.858643
Q9D0Q7	*Mrpl45*	-0.03	0.860183
Q9JMA2	*Qtrt1*	-0.03	0.869440
Q8K4Z3	*Naxe*	-0.02	0.880637
Q9CXW2	*Mrps22*	-0.02	0.876992
Q9WUM5	*Suclg1*	-0.02	0.908696
Q8VE22	*Mrps23*	-0.02	0.919921
P17665	*Cox7c*	-0.02	0.921864
Q8VDK1	*Nit1*	-0.01	0.928312
Q8BMS1	*Hadha*	-0.01	0.931592
Q9CXZ1	*Ndufs4*	-0.01	0.934121
Q9CPP6	*Ndufa5*	-0.01	0.935099
Q9JLJ2	*Aldh9a1*	-0.01	0.936764
Q91VA6	*Poldip2*	-0.01	0.964522
O08749	*Dld*	-0.01	0.964375
Q8JZQ2	*Afg3l2*	-0.01	0.967004
Q3TUH1	*Tamm41*	-0.01	0.967012
Q9DCU6	*Mrpl4*	-0.01	0.968927
Q8BG51	*Rhot1*	-0.01	0.970048
Q8K199	*Cmc2*	-0.01	0.975126
Q9Z210	*Pex11b*	0.00	0.982183
P47738	*Aldh2*	0.00	0.988799
Q99N84	*Mrps18b*	0.00	0.993241
B7ZMP1	*Xpnpep3*	0.00	0.992062
Q9JHS4	*Clpx*	0.00	0.988962
Q99MN9	*Pccb*	0.00	0.977942
Q9Z2I9	*Sucla2*	0.01	0.973895
Q9CQA3	*Sdhb*	0.01	0.938309
Q99KR3	*Lactb2*	0.01	0.933416
Q3UFY8	*Trmt10c*	0.02	0.913072
A6H611	*Mipep*	0.02	0.913573
Q3URE1	*Acsf3*	0.02	0.910239
Q9D7B1	*Dus2*	0.02	0.901730

Uniprot ID	Genes	FC [log2]	q-value
Q2TPA8	*Hsdl2*	0.02	0.889479
P62077	*Timm8b*	0.02	0.880730
Q99JR1	*Sfxn1*	0.02	0.871554
Q9CQF0	*Mrpl11*	0.02	0.881597
Q9DC29	*Abcb6*	0.03	0.857332
P97823	*Lypla1*	0.03	0.869570
Q99M87	*Dnaja3*	0.03	0.850906
O35129	*Phb2*	0.03	0.828693
Q9Z2I0	*Letm1*	0.03	0.823032
Q9D338	*Mrpl19*	0.03	0.826659
D3Z7P3	*Gls*	0.04	0.818951
Q9JKF7	*Mrpl39*	0.04	0.815103
Q8BIP0	*Dars2*	0.04	0.815300
Q9DB77	*Uqcrc2*	0.04	0.811523
Q9CYF5	*Rcc1l*	0.04	0.800416
Q91VT4	*Cbr4*	0.04	0.813091
Q8BH95	*Echs1*	0.04	0.772934
Q9CXT8	*Pmpcb*	0.05	0.741246
Q61578	*Fdxr*	0.05	0.751059
P19783	*Cox4i1*	0.05	0.750600
Q921S7	*Mrpl37*	0.05	0.740546
Q99N87	*Mrps5*	0.05	0.717960
Q9D0C4	*Trmt5*	0.06	0.730321
Q9DC61	*Pmpca*	0.06	0.699216
Q9CR68	*Uqcrfs1*	0.06	0.700441
Q9D5T0	*Atad1*	0.06	0.697733
Q9Z1J3	*Nfs1*	0.06	0.699920
O08709	*Prdx6*	0.06	0.695676
Q8BGH2	*Samm50*	0.06	0.695802
Q921H8	*Acaa1a*	0.07	0.694755
Q9D0G0	*Mrps30*	0.07	0.672814
Q80ZS3	*Mrps26*	0.07	0.661707
Q78PY7	*Snd1*	0.07	0.654233
Q91ZA3	*Pcca*	0.07	0.648844
Q922H2	*Pdk3*	0.07	0.639665
Q9WTP6	*Ak2*	0.07	0.641413
Q8BX10	*Pgam5*	0.07	0.645702
Q8JZN5	*Acad9*	0.07	0.633619
P48771	*Cox7a2*	0.08	0.646003
Q8K411	*Pitrm1*	0.08	0.620656
Q99N89	*Mrpl43*	0.08	0.627106
Q8K3J1	*Ndufs8*	0.08	0.637122
Q91V12	*Acot7*	0.08	0.620687
Q9DCJ5	*Ndufa8*	0.08	0.635225
O35972	*Mrpl23*	0.08	0.639717
Q60759	*Gcdh*	0.08	0.627135

Uniprot ID	Genes	FC [log2]	q-value
Q791V5	*Mtch2*	0.08	0.631964
Q64433	*Hspe1*	0.08	0.615325
Q9Z110	*Aldh18a1*	0.08	0.614780
Q8C163	*Exog*	0.08	0.633447
Q91V92	*Acly*	0.08	0.605019
Q8R3K3	*Ptcd2*	0.08	0.639815
Q8BMD8	*Slc25a24*	0.08	0.597753
Q9CWE0	*Mtfr1l*	0.08	0.614109
Q9CQJ8	*Ndufb9*	0.08	0.628121
P42125	*Eci1*	0.09	0.602057
Q8BU88	*Mrpl22*	0.09	0.589653
Q14C51	*Ptcd3*	0.09	0.586537
Q9D855	*Uqcrb*	0.09	0.577225
Q8BK72	*Mrps27*	0.09	0.560800
Q9D1B9	*Mrpl28*	0.10	0.534825
Q922W5	*Pycr1*	0.10	0.549678
Q9D773	*Mrpl2*	0.10	0.527868
Q9DCL9	*Paics*	0.10	0.517068
Q9DCS9	*Ndufb10*	0.10	0.547762
Q9CY16	*Mrps28*	0.10	0.516335
Q9CQF8	*Mrpl57*	0.10	0.544074
Q9JK81	*Myg1*	0.11	0.506209
Q99M04	*Lias*	0.11	0.554840
Q3U2A8	*Vars2*	0.11	0.506616
Q8QZS1	*Hibch*	0.11	0.526521
O88587	*Comt*	0.11	0.511694
Q99JY0	*Hadhb*	0.11	0.521604
P58064	*Mrps6*	0.11	0.497050
Q9WV98	*Timm9*	0.12	0.478344
Q9CZ13	*Uqcrc1*	0.12	0.467017
Q3TC33	*Ccdc127*	0.12	0.451693
Q922Q1	*Mtarc2*	0.12	0.443672
Q9CQN7	*Mrpl41*	0.13	0.440822
P53395	*Dbt*	0.13	0.450846
O88967	*Yme1l1*	0.13	0.443111
P18155	*Mthfd2*	0.13	0.499754
Q9DCS3	*Mecr*	0.13	0.454633
Q9ER88	*Dap3*	0.13	0.441969
Q8R035	*Mrpl58*	0.14	0.424631
O88696	*Clpp*	0.14	0.435598
Q9WU56	*Pus1*	0.14	0.412717
Q91VN4	*Chchd6*	0.14	0.407178
P63038	*Hspd1*	0.14	0.406809
Q9CR59	*Gadd45gip1*	0.14	0.409965
P08074	*Cbr2*	0.14	0.394177
P51174	*Acadl*	0.14	0.399221

Uniprot ID	Genes	FC [log2]	q-value
Q9D8S9	*Bola1*	0.14	0.385198
Q8JZN7	*Rhot2*	0.14	0.384872
Q9CY73	*Mrpl44*	0.15	0.393067
Q9CQQ7	*Atp5pb*	0.15	0.388468
Q8K2Y7	*Mrpl47*	0.15	0.425345
Q8K1R3	*Pnpt1*	0.15	0.388355
Q924T2	*Mrps2*	0.15	0.386412
Q8BWM0	*Ptges2*	0.15	0.386849
Q9CRB9	*Chchd3*	0.16	0.364386
Q8BGA9	*Oxa1l*	0.16	0.371517
O35465	*Fkbp8*	0.16	0.356944
Q9R0X4	*Acot9*	0.16	0.358953
Q9D8P4	*Mrpl17*	0.16	0.364684
P08228	*Sod1*	0.16	0.345536
Q9D7N3	*Mrps9*	0.16	0.336323
P70349	*Hint1*	0.17	0.349548
Q80X85	*Mrps7*	0.17	0.353004
Q8K2C6	*Sirt5*	0.17	0.350703
Q9CWG8	*Ndufaf7*	0.17	0.337636
Q61425	*Hadh*	0.17	0.327303
P47802	*Mtx1*	0.17	0.330794
Q8BGX2	*Timm29*	0.17	0.326587
Q80SW1	*Ahcyl1*	0.18	0.370172
Q99LP6	*Grpel1*	0.18	0.328231
Q9CQL5	*Mrpl18*	0.18	0.337018
P58281	*Opa1*	0.18	0.314403
Q9QZH6	*Ecsit*	0.18	0.352491
O35857	*Timm44*	0.18	0.311106
Q8C5H8	*Nadk2*	0.18	0.310981
Q920A7	*Afg3l1*	0.18	0.323175
P05202	*Got2*	0.18	0.329365
Q9D1H8	*Mrpl53*	0.18	0.344243
O35855	*Bcat2*	0.18	0.326286
P35486	*Pdha1*	0.19	0.297632
Q9Z2Z6	*Slc25a20*	0.19	0.310891
Q9CPV4	*Glod4*	0.19	0.305059
Q9Z2Y8	*Plpbp*	0.19	0.310969
Q9DC50	*Crot*	0.19	0.300268
Q99N94	*Mrpl9*	0.19	0.292041
P20108	*Prdx3*	0.20	0.300771
Q9DC71	*Mrps15*	0.20	0.285997
Q9D0M3	*Cyc1*	0.20	0.289997
P70444	*Bid*	0.20	0.319223
Q9D0S9	*Hint2*	0.20	0.281810
Q922E6	*Fastkd2*	0.20	0.316395
Q99KI0	*Aco2*	0.20	0.272201

Uniprot ID	Genes	FC [log2]	q-value
P09671	*Sod2*	0.20	0.304072
Q3TX08	*Trmt1*	0.20	0.282717
Q921G7	*Etfdh*	0.21	0.278215
P05132	*Prkaca*	0.21	0.291954
O08734	*Bak1*	0.21	0.293278
Q99N93	*Mrpl16*	0.21	0.544049
Q9CQX2	*Cyb5b*	0.21	0.281043
Q9JKX6	*Nudt5*	0.22	0.257986
Q9CQ69	*Uqcrq*	0.22	0.281147
Q8BH59	*Slc25a12*	0.22	0.266875
P08249	*Mdh2*	0.22	0.253283
Q99N95	*Mrpl3*	0.23	0.271077
Q921H9	*Coa7*	0.23	0.258887
O08756	*Hsd17b10*	0.23	0.248309
Q60931	*Vdac3*	0.23	0.257059
Q8K409	*Polb*	0.24	0.252221
Q6PB66	*Lrpprc*	0.24	0.237481
Q9CQY6	*Uqcc2*	0.24	0.241349
Q99PU8	*Dhx30*	0.24	0.241350
Q8R3F5	*Mcat*	0.24	0.236627
Q9WTP7	*Ak3*	0.25	0.243770
Q9D125	*Mrps25*	0.25	0.234972
Q9CPZ8	*Cmc1*	0.25	0.259914
Q8BIJ6	*Iars2*	0.25	0.236058
Q9JIY5	*Htra2*	0.26	0.237521
Q14CH7	*Aars2*	0.26	0.234221
Q8K0Z7	*Taco1*	0.26	0.234792
Q791T5	*Mtch1*	0.26	0.238030
Q8CAQ8	*Immt*	0.27	0.218919
A2ADA5	*Pusl1*	0.27	0.326592
Q9D051	*Pdhb*	0.27	0.222238
Q9D8T7	*Slirp*	0.27	0.230479
P50136	*Bckdha*	0.27	0.226820
P59017	*Bcl2l13*	0.28	0.268585
P70677	*Casp3*	0.28	0.213335
Q9JHR7	*Ide*	0.28	0.203170
P54116	*Stom*	0.28	0.219667
P99028	*Uqcrh*	0.28	0.211573
Q9CYG7	*Tomm34*	0.28	0.207265
Q91VC9	*Ghitm*	0.28	0.247641
O55126	*Nipsnap2*	0.29	0.207100
P46656	*Fdx1*	0.29	0.209610
Q99J99	*Mpst*	0.30	0.200983
Q99MR8	*Mccc1*	0.30	0.211425
O09111	*Ndufb11*	0.30	0.239431
P24270	*Cat*	0.30	0.198138

Uniprot ID	Genes	FC [log2]	q-value
Q3V384	*Afg1l*	0.30	0.237602
P51881	*Slc25a5*	0.30	0.195292
Q8BGT5	*Gpt2*	0.30	0.211563
Q8BVI4	*Qdpr*	0.31	0.207211
Q1HFZ0	*Nsun2*	0.31	0.198758
Q9CR98	*Fam136a*	0.31	0.198189
Q64105	*Spr*	0.31	0.198399
Q14AI6	*Rpusd3*	0.31	0.198183
Q9CPY7	*Lap3*	0.32	0.193160
Q91YP2	*Nln*	0.33	0.184688
Q9DB15	*Mrpl12*	0.33	0.186449
Q59J78	*Ndufaf2*	0.33	0.191701
Q9D6R2	*Idh3a*	0.34	0.186284
Q61941	*Nnt*	0.35	0.170934
Q9Z0X1	*Aifm1*	0.35	0.169587
Q9DBL7	*Coasy*	0.35	0.187222
Q9CWX4	*Rpusd4*	0.35	0.184962
Q3UJU9	*Rmdn3*	0.35	0.188196
P48962	*Slc25a4*	0.35	0.174833
Q9CWU6	*Uqcc1*	0.35	0.179435
Q9EP89	*Lactb*	0.35	0.187072
Q9QZD8	*Slc25a10*	0.35	0.187495
Q8C2E4	*Ptcd1*	0.35	0.174888
Q9D0K2	*Oxct1*	0.35	0.180737
Q9CQ43	*Dut*	0.35	0.174598
Q99L13	*Hibadh*	0.36	0.179341
O08807	*Prdx4*	0.36	0.168266
P53702	*Hccs*	0.36	0.187232
Q4VAE3	*Tmem65*	0.37	0.281102
Q9CQ06	*Mrpl24*	0.37	0.179823
Q3ULF4	*Spg7*	0.38	0.226686
Q71RI9	*Kyat3*	0.38	0.259811
A2APY7	*Ndufaf5*	0.38	0.198373
Q91WS0	*Cisd1*	0.39	0.174535
Q9D6K8	*Fundc2*	0.39	0.156486
Q8R4U6	*Top1mt*	0.39	0.213742
Q9WV84	*Nme4*	0.39	0.173662
Q61171	*Prdx2*	0.39	0.150524
Q9JLZ3	*Auh*	0.40	0.185031
Q8K4F5	*Abhd11*	0.40	0.172739
P55096	*Abcd3*	0.40	0.158879
Q80XL6	*Acad11*	0.40	0.195152
Q9JJG9	*Noa1*	0.40	0.151703
Q3ULD5	*Mccc2*	0.41	0.155057
Q9Z2I8	*Suclg2*	0.41	0.146199
Q91WG3	*Trub2*	0.41	0.178748

Uniprot ID	Genes	FC [log2]	q-value
Q8CBY0	*Gatc*	0.42	0.187749
Q9JHI5	*Ivd*	0.42	0.142576
Q9CQL4	*Mrpl20*	0.43	0.290929
Q99N96	*Mrpl1*	0.44	0.163748
Q8BKZ9	*Pdhx*	0.44	0.132949
Q8K0D5	*Gfm1*	0.44	0.139602
Q3URS9	*Ccdc51*	0.44	0.147646
P70404	*Idh3g*	0.45	0.128030
Q8QZT1	*Acat1*	0.45	0.135882
P47968	*Rpia*	0.45	0.127350
Q61576	*Fkbp10*	0.46	0.123739
Q8BMF4	*Dlat*	0.46	0.123282
Q8VCF0	*Mavs*	0.47	0.128305
O88986	*Gcat*	0.47	0.142818
O08600	*Endog*	0.47	0.192078
Q99KR7	*Ppif*	0.48	0.145422
Q3UN04	*Usp30*	0.49	0.127887
Q9CYK1	*Wars2*	0.49	0.141003
P52196	*Tst*	0.50	0.116068
Q811U4	*Mfn1*	0.52	0.139783
Q64521	*Gpd2*	0.53	0.101225
Q91YP0	*L2hgdh*	0.53	0.107771
Q9JIQ3	*Diablo*	0.54	0.119448
Q75NR7	*Recql4*	0.54	0.103886
Q9ESW4	*Agk*	0.56	0.107261
Q8C5Q4	*Grsf1*	0.56	0.111539
Q8BHC4	*Dcakd*	0.57	0.092462
P47791	*Gsr*	0.58	0.094819
Q99KB8	*Hagh*	0.59	0.087708
Q9D3P8	*Plgrkt*	0.59	0.125159
P16332	*Mmut*	0.59	0.101368
Q99LY9	*Ndufs5*	0.59	0.182793
Q8BYM8	*Cars2*	0.60	0.081537
Q8R3J4	*Mterf3*	0.61	0.110225
Q8R164	*Bphl*	0.62	0.154431
P97931	*Ung*	0.63	0.102440
Q9D0I4	*Stx17*	0.66	0.173539
P41216	*Acsl1*	0.66	0.074917
P62075	*Timm13*	0.66	0.104815
A2ASZ8	*Slc25a25*	0.69	0.066781
P47934	*Crat*	0.71	0.065127
Q07417	*Acads*	0.71	0.073353
Q61102	*Abcb7*	0.73	0.065437
Q9CWT6	*Ddx28*	0.76	0.065897
Q9CWX2	*Ndufaf1*	0.77	0.136928
Q61337	*Bad*	0.78	0.078179

Uniprot ID	Genes	FC [log2]	q-value
O88441	*Mtx2*	0.82	0.096331
Q4KMM3	*Oxr1*	0.84	0.109729
Q9CR88	*Mrps14*	0.85	0.054160
Q9CQV5	*Mrps24*	0.87	0.121678
O35435	*Dhodh*	0.99	0.107441
Q9CQR4	*Acot13*	1.14	0.030905
Q91ZE0	*Tmlhe*	1.16	0.024349
Q8BWF0	*Aldh5a1*	1.18	0.041541
Q8BP40	*Acp6*	1.28	0.073610
Q9WVA2	*Timm8a1*	1.37	0.068513
Q99N85	*Mrps18a*	1.40	0.063610
Q8K248	*Hpdl*	1.52	0.013962
Q9WUR2	*Eci2*	1.62	0.020892
Q8BTX9	*Hsdl1*	1.70	0.039325
O08715	*Akap1*	2.08	0.034028
Q8BHF7	*Pgs1*	2.10	0.019873
Q3U5Q7	*Cmpk2*	2.19	0.000000
Q9D964	*Gatm*	2.55	0.003024